Understanding Chemokines in the Oral Mucosa

Robert James Rees Reilly

BDS, MFDS RCPS (Glasg)

Submitted in fulfilment of the requirements for the Degree of Doctor of Philosophy

School of Infection and Immunity

College of Medical, Veterinary & Life Sciences

University of Glasgow

July 2023

Author’s declaration

I declare that, except where explicit reference is made to the contribution of others, that this dissertation is the result of my own work and has not been submitted for any other degree at the University of Glasgow or any other institution.

Robert Reilly

Abstract

Introduction: The gingiva is a unique barrier tissue exposed to masticatory forces, microbial insult, and food and airborne antigens. A bespoke immune network is essential to maintain homeostasis in this dynamic environment. Leukocytes, including CD4+ T cells, are central to maintaining oral health and are pivotal in oral disease pathogenesis. There is currently limited insight into the molecular mechanisms that regulate cellular recruitment to the gingival barrier. Chemokines, the main *in vivo* regulator of leukocyte recruitment, are likely to orchestrate cellular recruitment to the gingiva as they are crucial to maintaining homeostasis at other barrier tissues. This thesis sought to define the chemokine landscape in healthy gingiva, compare chemokine expression between health and periodontitis and characterise the chemokine receptor repertoire of CD4+ T cells in the gingiva.

Results: The chemokine landscape in the gingiva differed from the skin and small intestine. In gingival tissues, the CXCL12/CXCL14/CXCR4/ACKR3 axis was highly expressed and conserved between mammalian species. The chemokine landscape was similar in health and periodontitis, except for neutrophil chemo-attractants and CXCL14, which were upregulated and downregulated, respectively, in periodontitis. The chemokine receptor CXCR4 was highly expressed on gingival CD4+ T cells and upregulated compared to lymph node CD4+ T cells. Chemokine receptors responsible for skin and small intestine homing were minimally expressed on gingival CD4+ T cells.

Conclusions: The gingival chemokine landscape is unique compared to other barrier tissues. The mechanisms regulating CD4+ T cells migration to gingiva are likely distinct from the skin and small intestine. The similarity in chemokine expression between health and periodontitis may reflect the need for constant immunosurveillance at the gingival barrier. These findings, in the context of previously published data, suggest a prominent role for CXCL12/CXCL14/CXCR4 and ACKR3 in regulating homeostasis at the oral barrier. Further investigation is warranted to understand the precise role of this axis in more detail, and this may identify novel therapeutic targets to treat immune-mediated oral disease.

Acknowledgements

I would like to express my deepest gratitude to all those that have supported me on this incredible journey; without you, this simply would have been impossible. Firstly, I would like to thank my supervisors. Professor Shauna Culshaw and Professor Gerry Graham for your unwavering encouragement and support throughout my PhD. Shauna's wisdom, knowledge and experience has ensured a rewarding transition to clinical academia. Gerry's expertise and guidance, particularly when securing funding for my PhD, was invaluable and the skills developed through 'interview boot camp' will be essential in my continuing career. I will be forever grateful for the support, immense patience and friendship of Doctor Alan Hayes. His guidance in the laboratory ensured I had a wonderful PhD experience whilst learning skills beyond what I thought possible for a simple dentist.

To my funders; The Medical Research Council, The Royal College of Physicians and Surgeons of Glasgow and the British Oral and Dental Research Trust, thank you for your financial support.

Thank you to all the Chemokine Research Group members and William Johnston, your teaching of experimental techniques, feedback in lab meetings and generally making the lab a great place to work and study. Your skill, dedication and love for science have left me inspired.

I would also like to extend my appreciation to our collaborators Professor Sandra Fukada, Thaise Mayumi Taira, and Letícia Fernanda Duffles, at the University of Sao Paolo, for teaching me the ligature model, and supporting these experiments. It was a privilege getting to visit your beautiful city. Thank you to Professor Jeffery Ebersole, for his kindly sharing his non-human primate data set with us.

Next, I would like to extend thanks to the University of Glasgow Central Research Facility and Flow Core Facility, particularly Diane Vaughn and Alana Hamilton. I would like to thank John Cole for teaching me how to conduct RNA Sequencing analysis and Lauren Campbell for sharing her RNA Sequencing data

set with me. My time out of the lab during COVID-19 would have been much less productive without your contributions.

To my clinical colleagues in the Oral Medicine department at Glasgow Dental Hospital, thank you for accommodating me during my PhD and for all your support while I have been writing my thesis.

To my Mum, Dad and Andrew, thank you for everything you have done. Not simply during my PhD or when writing my thesis, but for your continuous support of my ambitions and aspirations, I would not be where I am today without you all.

Finally, I would like to thank Alison, you have inspired me throughout this journey, you have celebrated my successes and more importantly supported me when I have faced setbacks. For all your love, care and encouragement I am eternally grateful.

Table of Contents

List of Figures

Chapter 1

Chapter 2

Chapter 3

Chapter 4

Chapter 5

Chapter 6

List of Tables

Chapter 1

Chapter 2

Chapter 3

Chapter 4

Chapter 5

Abbreviations

ANOVA	**Analysis of variance**
BCA	**Bicinchoninic acid**
B-Me	**Beta mercaptoethanol**
bp	**Base pair**
BPE	**Brief periodontal examination**
CD	**Cluster of differentiation**
cDNA	**Complementary DNA**
CEJ	**Cementoenamel junction**
CLCG	**Contra-lateral control gingiva**
CMC	**Carboxymethyl cellulose**
CT	**Cycle threshold**
DapB	**Bacillus subtilis dihydrodipicolinate reductase**
DC	**Dendritic cell**
DNA	**Deoxyribonucleic acid**
EDTA	**Ethylenediaminetetraacetic acid**
ELISA	**Enzyme linked immunosorbent assay**
FCS	**Foetal calf serum**
FFPE	**Formalin fixed and paraffin embedded**
FPKM	**Fragments per kilobase of transcript per million**
GCF	**Gingival crevicular fluid**
GDC	**Genomic DNA contamination control**
gDNA	**Genomic DNA**
GF	**Germ free**
GPCR	**G-protein coupled receptors**
H&E	**Haematoxylin and eosin**
HKG	**Housekeeping gene**

HRP	**Horseradish peroxidase**
HSC	**Haematopoietic stem cell**
IBD	**Inflammatory bowel disease**
IFN	**Interferon**
IL	**Interleukin**
JE	**Junctional epithelium**
LFA-1	**Leukocyte function-associated antigen**
LG	**Ligated gingiva**
MFI	**Mean fluorescence intensity**
MHC	**Major histocompatibility complex**
mRNA	**Messenger RNA**
MSC	**Mesenchymal stem cell**
NBF	**Neutral buffered formalin**
NHP	**Non-human primate**
OVA	**Ovalbumin**
P. gingivalis	**Porphyromonas gingivalis**
PBS	**Phosphate buffered saline**
PCA	**Principal component analysis**
PCR	**Polymerase chain reaction**
PISA	**Periodontally inflamed surface area**
PMN	**Polymorphonuclear leukocytes**
PMPR	**Professional mechanical plaque removal**
PPC	**Positive PCR control**
Ppib	**Peptidylprolyl isomerase B**
qPCR	**Quantitative PCR**
RANKL	**Receptor activator of nuclear factor kappa-B ligand**
RDD	**RNeasy DNase digest**
RG	**Resting gingiva**

RIN	**RNA integrity number**
RNA	**Ribonucleic acid**
RPMI	**Roswell Park Memorial Institute Medium**
RTC	**Reverse transcription control**
RW1	**RNeasy wash buffer**
SPF	**Specific pathogen free**
STWS	**Scott's tap water solution**
Th	**T helper**
TNF	**Tumour necrosis factor**
WHIM	**Warts, hypogammaglobulinemia, infections, and myelokathexis**

Chapter 1 - Introduction

1.1 Chemokines

1.1.1 What are chemokines?

Chemokines are a family of around 50 small, highly conserved, cytokines. Chemokines are best known for their critical role in chemotaxis, most notably of leukocytes. However, chemokine-mediated recruitment of mesenchymal and haemopoietic stem cells are also well described. The term chemokine is a contraction of chemotactic cytokine. (Hughes and Nibbs, 2018; Oo, Shetty and Adams, 2010; Jiang *et al.*, 2017; Hocking, 2015; Surmi and Hasty, 2010).

Function alone does not define a chemokine; chemokines have a canonical arrangement of cysteine residues (Bhusal, Foster and Stone, 2020; Schall, 1991). Chemokines are classified by the arrangement of cysteine residues at the protein N-terminus. Four arrangements have been identified: CC, CXC, CX3C and C chemokines. C Chemokines have only one cysteine residue in the N-terminus. The 'X' in chemokine nomenclature represents any amino acid in the mature protein sequence. The N-terminus cysteine residues bind to C-terminus cysteine residues via disulphide bonds. The highly conserved structure is crucial to a chemokines function (Kufareva, Salanga and Handel, 2015; Jin *et al.*, 2011; Clore and Gronenborn, 1995) **(Figure 1.1).**

As previously reviewed, chemokines direct cell migration by signalling through cell membrane-bound G-protein coupled chemokine receptors (Hughes and Nibbs, 2018; Thelen and Stein, 2008). A promiscuous relationship exists between chemokines and their receptors, one chemokine may signal through multiple receptors, and one receptor may bind to multiple chemokines with differing affinity (Raport *et al.*, 1996). This makes elucidating and understanding the relationship between chemokines and their receptors *in vivo* challenging (Kufareva, Salanga and Handel, 2015). There are four known non-signalling chemokine receptors, termed atypical chemokine receptors, the primary function of these is to scavenge chemokines, thus regulating chemokine

availably and sculpting cell migration (Bonecchi and Graham, 2016; Thelen and Stein, 2008).

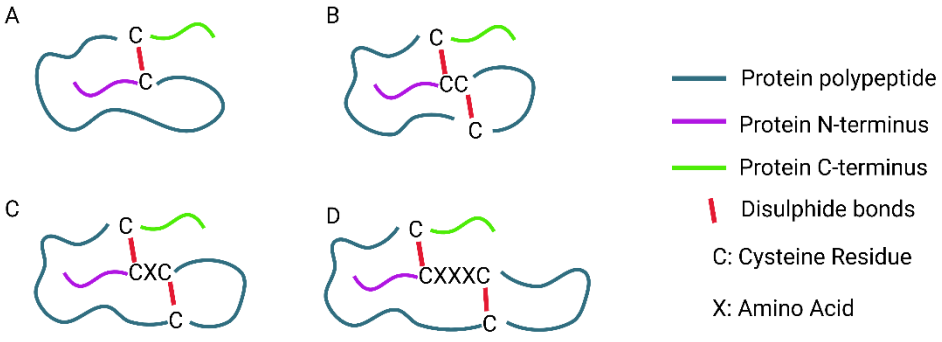

Figure 1. 1 Schematic of chemokine structure

Outline of the four conserved chemokine structures. **(A)** C chemokines. **(B)** CC chemokines. **(C)** CXC chemokines. **(D)** CX3C chemokines. Figure adapted from (Sahingur and Yeudall, 2015) created with BioRender.com.

1.1.2 Function of chemokines

To mediate their protective effects leukocytes must traffic to precise tissue locations at the right time. Chemokines are central to this by regulating leukocyte trafficking and have crucial roles in directing cellular extravasation. Following extravasation, cells are then precisely guided to their required locale within tissue through chemokine gradients (Middleton *et al.*, 2002; Weber *et al.*, 2013). In addition to cellular migration, chemokines can regulate cell adhesion; retaining cells at a specific tissue site (Janssens, Struyf and Proost, 2018). Non-leukocyte cells may also respond to chemokines and there are multiple reports of chemokines playing a role in angiogenesis and cancer metastasis (Hughes and Nibbs, 2018; Dimberg, 2010; Zlotnik, Burkhardt and Homey, 2011).

Given the vast array of chemokine functions it is unsurprising that chemokines are secreted by myriad cells, including leukocytes, endothelial cells, epithelial cells, and stromal cells (Hillyer *et al.*, 2003; Zimmerman *et al.*, 2008; Hussain *et*

al., 2020; Williams *et al.*, 2021). Furthermore, no one chemokine acts exclusively on one leukocyte sub-type, and chemokine-secreting cells can produce multiple chemokines, often with an overlapping spectrum of action. (Mantovani, 1999).

Chemokines direct cellular recruitment in health and during inflammation. Chemokines constitutively expressed in healthy tissue are termed homeostatic chemokines, whilst those induced during inflammation are defined as inflammatory chemokines (Chen *et al.*, 2018). The expression of homeostatic chemokines differs between tissues and is responsible for regulating processes in specific tissue niches (Rot and von Andrian, 2004). In contrast, inflammatory chemokines are indiscriminately expressed during inflammation. Thus, the inflammatory chemokines observed in infection will be like those observed in a chronic inflammatory condition, irrespective of the tissue site. Some chemokines have both homeostatic and inflammatory properties, named dual chemokines and a small number are yet to have their function defined (Zlotnik, Yoshie and Nomiyama, 2006) **(Fig. 1.2).**

Chemokines have functions beyond cellular recruitment and retention. For example, chemokines have been shown to have anti-microbial activity. In this context chemokines are thought to act like anti-microbial peptides, which are key components of innate immunity. Like chemokines, anti-microbial peptides have ancient embryological origins and are well conserved, furthermore chemokines and some anti-microbial peptides share structural similarities. In total 23 chemokines have been reported to demonstrate anti-microbial activity *in vitro*. Replicating these effects *in vivo* has proved challenging (Wolf and Moser, 2012; Krijgsveld *et al.*, 2000).

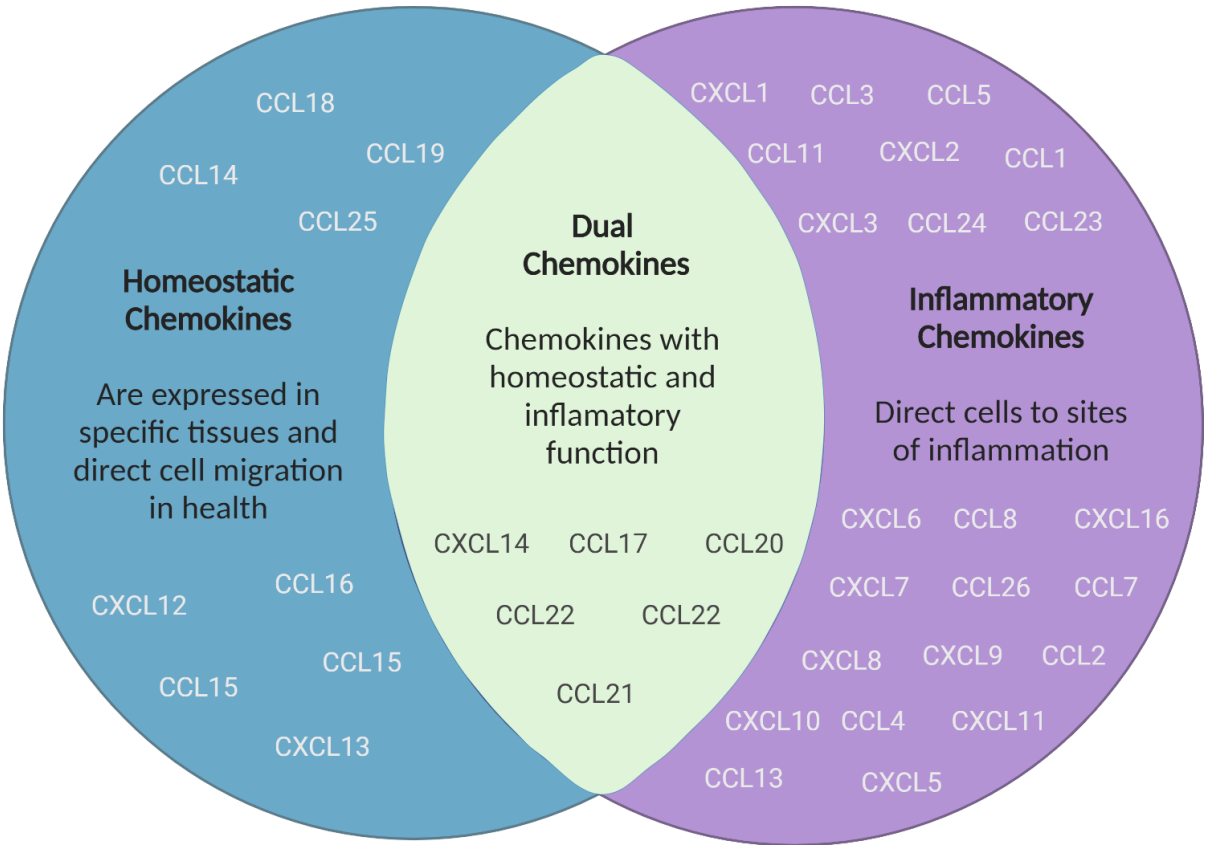

Figure 1. 2 Venn diagram of chemokine function

Chemokines are categorised as homeostatic or inflammatory depending on their function and expression patterns. A small number of chemokines have both homeostatic and inflammatory functions.

1.1.3 Chemokine receptors

Chemokine directed cell migration is dependant on signalling through chemokine receptors. There are approximately 18 signalling chemokine receptors. Chemokine receptors are 7 transmembrane G-protein couple receptors expressed on the cell surface of multiple cell types. Like chemokines, the receptors have a well conserved structure. However, there are fewer chemokine receptors, thus multiple chemokines will signal through the same receptor. There are a small number of chemokines, typically homeostatic chemokines, that have a monogamous relationship with the receptor (**Table 1.1**). This complex relationship has led to a paradigm of chemokine redundancy, ensuring robust outputs for cellular recruitment, this is particularly true for inflammatory chemokines (Mantovani, 1999; Bhusal, Foster and Stone, 2020; Zlotnik, Yoshie and Nomiyama, 2006). More recently an increased appreciation of the nuances of chemokine/chemokine receptor networks have emerged. A study using multi-

receptor reporter mice, exploring the expression patterns of CCR1, CCR2, CCR3 and CCR5, demonstrated that myeloid cells selectively express these receptors at specific times and places, and individual leukocytes are unlikely to express all four inflammatory chemokine receptors simultaneously. These findings suggest each receptor has a precise role regulating leukocyte recruitment, refuting the dogmatic view of redundancy, instead suggesting a more sophisticated system with greater specificity (Medina-Ruiz *et al.*, 2022). In addition to the 18 signalling receptors there are four non-signalling receptors termed Atypical Chemokine Receptors (ACKR). The ACKRs are also cell surface receptors with seven transmembrane domains, but lack, or have a modified, DRYLAIV motif; a highly conserved amino-acid sequence present in the second intracellular loop of a chemokine receptor essential for chemokine ligand-induced signalling (Nibbs, Graham and Rot, 2003). This results in a failure to induce classical GPCR signalling upon chemokine binding, and thus ACKRs do not direct migration. However, ACKRs have retained the ability to internalise chemokines. The primary role of ACKRs is to scavenge chemokines, reducing the availability of free chemokines in tissue, which limits cellular recruitment through those ligands. Like chemokine receptors, multiple ligands can bind to a single ACKR (Bonecchi and Graham, 2016; Nibbs and Graham, 2013).

1.1.4 Chemokine and chemokine receptor interactions

For a chemokine to direct cell trafficking it must bind to a signalling chemokine receptor. This is a complex process, which has been challenging to elucidate due to flexibility in chemokine receptor shape, post-translational modification of chemokines and the promiscuous relationship between chemokines and receptors. However, multiple studies have led to the two site model of chemokine to chemokine receptor binding; where the N-terminus of a chemokine receptor binds to the chemokine core domain, whilst the chemokine N-terminus binds to the chemokine receptor ligand-binding pocket (Monteclaro and Charo, 1996; Kufareva, Salanga and Handel, 2015).

Following chemokine-induced activation of a chemokine receptor, a complex downstream signalling cascade is initiated. Pathways regulating cytoskeleton rearrangement and cell adhesion are activated. Jak-STAT pathways are activated by chemokine-chemokine receptor binding, which influences cellular

polarisation, through calcium influx, which is critical for chemotaxis (Soriano *et al.*, 2003; Legler and Thelen, 2018).

1.1.5 Chemokines in cell migration and the leukocyte adhesion cascade

Recruitment of leukocytes to specific tissues depends on cellular extravasation. This is mediated through a tightly controlled process called the leukocyte adhesion cascade. The initial step contributing to trans-endothelial migration is rolling adhesion. In this process the velocity of circulating leukocytes is reduced through the binding of, P-Selectin and E-Selectin, expressed on the vascular endothelium, to extra-cellular glycoproteins on circulating cells, resulting in 'rolling' of leukocytes along the endothelial cell wall (Kunkel and Ley, 1996; Lorant *et al.*, 1993). Next, cell adhesion molecules on the endothelial wall bind to integrins on the rolling cell's membrane. Due to the reduced cellular velocity and close proximity to the endothelium, chemokines bound to glycosaminoglycans (GAGs) on the endothelial wall can recognise and bind to their cognate receptor, expressed upon the circulating cell. This induces conformational change and increases integrin expression, resulting in further bonds between integrins and adhesion molecules resulting in arrested movement. This facilities cellular transmigration via diapedesis, regulated by cell adhesion molecules (Ley *et al.*, 2007; Muller, 2013; Granger DN, 2010). Once a cell has transmigrated, interstitial cellular directional migration is thought to be regulated by chemokine gradients; a cell migrates from an area of low to high chemokine expression. The arrangement of a chemokine gradient is a highly complex process which is affected by chemokine abundance, chemokine scavenging by atypical chemokine receptors, chemokine affinity to GAGs, the extra-cellular matrix, and a host of other physiological features **(Fig. 1.3)** (Moore, Brook and Nibbs, 2018; Cardona *et al.*, 2008; Handel *et al.*, 2005).

Chemokine	Chemokine Receptor	Inflammatory or Homeostatic	Cells Attracted	Organism	Aliases
CC Chemokines					
CCL1	CCR8	I	Monocytes, T cells, B Cells	Hu, M	TCA-3
CCL2	CCR2	I	Monocytes, T cells, NK Cells, immature dendritic cells	Hu, M	JE
CCL3	CCR1, CCR5	I	Monocytes, macrophages, NK Cells, T cells, Immature dendritic cells	Hu, M	MIP-1α
CCL4	CCR5	I	Monocytes, T cells, immature dendritic cells	Hu, M	MIP-1ß
CCL4L1	CCR5	I	Monocytes, T cells, immature dendritic cells	Hu	
CCL5	CCR1, CCR3, CCR5	I	Monocytes, macrophages, eosinophils, NK Cells, T cells, immature dendritic cells	Hu, M	RANTES
CCL6 (Murine homologue of CCL23)	CCR1	I		M	C10
CCL7	CCR1, CCR3,CCR5	I	Monocytes, macrophages, NK Cells, T cells, immature dendritic cells	Hu, M	MARC
CCL8	CCR1, CCR2, CCR3, CCR5	I	Eosinophils, basophils, mast cells, T cells	Hu, M	MCP-2
CCL9/10 (Murine homologue of CCL15)	CCR1	H		M	MMRP2, CCF18, MIP-1γ
CCL11	CCR3	I	eosinophils, basophils, mast cells, T cells	Hu, M	Eotaxin
CCL12	CCR1, CCR2, CCR3, CCR5	I		M	MCP-5
CCL13	CCR1, CCR2, CCR3	I	Monocytes, T cells, NK Cells, immature dendritic cells, eosinophils, basophils, mast cells	Hu	MCP-4

Chemokine	Chemokine Receptor	Inflammatory or Homeostatic	Cells Attracted	Organism	Aliases
CCL14	CCR1	H	Monocytes, macrophages, NK cells, T cells	Hu	HCC-1
CCL15	CCR1, CCR3	H	Monocytes, macrophages, NK Cells, T cells, eosinophils, basophils, mast cells	Hu	HCC-2
CCL16	CCR1, CCR2, CCR5	H	Monocytes, macrophages NK Cells, T cells	Hu	HCC-4 LEC
CCL17	CCR4	D	T cells, macrophages	Hu, M	TARC
CCL18	Unknown	H	T cells	Hu	PARC
CCL19	CCR7	H	T cells, B Cells, mature dendritic cells	Hu, M	MIP3ß, ELC
CCL20	CCR6	D	T cells, B Cells, immature dendritic cells	Hu, M	MIP3α, LARC
CCL21	CCR7	D	T cells, B Cells, mature dendritic cells	Hu, M	SLC
CCL22	CCR4	D	T cells, macrophages	Hu, M	MDC, ABCD-1
CCL23	CCR1, FPRL-1	I	T cells, monocytes	Hu	MPIF-1
CCL24	CCR3	I	Eosinophils, basophils, mast cells, T cells	Hu	Eotaxin-2
CCL25	CCR9	H	T cells	Hu, M	TECK
CCL26	CCR3	I	Eosinophils, basophils, mast cells, T cells	Hu, M	Eotaxin 3
CCL27	CCR10	H	T cells, monocytes, B Cells, immature dendritic cells	Hu, M	CTACK, ILC
CCL28	CCR10, CCR3	Unknown	T cells	Hu, M	MEC
CXC Chemokines					
CXCL1	CXCR1, CXCR2	I	Neutrophils	Hu, M	Groα
CXCL2	CXCR2	I	Neutrophils	Hu, M	Groß, MIP-2
CXCL3	CXCR2	I	Neutrophils	Hu, M	Groγ, Dcip1
CXCL4	CXCR3B	U	Fibroblasts, endothelial cells	Hu, M	PF4
CXCL4V1	CXCR3B	U	Fibroblasts, endothelial cells	Hu	
CXCL5	CXCR2	I	Neutrophils	Hu, M	ENA-78, LIX
CXCL6	CXCR1, CXCR2	I	Neutrophils, macrophages	Hu	GCP-2

Chemokine	Chemokine Receptor	Inflammatory or Homeostatic	Cells Attracted	Organism	Aliases
CXCL7	Unknown	I	Neutrophils	Hu, M	NAP-2, Ppbp
CXCL8	CXCR1, CXCR2	I	Neutrophil chemotaxis	Hu	IL-8
CXCL9	CXCR3, CXCRB	I	T cells, NK Cells	Hu, M	MIG
CXCL10	CXCR3, CXCR3B	I	T cells, NK Cells	Hu, M	IP-10
CXCL11	CXCR3, CXCR3B	I	T cells, NK Cells	Hu, M	I-TAC
CXCL12	CXCR4	H	Haematopoietic cell types, CD34+ progenitor cells, mesenchymal stem cells	Hu, M	SDF-1α/β
CXCL13	CXCR5	H	B Cells, CD4+ T cells	Hu, M	BLC, BCA-1
CXCL14	Unknown	D	Monocytes, immature dendritic cells, NK Cells	Hu, M	BRAK, Bolekine
CXCL15	Unknown	Unknown		M	Lungkine, Weche
CXCL16	Unknown	I	T cells	Hu, M	
CXCL17	Unknown	U	Unknown	Hu, M	DMC
Other Chemokines					
XCL1	XCR1	D	T cells, NK Cells	Hu, M	Lymphotactin, SCM-1α
XCL2	XCR1	D	T cells, NK Cells	Hu	SCM-1β
CX3CL1	CX3CR1	I	T cells, monocytes, neutrophils	Hu, M	Fractalkine

Table 1. 1 Chemokines and their function

Table showing chemokines, their receptors, function, cells they attract, if they are present in humans and mice and their synonyms. H: Homeostatic, D: Dual, I: Inflammatory, U: Unknown, Hu: Human, M: Mouse. (Zimmerman *et al.*, 2008; Hughes and Nibbs, 2018; Zlotnik, Yoshie and Nomiyama, 2006)

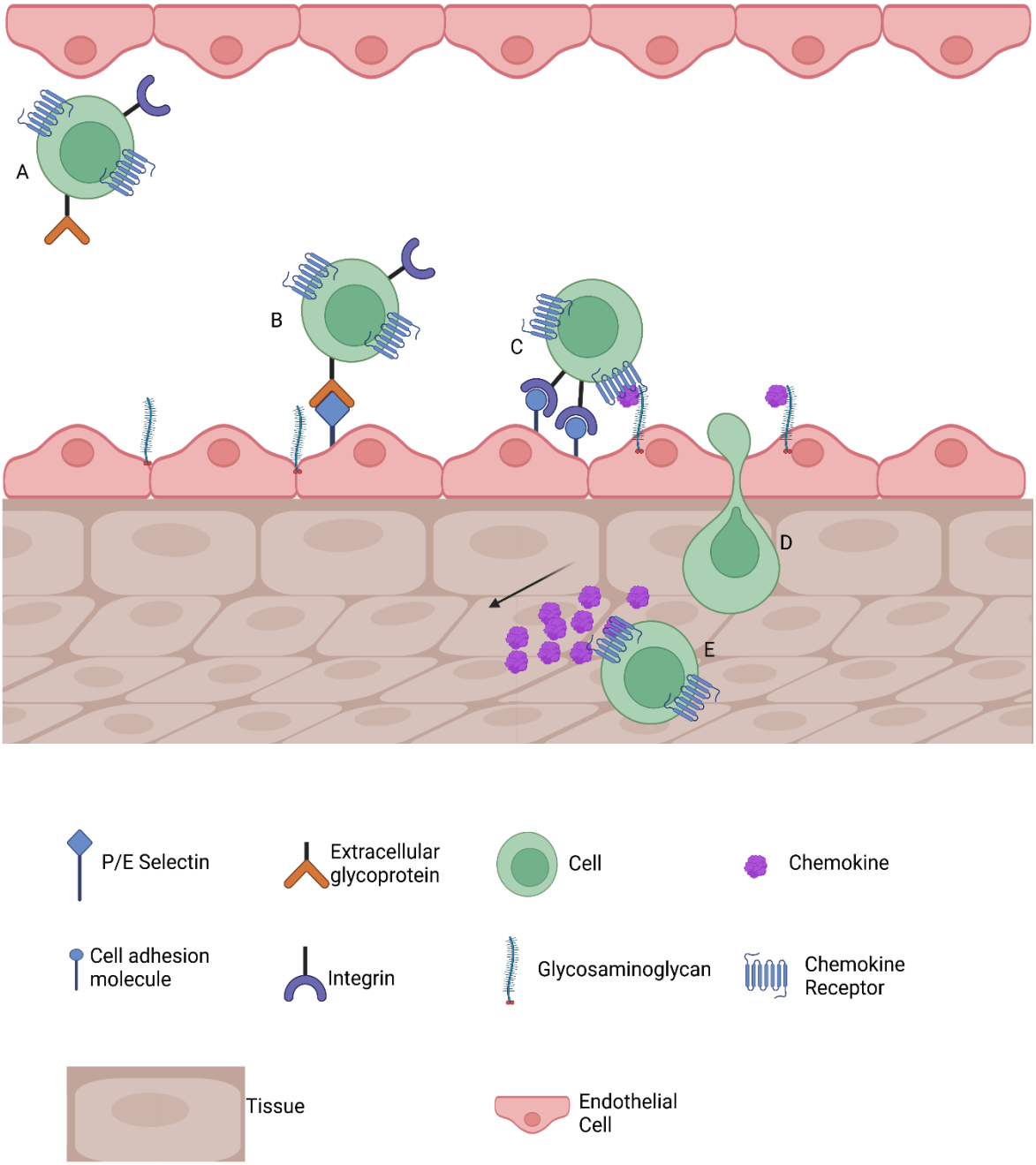

Figure 1. 3 The adhesion cascade

This figure outline the key steps in the adhesion cascade and tissue specific cellular migration. **(A)** Circulating leukocyte expressing chemokine receptors, integrins and extracellular glycoproteins. **(B)** Extracellular protein binding to selectin ligands present on vascular endothelium, resulting in cellular rolling. **(C)** Integrins and chemokine receptors on circulating cells binding to cell adhesion molecules and chemokine, presented on GAGs respectively, resulting in arrested cell movement. **(D)** Cell transmigrating via diapedesis **(E)** Cell migrating within tissue via a chemokine gradient Figure adapted from (Granger DN, 2010). Figure Created with BioRender.com.

1.1.6 Cellular address codes

Leukocytes and in particular T cells are crucial to tissue homeostasis (Mora and von Andrian, 2006). We now know specific chemokine and chemokine receptor interactions are essential for tissue specific T cell trafficking.

In lymph nodes the chemokines CCL19 and CCL21, ligands for CCR7, are responsible for the homing of T cells, B cells and dendritic cells, and this axis is a key contributor to the regulation of adaptive responses. The functional impact of this axis has been highlighted through CCR7 deficient mice; which lack T cells in the lymph node. Furthermore, adoptively transferred CCR7-deficient T cells are unable to traffic to the lymph nodes. Moreover, adaptive immune responses in CCR7 deficient mice are delayed (Forster *et al.*, 1999). Further studies have shown that in *Ccr7* knock out mice regulatory T cells, are unable to mediate their suppressive function, due to defective recruitment and positioning in the lymph node (Forster, Davalos-Misslitz and Rot, 2008).

In peripheral tissue, similar patterns have emerged that regulate T cell recruitment in homeostasis. The expression of homeostatic chemokines CCL25 and CCL27 is restricted to the small intestine and skin respectively. Moreover, the expression of CCL25 and CCL27 in their respective tissues are crucial for regulating T cell specific homing to these tissues in health (Mora and von Andrian, 2006; Reiss *et al.*, 2001). In the skin, T cell tropism is directed by CCL27 signalling through its receptor CCR10. In CCL27 knockout mice, an exaggerated skin inflammatory response is seen in a mouse model of psoriasis, suggesting disruption of the CCL27-CCR10 axis may contribute to disease (Davila *et al.*, 2022). Similarly, the CCL25/CCR9 axis directs T cell trafficking to small intestine in health. Mice lacking CCR9 had a diminished T cell compartment and were more susceptible to a murine model of colitis compared to controls (Wurbel *et al.*, 2001; Wurbel *et al.*, 2011).

The fate of small intestine and skin tropic T cells is determined upon activation in the lymph node and influenced by the presence of co-stimulatory factors presented by dendritic cells. For skin destined T cells activation in the presence of vitamin D derivatives influences T cell tropism by increasing CCR10 expression (Sigmundsdottir *et al.*, 2007). Whilst in small intestine tropic T cells retinoic acid

derivatives increase CCR9 expression as well as the integrin α4ß7 (Iwata *et al.*, 2004).

Overall, the concept that has now emerged is of cells bearing 'address codes' which regulate their tissue tropism, and chemokine receptors are dominant contributors to this code.

1.1.7 Chemokines in disease

Chemokines and their receptors are critical in facilitating immune cell function and as discussed are key contributors to homeostasis and the inflammatory response. Exacerbation or restriction of chemokine function is often associated with disease.

1.1.7.1 Skin disease

Chemokines have been implicated in the pathogenesis of several skin conditions. For example the CCL17/CCR4 axis is associated with atopic dermatitis. Patients with atopic dermatitis have an elevated serum CCL17, and following treatment a decrease in circulating CCL17 identified and was associated with improvements in disease activity. Furthermore, CCR4 expression is higher in peripheral blood CD4+ T cells in patients with atopic dermatitis compared to healthy controls (Kakinuma *et al.*, 2001). High serum levels of CCL17 are also associated with cutaneous T cell lymphoma (Kakinuma *et al.*, 2003). CCL11 and CCL26 are also found to be upregulated in numerous skin diseases. They signal through the chemokine receptor CCR3, expressed by eosinophils and T cells. Both are associated with atopic dermatitis, and CCL26 is associated with bullous pemphigoid and angioedema (Sugaya, 2015).

1.1.7.2 Inflammatory bowel disease

Crohn's disease and ulcerative colitis, are inflammatory bowel diseases (IBD) and present with gastrointestinal signs and symptoms, in the absence of infection or cancer (de Mattos *et al.*, 2015). In the sera of patients with IBD, CCL25, CCL23, CCL21, CCL23, CCL2, CCL1, CXCL6, CXCL13, CXCL5 and CXCL10 were found to be elevated compared to healthy controls. Due to its role in homeostasis, the importance of CCL25 in IBD pathogenesis is of particular interest. In a murine model of colitis, CCL2 deficient mice exhibited reduced disease severity and

decreased mortality compared to wild type controls, suggesting CCL2 is important in IBD immunopathogenesis (Singh *et al.*, 2016; Khan *et al.*, 2006).

1.1.7.3 Cancer

Chemokines are involved in multiple stages of cancer pathogenesis, including tumorigenesis and metastasis. Many tumours express chemokines that are suspected to modulate the tumour microenvironment, the quantity and specific chemokine released varies between cancer type. Moreover, tumour cells express chemokine receptors that can result in migration and potentially cancer metastases (Lazennec and Richmond, 2010).

Within the tumour microenvironment, CXCL12 and CCL20 are highly expressed in ovarian and breast cancer respectively (Bell *et al.*, 1999; Kryczek *et al.*, 2005). Both chemokines regulate Th17 cell trafficking to a tumour site; which may restrict tumour development, however, IL-17 produced by Th17 cells may promote tumour angiogenesis. Moreover CXCL12 can directly contribute to tumour angiogenesis (Zou and Restifo, 2010; Nagarsheth, Wicha and Zou, 2017). Furthermore, CCL22 produced by tumour cells, may recruit regulatory T cells to the tumours, which in turn promotes tumour development through immune response subversion, leading to decreased patient survival (Curiel *et al.*, 2004; Raman, Sobolik-Delmaire and Richmond, 2011). As previously reviewed both CXCL12/CXCR4 and CCL21/CCR7 axes are associated with cancer metastasis and local invasion in numerous cancer types (Raman, Sobolik-Delmaire and Richmond, 2011). The mechanisms regulating tumour cell migration are reflective of those that regulate leukocyte migration.

The chemokine landscape in cancer is complex, and contributes to tumour restriction, development, and metastasis, as such chemokines and chemokine receptors represent interesting therapeutic targets in the management of malignant disease.

1.1.8 Chemokines as therapeutics

Mutagenesis studies have shown that N-terminus modified chemokines can act as agonists or antagonists, giving rise to the potential use of chemokines as therapeutics. Given the importance of chemokines and chemokine receptors in cellular recruitment, their involvement in disease processes and their targetable

nature, chemokines and chemokine receptors represent exciting therapeutic targets.

Multiple clinical trials have investigated chemokines and chemokine receptors as therapeutic options, but only three licensed drugs are currently in use in the UK. Targeting chemokines therapeutically is challenging due to the promiscuous relationship between chemokines and receptors, non-specific bindings of chemokines, and signalling complexities. Chemokine signalling plays a role in disease pathogenesis, whilst also being essential in physiologic homeostasis. Making therapeutics to treat disease without disrupting health is challenging (Lai and Mueller, 2021).

In cancer studies, inhibitors of CCR1, CCR2, CCL2, CCR4, CCR5, CCR7, CXCR2, CXCR4 and ACKR3 have been developed (Mollica Poeta *et al.*, 2019). Of these, only Mogamulizumab, an anti-CCR4 monoclonal antibody, has been approved in the UK for the treatment of some T cell lymphomas (Moore *et al.*, 2020).

In addition to Mogamulizumab, two other chemokine therapies have been licensed for use in the UK. Maraviroc, is an allosteric CCR5 inhibitor that has successfully been used to treat HIV-1 R5 infection. CCR5 is a co-receptor for HIV viral cell entry, thus Maraviroc inactivating CCR5 prevents the further infection of CD4+ T cells (Tan *et al.*, 2013).

Plerixafor, a selective CXCR4 antagonist, is used to simplify haematopoietic stem cell (HSC) donation. Plerixafor mobilises HSCs, encouraging their migration from bone marrow into the circulation. This has revolutionised stem cell donation, as it no longer requires invasive bone marrow donation procedures. Plerixafor binds to CXCR4, expressed on bone marrow HSCs, thus restricting CXCL12 binding to CXCR4 and its ability to retain HSCs in the bone marrow. HSCs then migrate into peripheral blood, where they can be collected through a simple venous blood draw (**Fig. 1.4)** (Fricker, 2013).

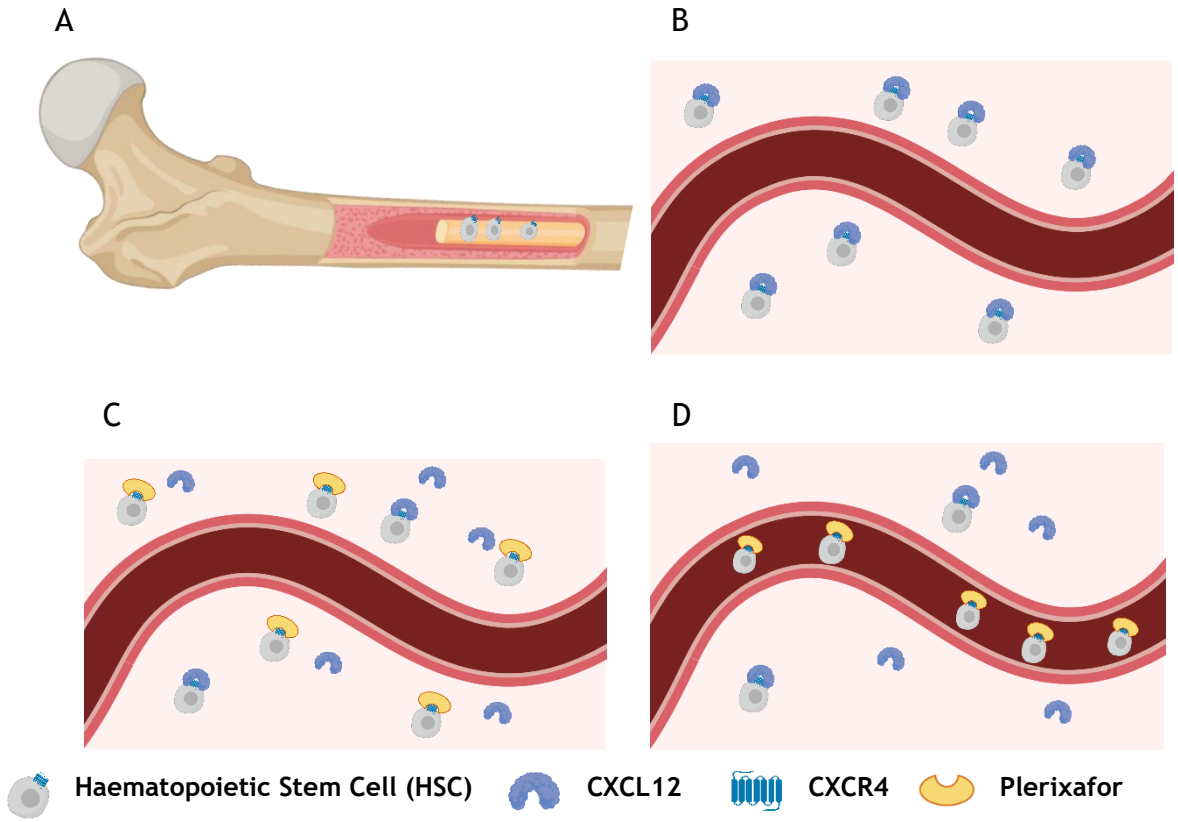

Figure 1.4 Plerixafor mechanism of action

(A) Bone marrow is rich source of HSCs. HSC allografts are regularly used in the treatment of haematological malignancy. **(B)** HSCs are retained in bone marrow by CXCL12 binding CXCR4, thus to retrieve HSCs often an invasive procedure to collect bone marrow tissue is needed. **(C)** Plerixafor is a CXCR4 antagonist, which limits the ability of CXCL12 to bind to CXCR4. **(D)** HSCs can mobilise and egress from bone marrow into peripheral circulation, allowing HSCs to be collected through venepuncture. Figure created with BioRender.com.

Despite the challenges in developing chemokine therapies, there have been some successes. As such, chemokines and chemokine receptors represent potentially effective therapeutic targets for treating numerous diseases. Furthermore, there are a wealth of chemokine-based therapies that have been unsuccessful in their original intended use. However, they may be suitable for repurposing and be effective for the management of other conditions. Further work exploring the complexities of chemokine and chemokine receptor biology is essential to develop our understanding of cellular recruitment, which may lead to successful chemokine-based therapeutics.

1.2 Oral Mucosa

1.2.1 Oral mucosa function

The oral mucosa is an epithelial barrier tissue, the primary function of which is to protect the host from chemical, microbial and physical insults, acting as a protective barrier between the environment and underlying structures. However, oral mucosa is more than a physical barrier; it constantly responds to pathogenic threats yet tolerates commensal microbes, food and airborne antigens and masticatory forces. To achieve this balance in the complex and unique ecological niche of the oral environment, a highly tailored immune network in combination with structural features that allow the barrier to function effectively is required (Moutsopoulos and Konkel, 2018; Brizuela and Winters, 2022).

1.2.2 Histology of oral mucosa

Oral mucosa typically consists of two layers; a stratified squamous epithelium and a deeper lamina propria. Where there is underlying bone, such as on the palate or covering the alveolus, a periosteal layer is present below the lamina propria. Where the epithelium is keratinised there are four layers; the stratum basale, stratum spinosum, stratum granulosum and stratum corneum (**Fig. 1.5** and **Table 1.2**).

Oral mucosa is heterogenous. The oral mucosa of the gingiva differs from that of the tongue and again from that of the buccal tissue and floor of mouth. This reflects the specific functions of the tissue. For example, the floor of mouth is non keratinised, which increases its movability; and the gingiva and palatal mucosa are keratinised to protect from occlusal forces. The tongue dorsum is a specialised mucosa, containing papillae which facilitate taste. Tongue mucosa may be keratinised or non-keratinised (Brizuela and Winters, 2022).

Figure 1. 5 Histology of oral mucosa

A section of murine palate following H&E staining. **(A)** Periosteum. **(B)** Lamina propria. **(C)** Stratum Basale. **(D)** Stratum spinosum **(E)** Stratum granulosum **(F)** Stratum corneum. Features and function of each layer are expanded upon in table 1. 2

Layer	Features	Function
Periosteum	• Fibrous outer layer • Cellular, osteogenic, layer • Rich vasculature	• Vascular supply and innervation to bone • Support bone growth and repair
Lamina propria	• Dense irregular connective tissue with blood vessels, nerves, fibroblast and leukocytes	• Innervation and vascular supply to the epithelium • Allows the epithelium to move independently of deeper structures
Stratum basale	• Cuboidal or columnar cells • Hemidesmosomes • Forms rete pegs with underlying lamina propria	• Attachment of epithelium to connective tissue • Mitosis and differentiation of cells to maintain mucosa
Stratum spinosum	• Larger prickle cells • Desmosome rich aiding intercellular attachment	• Development of keratinocytes
Stratum granulosum	• Cells with cytoplasmic granules • Stains heavily with haematoxylin • Fewer nuclei	• Cytoplasmic granules act as a water sealant
Stratum corneum	• Superficial layer • Flat cells, lacking nuclei • Stains pink with eosin	• Final stage of keratinocyte development • Barrier formation

Table caption overleaf

Table 1. 2 Features and function of different layers of oral mucosa

The histological features and the function of periosteum, lamina propria, stratum basale, stratum spinosum, stratum granulosum and stratum corneum are summarised (Nahian and Chauhan, 2022), (Brizuela and Winters, 2022), (Menon, Cleary and Lane, 2012).

1.2.3 Gingiva

The gingiva is unique as it forms a barrier by directly contacting the tooth or root surface. The epithelium adhering to the tooth/root is termed Junctional Epithelium (JE). The JE has wider inter-cellular spaces and is incredibly thin, as little as 3-4 cells thick (**Fig. 1.6**). JE is the front-line barrier, protecting the underlying hard and soft tissues from the environment. During physiological processes such as mastication, the JE can be breached; thus, rapid cellular regeneration, expression of defensive factors and secretion of inflammatory mediators are essential to maintaining homeostasis at this barrier site. Therefore, a tailored immune network is likely required to maintain gingival homeostasis (Moutsopoulos and Konkel, 2018; Bosshardt and Lang, 2005).

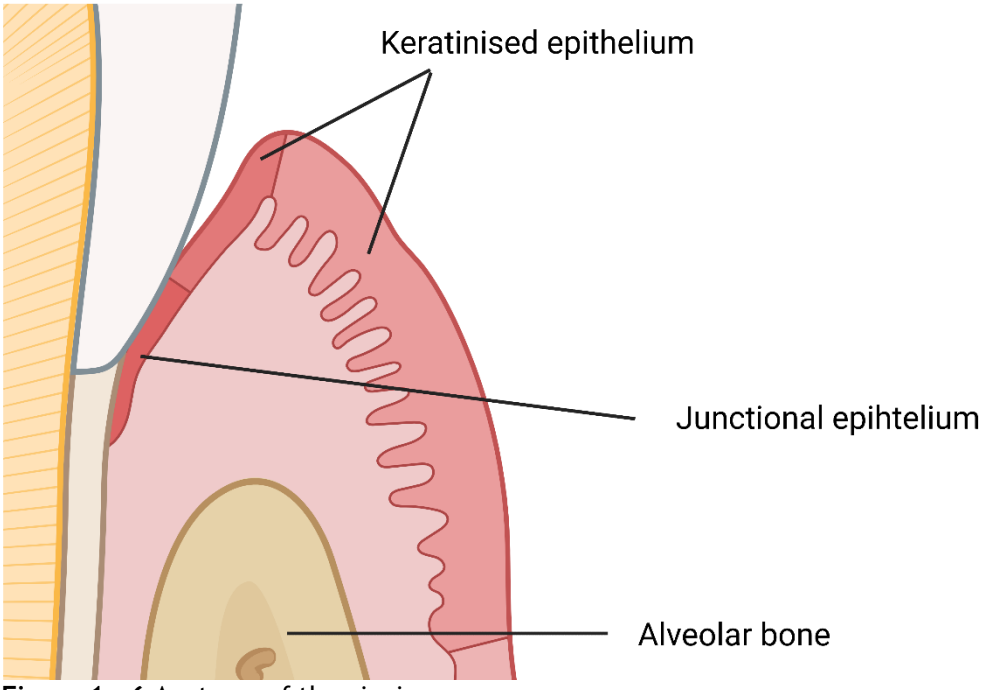

Figure 1. 6 Anatomy of the gingiva

Gingiva is a keratinised stratified squamous epithelium. It is unique due the junctional epithelium that binds it to the tooth and or root surface. Loss of the junctional epithelium results in transmigration of a plaque biofilm and a breach in the body, exposing it to environmental insult. Figure created with BioRender.com.

1.2.4 Leukocytes in gingival homeostasis

The cellular components of the immune system are vital to maintaining oral homeostasis. Neutrophils are the largest population of immune cells that are recruited to gingiva. Their importance in gingival homeostasis is supported by the numerous neutrophil associated pathologies that result in an increased susceptibility to periodontitis; such as Chediak-Higashi syndrome, Papillon-Lefevre syndrome and leukocyte adhesion deficiency disorders (Hajishengallis and Hajishengallis, 2014). Mice lacking leukocyte function-associated antigen-1 (LFA-1) demonstrated impaired neutrophil recruitment to the periodontium, higher bacterial loads and spontaneous alveolar bone loss, once more highlighting the protective role neutrophils have. However, excessive neutrophil recruitment has also been associated with disease (Hajishengallis *et al.*, 2011). Del-1 is an antagonist for LFA-1. Del-1 deficient mice have excessive neutrophil recruitment to the gingiva and increased alveolar bone loss (Hajishengallis and Chavakis, 2013).

T cells are also pivotal in maintaining gingival homeostasis. For example, IL-17, a cytokine primarily produced by Th17 and γδ T cells, has been shown to be protective against oral *Candida albicans* infection. Patients with IL-17 and IL-17RA deficiency are more susceptible to mucocutaneous candida infection, and in mice elevated numbers of Th17 and γδ T cells, and increased expression of IL-17 are observed following exposure to *Candida albicans* (Puel *et al.*, 2011; Conti *et al.*, 2014). However, murine studies have demonstrated δγ T cells limit gingival inflammation, and are protective against periodontitis, through the secretion of amphiregulin; and exaggerated Th17 responses are associated with inflammatory bone loss in periodontitis (Moutsopoulos *et al.*, 2014).

Both neutrophils and T cells are important in periodontal disease pathogenesis and maintaining gingival homeostasis, thus ensuring sufficient but non-pathological leukocyte populations in gingiva is crucial to maintaining oral health.

Yet our understanding of the mechanisms and specific contributions of the host, pathogens and environmental antigens that develop these tightly regulated networks remains limited.

The tooth surface is home to a diverse microbial community, and logically the interplay between the host and microbiome was thought to be important in conditioning tissue specific homeostasis. However, in mouse studies leukocyte numbers in gingiva of specific pathogen free (SPF) and germ free (GF) mice are similar, suggesting that other factors, such as the host or exposure to environmental factors are greater contributors to homeostatic immunity. Neutrophil migration into the gingival sulcus is detected in GF mice, albeit with decreased frequencies of neutrophils in GF compared to SPF mice, suggesting microbiome dependant mechanisms may still contribute to gingival homeostasis (Dutzan *et al.*, 2017).

Similarly, Th17 T cell accumulation in gingiva was independent of microbial colonisation. Instead, the presence of Th17 Cells was dependant on IL-6. Th17 T cell frequencies increased following mechanical damage of the murine palate, and induction of IL-6. These studies suggest mechanical trauma, can induce a Th17 Cell response in the gingiva, thus mastication may contribute to local tissue homeostasis (Dutzan *et al.*, 2017).

Oral mucosa repair and regeneration is essential to maintaining homeostasis, this requires an effective immune response, and neutrophils, macrophages, platelets, keratinocytes and fibroblasts are essential in this process. The accelerated healing in oral mucosa, may be in part due to, the presence of fibroblasts and a rich Mesenchymal Stem Cell (MSC) population in the lamina propria. MSCs in the gingiva are multipotent and have a high regenerative capacity (Smith and Martinez, 2018).

1.2.5 Cellular recruitment to the gingiva

The cellular network is indispensable in gingival homeostasis. However, there is a limited appreciation of the mediators that regulate cellular recruitment to the gingiva. As previously discussed, chemokines are the main *in vivo* regulators of leukocyte recruitment. Yet for many chemokines their specific role or indeed level of expression in the healthy periodontium is currently unknown.

A recent single cell transcriptomic analysis of human gingivae has provided some insight into the chemokines that may be regulating cellular recruitment to the gingiva. Within epithelial cells, the neutrophil chemo-attractants *CXCL1, CXCL6*

and *CXCL8* were primarily expressed. A similar expression pattern was observed in gingival fibroblasts with *CXCL1, CXCL2 and CXCL8* being strongly expressed. Fibroblasts highly expressed *CXCL12 and CXCL13*. *CXCL12* has a wide array of functions and is indispensable for life, and a wide variety of cellular recruitment is mediated through this chemokine; its precise role in gingiva remains elusive. Surprisingly, there was high expression of *CCL19*, typically responsible for regulating recruitment of *CCR7* expressing cells to secondary lymphoid organs, the specific function of this in gingiva is unknown (Yan *et al.*, 2019; Williams *et al.*, 2021).

The chemokine receptor *CXCR4* was widely expressed on leukocytes in this study. Supporting the importance of this transcript WHIM syndrome is also associated with periodontitis in humans. WHIM syndrome is a rare primary immunodeficiency disease characterised by Warts, Hypogammaglobulinemia, Infections and Myelokathexis. WHIM syndrome is caused by mutations to CXCR4 causing desensitisation and prolonged G protein and ß-arrestin responses. This results in neutropenia, monocytopenia and lymphopenia. Increased periodontitis susceptibility in WHIM syndrome may be related to decreased leukocyte recruitment, or impaired cellular differentiation, or cellular dysmorphia due to disrupted cellular development in the bone marrow (Hajishengallis and Hajishengallis, 2014; Heusinkveld *et al.*, 2019).

Yet there is evidence of resident immune cell populations in gingiva. A recent study has shown through a series of elegant murine models that a resident HSC population exist in healthy murine gingiva. The HSCs demonstrated the capacity to differentiate to cells of myeloid lineage, and these progenies were phenotypically similar to those in bone marrow. Upon ligature-induced inflammation, HSC activity increased, suggesting adaptations to the cellular landscape in gingiva can be locally controlled. This study represents a potentially significant paradigm shift in our understanding of cellular recruitment to the gingiva, furthermore, it may explain why CXCR4 and CXCL12 appear to be highly expressed in human gingiva, given its important role in HSC retention in bone marrow (Krishnan *et al.*, 2021).

The majority of research exploring chemokine expression in gingiva has focused on understanding the role of inflammatory chemokines in periodontitis, yet

homeostatic chemokines are important to maintain health at other barrier sites such as skin and small intestine. Both skin and small intestine have a barrier function and have adapted for their ecological niche. For example, skin is heavily keratinised, reflective of the physical trauma it is readily exposed to, the small intestine has thousands of small projections, increasing its surface area to facilitate absorption. Whilst address codes for gut and small intestine tropic T cells have been identified as discussed in section 1.1.6, no such mechanism has been identified in the oral mucosa.

1.3 Periodontal Disease

1.3.1 Overview

Periodontal diseases comprise of a wide range of conditions affecting the tooth supporting structures termed the periodontium. The most common periodontal diseases are gingivitis and periodontitis. Gingivitis is site specific inflammatory condition initiated by the accumulation of a dental plaque biofilm. Symptoms of gingivitis include gingival swelling, erythema and occasionally tenderness. However, many patients are unaware that they have the condition. Clinically gingivitis is defined by the presence of bleeding upon periodontal probing, without the presence of periodontal attachment loss. It is typically painless and resolves upon the removal of the causative plaque biofilm, without permanent damage to the periodontium **(Figure 1.7)** (Chapple *et al.*, 2018).

Left untreated, gingivitis may progress to periodontitis in susceptible patients. The chronic inflammation seen in periodontitis results in irreversible destruction of the periodontium leading to alveolar bone loss. These features result in the clinical finding of loss of attachment and increased periodontal pocket depths **(Figure 1.7)** . The resulting periodontal pockets create a niche favourable to microbial dysbiosis. Moreover, biofilm in periodontal pockets cannot be removed by toothbrushing, and a cycle of dysbiosis and inflammation is perpetuated. Periodontitis can result in tooth mobility and ultimately tooth loss, which negatively impact patient quality of life. However, the presence of gingivitis is not entirely predictive of periodontitis development (Listgarten, Schifter and Laster, 1985).

1.3.2 Global burden of periodontal disease

Periodontal diseases are amongst the most common chronic diseases, with up to 50% of the population affected and severe disease having a prevalence of 9.8%; this equates to 196 million people globally suffering from severe periodontitis (Nazir, 2017; Bernabe *et al.*, 2020). Periodontal disease is a global disease, and despite plaque and calculus control being poorer in developing nations, periodontal pockets between 4-5 mm are more common in adults in developed countries. Periodontitis prevalence increases with increasing age. In both developed and developing world populations, greater proportions of 65-74 year

olds had periodontal pockets greater than 6 mm, compared to younger adult populations (Nazir, 2017). A recent study estimated that in 2018 the direct and indirect costs of periodontal disease to be $154.06 billion and €158.64 billion in the US and Europe respectively (Botelho *et al.*, 2022). The majority of this was attributable to indirect costs, those associated with loss of productivity due to living with disease. In 2017 it was estimated globally, 5.2 million years were lived with disability due to periodontitis (Bernabe *et al.*, 2020). Between 1990 and 2017 there was a 6% increase in the years lived with periodontitis. It is hypothesised this trend will continue due to the association between aging and periodontitis and the rapidly aging population, the prevalence of periodontitis will increase and will result in increased economic burden (Clark, Kotronia and Ramsay, 2021).

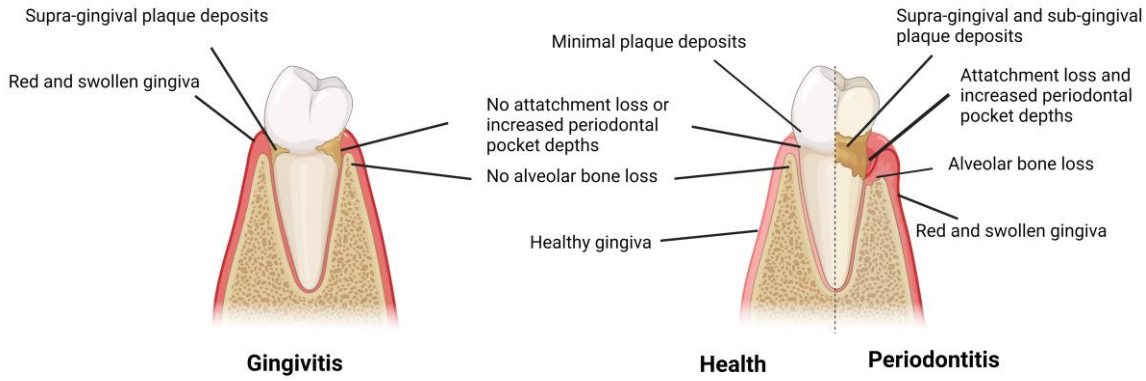

Figure 1. 7 Clinical characteristics of the gingiva in health and disease

Clinical features of the periodontium in gingivitis, health and periodontitis. Gingivitis presents with gingival erythema and oedema, supra-gingival plaque deposits. Periodontitis presents with the features of gingivitis and increased alveolar bone loss, periodontal pockets and sub-gingival plaque deposits. Figure created with BioRender.com.

1.3.3 Periodontal disease risk factors

Dental plaque alone is insufficient for the development of periodontitis (Löe *et al.*, 1986). This was alluded to by a study following male tea plantation workers in Sri Lanka who did not practice regular oral hygiene, thus presenting with significant plaque biofilms. Whilst gingival inflammation was present in all subjects, 11% of participants exhibited no periodontal attachment loss, 81% had moderate progression of attachment loss and 8% had rapid development of periodontitis. This suggests that periodontitis is not a directly caused by plaque alone. Periodontitis susceptibility varies between individuals with similar plaque biofilms, and myriad other risk factors for periodontitis have been identified (Van Dyke and Sheilesh, 2005).

As previously mentioned, periodontitis is more prevalent in the aged population, however, this is believed to be a result of cumulative destruction of the periodontium over time rather than increased rates of destruction with advanced age (Grossi *et al.*, 1995; Grossi *et al.*, 1994; Van Dyke and Sheilesh, 2005). Some recent work has refuted this, suggesting that age associated inflammation and immune response dysregulation may be responsible for the elevated level of periodontitis observed in the elderly (Clark, Kotronia and Ramsay, 2021).

A wealth of studies demonstrate that smoking is a major risk factor in the development of periodontitis. Smokers are around four times more likely then non-smokers to develop periodontitis (Tomar and Asma, 2000). Moreover, the risk of developing disease is dose dependent, with an odds ratio of 2.35 for light and 7.28 for heavy smokers respectively (Van Dyke and Sheilesh, 2005). Furthermore, the risk of periodontitis development decreases following smoking cessation (Tomar and Asma, 2000). Not only are smokers at increased risk of periodontitis, but it is typically more severe, develops quicker, and treatment outcomes are poorer (Johnson and Guthmiller, 2007). The immunomodulatory effects of smoking on the host immune system and changes in subgingival microflora of smokers are believed to be the main factors that contribute to an increased incidence of periodontitis amongst smokers (Jiang *et al.*, 2020; Lee, Taneja and Vassallo, 2012).

Diabetes is a well-established risk factor for periodontitis (Salvi, Carollo-Bittel and Lang, 2008; Chapple and Genco, 2013). Type 1 diabetes arises from the autoimmune destruction of insulin-secreting β cells, resulting in decreased, and in some instances complete loss of, insulin production and elevated blood glucose levels. Chronic hyperglycaemia damages the cardiovascular system, kidneys and eyes, and patients are often immunocompromised. Diabetes is diagnosed through the identification of an elevated HbA1c level, and work has shown that a HbA1c of greater then 7.0% positively identifies diabetic patients at an increased risk of periodontitis. In all periodontitis is 2-3 times more common in diabetics compared to non-diabetics (Casanova, Hughes and Preshaw, 2015). The link between diabetes and periodontitis is bi-directional. Diabetics with untreated periodontitis have poorer glycaemic control, and in type two diabetics successful periodontitis treatment has been shown to reduce HbA1c levels by 0.46% (Darre *et al.*, 2008). These findings highlight the importance of both good glycaemic control and maintaining periodontal health in patients with diabetes.

The variation in periodontal disease severity in response to microbial plaque raised the possibility of a genetic component to periodontitis susceptibility. To date more than 65 genes have been associated with periodontitis. Importantly, there appears to be no single gene that is a complete determinant of periodontitis, once again highlighting the multi-factorial nature of periodontitis. Studies involving families and twins with high rates of early onset periodontitis, have suggested genetics contributes up to 50% of the risk for periodontitis. In older patient studies genetic variation accounts for up to 25% of risk. No genetic link for gingivitis has been identified (Loos and Van Dyke, 2020; Michalowicz *et al.*, 2000). More recent studies have shown gene polymorphisms of pro-inflammatory cytokines, IL-6, IL-1β, and IFN-γ may be associated with periodontitis (Heidari, Moudi and Mahmoudzadeh-Sagheb, 2019).

1.3.4 Microbiology of periodontitis

In the development of periodontitis, there are broadly two categories of plaque biofilm; supra and subgingival. Despite being physically connected their ecological niche and microbial composition differ. The most important difference is the level of oxygenation. The supra-gingival plaque biofilm is an oxygen-rich environment; in contrast, the subgingival biofilm situated within the

periodontal pocket is anaerobic/facultative anaerobic, resulting in a change in microbial composition. Due to the inability of supragingival plaque removal alone to resolve periodontitis, most work has focused on understanding the subgingival plaque biofilm.

Socransky identified three 'red complex' bacterial species that were commonly associated with periodontitis; *Porphyromonas gingivalis (P. gingivalis), Tannerella forsythia (T. forsythia) and Treponema denticola (T. denticola)* (Socransky et al., 1998). *P. gingivalis* was later identified as a 'keystone pathogen', due to its ability to modulate the biofilm, despite being present in small numbers (Hajishengallis, Darveau and Curtis, 2012). However, *P. gingivalis* colonisation in GF mice did not result in alveolar bone loss, highlighting that *P. gingivalis* does not directly cause alveolar bone loss, and commensal microbiota play an obligatory role in periodontitis pathogenesis.

Following the explosion of 16S sequencing studies, a further 18 species of bacteria have demonstrated a significant association with periodontitis. Indeed, several studies document that some species health-associated species are also associated with periodontitis (Griffen *et al.*, 2012). These studies have been reinforced by a recent systematic review that identified 17 microbial species, beyond the traditional red-complex, that are associated with periodontitis (Perez-Chaparro *et al.*, 2014). The myriad bacterial species that were associated with periodontitis suggested the inflammation and resulting alveolar bone loss results from a polymicrobial infection mediated by the presence of *P. gingivalis*. These recent advances suggest a paradigm shift in our understanding of periodontitis from one of a simple direct infection model of disease to polymicrobial synergy and dysbiosis. In this model, periodontitis results from the synergy of a vast polymicrobial community, wherein each microbe has a specific function that causes inflammation in the periodontium. This is facilitated by the presence of 'key-stone' pathogens that can manipulate the typically symbiotic community to one of dysbiosis. Nevertheless, the presence of such pathogens alone is insufficient for disease progression, and the crosstalk between the host inflammatory response and the microbial community is crucial to periodontitis pathogenesis (Hajishengallis *et al.*, 2015).

1.3.5 The host response in periodontitis

Plaque and the presence of the key pathogen *P. gingivalis* alone are insufficient for the development of periodontitis, the host immune response plays a critical role in periodontal disease pathogenesis.

1.3.5.1 The development of the immune response

The host response in gingivitis and subsequently periodontitis was initially categorised into a sequential series of four key stages; 'initial', 'early', 'established' and 'advanced' lesions by Page & Schroeder in 1976. Each stage described the immune environment and histopathology encountered in the gingiva during periodontitis development (Page and Schroeder, 1976). Whilst the core principles remain useful and largely hold true, a more thorough understanding of the host response in periodontitis exists today (Hajishengallis and Korostoff, 2017) .

The 'initial lesion' presents after around four days following initial plaque exposure, and no clinical signs of disease are seen. However, histologically there is evidence of oedema, increased numbers of polymorphonuclear leukocytes (PMNs), and loss of connective. These clinical features are associated with complement cascade activation and release of proinflammatory mediators. These factors lead to increased vascular permeability and enhanced migration of PMNs. Recruited neutrophils release a barrage of anti-microbial mediators to manage the bacterial threat, however, this leads to iatrogenic connective tissue destruction (Jiang *et al.*, 2021). More recently it has been demonstrated, that pathogenic bacteria rely on by products of connective tissue destruction mediated by neutrophils, thus their presence in periodontitis pathogenesis is multifactorial (Hajishengallis, 2014) .

Our understanding of neutrophil biology has improved, and as discussed, neutrophils are key contributors to gingival homeostasis, without which periodontal disease rapidly progresses. When the Page & Schroeder model was first described, neutrophils were believed to simply cause 'by-stander' damage to the connective tissue in response to microbial plaque. Since then we have come to understand that neutrophils have a wider array of functionality, they have the ability to regulate CD4 + T cell and B cell recruitment, and influence adaptive immunity through dendritic cell interactions in lymphoid tissue, thus

neutrophils in gingiva may play a role in influencing the adaptive immune response in periodontitis (Mantovani *et al.*, 2011; Hajishengallis and Korostoff, 2017). Furthermore, the homogeneity of neutrophils is disputed, with subsets exhibiting specialised function being identified.

The next stage, termed the 'early lesion', occurs following 4 -7 days of plaque accumulation. On the cellular level there is shift in the primary leukocyte subsets from PMNs to increased frequencies of macrophages and lymphocytes. Increased vascularity and intercellular spaces of junction epithelial cells, results in bacterial product ingress to the gingiva leading to further inflammation (Jiang *et al.*, 2021; Fine *et al.*, 2016).

The role of macrophages has also been further elucidated since the publication of this model. Generally, the pathogenic role previously suggested holds true; increased macrophage populations are associated with developing periodontitis, and in macrophage deficient mice *P. gingivalis* colonisation is reduced. They are believed to mediate tissue damage directly by releasing pro-inflammatory mediators and reactive oxygen species. It is suggested *P. gingivalis* can influence Toll-like receptor 2 signalling macrophages, to evade clearance (Hajishengallis and Korostoff, 2017).

Between 14 and 21 days of plaque exposure the 'established' lesion develops in susceptible individuals. The early lesion will continue to develop and between 12 and 21 days there are increased lymphocytes, which then account for 70% of cells within the tissue (Seymour, Powell and Aitken, 1983). The cellular hallmark of the established lesion is an elevated B/plasma cell response. Further connective tissue breakdown at the JE occurs resulting in further ingress of microbial products, leading to endogenous release of pro-inflammatory mediators and continued tissue destruction. Clinically, the features of gingivitis are present. As the inflammatory response cannot remove the bacterial challenge, inflammation persists. Removal of the microbial challenge with physical debridement is the only way to resolve the inflammation. Resolution of inflammation at this juncture will typically lead to complete healing of the periodontium with no lasting defects. A prolonged period of inflammation beyond this stage may result in the transition from gingivitis to periodontitis.

Failure to resolve the inflammation in susceptible individuals will lead to the 'advanced' lesion. In 'advanced' periodontal lesions there is little change in the cellular composition of the gingiva, compared with the 'established' lesion however, periodontal attachment and alveolar bone loss are observed.

The mechanisms of alveolar bone loss are also better understood. This is now understood to be primarily driven through osteoclast differentiation and activation through RANK and RANKL. Osteoclasts are the only cellular mediator of bone resorption, in periodontitis osteoclast activity relative to osteoblasts is elevated, resulting in an equilibrium shift and alveolar bone loss occurring. The adaptive immune response is the key contributor of RANKL in the periodontium It is estimated around 50% and 90% of T and B cells respectively express RANKL, and Th17 cells are shown to activate osteoclasts directly though cell-cell contact. RANKL production can be also stimulated by multiple inflammatory mediators such as IL-1 and IL-6 that are seen in periodontitis (Usui *et al.*, 2021; Chen *et al.*, 2014; Hajishengallis and Korostoff, 2017).

Whilst this model is simplistic, it provides a useful framework for exploring periodontitis progression. Yet, our understanding since the publication of this model has progressed extensively. The primary change in our understanding is that periodontitis pathogenesis is not a linear response to periodontal pathogens, resulting in 'by-stander' damage; instead it is a result of complex crosstalk between the host epithelium, innate and adaptive leukocyte populations in response to microbial dysbiosis (Hajishengallis and Korostoff, 2017).

1.3.5.2 Leukocytes in periodontitis

Innate and adaptive cellular immune responses play crucial roles in the pathogenesis of periodontitis and the immune cell composition in the gingiva varies between different stages of disease progression.

Neutrophils are important in maintaining gingival homeostasis, demonstrated by patients that are deficient in or have neutrophil defects are more susceptible to periodontitis. Neutrophils in gingiva are effective at destroying periodontal pathogens through the oxidative burst or through lytic and proteolytic enzymes, however, without mechanical removal of plaque, neutrophils will persistently try – and fail - to neutralise the periodontal pathogens resulting in bystander

damage. (Scott and Krauss, 2012). Moreover peripheral blood neutrophils, isolated from patients with periodontitis were found to have impaired chemotaxis to CXCL8, thus may have restricted ability to manage pathogenic threat. Further to this, neutrophils from patients with periodontitis are hyperactive and hyperreactive when exposed to reactive oxygen species, which in turn may exacerbate local tissue destruction. Interestingly, following periodontal therapy responsiveness to CXCL8 improved, suggesting neutrophil function is influenced at least in part by active periodontitis (Matthews *et al.*, 2007; Roberts *et al.*, 2015).

Dendritic cells (DCs) are professional antigen presenting cells, that link innate and adaptive immune responses. Their primary role is to activate T cells, classically within the lymph node, and thus initiate an adaptive immune response against a specific antigen (Hovav, 2014). Immune tolerance is crucial at barrier sites to prevent inappropriate responses to environmental stimuli, and some DCs appear to have a protective role against periodontitis. Mice with reduced DC function demonstrate increased alveolar bone loss in murine models of periodontitis (Xiao *et al.*, 2015). However, there is evidence of DCs contributing to osteolytic activity following oral infection, this is thought to be through the induction of Th1 or Th17 lymphocytes. Furthermore, there is evidence of CXCL8 production by DCs and epithelial cells resulting in further neutrophil accumulation (Song *et al.*, 2018).

T cells are crucial to adaptive immune responses and are essential to the orchestration of tolerance and pathogenesis of oral disease. In brief, T cells recognise a specific antigen in the context of the major histocompatibility complex (MHC) II or MHC I complexes for CD4+ and CD8+ T cells respectively. Recognition of the T cells cognate peptide and nuances of co-stimulatory molecules as well as the presence of soluble mediators determine the fate of the T cell. Upon activation, T cells can enter tissue and induce regulatory or inflammatory effects. Classically, T cells have been categorised as either cytotoxic CD8+ cytotoxic T cells or CD4+ T cells.

Activated cytotoxic CD8+ T cells, as the name suggests, can directly mediate cell death upon recognition of their cognate antigen in the context of MHC I on a cell surface. The role of CD8+ T cells in periodontitis is poorly understood. It has

been suggested they may be negative regulators of osteoclast activation in the periodontium (Cardoso and Arosa, 2017).

In contrast, CD4+ T cells have been widely implicated in the pathogenesis of periodontitis. Baker *et al*. elegantly demonstrated that mice deficient for CD4+ but not CD8+ T cells had abrogated alveolar bone loss in a gavage model of periodontitis. Following activation, CD4+ T cells migrate and mediate their protective or pathogenic affect through the release of inflammatory mediators, such as IFN gamma, IL-17, IL-4 and IL-10. The specific inflammatory mediators released by T cells is dictated by the subset they belong to (**Fig. 1.8)**.

Th1, Th2 and Th17 cells have been implicated in periodontitis. For example, interferon gamma knockout mice exposed to *P. gingivalis* appear to be protected from alveolar bone loss compared to controls (Baker *et al.*, 1999). However, exposure to the periodontal pathogen *Aggregatibacter actinomycetemcomitans*, in IFN-γ knockout mice, whilst resulting in diminished alveolar bone loss, was ultimately fatal (Garlet *et al.*, 2008). These studies show protective and pathogenic capabilities of IFN-γ, and thus Th1 cells in periodontitis. IL-33, a tissue derived cytokine that stimulates Th2 cell responses, is elevated in patients with periodontitis and mice exposed to *P. gingivalis*, compared to healthy control patients and control infected mice respectively. Moreover, mice exposed to *P. gingivalis* with additional IL-33 treatment showed exacerbated bone loss compared to *P. gingivalis* alone showing that IL-33, and by proxy Th2 cells, may play an important role in periodontitis pathogenesis (Malcolm *et al.*, 2015). A pleiotropic role has been suggested for Th17 cells; IL-17RA deficient mice show increased alveolar bone loss following *P. gingivalis* infection, suggesting a protective phenotype in periodontitis (Yu *et al.*, 2007). Conversely, humans with Th17 defects appear to be protected against periodontal bone loss (Dutzan *et al.*, 2018).

Whilst murine models point to a crucial function for CD4+ T cells in disease development, patients with HIV, and thus reduced CD4+ T cell frequencies, are more likely to experience necrotising periodontitis compared to healthy patients. The clinical features, mainly alveolar bone loss, are shared between necrotising periodontitis and periodontitis, but their aetiology differs. In contrast to the complex processes in periodontitis pathogenesis, necrotising periodontitis results from opportunistic bacterial infection, typically

Fusobacterium and *Treponema* species. Necrotising periodontitis can often be controlled acutely with antibiotics, periodontal therapy and management of predisposing risk factors such as HIV (Murayama *et al.*, 1994; Dufty, Gkranias and Donos, 2017). Thus, a CD4+ cell population may be protective against necrotising periodontitis, yet pathogenic in periodontitis. Further, implicating T cells in maintaining periodontal health; gingival overgrowth is a side effect of ciclosporin, a selective T cell immunosuppressant, the precise mechanisms resulting in gingival overgrowth are unknown. Interestingly recipients of ciclosporin do not present with rapid development of periodontitis, suggesting CD4+ T cell may be dispensable in periodontitis protection (Pejcic *et al.*, 2014) . The precise function of CD4+ T cells remains elusive and further work is necessary to delineate their role in gingival health and periodontitis.

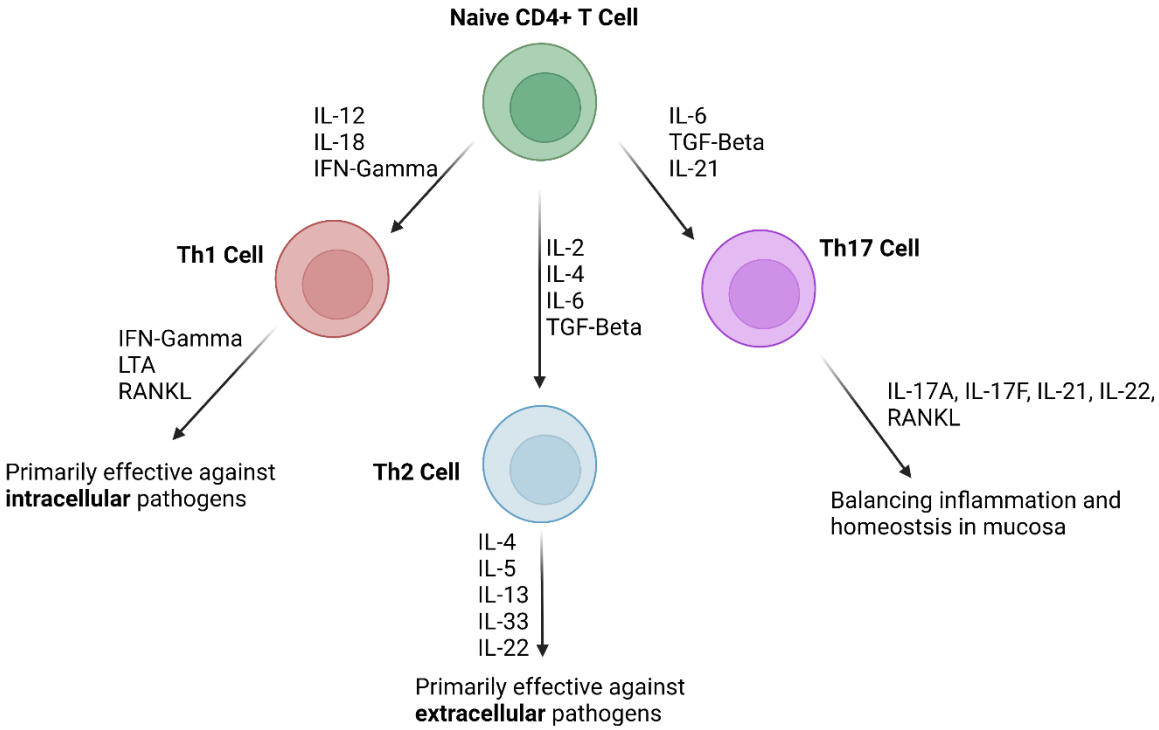

Figure 1. 8 CD4+ T cell subsets in periodontitis

Th1, Th2 and Th17 T cell subsets have been implicated in periodontitis. Activation of CD4+ T cells is dependant on exposure to their cognate antigen expressed upon MHC II, differentiation to a specific T cell subset is determined by the presence of specific inflammatory mediators simultaneously with activation. The function of each T helper cell subset is determined by the cytokines released. Adapted from (Campbell *et al.*, 2016). Figure created with BioRender.com.

1.3.5.3 Chemokines in periodontitis

For a leukocyte to mediate their protection or pathogenesis they must precisely migrate to a specific site at the correct time; chemokines are indispensable in this process.

CXCL8 is highly expressed in human gingiva in both health and during periodontitis. Due to the large neutrophil influx in periodontitis, it seems likely that CXCL8, previously plays its well-established in regulating neutrophil chemotaxis (Ertugrul *et al.*, 2013; Finoti *et al.*, 2017). Cellular expression of CXLC8 in the gingiva is highest at the superficial JE, this mirrors the spatial position of neutrophils in the gingiva, which also are in abundance at the JE (Tonetti, Imboden and Lang, 1998). There are reports of CXCL8 stimulating osteoclastogenesis, thus it may influence alveolar bone resorption directly, but given the presence of CXCL8 in health, the impact of this is unclear (Bendre *et al.*, 2003). Mice lack CXCL8, thus defining the importance of this in periodontitis pathogenesis has proved challenging.

CXCL1 and CXCL2 are also potent neutrophil chemoattractants, and are expressed in healthy gingiva, and are upregulated during periodontitis. Levels of CXCL1 and CXCL2 expression correlate with PMN migration (Rath-Deschner *et al.*, 2020; Zenobia *et al.*, 2013; Miyauchi *et al.*, 2004). Recent studies have suggested that CXCL1 and 2 may direct neutrophil recruitment to specific gingival sites in mice (Greer *et al.*, 2016).

CXCL1, 2 and 8 signal through the chemokine receptors CXCR1 and 2 with varying affinity. CXCL8 shows a bias for CXCR1; CXCL1 and 2 preferentially signal through CXCR2, along with several other chemokines (Sahingur and Yeudall, 2015). In CXCR2 knockout mice periodontitis spontaneously develops, and scant neutrophils are seen histologically in the gingivae, suggesting CXCR2 is the primary chemokine receptor responsible for neutrophil trafficking to murine gingivae (Hajishengallis *et al.*, 2011; Zenobia *et al.*, 2013).

Other inflammatory chemokines are also implicated in periodontitis. CCL2, CCL3 and CCL5 specifically recruit macrophages to the oral cavity and the expression of these mediators is associated with disease severity (Gemmell, Carter and Seymour, 2001; Hanazawa *et al.*, 1993; Kabashima *et al.*, 2002). Interestingly, CCL3 and CCL5 have been shown to regulate osteoclast differentiation and

migration respectively, and thus may directly regulate osteoclast function in periodontitis (Han *et al.*, 2001; Votta *et al.*, 2000).

CCL5 and CXCL10 have been implicated in Th1 cell recruitment in periodontitis. CCL1 has been associated with elevated Th2 cell recruitment. The chemokines CX3CL1, and CCL20 are elevated in periodontitis, both having T cell chemotactic properties, but no work has fully explored their role in periodontitis pathogenesis (Silva *et al.*, 2007).

The B cell chemoattractant CXCL13 is transcriptionally raised in periodontitis and gingivitis. In inflammation, CXCL13 positive cell frequencies increased which correlated with an increase in CD19+ cells. Thus, CXCL13 is involved in the recruitment of B cells to the periodontium in periodontitis (Nakajima *et al.*, 2008). CXCR5, the signalling receptor, is also expressed on osteoblasts, which suggests CXCL13 may also regulate osteoblast activity (Cekici *et al.*, 2014).

Multiple chemokines with overlapping function are expressed in periodontitis, and in healthy gingiva. Pinpointing the precise role a specific chemokine plays in disease progression has proved challenging. Furthermore, few studies have taken an unbiased approach to chemokine expression in periodontitis, with the majority of studies focusing on specific chemokines of interest.

1.3.6 Animal models of periodontitis

The overarching principals of 'Replace, Reduce, Refine' have accelerated the development on *in vitro* models that replicate elements of periodontitis pathogenesis. However, the complexities of the immune response, in particular with respect changes over time as cells move in a complex three-dimensional environment are impossible to capture *in vitro* (Millhouse *et al.*, 2014; NC3R, 2022). Animal models are of immense value in exploring periodontitis pathogenesis. Mice have immune systems with broad homology to humans and as mice are amenable to genetic modifications, they facilitate assessment of the evolving disease state and exploration of the roles of specific genes in disease development (Masopust, Sivula and Jameson, 2017; Hajishengallis, Lamont and Graves, 2015).

Reflecting human disease most accurately are non-human primate (NHP) models of periodontitis, due the significant similarities in transcriptomes and anatomy.

Like humans, NHPs are susceptible to periodontitis, and disease can be exacerbated using a ligature model, furthermore the clinical signs of disease are similar to those of humans, and can be measured, allowing for disease severity to be accurately recorded. Tissue and disease severity can be examined at multiple timepoints in the same animal, as tissue can be harvested from NHP under sedation or anaesthetic, whereas tissue in rodents is typically collected following euthanasia. However, there are significant ethical and cost implications associated with NHP which substantially limit their use (Oz and Puleo, 2011).

Rodent models of disease are frequently used to explore periodontitis pathogenesis. A key benefit of rodent, and in particular mouse models, are the wide array of genetically modified animals and an accessible array of reagents for evaluating immune responses. However, rodents are naturally resistant to periodontitis and their anatomy differs significantly from humans. Experimental models of periodontitis develop rapidly. Rats being larger results in larger immune cell infiltrates and makes evaluating alveolar bone loss easier, however they are more expensive to house and there are fewer commercially available reagents (Graves *et al.*, 2008).

Two commonly used mouse models for periodontitis are the ligature and gavage models. The ligature model involves placing suture material around a tooth, and leaving it in-situ to accelerate local alveolar bone loss (Prates *et al.*, 2014) . This model permits a split mouth approach, thus allowing a comparison between ligated and un-ligated tissue in the same mouse. Interestingly, GF mice do not develop alveolar bone loss in the ligature model; suggesting aggregation of bacteria at the ligature site are responsible for driving bone loss (Marchesan *et al.*, 2018).

Another model of murine periodontitis is the ‘gavage’ model, first described by Baker in 1994 (Baker, Evans and Roopenian, 1994). In this model, mice are repeatedly orally infected with a periodontal pathogen and alveolar bone loss occurs at around 6-10 weeks following the initial infection. This model is well suited to exploring the host-microbe interactions of specific pathogens, and the systemic alterations associated with periodontitis. Unlike the ligature model a split mouth approach can’t be used, and un-physiological numbers of pathogens are required to colonise the mouse and induce alveolar bone loss. As disease

progresses at a slower rate in the gavage model, different time points can be selected, to explore immune cell dynamics following infection (Graves *et al.*, 2008).

There are myriad animal models that can be employed to explore periodontitis, but none precisely replicate human disease, instead each has their own unique advantages and disadvantages a researcher should be aware of when interpreting results.

1.3.7 Management of periodontitis

Management of periodontitis focuses on the removal of dental plaque. Typically patients are provided with intensive oral hygiene instruction and professional mechanical plaque removal 'PMPR' aimed at removing plaque and calculus from the tooth and root surfaces to facilitate resolution of inflammation and reattachment of the periodontal tissues. In instances where non-surgical therapy is ineffective a surgical approach may be indicated to aid treatment. Smoking cessation is also key to periodontal therapy success. In some instance antimicrobial adjuncts may be used to aid the management of disease, but are not indicated without non-surgical mechanical periodontal therapy (SDCEP, 2014; Kapoor *et al.*, 2012). Treatment for periodontitis is time consuming, technique sensitive and multiple appointments are required. Access to periodontal treatment can be challenging. A recent study has shown non-surgical therapy to be effective in 39% of cases, success was dependant on tooth type with disease, with endodontically treated, molar teeth, furcation involvement and smoking negatively impacting treatment outcomes (Van der Weijden, Dekkers and Slot, 2019) .

Due to the significant immune component in periodontitis and the association with chronic inflammatory conditions it has been hypothesised that targeting inflammation may offer an effective adjunct to standard treatment – and may be preferable to extensive use of antibiotics. There have been investigations into the use of biologics to treat disease. A systematic review revealed that therapies targeting TNF-α (administered for treatment of other diseases such as rheumatoid arthritis) may reduce the rate of alveolar bone loss in periodontitis and improve treatment outcomes (Peddis *et al.*, 2019). There has been some work exploring a potential use of the RANKL inhibitors in periodontitis; in a

mouse model a RANKL inhibitor protected mice from alveolar bone loss in a ligature model of disease (Kuritani *et al.*, 2018). However, caution is required as many biologics are associated with medication related osteonecrosis of the jaw, and have significant side effect profiles.

Periodontitis remains a significant burden for patients and economies, and current management strategies are not entirely effective, particularly for those who cannot access services regularly. By improving our understanding of periodontitis pathogenesis and the mechanisms of cellular recruitment novel therapeutics may be identified to treat this debilitating disease.

1.4 Summary and Thesis Aims

The literature reviewed in this chapter shows the complex nature of oral mucosa homeostasis and the myriad factors that may contribute to this. The immune cell network is crucial to maintaining health, but the same cells may contribute to disease, thus a bespoke, regulated immune network is required to strike this delicate balance. Central to regulating cellular recruitment are the chemokines, yet we have only a rudimentary understanding of chemokine function in gingiva, and studies investigating them have often been selective and many chemokines have not been explored. Given the delicate balance that must be struck to achieve homeostasis, this has led to the hypothesis that the chemokine landscape in oral mucosa is distinct from other barrier tissue and that the chemokine expression in oral mucosa differs between health and periodontitis.

This thesis aims to:

- Characterise the chemokine landscape in murine palatal tissue compared to other barrier sites (Chapter 3)
- Identify the differences in chemokine landscape between health and periodontitis in mammalian species (Chapter 4)
- Identify a transcriptomic signature of CD4+ T cells in murine gingivae and draining lymph nodes following *P. gingivalis* or control infection (Chapter 5)
- Identify chemokine receptors that may contribute to gingival CD4+ T cell tissue tropism (Chapter 5).

Improving our understanding of chemokines in the oral mucosa has the potential to identify crucial components to the maintenance of oral mucosa homeostasis and identify potential therapeutic targets for the management of periodontitis and other oral inflammatory diseases.

Chapter 2 - Methods

2.1 Mice

To explore the chemokine landscape in healthy and diseased gingiva, 6–8-week-old C57BL/6 mice were used for a ligature-induced periodontitis model. Mice were housed at the Department of BioMolecular Sciences, School of Pharmaceutical Sciences of Ribeirão Preto. All experiments and husbandry were carried out following the Animal's Facility of the University of São Paulo code of conduct (number 215/2017).

For the gavage model of periodontal disease, 6–8-week-old female BALB/c mice were purchased from Harlan or Charles River Laboratories. Experiments were carried out in accordance with local and UK home office regulations (Licences 60/4041 and 70/8166).

Resting tissue was obtained from 7-9-week-old C57BL/6 mice purchased from Charles River Laboratories. Animals were housed for one-week acclimatisation at the Central Research Facility by Biological Services, University of Glasgow. Experiments were carried out in accordance with UK Home Office regulations.

2.2 Non-Human Primates

Chemokine and chemokine receptor data were obtained from a published NHP data set (Ebersole *et al.*, 2020). *Macaca mulatta* (*n* = 34) were distributed by age and disease status. The Institutional Animal Care and Use Committee of the University of Puerto Rico approved all work; this facilitated clinical measures of periodontal health and disease through assessing periodontal pocket depths and bleeding on probing at four sites per tooth throughout the dentition (Ebersole *et al.*, 2008). Experimental periodontitis was initiated through a ligature model by tying 3-0 silk sutures around the necks of maxillary and mandibular premolar and first and second molar teeth in 3 quadrants in each animal (Ebersole *et al.*, 2014). The untreated quadrant provided baseline healthy tissue from each animal. Individual buccal gingival samples from healthy or periodontitis-affected premolar/molar maxillary region tissues of each animal were taken after three

months of ligature application and frozen in RNAlater for microarray analysis (GeneChip Rhesus Gene 1.0 ST Array; Affymetrix) (Gonzalez *et al.*, 2011).

2.3 Human Studies

2.3.1 Ethics

Gingiva was collected from patients with and without periodontitis undergoing routine periodontal surgery. The study received ethical approval REC reference: 14/LO/2064. All samples were obtained, with written informed consent, from patients attending Glasgow Dental Hospital. Saliva and gingival crevicular fluid (GCF) samples were collected from patients with periodontitis. Samples were obtained from patients enrolled on the Randomised Control Trial "The Immune Response After Periodontal Treatment (IRAPT)" REC reference: 18/NI/0059, ClinicalTrials.gov Identifier: NCT03501316 (Johnston *et al.*, 2020). Healthy control saliva and GCF were collected from healthy volunteers under the study "Host-microbiota interactions in oral health and disease", project number: 2011002. The healthy control study received ethical approval from the University of Glasgow MVLS ethical committee.

2.3.2 Gingival tissue inclusion and exclusion criteria for healthy and periodontal disease participants

Healthy gingival samples (n = 5) were collected from patients undergoing routine gingival surgery without periodontal disease. Diseased gingival samples (n = 6) were collected from patients undergoing open flap debridement, with pocket depths of ≥5mm, due to severe periodontitis. All patients were free of significant systemic disease. All samples were obtained, with consent, from patients attending the Restorative Department at Glasgow Dental Hospital. Samples were collected and used in accordance with the approved study: The Immune Response in Periodontal Disease REC reference: 14/LO/2064 IRAS project ID: 149159.

2.3.3 Human saliva and gingival crevicular fluid collection

Inclusion criteria for periodontitis cases were periodontal probing depths of 5 mm on two or more teeth at non-adjacent sites excluding third molars requiring

periodontal treatment at Glasgow Dental Hospital (Davison *et al.*, 2021; Johnston *et al.*, 2020). Written and informed consent was obtained, and all subjects were ≥ 18 years of age. Patients were excluded if they had a known diagnosis of rheumatoid arthritis, other systemic conditions that may influence immune responses, known or suspected risk of tuberculosis, hepatitis B or HIV infections, bleeding disorders, required an interpreter, and non-English language written material to be provided.

The presence and extent of periodontitis were confirmed by clinical assessment at a baseline visit where the location of the gingival margin, periodontal probing depths and bleeding on probing were recorded by an experienced dental hygienist at six sites per tooth. An overall periodontal inflamed surface area (PISA) score was given for each patient and was calculated as previously described (Nesse *et al.*, 2008).

The samples selected for these experiments were from patients with periodontal disease with PISA scores > 1000 and were either ex or non-smokers.

Healthy controls were recruited from members of staff at the University of Glasgow. Participants were ex or non-smokers and free of systemic disease. A brief periodontal examination (BPE) was conducted, by a qualified dentist, to ensure there were no periodontal pockets > 3.5 mm; participants with a BPE score of three or above were excluded from the study.

2.3.4 Saliva collection

Whole saliva was collected using the passive drool method into 50 mL Falcon tubes (Grenier Bio-One, Gloucestershire, UK) (Yau *et al.*, 2022). Using a sterile Pasteur pipette, 1mL aliquots were made into Eppendorf tubes. Samples were then clarified via centrifugation at 13,000 RPM for 5 minutes (Eppendorf model 5415C, Hamburg, Germany). The supernatant was aliquoted into sterile Eppendorf tubes and immediately stored at -80°C until analysis. Saliva from periodontal disease patients was collected at the baseline visit. Samples with blood contamination were excluded from downstream analysis (Johnston *et al.*, 2020).

2.3.5 Gingival crevicular fluid collection

GCF was collected from a single site (preferentially ≥5 mm in the patients with periodontitis) in each quadrant, at baseline appointments from patients with periodontitis and healthy controls. The method used has been described by William Johnston, who eluted all GCF samples from patients with periodontitis. Gingival sites were dried and isolated using cotton rolls to avoid saliva contamination. PerioPaper® strips were placed into each pocket for 30 seconds (timed). Following collection, strips were put into a sterile Eppendorf and stored immediately at -80°C until analysis (Johnston, 2021).

Collected GCF strips were pooled together in a sterile Eppendorf and eluted using a method adapted from previously published work (Wassall and Preshaw, 2016, Fitzsimmons et al., 2010). PerioPaper® strips were eluted in 150 µLPBS/ 0.1% BSA. The tubes with PerioPaper were placed on a rocking shaker at 4ºC for 20 minutes (100 RPM). After rocking, tubes were centrifuged at 10,000 RPM for 2 minutes. The resulting solution was aliquoted into new sterile Eppendorf's and stored at -80°C until use (Johnston, 2021).

2.4 Murine Ligature Induced Periodontitis

2.4.1 Ligature application

A black silk suture ligature was placed at the left maxillary first molar; no ligature was applied to the contra-lateral molar of 6–8-week-old C57BL/6 mice. Ligatures were left in situ for 3, 7 and 10 days. Four mice served as a non-ligature control in which no ligature was applied. These control gingivae were harvested at day = 0. At the end of each time point, mice were euthanised, gingiva was harvested, and buccal alveolar bone loss was measured. The ligature model was ran at the Department of BioMolecular Sciences, School of Pharmaceutical Sciences of Ribeirão Preto, University of São Paulo, Brazil under the supervision of Professor Sandra Fukada by Robert Reilly, Thaise Mayumi Taira, and Letícia Fernanda Duffles.

2.4.2 Measurement of ligature-induced alveolar bone loss

Buccal alveolar bone loss was measured as previously described (Prates *et al.*, 2014). In brief, the maxillary alveoli were de-fleshed by treatment with 3% hydrogen peroxide, followed by the mechanical removal of residual tissue. The maxillae were stained with 0.3% methylene blue to highlight the cementoenamel junction (CEJ). The palatal aspect of each molar was photographed under 3.2X magnification (ZEISS CL1500 ECO) with a digital camera (Canon E0S 1000D). The palatal alveolar bone loss was measured using IMAGE J software by Thaise Mayumi Taira. The distomesial area (mm^2) between CEJ and the alveolar bone crest was determined. The bone loss measurements from the ligated sites were estimated by subtracting bone loss of the non-ligated contra-lateral side.

2.4.3 Gavage model of murine periodontitis

An existing RNA-Sequencing data set was used to explore the T cell transcriptome of mice with experimental gavage-induced periodontitis (Campbell, 2017). Six to eight-week-old female BALB/c mice were pre-treated with antibiotics (0.08% sulfamethoxazole and 0.016% trimethoprim) in drinking water for ten days, followed by two antibiotic-free days. The mice were equally divided between two cages. One cage of mice were orally infected, using a P200 pipette, with 75 µl of *P. gingivalis* (10^9 CFU) in 2% Carboxymethyl Cellulose (CMC) as previously described (Baker, Evans and Roopenian, 1994; Malcolm *et al.*, 2015; Campbell, 2017). The control group were treated with 75 µl of 2% CMC only. Mice were infected 3 or 4 times within seven days. Anti-*P. gingivalis* IgG Enzyme-Linked Immunosorbent Assays (ELISA) were used to confirm *P. gingivalis* exposure from venous blood obtained from tail bleeding one to two days before the 28 post-infection endpoints. At 28 days post-infection, mice were euthanised by neck dislocation. Gingivae and cervical draining lymph nodes were collected. These experiments were conducted by Lauren Campbell.

2.5 Mouse Tissue Collection

2.5.1 Dorsal flank skin harvesting

Doral flank tissue was collected from euthanised mice by removing dorsal hair tissue with hair clippers. An area of hairless skin was removed with scissors from the dorsal flank using tweezers to add tension. The skin was washed in cold PBS. The subcutaneous tissue was removed using a modified version of a previously described protocol (Li, Adase and Zhang, 2017). The skin piece was placed with the subcutaneous tissue facing the operator in a petri-dish with Phosphate Buffered Saline (PBS); a size ten scalpel blade was used to scrape the subcutaneous tissue from the epidermis and dermis until loose tissue had been removed. This method was used in most instances except for optimisation stages, where subcutaneous tissue was not removed as a control.

2.5.2 Ear skin harvesting

Ear skin was harvested from euthanised mice by cutting the ears off at the base, including cartilage, before rinsing briefly in cold PBS. The left ear was kept intact; the right ear had cartilage removed by using curved scissors to separate the dorsal and ventral surfaces from the cartilage with curved scissors before removing the cartilage with strong forceps, taking care not to traumatise the tissue (Kashem and Kaplan, 2018).

2.5.3 Small intestine harvesting

The small intestine was harvested from euthanised mice. The skin was sterilised with 100% ethanol before accessing the peritoneal cavity by making a 2 cm incision in the skin and peritoneum. The distal and proximal ends of the small intestine were identified, and cuts made 5 mm away from each end, ensuring 2-3 cm of small intestine was available per specimen. Connective tissue and fat were then dissected from the intestine. The small intestine was then cut longitudinally, and faeces were removed from the small intestine. The tissue was finally washed in cold PBS.

2.5.4 Palate harvesting

Whole palates were collected from euthanised mice by cutting both sides of the oral cavity, including cheeks and the ramus of the mandible, with scissors. Soft and hard tissues were cut 1 mm behind the third molars with a scalpel blade, and 2 mm in front of the first molar, followed by cutting the tissue connecting the maxilla to the cheek, taking care to avoid collection of nasal associated lymphoid tissue. The maxilla was then detached from the skull. The gingival and palatal tissues were carefully removed from the maxilla using tweezers. For most experiments, the entire palate was used for ligature-induced periodontitis experiments gingiva alone was used.

2.5.5 Lymph node harvesting

Cervical draining lymph nodes (dLN) were harvested by pinning the murine cadaver ventral side up on a cork board and sterilising the skin with 100% ethanol. An incision was made with scissors from the submental region to the thorax. The tissue was reflected and pinned back, allowing access to the deeper tissue layer. dLNs were identified, removed, and washed in cold PBS.

2.6 RNA Isolation

2.6.1 RNA sample storage

Tissue for RNA analysis was stored in RNA Later (RNAlater™ Stabilization Solution ThermoFisher) at -20^{o}C until sample purification steps.

2.6.2 RNA purification with Qiagen RNeasy Mini Kit

RNA was obtained from murine small intestine, palate, gingiva, lymph nodes, and human gingiva as follows. Tissue was removed from RNAlater solution using forceps. Tissue was then weighed to ensure no more than 30 mg was used. The tissue was placed into a 2 mL centrifuge tube with two 4 mm stainless steel beads (Qiagen) that had been precooled on dry ice and 600 µl of RNeasy Lysis Buffer (RLT) with beta-mercaptoethanol (ß-Me) (10 µl of ß-Me per 1 mL of RLT) was added to each sample. The tubes were then placed in a TissueLyser LT (Qiagen) at 50 Hz for 5-10 minutes until the tissue was disrupted. The lysate was

then centrifuged for three minutes at full speed. The supernatant was removed and transferred to a new 2 mL microcentrifuge tube. The supernatant was centrifuged for three minutes at full speed through the genomic DNA (gDNA) eliminator column with a 2 mL collecting tube. One volume of 70% ethanol was added to the lysate and mixed by pipetting, 700 µl of the sample and precipitate were transferred to an RNeasy spin column with a new 2 mL collection tube, which was then centrifuged for 15 seconds at over 8000 x g. The flow-through was discarded. Next, 350 µl buffer RW1 was added to the RNeasy column and centrifuged for 15 seconds at over 8000 x g. The DNase incubation mix was made by adding 10 µl DNase I stock solution to 70 µl RNeasy DNase Digest (RDD) buffer and mixing gently inverting the tube; 80 µl DNase I incubation mix was added directly to the RNeasy column membrane. The column, with the mix, was left on the benchtop for 15 minutes. 350 µl RNeasy Wash (RW1) buffer was added to the RNeasy column, centrifuged for 15 seconds at > 8000 x g, and the flow-through was discarded. Next, 700 µl RW1 buffer was added to the RNeasy spin column and centrifuge for 15 seconds at 8000 x g, and the flow through was discarded. Next, 500 µl Buffer RPE was added to the RNeasy spin column and centrifuge for 15 seconds at 8000 x g, and the flow through was discarded. The spin column was placed in a 1.5 mL collection tube and 30 µl RNase-free water directly to the spin column membrane and centrifuged for one minute at 8000 x g to elute the RNA.

2.6.3 RNeasy Fibrous Tissue Mini Kit

Skin tissue was first disrupted and homogenised as described in the RNeasy mini kit protocol. Following homogenisation, 590 µl RNase-free water and 10 µl proteinase K was added to the homogenate, mixed with a pipette, and incubated at 55^{o}C for 10 minutes. The samples were centrifuged at 10,000 x g for three minutes. The supernatant was transferred to a new tube, and 0.5 volumes, relative to the supernatant, of 96-100% ethanol were added and mixed. Next, 700 µl of the supernatant was transferred to the RNeasy mini spin column with a 2 mL collection tube and was centrifuged for 15 seconds at 8000 x g. The RNA was then washed, DNAse treated and eluted as section 2.6.3.

2.6.4 RNA purity and concentration analysis

To ensure the purified RNA was suitable for downstream analysis the RNA concentration and purity was assessed using a DeNovix DS-11 Spectrophotometer. The ultraviolet absorbance of 1 µl of RNA was analysed at 230 nm, 260 nm and 280 nm. The RNA concentration was determined by the absorbance at 260 nm. An absorbance reading of 1.0 in a 1 cm detection path corresponds to an RNA concentration of 40 µg/mL. The purity is judged by the 260 nm/280 nm ratio; for the RT^2 profiler array, an A260:A280 ratio of 1.8 - 2.0 was recommended. The ratio between 230 nm and 280 nm is a secondary measure of purity and assesses the sample for impurities such as EDTA or phenol contamination. For the downstream analysis, the A230:A260 ratio of > 1.7 was recommended.

2.6.5 RNA integrity analysis

RNA integrity analysis was conducted for a more detailed survey of RNA samples. This provides a higher accuracy assessment of RNA concentration and identifies if the RNA has been degraded. For an RT^2 profiler array an RNA Integrity Number (RIN) of greater than seven was required. This analysis was undertaken by Glasgow Polyomics using an Agilent 2100 bioanalyser.

2.6.6 RNA reverse transcription

cDNA was synthesised from RNA using a Qiagen RT^2 First Strand Kit, following the manufacturer's instructions. gDNA contamination was removed by adding 2 µl genomic elimination mix to 300 - 400 ng of total RNA. The mix was incubated for five minutes at 42°C and then placed on ice. The reverse transcription mix was prepared, and 10 µl of the mix was added to 10 µl gDNA elimination mix and gently pipetted up and down. The mix was incubated at 42°C for 15 minutes, then at 95°C for five minutes to stop the reaction. To the reverse transcribed mix, 91 µl of RNase-free water was added to each reaction and placed on ice until proceeding with the RT^2 profiler array protocol.

2.6.7 RT^2 Profiler Array

RT^2 SYBR was centrifuged, and 102 µl cDNA synthesis reaction, 650 µl of RT^2 SYBR, and 548 µl RNase-free water were mixed in a loading reservoir for each sample. Using a multichannel pipette 10 µl of the sample was added to the corresponding well. This was repeated for each sample. The RT^2 Profiler Array plate was sealed with an optical strip, centrifuged for one minute at 1000 x g at room temperature and placed on ice whilst setting up the real-time PCR thermocycler (ABI 7900HT). The cycler was programmed 95ºC for 10 minutes and then 40 cycles of 95ºC for 15 seconds and 60ºC for one minute. The absolute quantification of the fluorescent signal was selected. The baseline threshold was manually determined ensuring this was above the background signal but within the lower one-third to one-half of the linear phase of each amplification plot, this was kept constant between all RT^2 Profiler PCR Array runs in the same analysis. The resulting data were exported and analysed.

2.6.8 RT2 Profiler quality control and data analysis

Any cycle threshold (CT) values not detected, or reported as >35, were assigned a value of 35. Any sample with a value of 35 was considered to have a negative call for that analyte. Genomic contamination was determined by assessing the CT value for genomic DNA contamination control well (GDC). If the CT value was less than 35, genomic DNA contamination was identified, and the sample was omitted from subsequent analysis. To determine if reverse transcription was efficient the CT values from the positive PCR control (PPC) well were subtracted from the reverse transcription control (RTC) value, a value of greater than 5 suggested evidence of impurities that inhibited reverse transcription. Finally, the PPC well across samples and arrays should be 20 +/- 2 and not vary by more than 2 cycles between the arrays being compared. Gene of interest expression was determined by using the formulas 2^- (CT Gene of interest – CT Average of Housekeeping Genes) and then log transformed.

2.7 Histology

2.7.1 Paraffin embedding and slide mounting

Tissues used for Haematoxylin and Eosin (H&E) as well as RNA Scope staining protocols were paraffin embedded using the same method. Freshly harvested and washed tissues were completely submerged in 10% Neutral Buffered Formalin (NBF) (Leica) for 24 hours at room temperature. The samples were embedded in paraffin using a standard ethanol and xylene series. Embedded specimens were cut at a thickness of 6 um, suspended in a water bath and mounted on SuperFrost Plus™ Slides (Fisher Scientific).

2.7.2 Haematoxylin and Eosin staining

SuperFrost Plus™ Slides with mounted Formalin Fixed Paraffin embedded sections were placed in xylene for three minutes. The slides were then dipped in 100% ethanol 20 times then in 70% ethanol 10 times. The slides were washed in running tap water. The sections were stained in haematoxylin Z for seven minutes then rinsed with running tap water until the water ran clear. Next, the samples were dipped 12 times in acid alcohol solution (1% Hydrochloric acid in 70% ethanol) then washed in running water. The sections were blued by submerging the slides in Scott's Tap Water Solution (STWS) for two minutes and rinsed again in running water. Samples were then stained with eosin for four minutes and washed in tap water for two minutes. Samples were dipped ten times in 70% ethanol, then 20 times in 100% ethanol. The slides were cleared by placing them in xylene for one minute, this was repeated twice more using fresh xylene each time. Cover slips were placed and sealed using DPX mountant and left to dry overnight.

2.7.3 RNA Scope staining protocol

Samples were cut at 6 µm, suspended in a water bath at 40^{o}C, mounted on SuperFrost Plus™ Slides, and dried at room temperature overnight. Slides were then baked at 60^{o}C for one hour. Paraffin was removed from the slides by submerging them in xylene for five minutes, this step was then repeated. Subsequently, the slides were placed in 100% ethanol for one minute, this was then repeated. The slides were air dried and, once dry, a wax ring was drawn

around each sample with a hydrophobic barrier pen. RNAScope hydrogen peroxide was dropped onto each section and incubated at room temperature for ten minutes and tapped off prior to washing in distilled water for one minute, the slides were then washed a second time. The slides were lowered into boiling antigen retrieval agent for fifteen minutes. The slides were then washed in distilled water for one minute, followed by washing in 100% ethanol for one minute before being left to air dry. Each section was treated with RNAScope Protease Plus and incubated in the HybEZ oven for 30 minutes at 40ºC. The excess fluid was tapped off and slides were washed in distilled water for one minute. RNAScope probes were then hybridised to the sections by dropping each probe onto the relevant sample and incubating at 40ºC in the HybEZ oven for two hours. The signal was then amplified by sequentially dropping amplification solutions, incubating, and washing as directed in the protocol. The RED staining signal was then pipetted onto each sample and incubated, out of direct light, for ten minutes at room temperature. The samples were washed in fresh tap water for one minute twice, using fresh water each time. The slides were then counterstained by submerging a tissue rack into a dish with a 1:1 Gills Haematoxylin and distilled water solution for two minutes, the slides were washed with tap water until it ran clear before submerging them in STWS and moving the rack up and down 2-3 times. The slides were then dried in the oven at 60ºC until completely dry. The slides were dipped into fresh xylene, eco-mount solution was placed on each slide before placing a cover slip and allowing to dry overnight at room temperature. This was repeated for each target probe. There were three consecutive sections per slide, the sections were treated with either a positive control, negative control, or target probe (**Figure 2.1**). The reagents and probes used are outlines in **Table 2.1.**

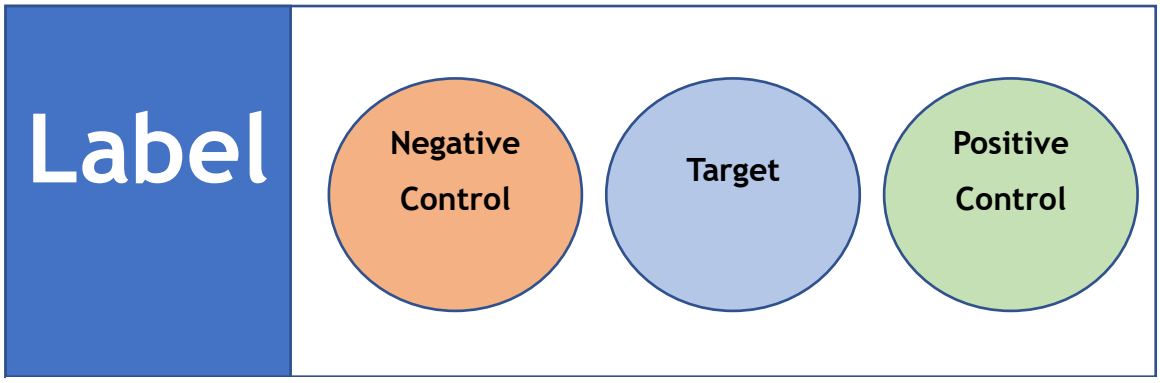

Figure 2. 1 RNA Scope slide configuration

Item	Product code
RNAScope 2.5HD Reagent Kit-RED	322350
RNAScope Negative Control Probe DapB	310043
Positive Control Probe Mm-Ppib	313911
ImmEdge Hydrophobic barrier pen	310018
Mm- Cxcl12 probe	422711
Mm- Cxcl17 probe	519621
Mm- Cxcr4 probe	425901
Mm- Ackr3 probe	482561
Mm- Cxcl14 probe	459741

Table 2. 1 RNA Scope Reagents

2.7.4 Imaging of histology slides

All slides were imaged using an EVOS M7000 digital microscope and ZEISS ZEN microscope software. All images were taken using transillumination. The magnification used for each image is stated in the relevant figure legend.

2.8 Murine Tissue Lysates

Murine tissue lysates were generated to analyse the concentration of chemokines in tissue. Mouse tissues were harvested as previously described. The tissue samples were weighed. Cell lysis buffer solution was made of 1:1 PBS and Cell Lysis Buffer (R&D Cell Lysis Buffer 2), 10 µl per ml of Halt Protease Inhibitor Cocktail (ThermoScientific). In a 2 mL microcentrifuge tube tissue and lysis buffer were added, at a 1:20 weight to volume ratio. The tissue was cut in the tube with spring scissors. Two stainless steel beads were added to the tubes, and tissue was homogenised at 50 Hz using the TissueLyserLT. Gut and lymph node were homogenised for ten minutes, skin and palate were homogenised for 15 minutes. Tissues were then lysed at room temperature for 30 min with gentle agitation and centrifuged at 40^{o}C for 20 minutes at 10,000 x g. The lysate was pipetted and aliquoted. The lysate was stored at -80^{o}C until required.

2.9 Detection and Quantification of Chemokines in Samples

2.9.1 Bicinchoninic acid assay

The total protein concentration in each murine tissue sample was determined using a Pierce™ Bicinchoninic Acid (BCA) Protein Assay Kit (ThermoFisher). In Brief, 25 µl of the standards or samples were pippeted into individual wells in a 96-well plate. The working reagent was mixed and 200 µl was added to each well and mixed on a plate shaker for 30 seconds. The plate was covered and incubated at 37ºC for 30 minutes. The plate was cooled to room temperature and the absorbance was determined at 562 nm on a spectrophotometer. The absorbance of the blank well was subtracted from each sample and a standard curve was generated; unknown sample concentrations were interpolated against the standard curve.

2.9.2 Enzyme linked immunosorbent assays

2.9.2.1 Reagents

R&D Systems DuoSet Enzyme linked immunosorbent assays (ELISAs) were used for all assays with R&D Systems DuoSet Ancillary Reagent Kit 2, except for CXCL4, where an R&D Systems Quantikine ELISA was used. Reagents were prepared as instructed for each protocol (**Table 2.2**).

2.9.2.2 ELISA method

Human and murine samples were collected as described. In brief, 100 µL of capture antibody was added to a 96-well flat-bottom microtiter plates and incubated overnight at room temperature (R&D Systems). The following day, wells were washed, in PBS Tween (R&D Systems) and 200 µL of blocking buffer was added. Plates were incubated for 1 hour at room temperature before further washing. Samples were added at appropriate dilutions alongside standard curves and blank controls, and plates were incubated for 2 hours at room temperature. Following incubation, plates were washed and 100 µL of biotin-conjugated detection antibodies were added for 1 hour. Plates were washed and 100 µL Streptavidin-HRP B to each well for 20 minutes. Plates were washed and 100 µL of Substrate Solution was added to each well and left for colour to

develop. 50 µl Stop Solution (2N sulphuric acid) (R&D Systems) was added to the wells and tapped to ensure thorough mixing. Plates were immediately read at 450 nm with correction at 540 nm. Signal from negative controls was subtracted from sample and standard wells, and the concentration of samples was determined by interpolation using a sigmoidal 4PL standard curve. Chemokine concentration for murine tissue was standardised per milligram of total protein in the sample.

Analyte	System	Product Code	Range of Standard Curve
Human CXCL8	DuoSet ELISA	DY208-05	31.3 – 2000 pg/mL
Human CXCL12	DuoSet ELISA	DY350-05	31.3 – 2000 pg/mL
Human CXCL14	DuoSet ELISA	DY866	125 – 4000 pg/mL
Mouse IL-1β	DuoSet ELISA	DY401-05	15.6 – 1000 pg/mL
Mouse CCL6	DuoSet ELISA	DY487	15.6 – 1000 pg/mL
Mouse CCL25	DuoSet ELISA	DY481	31.3 – 2000 pg/mL
Mouse CCL27	DuoSet ELISA	DY725	62.5 – 4000 pg/mL
Mouse CCL28	DuoSet ELISA	DY533	62.5 – 4000 pg/mL
Mouse CXCL4	Quantikine ELISA	MCX400	0.078 – 5.0 ng/mL

Table 2. 2 ELISA Reagents

2.9.3 LUMINEX

Human gingival crevicular fluid and saliva samples and murine barrier tissue lysates were evaluated using a Luminex™ assay (Custom multiplex assay, R&D Systems) to determine the concentrations of chemokines. For the human studies GCF and saliva were assayed from baseline sample collections from patients with periodontitis as well as healthy controls. Small intestine, skin, palate, and lymph node lysates were generated and assayed. The manufactures instructions were followed for all assays.

Briefly, standards were made as instructed in the user manual. The Microparticle cocktail and Biotin-Antibody Cocktails were centrifuged for 30 seconds at 1000 x g and gently vortexed. Each cocktail was diluted in RD2-1 diluent. Streptavidin-PE was centrifuged for 30 seconds at 1000 x g, vortexed gently and diluted in wash buffer. To each well 50 µl of samples or standards were added, a further

50 µl of diluted microparticle cocktail was then added, covered with the supplied foil plate sealer, and incubated for 2 hours at room temperature on a horizontal orbital shaker (0.12" orbit) at 800 rpm. The plate was then washed. To wash the plate the 96 well plate was inserted into a magnetic plate holder, one minute after insertion 100 µl of wash buffer was added to each well, left for one minute before removing the liquid; the plate was washed three times. Next, 50 µl per well of diluted Biotin-Antibody Cocktail was added and a foil plate sealer was securely fitted, and the plate incubated for one hour at room temperature on the orbital shaker at 800 rpm. The plate was washed three times as described above. 50 µl of diluted Streptavidin-PE was added to each well and the plate was covered with a foil plate sealer, the plate was incubated at room temperature for 30 minutes on an orbital shaker set at 800 rpm. The plate was washed three times as previously described. The microparticles were resuspended in 100 µl of Wash Buffer and incubated for two minutes at room temperature on an orbital shaker at 800 rpm. The human assays were analysed using a Bio-Plex 200 analyser (BioRad, Watford, UK). Murine samples were analysed using a Magpix multiplexer (Luminex, Austin, USA). Sample chemokine concentration was determined by interpolating the Mean Fluorescence Intensity (MFI) of samples against an asymmetric sigmoidal 5PL standard curve. All standards and samples were conducted in technical duplicate.

2.10 RNA Sequencing Analysis

2.10.1 Data set description

The RNA Sequencing data set used was generated by Lauren Campbell (Campbell, 2017). It comprises of RNA purified from murine gingiva and draining lymph node CD4+ T cell populations, with experimental periodontitis or controls. A gavage model of periodontitis was used as described in section **2.4.3.** Single-cell suspensions of palatal tissue harvested from mice with experimental periodontitis or controls. The suspension was generated from tissue pooled from five mice. Palatal tissue from a single mouse was minced using a scalpel blade in a 35 mm tissue culture dish containing 1 mL PBS + 2% FCS, 2 mg/mL collagenase II (Lorne Laboratories, Berkshire, UK) and 1 mg/mL DNase Type I. The minced gingival tissue was washed with 1 mL PBS + 2% FCS to collect remaining cells. Tubes were transferred to a shaking incubator (InnovaTM 4400, New Brunswick™)

for 30 minutes at 37°C and 200 rpm, with 0.5M EDTA added 10 minutes prior to the end of the incubations. The samples were topped up to 12mL with PBS + 2% FCS, then centrifuged. The supernatant was discarded, and the pellet was resuspended then the cells were passed through a 70 µm strainer into a new 50 mL centrifuge tube to remove the remaining tissue. Strained cells were then centrifuged at 380 x g for 5 minutes and the supernatant was discarded. To allow for more accurate cell counting, the pellet was resuspended in 300 µl PBS + 2% FCS. dLNs were collected into 6-well microtiter plates containing 4 mL RPMI 1640 medium supplemented with 10% HI-FCS, 2 mM L-glutamine, 100 U/mL penicillin and 100 µg/ml streptomycin. The dLNs were then transferred to a 40 µm cell strainer and mashed using the plunger from a 2.5 mL syringe into complete media to generate a single cell suspension.

dLN and gingivae single cell suspension were stained extracellularly for Flow Assisted Cell Sorting. The cells were stained with anti-CD45 (eBioscience), anti-CD4 (eBioscience) and viability dye (eBioscience). The cells were sorted using the BD FACSAria™ I or BD FACSAria™ III. Single, viable, CD45+ CD4+ T cells were sorted separately into 1.5 mL reaction tubes for downstream analysis. This yielded a 100% pure CD4+ T cell population (Campbell, 2017).

RNA extraction was performed using the Arcturus® PicoPure™ RNA isolation kit following the manufacturer's instructions. RNA concentration and integrity was validated via Bioanalysis (Aligent 2100, Aligent, Chesire, UK). Due to low RNA yield amplification steps were necessary.

2.10.2 Sequencing

High-quality total RNAs were used to construct Illumina mRNA sequencing libraries. RNA preamplification, cDNA synthesis and cDNA amplification were performed using SMART-seq v4 Ultra Low Input RNA Kit for Sequencing (Takara Bio, Saint-Germain-en-Laye, France). Samples were shipped to Source Bioscience for cDNA synthesis and RNA Sequencing. RNA sequencing was conducted by Source BioScience on the Illumina NextSeq 500 v2 platform. A 75 bp paired-end read protocol was selected and ran using one High-Output flow cell (12 indexes per flow cell).

The reads were aligned with HISAT 2 against Mus Musculus Genome version GRCm38 release 101 using the University of Glasgow galaxy server. Read counts were determined using ht-seq count. All normalisation of read counts and differential expression analysis was performed in R using the DESeq2 package. Genes with a mean expression of <1 were omitted from the analysis.

2.10.3 RNA Sequencing analysis

All RNA sequencing analysis was conducted in R with the use of additional packages **(Table 2.3).** The R script used for RNA Sequencing analysis can be found in Appendix 1. **Figure 2.2** outlines the steps taken in these experiments.

Package/Programme	**Function**
DESeq2	Differential Expression and statistical analysis
ggplot2	Graphical Representation of data
Another Multidimensional Analysis Package (AMAP)	Clustering and Principal Component Analysis
ggrepel	Prevents overlapping text labels
Corrplot	Visual exploratory tool on correlation matrix
Reshape2	Data transformation
BiocManager	Allows installation of projects from *Bioconductor* packages
GenomeInfoDb	Manipulating chromosome names, including modifying them to follow a particular naming style
clusterProfiler	methods to analyse and visualize functional profiles of genomic coordinates, gene and gene clusters
GO.db	annotation maps describing the entire Gene Ontology
Org.Mm.eg.db	Genome wide annotations for mice using Entrez Gene identifiers
Viridis / ViridisLite	Colour map to improve graphical readability

Table 2. 3 Packages and programmes used for RNA Sequencing analysis

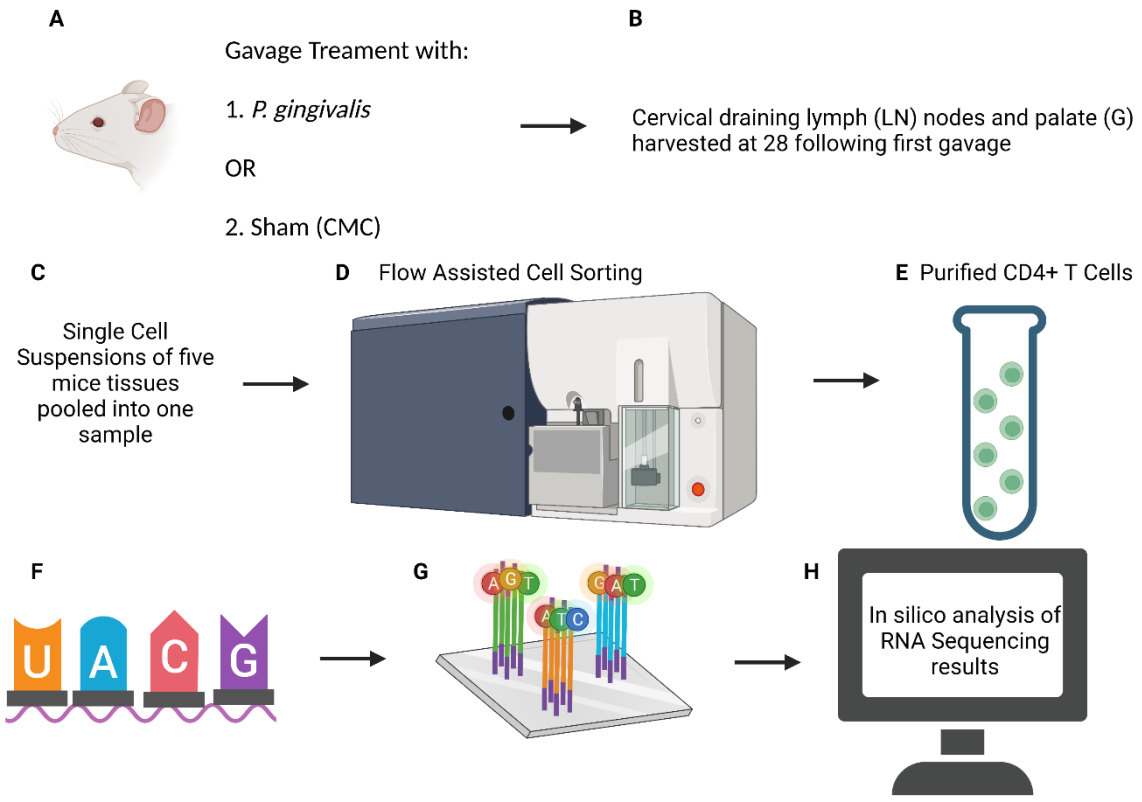

Figure 2. 2 RNA Sequencing methods

(A) Experimental periodontitis was induced using oral exposure to *P. gingivalis*. BALB/c mice received oral infection with *P. gingivalis* W83 in a carrying medium (2% Carboxy-Methyl Cellulose (CMC)) or carrying medium alone, as a control, via gavage at multiple timepoints. Exposure was confirmed by identifying *P. gingivalis* antibodies in circulation by ELISA. **(B)** At 28 days following initial infection gingiva and draining cervical lymph nodes were harvested. **(C)** Single cell suspensions of gingiva and lymph nodes were made by pooling the tissues from 5 mice. **(D)** Lymph nodes and gingiva single cell suspension were stained extracellularly for Flow Assisted Cell Sorting. **(E)** Viable CD45+, CD4+ cells were sorted thus isolating CD4+ T cells. **(F)** RNA was extracted and amplified from the purified CD4+ T cells. **(G)** High-quality total RNAs were used to construct Illumina mRNA sequencing libraries. **(H)** Analysis was conducted as described in section **2.10.3.**

2.11 Statistical Analysis

2.11.1 RNA Sequencing

RNA Sequencing analyses were conducted in R with the additional use of programs outlined in section **2.10.3.** All RNA Sequencing data were normalised to Fragments Per Kilobase of transcript per Million (FPKM) mapped reads and log

transformed for subsequent analysis. The distribution of the data was examined using density plots, revealing the data had a bimodal distribution. DESeq2 was used to determine differential expression and p-value by using Wald's test with a Benjamini-Hochberg adjustment.

All other statistical analyses were performed using GraphPad Prism® software version 9.

2.11.2 Murine ligature induced bone loss analysis

Murine ligature-induced periodontitis bone loss data was measured in mm and used to examine the level of alveolar bone loss at three time points. Data were normally distributed. Alveolar bone loss was compared between ligated and non-ligated sides using an unpaired t-test and corrected for multiple comparisons. To determine the changes in alveolar bone loss at the different timepoints a one-way ANOVA with Tukey's correction for multiple comparisons was used.

2.11.3 RT^2 Profiler Array statistical analysis

RT^2 Profiler Array data are displayed as the gene expression relative to housekeeping genes (HKG), or as the fold change relative to contra-lateral controls in murine models of periodontitis, or healthy gingiva in human studies. All data were log transformed for statistical analysis, due to skewed data distribution.

Ligature-induced murine periodontitis quantitative RT^2 Profiler Array data generated multi-variate, normally distributed data. The expression of thirty-four analytes in seven experimental conditions were assessed. The difference of means in each condition were compared using a 2way ANOVA and corrected using Tukey's multiple comparisons test. Outliers were identified using a Grubb's test and those identified were omitted from data analysis.

Simple linear regression analysis was used to determine associations between alveolar bone loss and analyte expression in ligature-induced murine periodontitis.

Human quantitative PCR (qPCR) data analysed the transcriptional expression of 84 analytes; from two experimental conditions; health and disease. As the

standard deviation of each analyte differed between health and disease, the statistical differences were analysed using a Welch's unpaired t-test, with a Holm-Sidak B correction for multiple comparisons, an alpha of 0.05 was used to determine significance.

2.11.4 Non-human primate microarray data

NHP micro-array data was normalised across the chips through Affymetrix RMA and the MAS 5 algorithms and log transformed for statistical analysis. The mean expression of 62, selected chemokine and chemokine receptor transcripts were identified, and expression was compared between six experimental groups. The data were normally distributed, and statistical comparisons were made using a Two-Way ANOVA and corrected for multiple comparisons using Tukey's test.

2.11.5 Protein analysis

The chemokine concentration in GCF and saliva were determined by ELISA and LUMINEX. The differences in chemokine concentration between patients with and without periodontitis were determined for each fluid using a Mann-Whitney U test, as the data was non-parametric. The results were corrected for multiple comparisons using the Holm-Sidak method.

Murine ELISA and Luminex data were standardised for total protein concentration per sample. For LUMINEX analysis the concentration of 16 analytes were compared across four experimental groups, the data was distributed normally. Each ELISA analyte was compared against across the four experimental groups, the distribution of the data was assumed to be normal. Group means were compared using a Two-way ANOVA and corrected for multiple comparisons using a Tukey's test.

2.11.6 Sample size determination

In the majority of cases the experiments conducted were both entirely novel and exploratory and therefore an a priori sample size calculation was not possible.

Chapter 3 – The Chemokine Landscape in Murine Barrier Tissues

3.1 Introduction

The gingivae occupy a unique ecological niche which is exposed to food and airborne antigens, diverse microbiota, and masticatory forces (Dewhirst *et al.*, 2010; Wu *et al.*, 2014; Dutzan *et al.*, 2017). As such it is crucial to both local and systemic health that immune mechanisms in the gingivae are tailored to its specific requirements (Moutsopoulos and Konkel, 2018). Signalling within the gingiva allows for the initiation of effective immune responses towards pathogens and facilitates repair following trauma whilst being tolerant of commensal micro-organisms and harmless antigens (Moutsopoulos and Konkel, 2018). If the gingival immune response becomes ineffective opportunistic infections may occur, such as candidiasis (Conti *et al.*, 2014). Contrastingly, a dysregulated immune response may damage the host, as seen in periodontitis (Yucel-Lindberg and Bage, 2013).

Leukocytes are the fundamental mediators of tissue-specific immune responses and to mediate their protective, or pathogenic effects leukocytes must traffic to precise tissue locations.

Chemokines are the major *in vivo* regulators of leukocyte migration (Mantovani, 1999). Mammals have approximately 45 chemokines (Zlotnik, Yoshie and Nomiyama, 2006), which are broadly categorised as being inflammatory or homeostatic, according to the contexts in which they function (Mantovani, 1999). Thus, inflammatory chemokines regulate inflammatory leukocyte recruitment to any damaged or infected tissue site and can probably be produced by any cell type in the vicinity of tissue damage. In contrast homeostatic chemokines are constitutively expressed and are important in the precise navigation of cells to specific tissues (Rot and von Andrian, 2004). Several chemokines have both homeostatic and inflammatory functions, termed dual chemokines, and some are yet to have their function defined (Zlotnik, Yoshie and Nomiyama, 2006; Chen *et al.*, 2018). To induce cellular migration

chemokines must interact with their cognate chemokine receptor, however, chemokine biology is further complicated by the promiscuous relationship between chemokines and chemokine receptors, especially in the context of inflammation (Hughes and Nibbs, 2018).

Our understanding of chemokines in gingiva has largely focused on those present in periodontitis and multiple studies have analysed the expression of inflammatory chemokines in periodontal disease compared to health (Silva *et al.*, 2007). There have been limited studies investigating homeostatic chemokine expression in gingiva.

Examples of homeostatic chemokines include CCL27, which attracts T cells specifically to the skin; and CCL25, which attracts T cells to the gut (Mora and von Andrian, 2006). Chemokines interact with target T cells by binding to receptors belonging to the 7-transmembrane spanning family of G-protein coupled receptors (GPCR) (Zlotnik, Yoshie and Nomiyama, 2006). In terms of receptors regulating homeostatic immune cell migration individual receptors confer discrete tissue homing capacity on lymphocytes. Thus, CCR10 is the receptor for CCL27 and is expressed on immune cells that migrate to the skin; CCR9 mediates immune cell migration to the gut by binding CCL25; CCR7 is expressed on T cells and dendritic cells and is essential for their efficient migration to secondary lymphoid organs (Mora and von Andrian, 2006).

The concept that has now emerged is of cells bearing ‘address codes’ which regulate their tissue tropism, and chemokine receptors are dominant contributors to this code. To date, our understanding of address codes is relatively restricted to secondary lymphoid organs, the gut, and the skin. The role played by chemokines and their receptors in attracting leukocytes to other body sites during immune responses is relatively poorly understood. Such an understanding is central for our overall appreciation of the orchestration of immune responses but also, importantly, would highlight novel therapeutic targets for tissue specific immune modulation. A single chemokine can often bind to multiple receptors, and a single receptor may bind multiple ligands with high affinity (Mantovani, 1999; Hughes and Nibbs, 2018). In addition to the classical chemokine receptors there is a small subfamily of atypical chemokine receptors that actively degrade chemokines thereby sculpting in vivo chemokine

gradients and contributing to the overall regulation of tissue-specific leukocyte recruitment (Bonecchi and Graham, 2016).

It is not yet clear which chemokines are essential to gingival homeostasis and which drive inflammatory responses in the oral mucosa. The experiments in this chapter aimed to explore the chemokine landscape in oral mucosa compared to skin and small intestine; hypothesising that a distinct chemokine signature is present in oral mucosa to other barrier sites. Thus, clarifying similarities and differences in chemokine expression in barrier tissue and identify targets that may be responsible for maintaining oral health.

Hypothesis:

The chemokine and chemokine receptor expression profile in murine palate is distinct from skin and small intestine.

The research questions posed to investigate this hypothesis included:

- Are there quantitative differences in the chemokine and chemokine receptor gene and protein expression in murine palate compared with skin and small intestine?
- Which chemokines are highly expressed in murine palate in health?
- Where in the tissues are chemokine and chemokine receptor transcripts expressed?

3.2 Results

3.2.1 Chemokine and chemokine receptor expression in murine palate

To begin exploring the chemokine and chemokine receptor patterns in oral mucosa, the transcriptional expression in murine palate (n = 4) was determined by qPCR. Bioanalysis and Qubit analysis revealed, for all samples, sufficient RNA quantities and integrity for downstream analysis with a Qiagen RT^2 Profiler Array **(Table 3.1)**.

Following RNA isolation 400 ng of RNA from each sample were reverse transcribed prior to analysis by qPCR with a Qiagen RT2 Profiler array for chemokines and chemokine receptors (**Table 3.2)**. The qPCR array has five inbuilt HKG and controls for genomic contamination, reverse transcription, and positive PCR controls, all samples passed quality control.

Sample	RNA Concentration (ng/ul)	RNA Integrity Number (RIN)
P1	431	10
P2	588	10
P3	317	10
P4	187	10

Table 3. 1 Concentration and RNA integrity numbers of RNA isolated from four murine palates

Position	Gene Symbol	Description	Role
A01	*C5ar1*	Complement component 5a receptor 1	Analyte
A02	*Ccbp2 (ACKR2)*	Chemokine binding protein 2 (Atypical Chemokine Receptor 2)	Analyte
A03	*Ccl1*	Chemokine (C-C motif) ligand 1	Analyte
A04	*Ccl11*	Chemokine (C-C motif) ligand 11	Analyte
A05	*Ccl12*	Chemokine (C-C motif) ligand 12	Analyte
A06	*Ccl17*	Chemokine (C-C motif) ligand 17	Analyte

Position	Gene Symbol	Description	Role
A07	*Ccl19*	Chemokine (C-C motif) ligand 19	Analyte
A08	*Ccl2*	Chemokine (C-C motif) ligand 2	Analyte
A09	*Ccl20*	Chemokine (C-C motif) ligand 20	Analyte
A10	*Ccl22*	Chemokine (C-C motif) ligand 22	Analyte
A11	*Ccl24*	Chemokine (C-C motif) ligand 24	Analyte
A12	*Ccl25*	Chemokine (C-C motif) ligand 25	Analyte
B01	*Ccl26*	Chemokine (C-C motif) ligand 26	Analyte
B02	*Ccl28*	Chemokine (C-C motif) ligand 28	Analyte
B03	*Ccl3*	Chemokine (C-C motif) ligand 3	Analyte
B04	*Ccl4*	Chemokine (C-C motif) ligand 4	Analyte
B05	*Ccl5*	Chemokine (C-C motif) ligand 5	Analyte
B06	*Ccl6*	Chemokine (C-C motif) ligand 6	Analyte
B07	*Ccl7*	Chemokine (C-C motif) ligand 7	Analyte
B08	*Ccl8*	Chemokine (C-C motif) ligand 8	Analyte
B09	*Ccl9*	Chemokine (C-C motif) ligand 9	Analyte
B10	*Ccr1*	Chemokine (C-C motif) receptor 1	Analyte
B11	*Ccr10*	Chemokine (C-C motif) receptor 10	Analyte
B12	*Ccr1|1*	Chemokine (C-C motif) receptor 1 -like 1	Analyte
C01	*Ccr2*	Chemokine (C-C motif) receptor 2	Analyte
C02	*Ccr3*	Chemokine (C-C motif) receptor 3	Analyte
C03	*Ccr4*	Chemokine (C-C motif) receptor 4	Analyte
C04	*Ccr5*	Chemokine (C-C motif) receptor 5	Analyte
C05	*Ccr6*	Chemokine (C-C motif) receptor 6	Analyte
C06	*Ccr7*	Chemokine (C-C motif) receptor 7	Analyte
C07	*Ccr8*	Chemokine (C-C motif) receptor 8	Analyte
C08	*Ccr9*	Chemokine (C-C motif) receptor 9	Analyte
C09	*Ccrl1 (ACKR4)*	Chemokine (C-C motif) receptor -like 1 (Atypical Chemokine Receptor 4)	Analyte
C10	*Ccrl2*	Chemokine (C-C motif) receptor -like 2	Analyte
C11	*Cmklr1*	Chemokine-like receptor 1	Analyte
C12	*Cmtm2a*	CKLF-like MARVEL transmembrane domain containing 2A	Analyte

Position	Gene Symbol	Description	Role
D01	*Cmtm3*	CKLF-like MARVEL transmembrane domain containing 3	Analyte
D02	*Cmtm4*	CKLF-like MARVEL transmembrane domain containing 4	Analyte
D03	*Cmtm5*	CKLF-like MARVEL transmembrane domain containing 5	Analyte
D04	*Cmtm6*	CKLF-like MARVEL transmembrane domain containing 6	Analyte
D05	*Cx3Cl1*	Chemokine (C-X3-C motif) ligand 1	Analyte
D06	*Cx3cr1*	Chemokine (C-X3-C) receptor 1	Analyte
D07	*Cxcl1*	Chemokine (C-X-C motif) ligand 1	Analyte
D08	*Cxcl10*	Chemokine (C-X-C motif) ligand 10	Analyte
D09	*Cxcl11*	Chemokine (C-X-C motif) ligand 11	Analyte
D10	*Cxcl12*	Chemokine (C-X-C motif) ligand 12	Analyte
D11	*Cxcl13*	Chemokine (C-X-C motif) ligand 13	Analyte
D12	*Cxcl14*	Chemokine (C-X-C motif) ligand 14	Analyte
E01	*Cxcl15*	Chemokine (C-X-C motif) ligand 15	Analyte
E02	*Cxcl16*	Chemokine (C-X-C motif) ligand 16	Analyte
E03	*Cxcl2*	Chemokine (C-X-C motif) ligand 2	Analyte
E04	*Cxcl3*	Chemokine (C-X-C motif) ligand 3	Analyte
E05	*Cxcl5*	Chemokine (C-X-C motif) ligand 5	Analyte
E06	*Cxcl9*	Chemokine (C-X-C motif) ligand 9	Analyte
E07	*Cxcr1*	Chemokine (C-X-C motif) receptor 1	Analyte
E08	*Cxcr2*	Chemokine (C-X-C motif) receptor 2	Analyte
E09	*Cxcr3*	Chemokine (C-X-C motif) receptor 3	Analyte
E10	*Cxcr4*	Chemokine (C-X-C motif) receptor 4	Analyte
E11	*Cxcr5*	Chemokine (C-X-C motif) receptor 5	Analyte
E12	*Cxcr6*	Chemokine (C-X-C motif) receptor 6	Analyte
F01	*Cxcr7*	Chemokine (C-X-C motif) receptor 7 Atypical Chemokine Receptor 3	Analyte
F02	*Darc (Ackr1)*	Duffy blood group, chemokine receptor Atypical Chemokine Receptor 1	Analyte
F03	*Fpr1*	Formyl peptide receptor 1	Analyte

Position	Gene Symbol	Description	Role
F04	*Gpr17*	G protein-coupled receptor 17	Analyte
F05	*Hif1a*	Hypoxia inducible factor 1, alpha subunit	Analyte
F06	*Ifng*	Interferon gamma	Analyte
F07	*IL16*	Interleukin 16	Analyte
F08	*Il1b*	Interleukin 1 beta	Analyte
F09	*Il4*	Interleukin 4	Analyte
F10	*Il6*	Interleukin 6	Analyte
F11	*Itgam*	Integrin alpha M	Analyte
F12	*Itgb2*	Integrin beta 2	Analyte
G01	*Mapk1*	Mitogen-activated protein kinase 1	Analyte
G02	*Mapk14*	Mitogen-activated protein kinase 14	Analyte
G03	*Pf4* *(Cxcl4)*	Platelet factor 4 Chemokine (C-X-C motif) ligand 4	Analyte
G04	*Ppbp* *(Cxcl7)*	Pro-platelet basic protein Chemokine (C-X-C motif) ligand 7	Analyte
G05	*Slit2*	Slit homolog 2 (Drosophila)	Analyte
G06	*Tgfb1*	Transforming growth factor, beta 1	Analyte
G07	*Tlr2*	Toll-like receptor 2	Analyte
G08	*Tlr4*	Toll-like receptor 4	Analyte
G09	*Tnf*	Tumour necrosis factor	Analyte
G10	*Tymp*	Thymidine phosphorylase	Analyte
G11	*Xcl1*	Chemokine (C motif) ligand 1	Analyte
G12	*Xcr1*	Chemokine (C motif) receptor 1	Analyte
H01	*Actb*	Actin, beta	HKG
H02	*B2m*	Beta-2 microglobulin	HKG
H03	*Gapdh*	Glyceraldehyde-3-phosphate dehydrogenase	HKG
H04	*Gusb*	Glucuronidase, beta	HKG
H05	*Hsp90ab1*	Heat shock protein 90 alpha (cytosolic), class B member 1	HKG
H06	MGDC	Mouse Genomic DNA Contamination	Control
H07	RTC	Reverse Transcription Control	Control
H08	RTC	Reverse Transcription Control	Control

Position	Gene Symbol	Description	Role
H09	RTC	Reverse Transcription Control	Control
H10	PPC	Positive PCR Control	Control
H11	PPC	Positive PCR Control	Control
H12	PPC	Positive PCR Control	Control

Table 3. 2 Qiagen Chemokine and Receptors RT2 Profiler Array (PAMM-022ZE-4) targets and well location

Analyte expression was determined relative to the mean housekeeping gene expression. *Ccl19* exhibited the highest expression; the chemokines in the highest quartile of expression were: *Cxcl16, Cxcl7, Ccl11, Cxcl5, Ccl6, Cxcl12, Cxcl14* and *Cxcl13* **(Fig. 3.1A)**. In terms of receptors in murine palate, a broad expression pattern was observed with detectable expression of *Cxcr4, Ccr2, Ccr6, Ackr1* and *Ackr4*. *Ackr3* was the atypical chemokine receptor with the highest expression, whilst *Cxcr4* was the most highly expressed typical chemokine receptor **(Fig. 3.1B)**. Other transcripts related to cell migration were included on the assay, this showed high expression of *Hif1a, Mapk1, Cmtm6*, and *Mapk14* (**Fig. 3.1C)**.

These data highlighted transcripts of interest which warranted further investigation, in particular the chemokines *Ccl6, Ccl11, Ccl19, Cxcl5, Cxcl12, Cxcl13, Cxcl14* and the chemokine receptors *Cxcr4* and *Ackr3*.

A

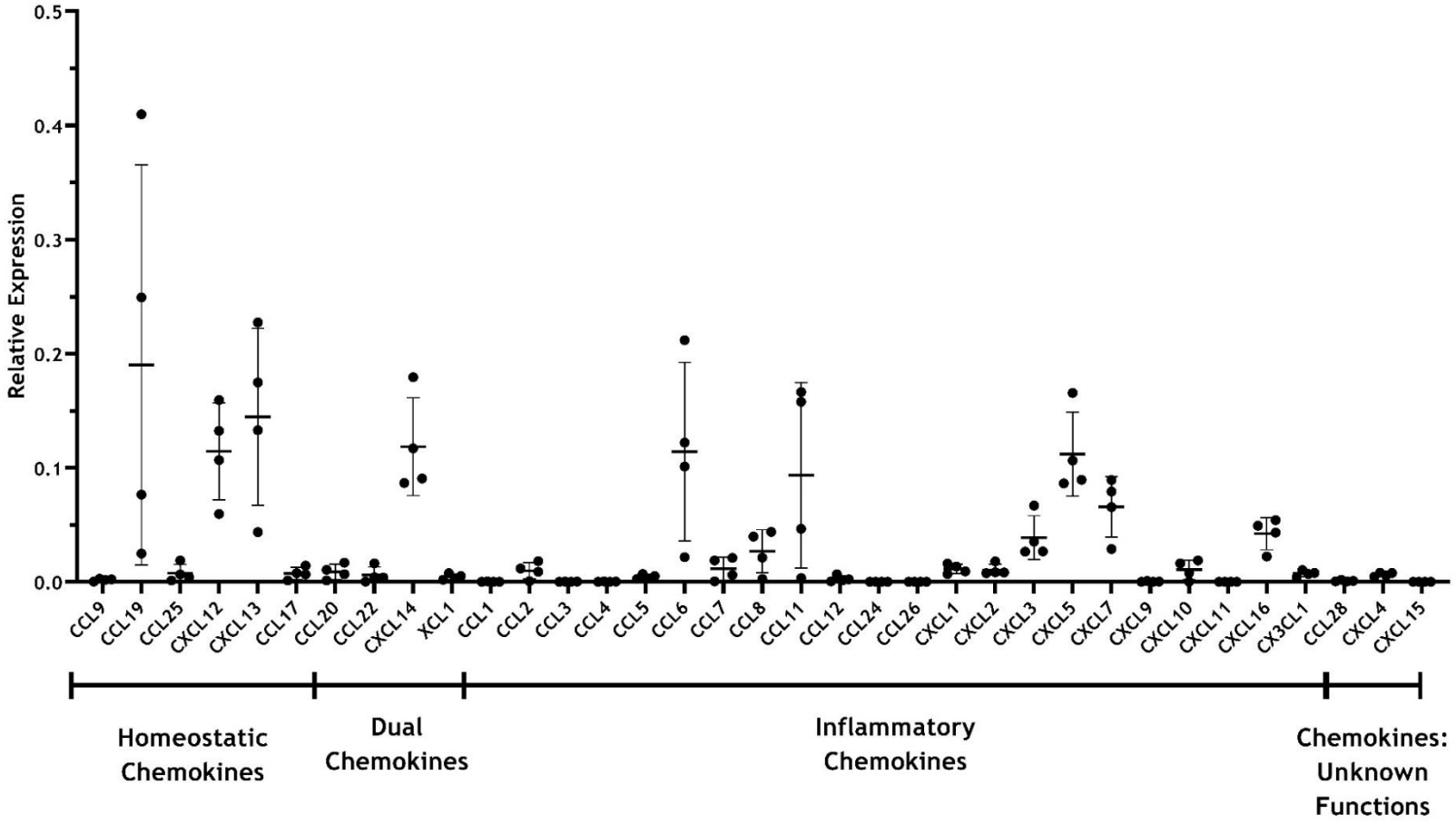

Figure 3.1 legend on page 71

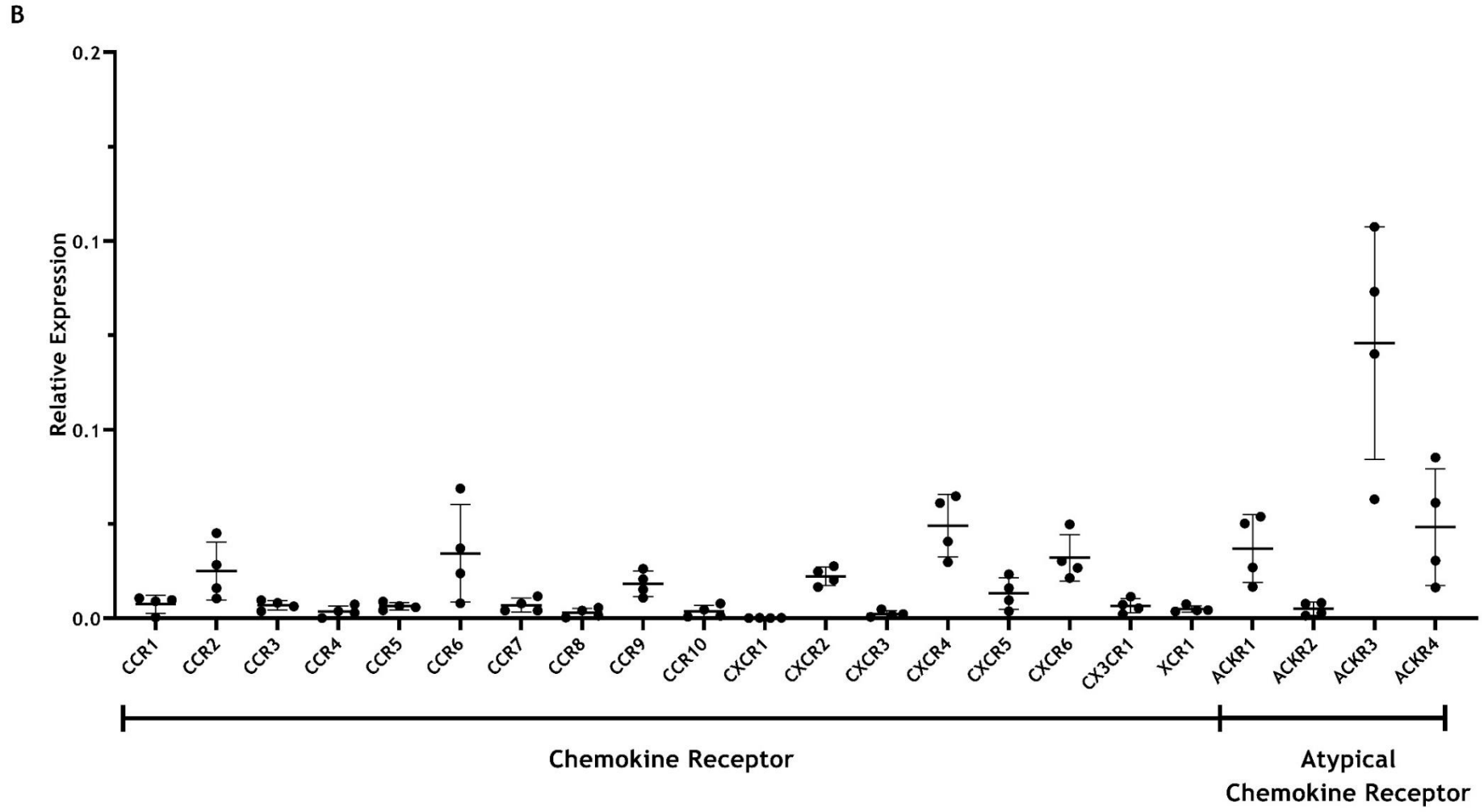

Figure 3.1 legend on page 71

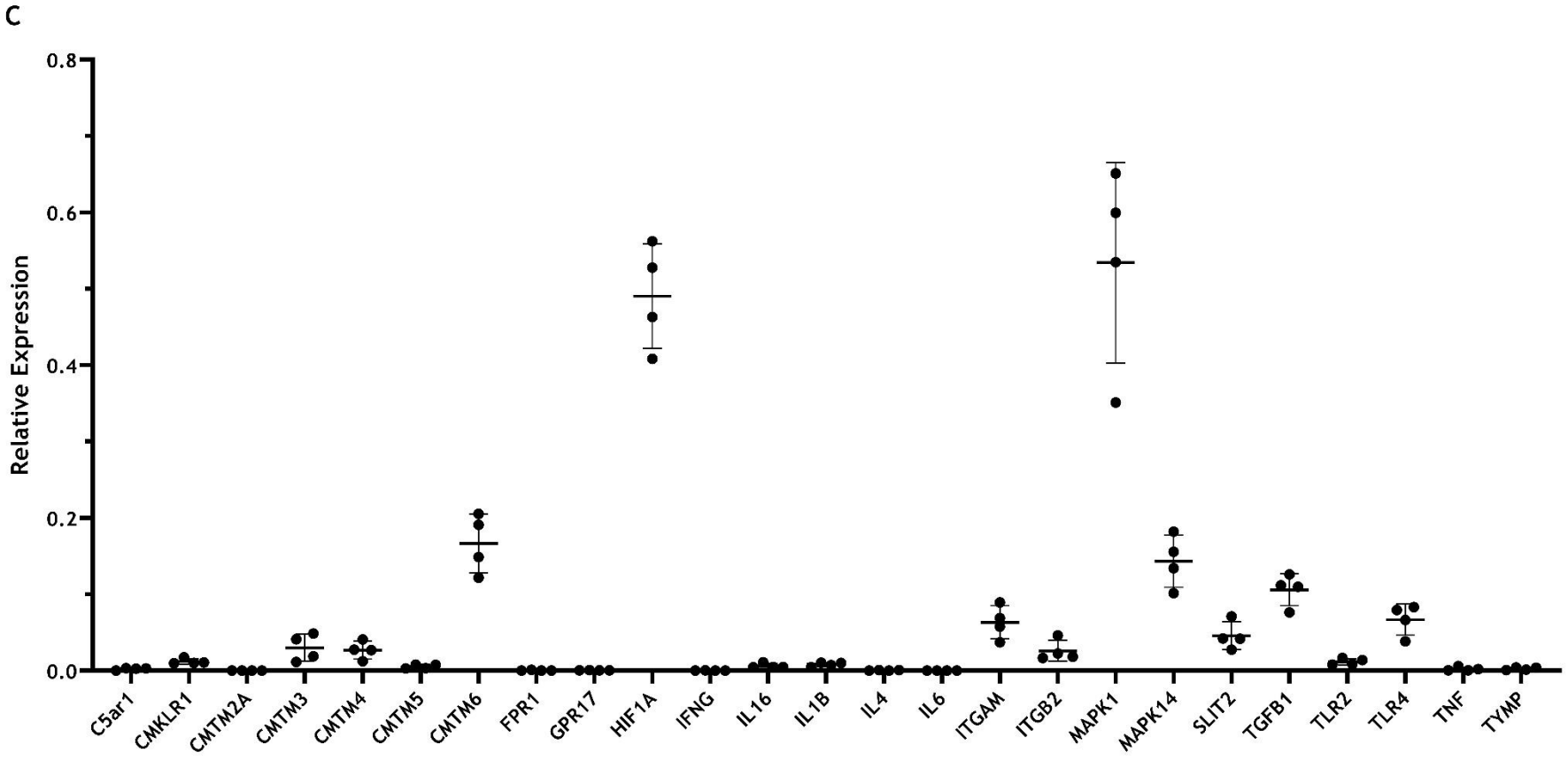

Figure 3.1 Chemokine and chemokine receptor expression in healthy murine palate

RNA was isolated from palatal tissue collected from healthy mice (*n*=4). The expression of chemokines, chemokine receptors was determined by qPCR. Mean indicated by horizontal bar, error bars show standard deviation of the mean. **(A)** Chemokine expression in healthy murine palate. **(B)** Chemokine receptor expression in healthy murine palate. **(C)** Other transcripts related to cell migration in healthy murine palate.

3.2.2 Chemokine and chemokine receptor expression in murine barrier tissue

To identify if the chemokine and chemokine receptor signature observed is unique to the oral mucosa, we explored the chemokine and chemokine receptor landscape in oral mucosa compared to other barrier tissues in health.

An abbreviated Qiagen Custom RT2 Profiler was used, to allow for increased sample numbers and thus improved statistical power (**Table 3.3**). This included reducing the number of HKG to three, as recommended by the manufacturer, the genes selected were *Actb, B2m* and *Tbp*.

Position	Gene Symbol	Description	Role
A1	*Gdc*	Mouse Genomic DNA Contamination	Control
A2	*Ppc*	Positive PCR Control	Control
A3	*Rtc*	Reverse Transcription Control	Control
B1	*Actb*	Actin, beta	HKG
B2	*B2m*	Beta-2 microglobulin	HKG
B3	*Tbp*	TATA-binding protein	HKG
C1	*Ccl2*	Chemokine (C-C motif) ligand 2	Analyte
C2	*Ccl3*	Chemokine (C-C motif) ligand 3	Analyte
C3	*Ccl4*	Chemokine (C-C motif) ligand 4	Analyte
D1	*Ccl5*	Chemokine (C-C motif) ligand 5	Analyte
D2	*Ccl6*	Chemokine (C-C motif) ligand 6	Analyte
D3	*Ccl11*	Chemokine (C-C motif) ligand 11	Analyte
E1	*Ccl19*	Chemokine (C-C motif) ligand 19	Analyte
E2	*Ccl20*	Chemokine (C-C motif) ligand 20	Analyte
E3	*Ccl22*	Chemokine (C-C motif) ligand 22	Analyte
F1	*Ccl25*	Chemokine (C-C motif) ligand 25	Analyte
F2	*Ccl27b*	Chemokine (C-C motif) ligand 27b	Analyte

Position	Gene Symbol	Description	Role
F3	*Ccl28*	Chemokine (C-C motif) ligand 28	Analyte
G1	*Cxcl1*	Chemokine (C-X-C motif) ligand 1	Analyte
G2	*Cxcl2*	Chemokine (C-X-C motif) ligand 2	Analyte
G3	*Pf4*	Platelet factor 4 (Chemokine (C-X-C motif) ligand 4)	Analyte
H1	*Cxcl5*	Chemokine (C-X-C motif) ligand 5	Analyte
H2	*Cxcl12*	Chemokine (C-X-C motif) ligand 12	Analyte
H3	*Cxcl13*	Chemokine (C-X-C motif) ligand 13	Analyte
I1	*Cxcl14*	Chemokine (C-X-C motif) ligand 14	Analyte
I2	*Cxcl16*	Chemokine (C-X-C motif) ligand 17	Analyte
I3	*Cxcl17*	Chemokine (C-X-C motif) ligand 17	Analyte
J1	*Ccr1*	Chemokine (C-C motif) receptor 1	Analyte
J2	*Ccr2*	Chemokine (C-C motif) receptor 2	Analyte
J3	*Ccr3*	Chemokine (C-C motif) receptor 3	Analyte
K1	*Ccr5*	Chemokine (C-C motif) receptor 5	Analyte
K2	*Ccr6*	Chemokine (C-C motif) receptor 6	Analyte
K3	*Cxcr2*	Chemokine (C-X-C motif) receptor 2	Analyte
L1	*Cxcr4*	Chemokine (C-X-C motif) receptor 4	Analyte
L2	*Cxcr5*	Chemokine (C-X-C motif) receptor 5	Analyte
L3	*Cxcr6*	Chemokine (C-X-C motif) receptor 6	Analyte
M1	*Darc*	Duffy blood group, chemokine receptor (Atypical Chemokine Receptor 1)	Analyte
M2	*Ccbp2*	Chemokine binding protein 2 (Atypical Chemokine Receptor 2)	Analyte
M3	*Cxcr7*	Chemokine (C-X-C motif) receptor 7 (Atypical Chemokine Receptor 3)	Analyte

Position	Gene Symbol	Description	Role
N1	*Ccrl1*	Chemokine (C-C motif) receptor -like1 (Atypical Chemokine Receptor 4)	Analyte
N2	*Tnfsf11*	Receptor Activator Of Nuclear Factor Kappa B Ligand (RANKL)	Analyte
N3	*Tnfrsf11b*	Osteoprotegerin	Analyte
O1	*Il17a*	Interleukin-17A	Analyte
O2	*Niacr1*	G Protein-Coupled Receptor 109A	Analyte
O3	*Ffar3*	G-Protein Coupled Receptor 41	Analyte
P1	*Ffar2*	G-Protein Coupled Receptor 43	Analyte
P2	*Tlr9*	Toll-Like Receptor 9	Analyte
P3	*Tlr2*	Toll-Like Receptor 2	Analyte

Table 3. 3 Qiagen Custom RT2 Profiler Array (CLAM36735) targets and well location

Small intestine and skin were selected as comparator tissues as they have a well described chemokine landscape, are barrier tissues, and as such share similarities in function and structure to palate (Wermers *et al.*, 2011; Homey *et al.*, 2002; Moutsopoulos and Konkel, 2018). Methods of tissue harvesting for palate and small intestine are generally standardised. However, there are several different methods and sites described for skin.

3.2.2.1 Optimisation of barrier tissue harvesting

To determine the most suitable site, and method, for skin preparation, skin from mouse ear, with and without cartilage removal was compared to murine dorsal flank skin, with and without subcutaneous tissue removal. Initial histological comparison demonstrated which preparation would offer the most suitable comparison between barrier tissues. Palate, small intestine, and skin were formalin fixed and paraffin embedded (FFPE) and stained with H&E. Small intestine (**Fig. 3.3A**) and palatal tissue (**Fig. 3.3B**) comprised of an epithelium and lamina propria, whilst skin from the dorsal flank (**Fig. 3.3C**) and ear (**Fig. 3.3E**) had significant accompanying subcutaneous tissue. As such, steps were taken to remove of the subcutaneous tissue allowing for an accurate comparison of the barrier tissue chemokine landscapes.

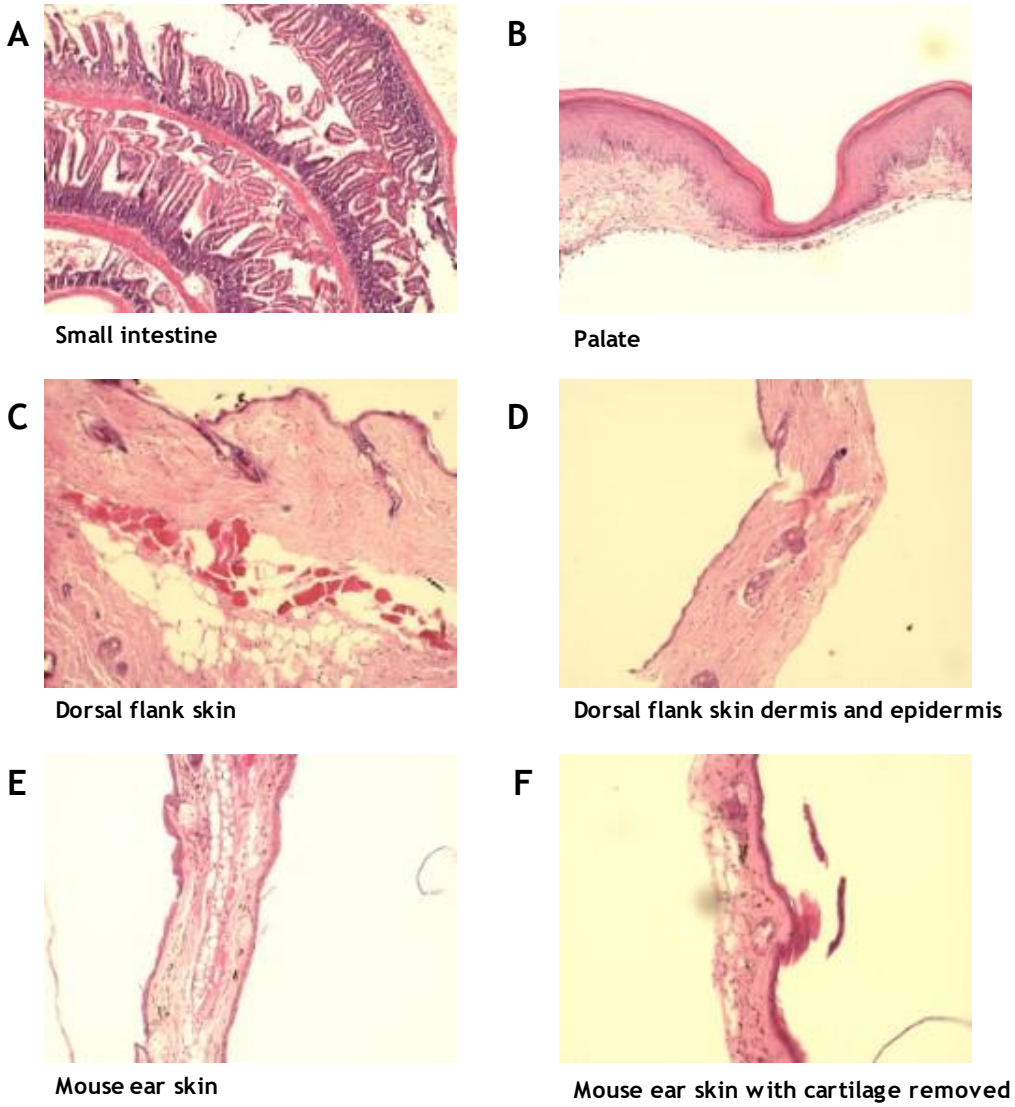

Figure 3. 2 H&E stained barrier tissue from adult male mice

Formalin fixed and paraffin embedded murine barrier tissues were stained with H&E to compare the histological structure of tissues under x 20 magnification with EVOS microscope. (**A)** Small intestine (**B)** Palatal tissue (**C)** Whole skin from mice flank (**D)** Skin from flank with subcutaneous tissue removed (**E)** Mouse ear (**F)** Mouse ear with cartilage removed.

To remove subcutaneous tissue from flank and cartilage from ears a modified version of the protocols used by Kashem and Kaplan was employed (Kashem and Kaplan, 2018). This satisfactorily removed subcutaneous tissue whilst leaving the epidermis and dermis intact from flank (**Fig. 3D**). It was also beneficial in reducing the amount of cartilage from ear tissue **(Fig. 3F)**. However, cartilage removal, yielded inconsistent results. Thus, skin from the mouse dorsal flank was

used, with subcutaneous tissue removed, as a comparator to palate and small intestine.

3.2.2.2 Chemokine and chemokine receptor analysis RT^2 Profiler Array

Following the same RNA isolation protocol as previously described, RNA from small intestine and palate were isolated at concentrations suitable for downstream analysis. RNA was isolated from skin with a Qiagen RNEasy Mini Fibrous Tissue kit which consistently yielded sufficient RNA for downstream analysis. Furthermore, all samples had satisfactory A260:280 and A260:230 ratios reinforcing the suitability for the preparation method for the array **(Table 3.4).** Samples that did not pass quality control were omitted from further analysis.

Sample	RNA Conc.(ng/µl)	A260:230	A260:280	Used in array	Passed RT2 QC
P1	427.541	2.175	2.085	Yes	Yes
P2	365.527	1.814	2.091	Yes	Yes
P3	362.395	1.851	2.085	Yes	Yes
P4	177.922	1.285	2.107	Yes	No – Genomic Contamination
P5	153.489	1.728	2.084	Yes	Yes
P6	95.505	0.838	2.081	No	NA
P7	144.757	0.931	2.054	Yes	Yes
P8	216.784	1.373	2.071	Yes	Yes
P9	463.07	2.22	2.085	Yes	Yes
P10	336.392	2.162	2.082	Yes	Yes
P11	287.592	2.16	2.071	Yes	Yes
P12	262.441	1.362	2.07	Yes	Yes
G1	626.269	2.14	2.115	Yes	Yes
G2	252.596	1.707	2.077	Yes	Yes
G3	494.402	1.983	2.076	Yes	Yes

Sample	RNA Conc.(ng/µl)	A260:230	A260:280	Used in array	Passed RT2 QC
G4	78.197	1.536	2.051	No	NA
G5	685.89	2.239	2.131	Yes	Yes
G6	126.799	2.016	2.052	No	NA
G7	485.423	2.01	2.101	Yes	Yes
G8	494.308	2.158	2.089	Yes	Yes
G9	603.911	1.829	2.109	Yes	Yes
G10	568.838	2.152	2.096	Yes	Yes
G11	877.014	2.111	2.15	Yes	Yes
G12	856.06	2.16	2.149	Yes	Yes
S1	329.362	2.139	2.084	Yes	Yes
S2	153.045	1.68	2.053	Yes	Yes
S3	336.636	1.906	2.075	Yes	Yes
S4	970.493	2.131	2.067	Yes	Yes
S5	416.634	2.123	2.074	Yes	Yes
S6	552.705	2.152	2.097	No	NA
S7	250.389	1.919	2.061	Yes	Yes
S8	428.924	1.858	2.2024	Yes	Yes
S9	773.527	2.207	2.129	Yes	Yes
S10	293.584	2.01	2.064	Yes	No – Pipetting Error
S11	232.721	2.044	2.054	Yes	Yes
S12	606.645	2.215	2.096	Yes	Yes

Table 3. 4 Murine barrier tissue samples

This table outlines the RNA concentration of each sample, the A260:230, A260:280 ratio, if it was analysed on the array and if it passed the RT2 profiler quality control. P=Palate, G=Small Intestine, S=Skin.

Purified RNA was reverse transcribed and analysed. Quality controls revealed one sample had evidence of genomic contamination, another sample was omitted due to a pipetting error. All other samples passed quality control. The combined mean expression of the three housekeeping genes relative to the gene of interest expression was determined using the formula Log10((2^-(HKG CT – GOI CT)) *-1).

Reflecting the observations from **Figure 3.1**, all chemokine and chemokine receptors analysed had detectable levels of expression in palate. *Ccl19, Cxcl5, Cxcl12, Cxcl13, Cxcl14, Cxcl16* and *Cxcl17* were highly expressed and *Ackr3* demonstrated high expression relative to other chemokine receptors in murine palate. Multiple chemokines had similar expression across tissues; however, many exhibited significant differential expression **(Fig. 3.3)**.

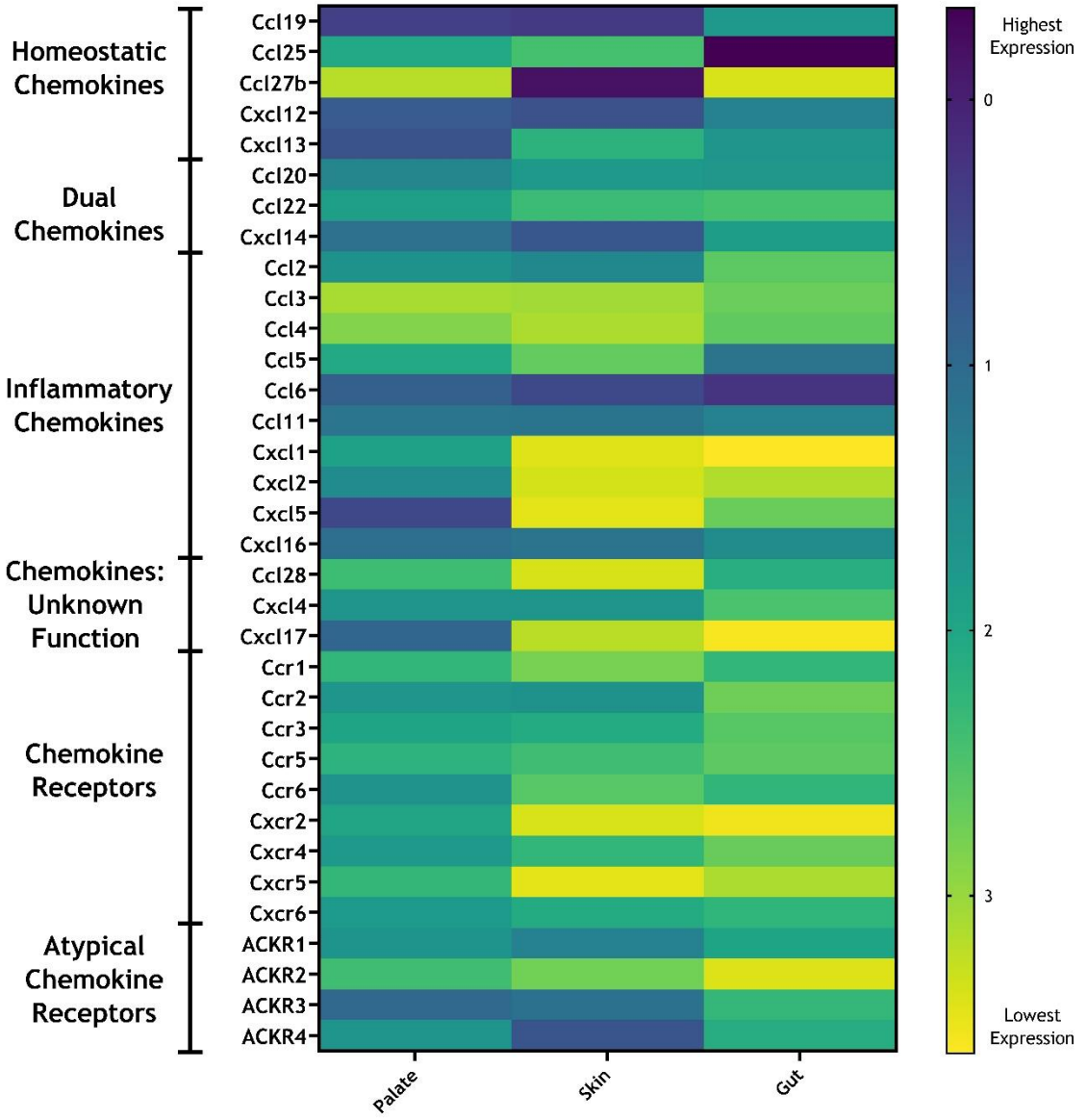

Figure 3. 3 Heatmap of chemokine and chemokine receptor expression in murine barrier tissue

RNA isolated from murine palate (n = 10), skin (n = 10) and small intestine (n = 10) was reverse transcribed and analysed using a Custom Qiagen RT2 Profiler Array. Expression was measured relative to the average of three housekeeping genes, and log transformed. The mean expression for each analyte in palate, skin and small intestine was determined and is represented as a colour, indicating the level of expression.

3.2.2.3 Differential transcript analysis

Twenty-seven chemokines and receptors demonstrated differential expression between the barrier tissues. Eight transcripts: *Cxcl1, Cxcl2, Cxcl5, Cxcl13, Cxcl17, Ccr6, Cxcr2,* and *Cxcr5,* were significantly upregulated in palate compared to dorsal skin and small intestine **(Fig. 3.5 and Fig. 3.6)**. *Ccl2, Cxcl12, Cxcl14, Ccr2, Ccr3, Ackr2,* and *Ackr3* were significantly upregulated in palate and skin compared to small intestine **(Fig. 3.4, Fig. 3.5, and Fig. 3.6)**. *Ccl5, Ccl28, Cxcl4, Cxcl5,* and *Ccr1* were upregulated in palate and small intestine compared to skin intestine **(Fig. 3.4, Fig. 3.5, and Fig. 3.6)**. The T cell chemo-attractants *Ccl25* and *Ccl27* exhibited low expression in murine palate and significantly upregulated in small intestine and skin respectively **(Fig. 3.4)**. *Ccl19, Ccl6, Ccl11* and *Cxcl16* were highly expressed in all tissues and did not exhibit differential levels of expression **(Fig. 3.3)**.

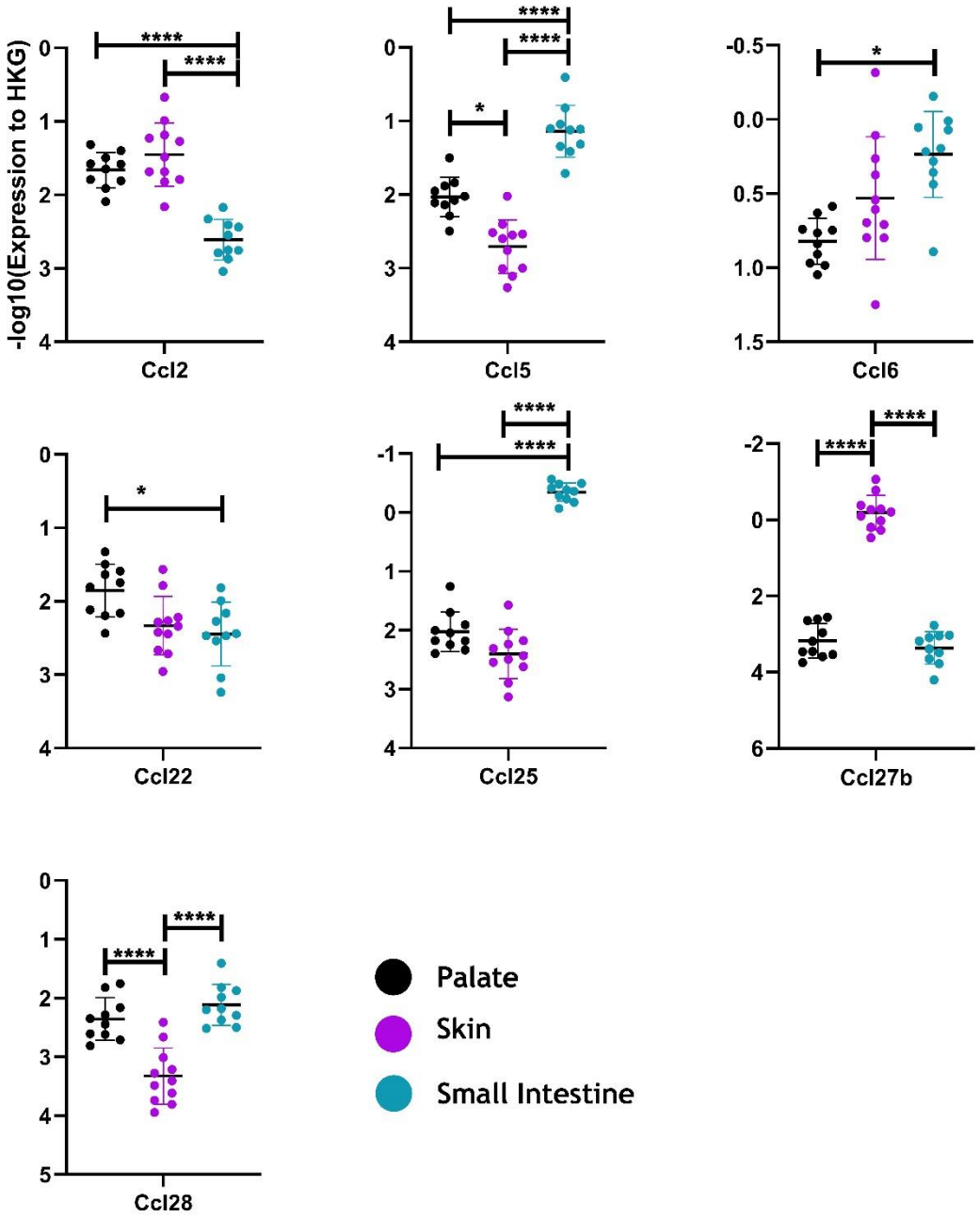

Figure 3. 4 Significantly differentially expressed C-C chemokines between murine barrier tissue

RNA isolated from murine palate (n=10), skin (n=10) and small intestine (n=10) was reverse transcribed and analysed using a Custom Qiagen RT2 Profiler Array. Expression was measured relative to the average of three HKGs, and log transformed. The black line represents the mean expression, and the error bars the standard deviation of the mean. Significance was determined using a 2way ANOVA and corrected using Tukey's multiple comparisons test. *(P≤0.05), **(P≤0.01), ***(P≤0.001), ****(P≤0.0001).

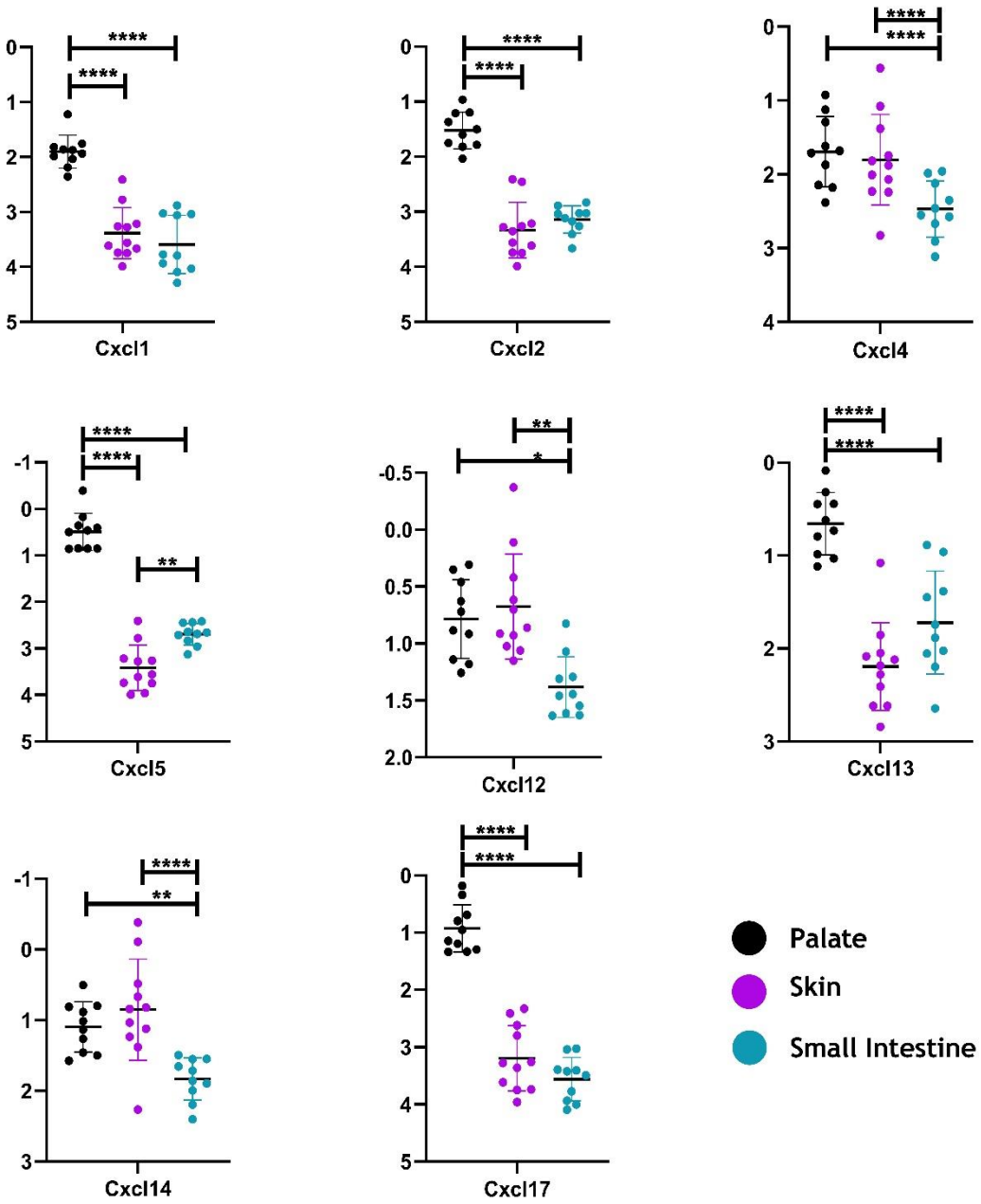

Figure 3. 5 Significantly differentially expressed C-X-C chemokines between murine barrier tissues

RNA isolated from murine palate (n=10), skin (n=10) and small intestine (n=10) was reverse transcribed and analysed using a Custom Qiagen RT2 Profiler Array. Expression was measured relative to the average of three HKGs, and log transformed. The black line represents the mean expression, and the error bars the standard deviation of the mean. Significance was determined using a 2way ANOVA and corrected using Tukey's multiple comparisons test. *(P≤0.05), **(P≤0.01), ***(P≤0.001), ****(P≤0.0001).

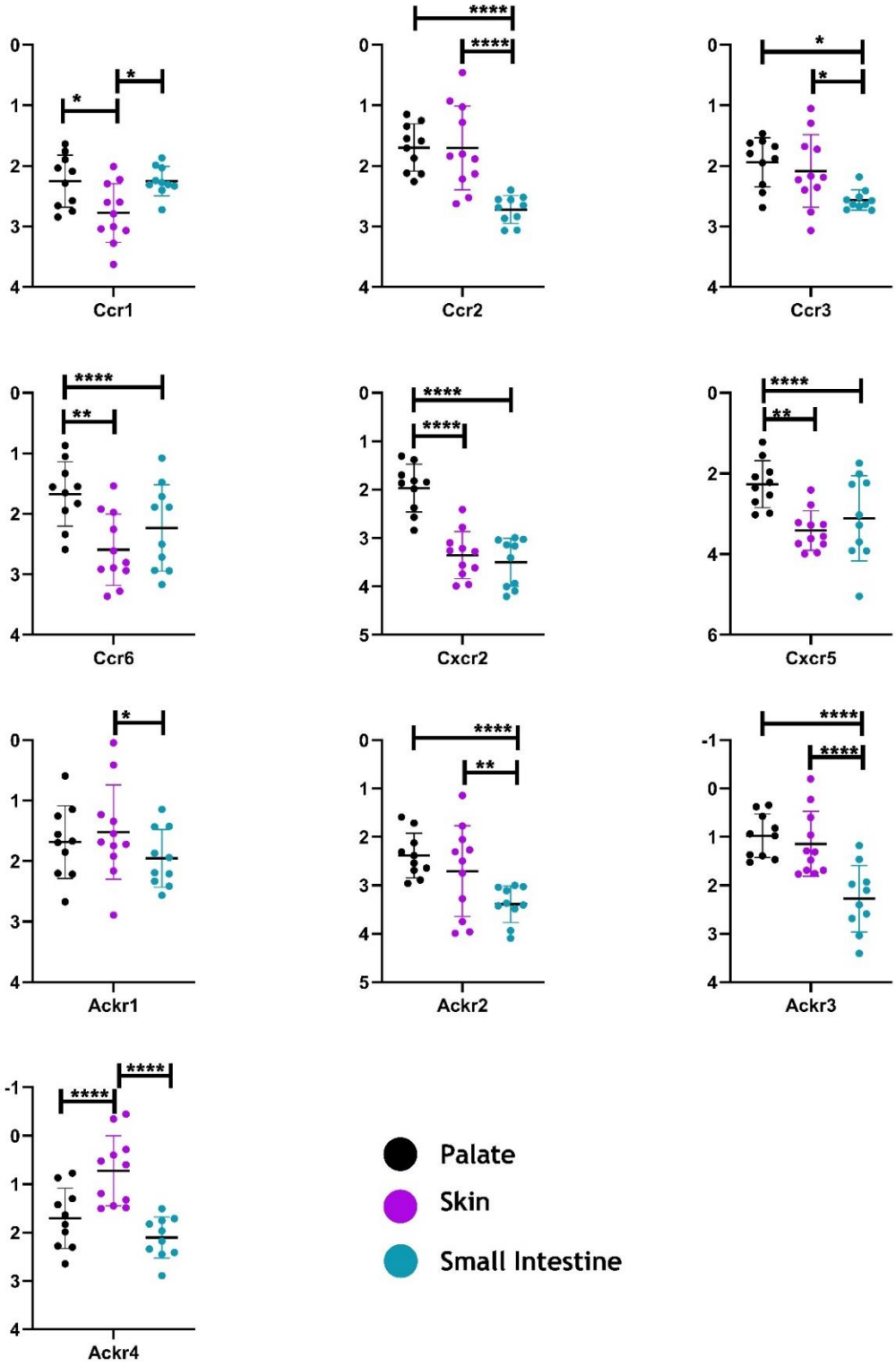

Figure 3. 6 Significantly differentially expressed chemokine receptors between murine barrier tissues

RNA isolated from murine palate (n=10), skin (n=10) and small intestine (n=10) was reverse transcribed and analysed using a Custom Qiagen RT2 Profiler Array. Expression was measured relative to the average of three HKGs, and log transformed. The black line represents the mean expression, and the error bars the standard deviation of the mean. Significance was determined using a 2way ANOVA and corrected using Tukey's multiple comparisons test. *(P≤0.05), **(P≤0.01), ***(P≤0.001), ****(P≤0.0001).

3.2.2.4 Principal component analysis

Principle component analysis was used to determine if differences in chemokine and chemokine receptor expression lead to clustering of samples. Principal component 1 accounted for 20.45% of the variance between samples, and palatal tissue clustered separately from both skin and small intestine. Principal component 2 accounted for 18.14% of the sample variance and all three tissues clustered separately. These findings suggested a distinct chemokine and chemokine receptor expression profile is present in palate, skin, and small intestine tissue **(Fig. 3.7)**.

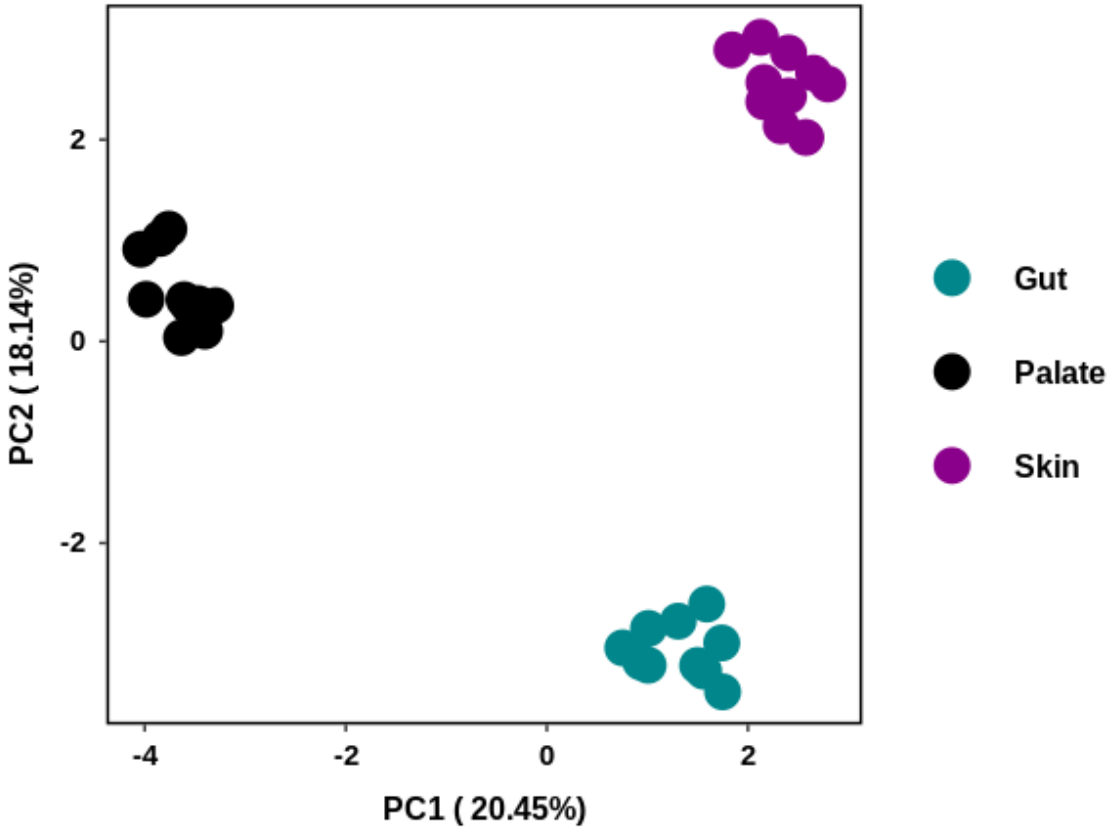

Figure 3. 7 Principal component analysis of chemokines in murine barrier tissue

RNA isolated from murine palate (n=10), skin (n=10) and small intestine (n=10) was reverse transcribed and analysed using a Custom Qiagen RT2 Profiler Array. Expression was measured relative to the average of three housekeeping genes. Expression was scaled and Z-score of components determined using R prior to principal component analysis.

In all these data show that the chemokine and chemokine receptor landscape in murine oral mucosa is distinct from murine skin and gut, but some chemokines have similar expression patterns in all three tissues. From these analyses, *Cxcl12* and its signalling and scavenging receptors *Cxcr4* and *Ackr3* are highly expressed in murine palate, as were *Cxcl14* and *Cxcl17*. The chemokine receptor *Cxcr2* and its ligands *Cxcl1, Cxcl2* and *Cxcl5* were also prominent in palate. In addition *Cxcl13* and its primary signalling receptor, *Cxcr5* were also highly expressed.

3.2.3 The spatial position of homeostatic chemokines in murine barrier tissue

To identify the spatial position of *Cxcl12, Cxcl14, Cxcl17, Cxcr4* and *Ackr3* the in-situ hybridisation platform RNA Scope was used. These transcripts were selected for further investigation due to our limited insight into their role in the gingiva. Here we analysed the spatial expression patterns of these transcripts in barrier tissue of three B6 female mice.

Cxcl12 demonstrated expression in palate, skin, and small intestine. Expression was focused in the lamina propria of palate and small intestine, and the dermis of murine skin. Spatial expression patterns of *Cxcl12* were consistent between barrier tissues **(Fig. 3.8 G, H, I)**.

Cxcl14 was expressed in all barrier tissues. In palate it was primarily expressed at the basement membrane of the epithelium. In skin *Cxcl14* expression was focused around the hair follicles and in small intestine expression was restricted to the lamina propria **(Fig. 3.8 J, K, L)**.

Cxcl17 in contrast only exhibited expression in palatal tissue. In palatal tissue *Cxcl17* expression was restricted to the periosteum, no expression was detected in the lamina propria or the epithelium **(Fig. 3.8 M, N, O)**.

In contrast, chemokine receptor expression was less distinct. *Cxcr4* had a weak signal in palate, skin, and small intestine, but the expression pattern mimicked that of *Cxcl12* in all tissues. In palate and small intestine *Cxcr4* was expressed in the lamina propria, and in skin expression was focused in the dermis. **(Fig. 3.9 G, H, I)**.

Ackr3 was detectable in the epithelium and lamina propria of murine palate. In skin *Ackr3* was expressed in the epidermis and in the small intestine *Ackr3* expression was focused in the lamina propria **(Fig. 3.9 J, K, L)**.

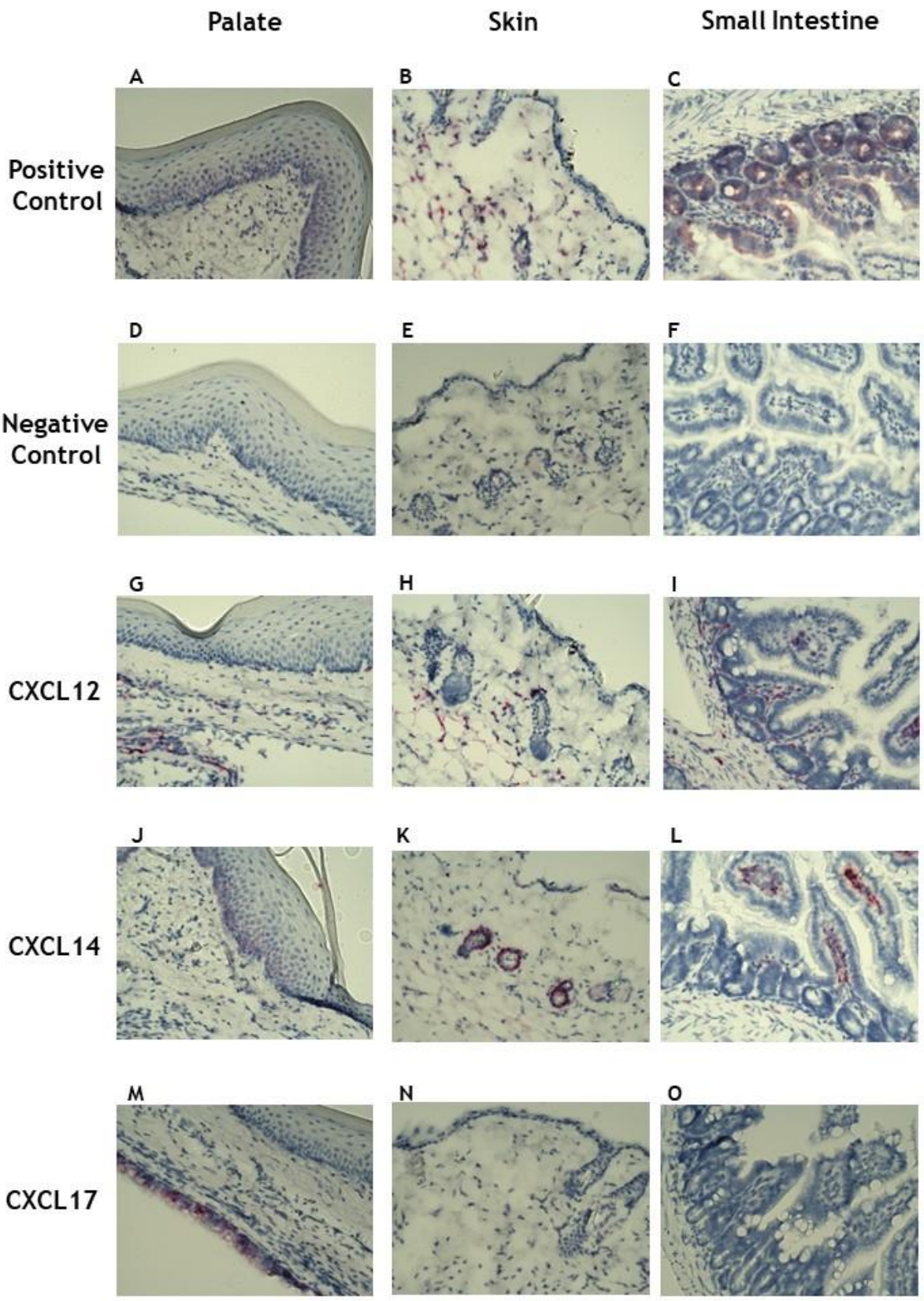

Figure 3.8 legend overleaf

Figure 3.8 Spatial position of chemokine ligand transcripts

Palate, skin, and gut tissue was harvested from 9-week-old female C57BL/6J mice. Harvested tissue was FFPE and treated with RNAScope 2.5 HD Assay-RED kit and the appropriate RNAScope probes prior to imaging with a microscope at 20 x magnification. (**A)** Palatal tissue stained with *Ppib* positive control probe. **(B)** Skin tissue stained with *Ppib* positive control probe. **(C)** Small intestine tissue stained with *Ppib* positive control probe. **(D)** Palatal tissue stained with *DapB* negative control probe. **(E)** Skin tissue stained with *DapB* negative control probe. **(F)** Small intestine tissue stained with *DapB* negative control probe. **(G)** Palatal tissue stained with *Cxcl12* probe. **(H)** Skin tissue stained with *Cxcl12* probe. **(I)** Small intestine tissue stained with *Cxcl12* probe. **(J)** Palatal tissue stained with *Cxcl14* probe. **(K)** Skin tissue stained with *Cxcl14* probe. **(L)**Small intestine tissue stained with *Cxcl14* probe. **(M)** Palatal tissue stained with *Cxcl17* probe. **(N)** Skin tissue stained with *Cxcl17* probe. **(L)** Small intestine tissue stained with *Cxcl17* probe.

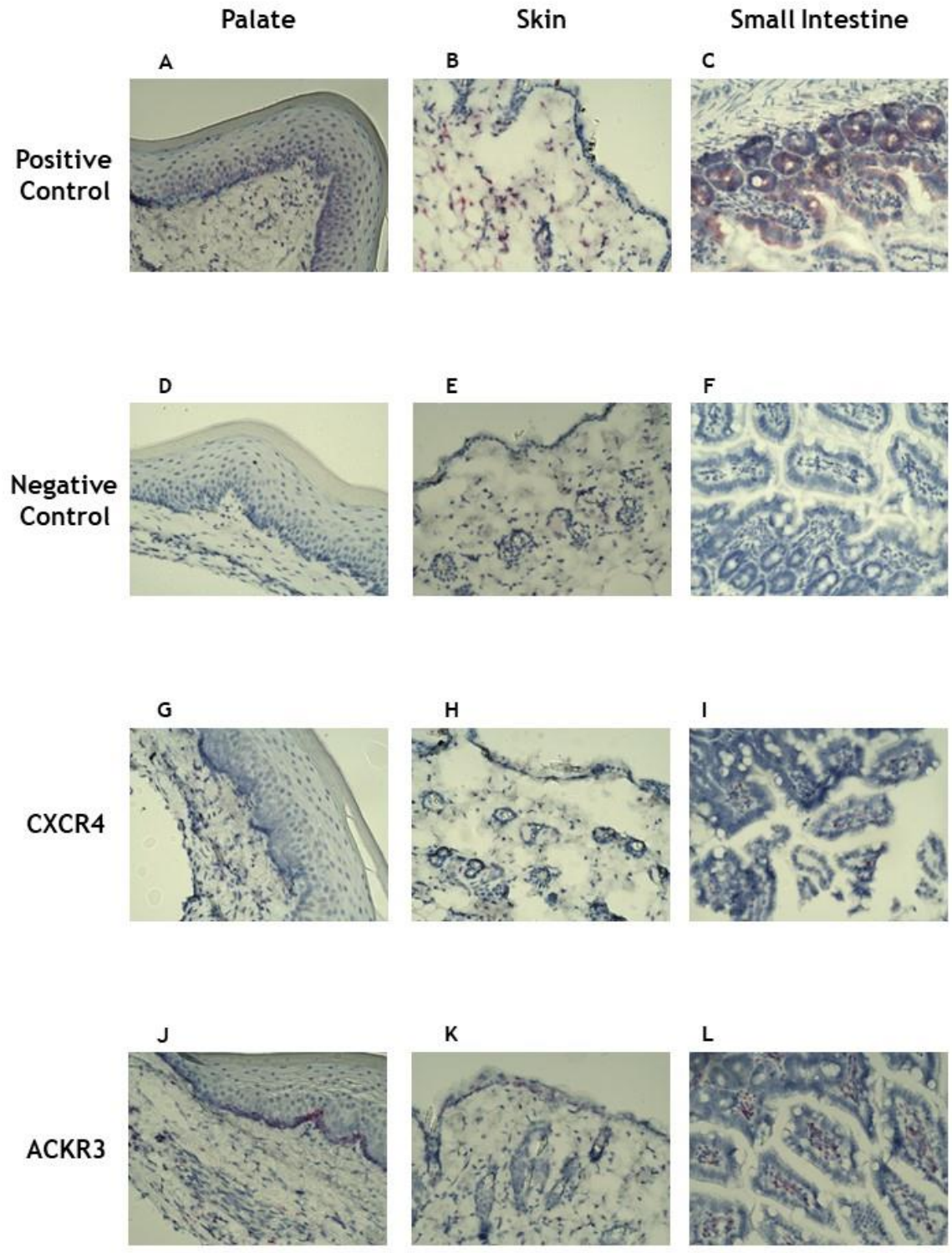

Figure legend overleaf

Figure 3. 9 Spatial position of chemokine receptor transcripts

Palate, skin, and gut tissue was harvested from 9-week-old female C57BL/6J mice. Harvested tissue was FFPE and treated with RNAScope 2.5 HD Assay-RED kit and the appropriate RNAScope probes prior to imaging with a microscope at 20x magnification. (**A)** Palatal tissue stained with *Ppib* positive control probe. **(B)** Skin tissue stained with *Ppib* positive control probe. **(C)** Small intestine tissue stained with *Ppib* positive control probe. **(D)** Palatal tissue stained with *DapB* negative control probe. **(E)** Skin tissue stained with *DapB* negative control probe. **(F)** Small intestine tissue stained with *DapB* negative control probe. **(G)** Palatal tissue stained with *Cxcr4* probe. **(H)** Skin tissue stained with *Cxcr4* probe. **(I)** Small intestine tissue stained with *Cxcr4* probe. **(J)** Palatal tissue stained with *Ackr3* probe. **(K)** Skin tissue stained with *Ackr3* probe. **(L)** Small intestine tissue stained with *Ackr3* probe.

These data describe the transcriptional landscape of chemokine and chemokine receptor expression and the spatial expression of *Cxcl12, Cxcl14, Cxcl17, Cxcr4 and Ackr3* in murine barrier tissues.

3.2.4 Chemokine concentrations in murine barrier tissue and lymph node

Next, chemokine and chemokine receptor protein concentrations were determined, in palate, small intestine, skin, and lymph node. These studies sought to assess similarities and differences in chemokine concentrations between tissues and to determine if these findings reflected those observed at the transcriptional level.

Tissue protein lysates were generated from murine barrier tissues. To provide sufficient tissue lysate for all downstream analysis each tissue sample was pooled from four mice for an n = 1. Protein at consistent concentration, suitable for downstream analysis was obtained from tissue lysates **(Fig. 3.10).** Small intestine tissue had the highest total protein concentration, whilst skin, plate and lymph node lysates had similar concentrations.

To determine the concentration of chemokines in tissue lysates a combination of single analyte ELISAs and a 16-plex LUMINEX from R&D systems were used.

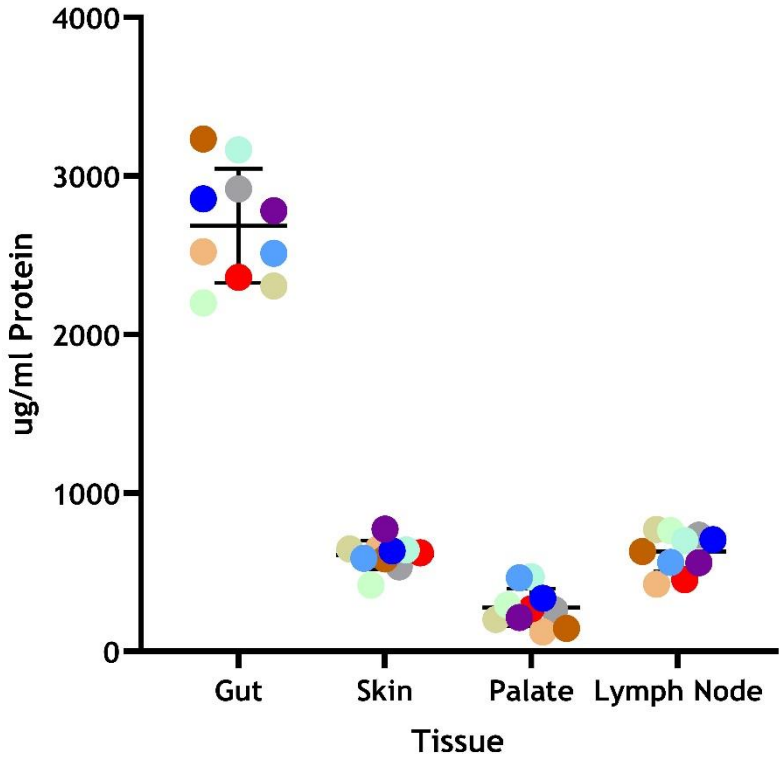

Figure 3. 10 Protein concentration in murine tissue

Small intestine, skin, palate, and lymph node tissues were harvested from 40 7-week-old female C57BL/6J mice. Each dot represents one sample, which was formed by combining the respective tissue from four mice to give an n = 1. Each tissue has an n = 10. Tissue was lysed and protein isolated. Protein concentration of each sample was determined by Pierce BCA Protein Assay, following the manufacturers instruction. Samples were interpolated against the Bovine-Serum Albumin standards using Graph-pad prism software. The black line represents the mean expression, and the error bars the standard deviation of the mean.

Chemokine concentrations in each sample were standardised per milligram of total protein, allowing for comparison between tissues. In murine palate CXCL1, CCL2, CXCL13, CCL5, CCL4, CCL20, CXCL12 and CCL2 were detected. CCL19, CXCL1, CXCL2 and CXCL16, chemokines that demonstrated very high levels of expression transcriptionally in murine palate, were not detected on the LUMINEX assay (**Fig. 1.11**). In murine palate CCL2, CCL5 and CXCL13 had significantly higher concentration when compared to skin, small intestine, and lymph node (**Fig. 1.12**).

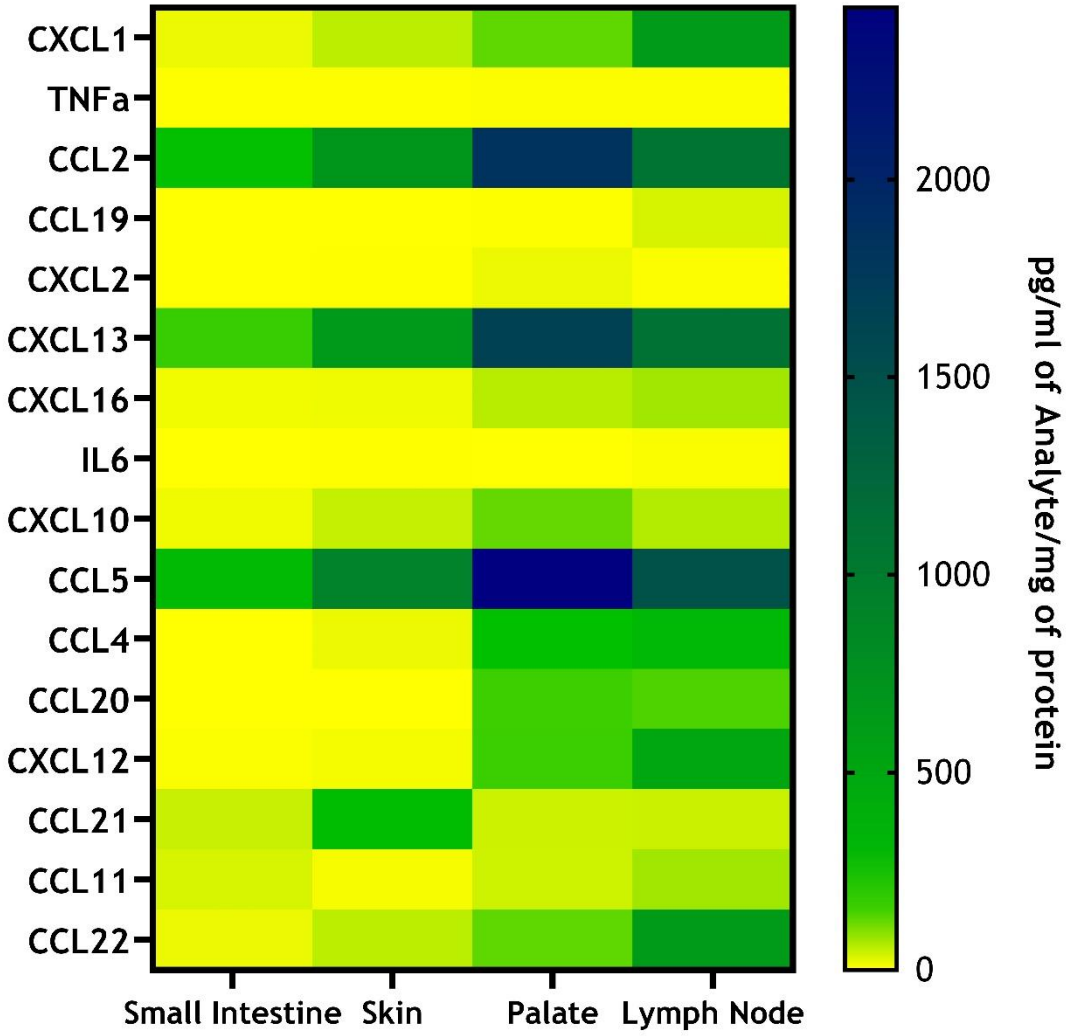

Figure 3. 11 Heatmap of chemokine protein concentration in murine barrier tissues

Small intestine, skin, palate, and lymph node tissues were harvested from 40 7-week-old female C57BL/6J mice. Each dot represents one sample, which was formed by combining the respective tissue from four mice to give an n = 1. Each tissue has an n = 10. Tissue was lysed and protein isolated. Protein concentration of each sample was determined by Pierce BCA Protein Assay, following the manufacturers instruction. Chemokine ligand concentrations were determined using a R&D system Custom Magnetic Mouse LUMINEX Assay. Chemokine concentrations were determined by interpolating the Mean Fluorescence Intensity (MFI) of the sample analytes relative to the known standards. Chemokine concentration was then standardised per mg of protein, as determined by BCA analysis. The mean value of each analyte is represented as a colour in a heatmap.

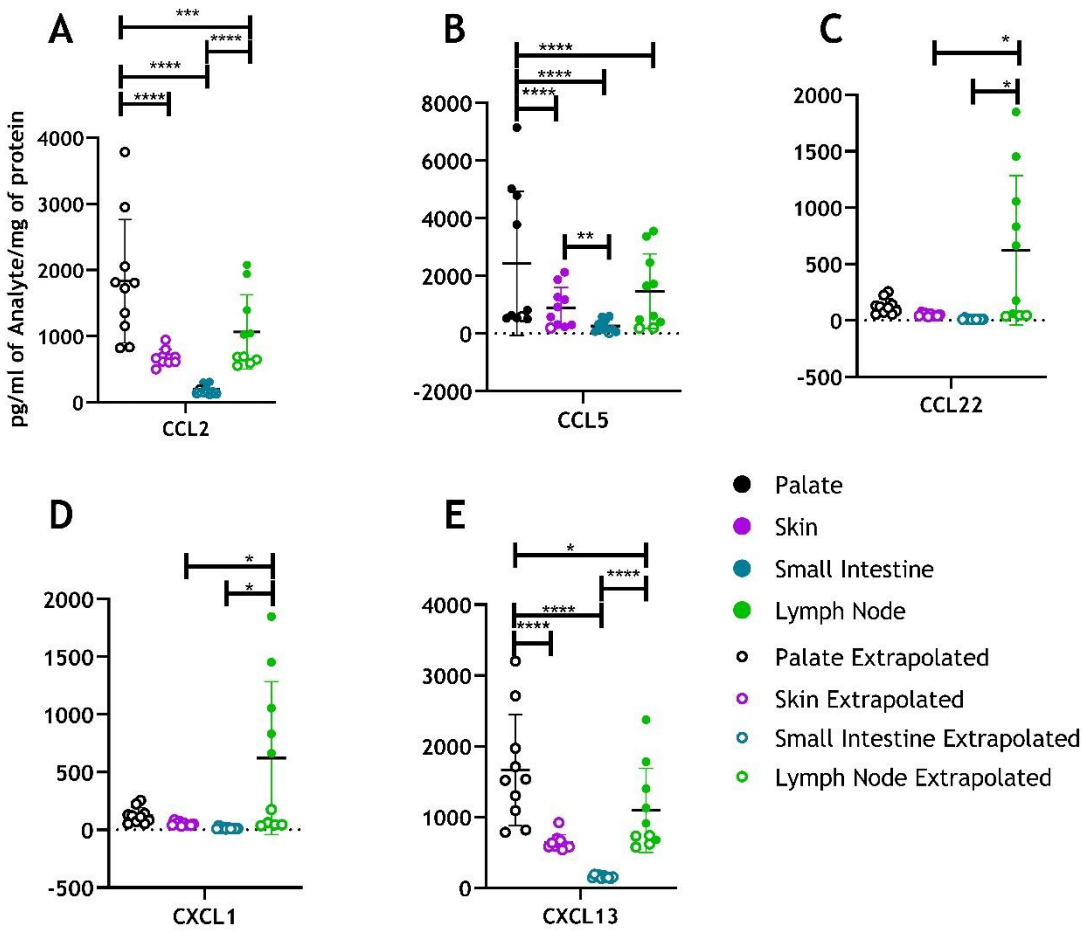

Figure 3. 12 Dot plot of significantly differentially expressed chemokines in murine barrier tissue

Small intestine, skin, palate, and lymph node tissues were harvested from 40 7-week-old female C57BL/6J mice. Each dot represents one sample, which was formed by combining the respective tissue from four mice to give an n = 1. Each tissue has an n = 10. Tissue was lysed and protein isolated. The protein concentration of each sample was determined by a Pierce BCA Protein Assay, following the manufacturers instructions. Chemokine ligand concentrations were determined using a R&D system Custom Magnetic Mouse LUMINEX Assay. Chemokine concentrations were determined by interpolating the Mean Fluorescence Intensity (MFI) of the sample analytes relative to the known standards. Chemokine concentration was then standardised per mg of protein, as determined by BCA analysis. **(A)** CCL2 protein expression in murine barrier tissue. **(B)** CCL5 protein expression in murine barrier tissue. **(C)** CCL22 protein expression in murine barrier tissue. **(D)** CXCL1 protein expression in murine barrier tissue. **(E)** CXCL13 protein expression in murine barrier tissue. Solid dots represent samples where the concentration was interpolated from the standard curve, rings represent samples that had fluorescence below the limit of detection and were extrapolated from the standard curve. The black line represents the mean expression, and the error bars the standard deviation of the mean. *(P≤0.05), **(P≤0.01), ***(P≤0.001), ****(P≤0.0001).

Supplemental ELISAs were performed for CCL6, CCL25, CCL27, CCL28, CXCL4, and CXCL14 as they were not available on the LUMINEX assay. All these chemokines were detected. Reflecting the transcriptional findings CCL25 had higher expression in small intestine, than all other tissues analysed. In contrast, CCL27 was most highly expressed in small intestine, rather than skin. CXCL14 was detected in all tissues. CXCL4 had higher expression in palate compared to other barrier tissue. CCL6 was detectable in all tissues, however, was significantly more highly expressed in small intestine **(Fig. 3.13).**

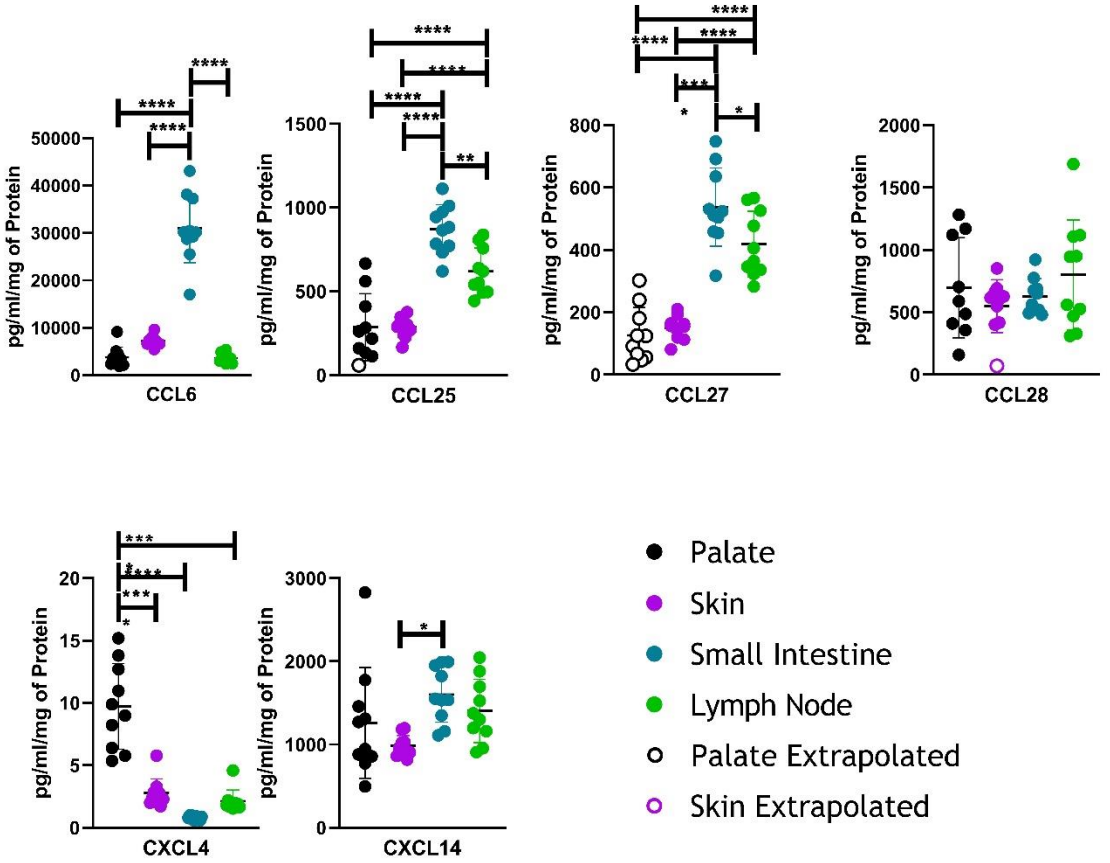

Figure 3.13 Chemokine protein concentration in murine barrier tissues measured by ELISA

Small intestine, skin, palate, and lymph node tissues were harvested from 40 7-week-old female C57BL/6J mice. Each dot represents one sample, which was formed by combining the respective tissue from four mice to give an n = 1. Each tissue has an n = 10. Tissue was lysed and protein isolated. The protein concentration of each sample was determined by using a Pierce BCA Protein Assay, following the manufacturers instruction. Chemokine ligand concentrations were determined using a R&D system Custom Magnetic Mouse LUMINEX Assay. Chemokine concentrations were determined by interpolating the Mean Fluorescence Intensity (MFI) of the sample analytes relative to the known standards. Chemokine concentration was then standardised per mg of protein, as determined by BCA analysis. Chemokine ligand concentrations were determined using a R&D system DuoSet or Quantikine ELISA kits. Chemokine concentrations

Figure 3.13 continued

were determined by interpolating wavelength and blank corrected absorbance against that of the know standard. Chemokine concentration was then standardised per mg of protein, as determined by BCA analysis. **(A)** CCL6 protein expression in murine barrier tissue. **(B)** CCL25 protein expression in murine barrier tissue. **(C)** CCL27 protein expression in murine barrier tissue. **(D)** CCL28 protein expression in murine barrier tissue. **(E)** CXCL4 expression in murine barrier tissue. **(F)** CXCL14 protein expression in murine barrier tissue. Solid dots represent samples where the concentration was interpolated from the standard curve, rings represent samples that had fluorescence below the limit of detection and were extrapolated from the standard curve. The black line represents the mean expression, and the error bars the standard deviation of the mean. *(P≤0.05), **(P≤0.01), ***(P≤0.001), ****(P≤0.0001).

3.3 Discussion

These data provide the most comprehensive overview to date of the transcriptional and protein expression of chemokine ligands and receptors in murine palate. It shows the chemokine landscape in palate is unique compared to skin and small intestine. Furthermore, highly expressed homeostatic chemokines have distinct expression patterns in murine palate.

These initial studies show that multiple chemokines are expressed in murine palate, including homeostatic, inflammatory, and dual chemokines. Whilst it may be surprising to see inflammatory chemokines to be present in uninflamed oral tissues, this may be reflective of the continued need for immunosurveillance given the constant exposure to masticatory forces, food, and airborne antigens as well as microbial insult (Moutsopoulos and Konkel, 2018).

High transcriptional expression of homeostatic and dual chemokines including *Cxcl12, Cxcl13, Cxcl14* and *Cxcl17* was observed in murine palate. As previously mentioned, homeostatic chemokines direct cells to specific sites out with the context of inflammation and are often tissue specific, this suggests these may play an important role in maintaining homeostasis in the oral cavity.

Data from both RT^2 Profiler Arrays show the homeostatic chemokine, *Cxcl12* and its receptor *Cxcr4*, are highly expressed murine gingiva. Due to its wide range of functions, suggested role in cancer development and being indispensable to

development CXCL12 has been studied extensively (Portella, Bello and Scala, 2021; Janssens, Struyf and Proost, 2018). CXCL12 is highly conserved and is essential for successful embryonic development (Nagasawa *et al.*, 1996). It plays crucial roles in stem cell migration during embryogenesis and stem cell retention in bone marrow, lymphopoiesis and angiogenesis in the adult animal (DeVries *et al.*, 2006; Janssens, Struyf and Proost, 2018). Furthermore, the CXCL12-CXCR4 axis has been shown to promote MSC mobilisation. Given the potent MSC populations in oral mucosa this axis may have a similar role in gingival tissue, encouraging gingival regeneration and wound healing (Krishnan *et al.*, 2021; Hu *et al.*, 2013; Zhang *et al.*, 2012).

The other known chemokine receptor for CXCL12 is the atypical chemokine receptor ACKR3 which was also highly expressed in mouse (Murphy and Heusinkveld, 2018). Atypical chemokine receptors do not signal through typical G protein pathways and their primary function is to regulate chemokine availability within tissues, through internalisation and degradation of chemokine ligand. It has also been shown that ACKR3 is capable of heterodimerizing with CXCR4, thus modifying the cellular response to CXCL12 (Nibbs and Graham, 2013). ACKR3 therefore represents an important regulator of the CXCL12/CXCR4 interaction and provides an essential third arm to this axis.

In addition to binding CXCL12, CXCR4 is also capable of binding to CXCL14, but the latter does not induce downstream signalling (Collins *et al.*, 2017). Whilst no signalling chemokine receptor has been identified for CXCL14, it has been shown to potentiate CXCL12-CXCR4 directed cell migration through conformational change or dimer formation of CXCR4 *in vitro* (Collins *et al.*, 2017). In contrast other studies have shown CXCL14 to reduce CXCL12 mediated cell migration *in vitro* or to have no modulatory effect on CXCR4 (Tanegashima *et al.*, 2013; Otte *et al.*, 2014). The precise role for CXCL14 remains unknown. Like CXCL12, CXCL14 is an ancient chemokine, and its origin can be traced back at least 450 million years. CXCL14 is highly conserved amongst vertebrates and shares significant homology with its homologue in chickens and zebrafish (DeVries *et al.*, 2006). Furthermore, the semi lethal phenotype observed in CXCL14 knockout mice demonstrates it is essential in embryogenesis (Tanegashima *et al.*, 2010). There are indications that CXCL14 may influence dendritic cell precursor recruitment and macrophage development (Schaerli *et al.*, 2005).

Our data show that CXCL13 was highly expressed in palatal tissue in health and was detected at the protein level. CXCL13 is important for B cell recruitment through binding to CXCR5 (Forster *et al.*, 1996). It is likely CXCL13 assumes this role in the context in gingival tissue, given the B cell populations observed in healthy gingiva and their abundance in periodontally diseased gingiva (Nakajima *et al.*, 2008; Mahanonda *et al.*, 2016).

CXCL4 in the palate had similar expression levels to skin and was more highly expressed when compared to small intestine. At the protein level CXCL4 demonstrated significantly higher expression in palate compared to skin, small intestine and lymph node. CXCL4 is reported to protective against viral infection, aid platelet aggregation, and wound repair (Guo *et al.*, 2017; Vandercappellen, Van Damme and Struyf, 2011). Given the healing propensity of oral mucosa CXCL4 may assume a similar role in murine palate.

Interestingly CCL25 and CCL27, chemokines that are crucial for T cell homing to healthy gut and skin respectively, demonstrated low expression and the transcriptional and protein levels in murine palate (Kunkel and Butcher, 2002; Wurbel *et al.*, 2007; Xia *et al.*, 2014). This suggests that a chemokine-chemokine receptor axis distinct from skin or small intestinal tissue may regulate T cell migration to the gingiva in health and disease. This is reinforced when the chemokine expression of CCL25 and CCL27 were significantly upregulated in small intestine and skin respectively when compared to other barrier tissues in qPCR.

Advancing the concept of oral mucosa having a distinct chemokine landscape a principal component analysis of chemokine and chemokine receptor transcriptional expression shows that palatal tissue is distinct from skin and small intestine. However, there were also similarities observed between skin and small intestine. This suggests there are unique requirements for specific cell recruitment to the oral cavity, but also common features required in all three barrier tissues to maintain homeostasis.

Interestingly the highly expressed transcripts *Cxcl12, Cxcl14*, and *Cxcl17* have distinct patterns of spatial expression. *Cxcl12* expression, in palate, was focused in the lamina propria, *Cxcl14* at the basement membrane of epithelium and

Cxcl17 in the periosteum. Supporting results from the RT^2 Profiler Array data *Cxcl17* was not detected in skin or small intestine with in-situ hybridisation. CXCL17 therefore may play a role in tailoring cellular recruitment specific to maintaining oral mucosa homeostasis. Unfortunately, there is no known receptor for CXCL17, and its function is largely unknown.

An important limitation of the array-based approach is that the analytes of interest are selected specifically, introducing bias. In these studies chemokines, which demonstrated low levels of expression in the initial exploratory assay, or were not homeostatic in nature, were omitted from the array used to compare the transcriptional expression between barrier tissues. An alternative approach would be the use of RNA Sequencing, which would have reduced the risk of bias, however, this was cost prohibitive. A further limitation relates to species differences. Despite chemokines being generally well conserved between mammalian species, the chemokine CXCL8 does not exist in mice and has no functional homologue. As previously discussed, CXCL8 contributes to neutrophil chemotaxis in human gingiva, thus the murine models used do not directly replicate the human chemokine landscape, limiting the applicability of these findings to humans.

Like *Cxcl12, Cxcl14 and Cxcl17*, the chemokine receptors *Cxcr4* and *Ackr3* had differing spatial expression patterns. *Cxcr4* was mainly expressed in the lamina propria of palate, *Ackr3* was expressed at the basement membrane of the epithelium, this suggests ACKR3 may be important in regulating CXCL12 expression at the basement membrane, as they had similar spatial expression patterns. This suggests there is no single homeostatic chemokine in the oral mucosa, but multiple chemokines with differing functions. Further work is important to identify the cell types that are expressing these transcripts to elucidate the role of these homeostatic chemokines in regulating oral mucosa homeostasis.

Protein analysis reinforced that the chemokine landscape in murine palate differs from skin and small intestine, yet there were some similarities too. However, CCL19 and CXCL2 had low protein expression, despite having relatively high transcriptional expression in palatal tissue. One explanation for this is ACKR4, a scavenging receptor for CCL19, may reduce the availability of CCL19 in

tissue as ACKR4 had high transcriptional expression in palate. CCL27 demonstrated higher expression in small intestine than skin at the protein level, despite transcriptionally it's expression being significantly higher in skin and its known function in directing cells specifically to skin in health, however, CCL27 was still detected in skin. There are limitations of ELISA and LUMINEX as well as tissue preparation protocols, the assays as such may not have been sensitive enough to accurately detect differential expression, or processing methods may have impacted these chemokines specifically. Furthermore, chemokines are susceptible to post translation modification, and such variants may not have been detected on the platforms used (Vanheule *et al.*, 2018).

In conclusion this chapter has identified multiple chemokines that may play a pivotal role in maintain oral homeostasis. Specifically, the CXCL12, CXCL14, CXCR4, ACKR3 axis and CXCL17 are interesting targets. Moreover, these data show the chemokine landscape in oral mucosa is distinct from skin and small intestine, which is likely representative of the unique ecological niche. Expression patterns of CXCL12, CXCL14 and CXCL17 is restricted to specific histological sites within murine palate, suggesting each chemokine may have differing functions in oral mucosa, and finally the protein chemokine landscape reflects the transcriptional findings.

The key findings from the posed research questions for this chapter are:

- Are there quantitative differences in the chemokine and chemokine receptor gene and protein expression in murine palate compared with skin and small intestine?
    - The chemokine and chemokine receptor landscape in murine palatal mucosa is distinct from skin and small intestine, at the transcriptional and protein levels.
    - CXCL17 is uniquely highly expressed in murine palate compared to other barrier tissues.
- Which chemokines are highly expressed in murine palate in health?
    - There are multiple highly expressed chemokines in murine palatal mucosa, and in health the CXCL12/CXCL14/CXCR4/ACKR3 axis is prominently expressed in murine palatal tissue.

- Where in the tissues are chemokine and chemokine receptor transcripts expressed?
    - CXCL12, CXCL14 and CXCL17 have distinct patterns of spatial expression in murine palate

These findings support the hypothesis that the chemokine landscape in murine palatal mucosa is distinct from skin and small intestine.

Chapter 4 - The Chemokine Landscape in Periodontitis

4.1 Introduction

Chapter three demonstrated that the murine oral mucosae's chemokine and chemokine receptor landscape is unique compared with other barrier tissues. However, immune cell populations change during oral inflammation. Thus, the chemokine and chemokine receptor profiles in diseased gingiva may be different to health. Periodontitis is a highly prevalent oral immune-mediated condition with severe forms affecting 11.2% of the population (Bernabe *et al.*, 2020). The hallmark of periodontitis is alveolar bone loss mediated by the host immune response (Kwon, Lamster and Levin, 2020; Loos and Van Dyke, 2020). Furthermore, there are multiple well-described murine models of periodontitis (Baker, Evans and Roopenian, 1994; Prates *et al.*, 2014; Abe and Hajishengallis, 2013). This has led to comprehensive research identifying the changes in immune cell populations in periodontitis compared to health. There are increases in plasma cells, naïve B cells and neutrophil populations in periodontitis gingiva compared to healthy tissue, and T cells are pivotal to periodontal disease progression (Li, Zhang and Wang, 2020; Figueredo, Lira-Junior and Love, 2019). Despite these changes and their crucial role in periodontal disease pathogenesis, the mechanisms and molecules regulating cellular recruitment in periodontitis remain poorly defined. Previous work has explored several inflammatory chemokines and their role in gingival leukocyte recruitment in health compared to periodontitis.

The research to date exploring gingival chemokines has focused on the neutrophil chemo-attractants CXCL1,2 and 8. This is due to the large neutrophil infiltrate seen in the periodontium, and the role neutrophils play both in maintaining health and in disease (Hajishengallis and Hajishengallis, 2014).

These studies consistently show an elevated CXCL2 and CXCL8 expression in periodontitis. There is disagreement if CXCL1 expression increases in periodontitis compared to healthy gingiva (Greer *et al.*, 2016; Rath-Deschner *et*

al., 2020). Other chemokine ligands essential in neutrophil trafficking, such as CXCL3,5,6 and 12 have not been comprehensively analysed in the diseased periodontium (Capucetti, Albano and Bonecchi, 2020). The macrophage chemo-attractants CCL2, CCL3 and CCL5, and the B cell chemoattractant CXCL13 show higher expression in periodontitis than health, and in mouse models inhibition of CCL2 lead to decreased alveolar bone loss (Silva *et al.*, 2007; Nakajima *et al.*, 2008; Shen *et al.*, 2021).

Currently, there are indications that chemokines are important in oral mucosa function and periodontal disease pathogenesis. However, previous studies have primarily focused on single or small groups of chemokines, which may fail to account for chemokines with overlapping functions. There is little work exploring homeostatic chemokines in periodontal tissues; and there has been little comparison of the chemokine landscape between humans and mice. Mammalian species share significant transcriptional homology; however, there is limited insight into chemokine expression similarities and differences in human periodontitis and experimental periodontitis in mice, limiting the translation of mouse models.

Due to the pathogenesis, prevalence, existing mouse models and well described immune cell landscape; periodontitis is the ideal disease to identify how the chemokine landscape changes during inflammation in the oral mucosa.

Hypotheses:

- The gingival chemokine and chemokine receptor expression profile differs between health and periodontitis.
- Chemokine and chemokine receptor expression is conserved across mammalian species.

The research questions posed to investigate these hypotheses included:

- Does the expression of chemokine or chemokine receptor transcripts change between health and periodontitis in mice, non-human primates, and humans?
- Does the transcriptional expression of chemokines and chemokine receptors differ between mice, non-human primates, and humans?

4.2 Results

4.2.1 Transcriptional expression of chemokines in murine periodontitis

The chemokine landscape was explored, at different time points, in a ligature model of periodontitis: an overview of the experimental design is shown in **Figure. 4.1**. Ligature-induced bone loss was calculated by subtracting the bone loss area observed in the contra-lateral non-ligated control site from the ligated side (**Table 4.1**). There was a significant increase in ligature-induced bone loss on day ten (D10) compared to day three (D3). A non-significant increase was observed between D3 and day seven (D7) and between D7 and D10 **(Fig. 4.2).** These results confirmed that mice developed alveolar bone loss at the ligated sites and that bone loss increased over time. Mice that failed to develop measurable bone loss or where ligatures failed (D3, n=2/10; D7 n=7/10; D10 n=3/10) were excluded from downstream analysis.

RNA was purified from ligated and contra-lateral control gingiva from D3, D7 and D10 timepoints. Gingivae from five mice served as non-ligated controls. RNA concentration was determined by absorbance at A260 and purity by 260:280 and 260:230 absorbance ratios. RINs were obtained from ten samples, to ensure RNA isolation methods were adequate. One sample did not yield suitable RNA and was omitted from subsequent assessment and analysis **(Table 4.2).**

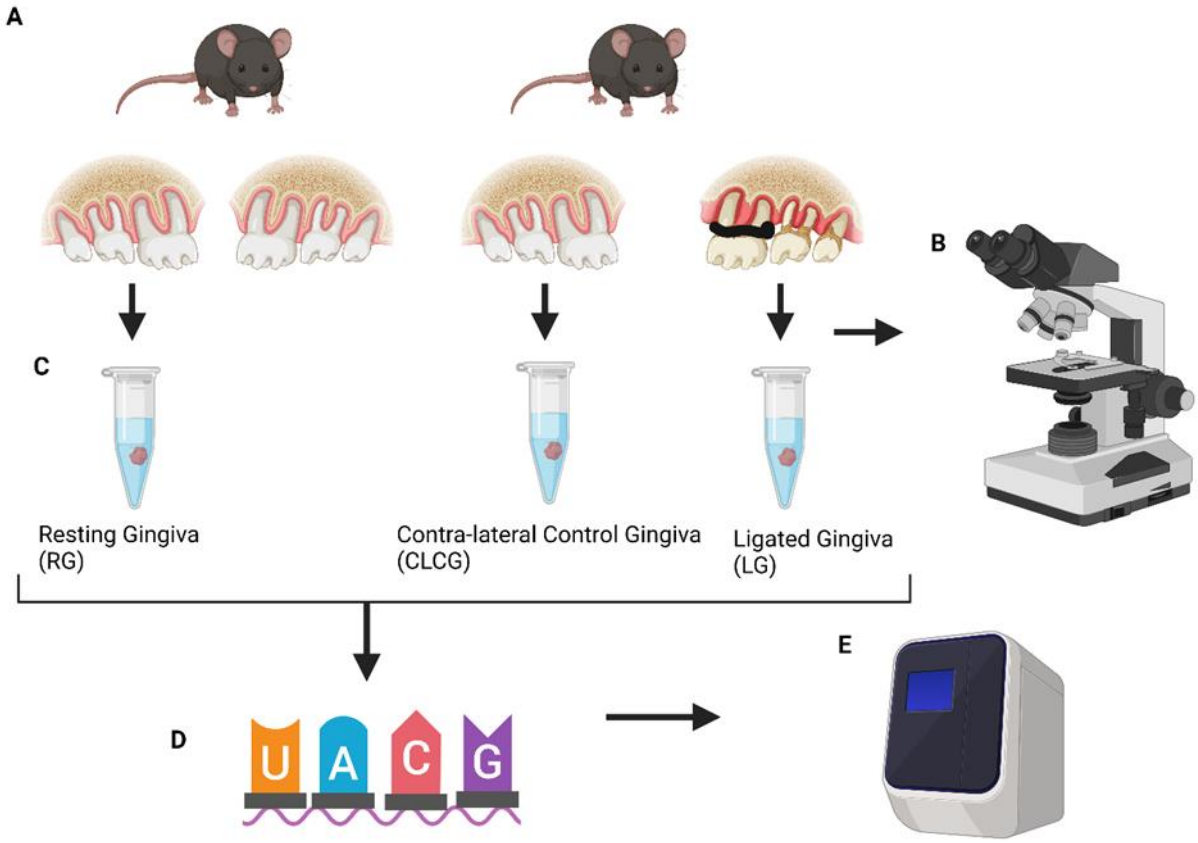

Figure 4. 1 Ligature-induced periodontitis experimental outline

(A) A ligature was applied to the left maxillary first molar (LG), the right maxillary first molar was not ligated (CLCG), and ligatures were left in situ for three, seven and ten days. As a control, five mice had no ligature applied (RG). At the end of each time point, mice were euthanised. **(B)** Gingiva was harvested from the right and left maxilla, and alveolar bone loss was measured at the ligated and control sites. **(C)** Harvested tissue was stored in RNA later at -80^{O}C. **(D)** RNA was isolated from gingiva and reverse transcribed. **(E)** Chemokine and chemokine receptor expression were determined by qPCR. Figure created with BioRender.com.

Mouse	Control Alveolar Bone Loss (mm^2)	Ligature induced alveolar bone loss (mm^2)	Relative Ligature induced alveolar bone loss (mm^2)
Day 3			
D3 M1	0.200	0.234	0.034
D3 M2	0.214	0.252	0.038
D3 M3	0.169	0.196	0.027
D3 M4	0.203	0.251	0.048
D3 M5	0.173	0.200	0.027
D3 M6	0.187	0.202	0.015
D3 M7	0.169	0.236	0.067
D3 M8	0.213	0.247	0.034
D3 M9	0.226	0.225	-0.001
D3 M10*	0.194	0.251	0.057
D3 Mean	0.195	0.229	0.035
Day 7			
D7 M1*	0.225	0.262	0.037
D7 M2*	0.243	0.435	0.192
D7 M3*		0.335	
D7 M4*	0.218		
D7 M5	0.244	0.328	0.084
D7 M6*	0.231		
D7 M7	0.217	0.295	0.078
D7 M8	0.230	0.243	0.013
D7 Mean	0.229714286	0.316333333	0.0808
Day 10			
D10 M1*	0.196		
D10 M2	0.265	0.362	0.097
D10 M3	0.201	0.311	0.11
D10 M4	0.395	0.430	0.035
D10 M5	0.195	0.391	0.196
D10 M6	0.180	0.405	0.225
D10 M7	0.202	0.313	0.111
D10 M8*	0.247		
D10 M9	0.211	0.201	-0.01
D10 M10	0.250	0.399	0.149
D10 Mean	0.2342	0.3515	0.114125

Table 4. 1 Ligature induced alveolar bone loss

Table showing the root surface area of maxillary first molar surface palatal roots between the CEJ and alveolar crest. Measurements were taken from ligated gingiva and contra-lateral control gingiva teeth. The control surface area was subtracted from the ligated surface area to give the relative alveolar bone loss. * denotes samples that bone loss measurements were not obtained from.

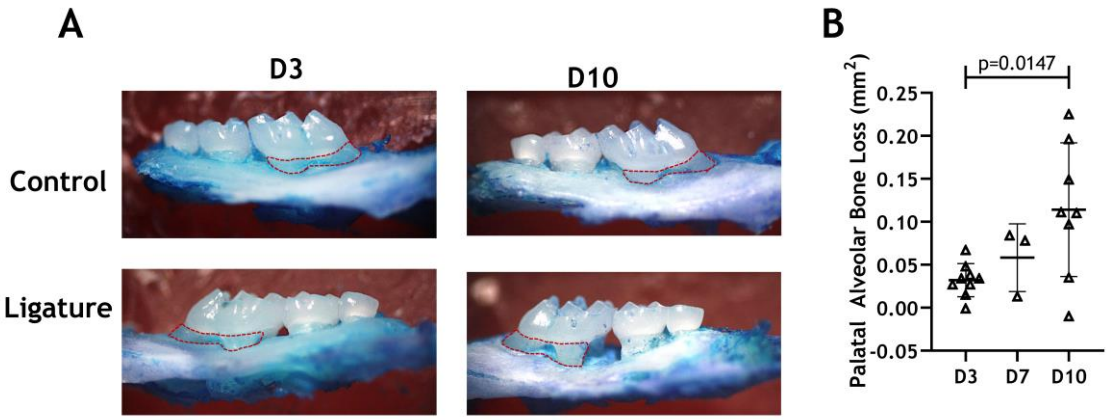

Figure 4. 2 Measurement of ligature induced alveolar bone loss

Ligatures were placed around the left maxillary first molar teeth (LG). The contralateral tooth served as control (CLCG). A further control group had no ligature (RG) (n=5). On day three (D3), day seven (D7) and day ten (D10), mice were culled, gingival tissue collected, and bone loss measured (n=10 mice/group/time point). **(A)** Representative alveolar bone loss following ligature application compared with controls, the red line identifies the area measured in bone loss analysis. **(B)** Bone loss area relative to contralateral control at D3 (n = 9), D7 (n = 3) and D10 (n = 8). Data shown are median and inter-quartile ranges, analysed by unpaired t-test and corrected for multiple comparisons.

Sample	Control or Ligature	Conc. ng/µl	A260:280	A260:230	RIN	Suitable for Profiler Array	RT2 Quality Control
D3 M1	Ligature	280.8	2.073	1.455	10	Yes	Pass
D3 M1	Control	312.7	2.069	2.108	9.90	Yes	Pass
D3 M2	Ligature	139.5	2.054	0.501	9.50	Yes	Pass
D3 M2	Control	190.6	2.069	1.618	NA	Yes	Pass
D3 M3	Ligature	147	2.054	2.046	NA	Yes	Pass
D3 M3	Control	338.4	2.077	1.601	10	Yes	Pass
D3 M4	Ligature	138	2.059	1.801	NA	Yes	Pass
D3 M4	Control	235.5	2.067	2.272	NA	Yes	Pass
D3 M5	Ligature	238.3	2.079	1.749	NA	Yes	Pass
D3 M5	Control	230.2	2.039	2.271	NA	Yes	Pass
D3 M6	Ligature	283.4	2.060	2.196	NA	Yes	Pass
D3 M6	Control	181.6	2.083	1.161	9.80	Yes	Pass
D3 M7	Ligature	310.5	2.064	1.916	NA	Yes	Pass
D3 M7	Control	173.1	2.065	1.202	9.90	Yes	Pass
D3 M8	Ligature	198.2	2.047	1.777	NA	Yes	Pass
D3 M8	Control	134.8	2.063	0.919	9.60	Yes	Pass
D3 M9	Ligature	75.6	1.993	0.625	8.50	Yes	Pass
D3 M9	Control	315.9	2.064	2.072	NA	Yes	Pass
D3 M10	Ligature	302.8	2.077	1.873	NA	Yes	Pass
D3 M10	Control	155.2	2.039	1.878	NA	No: Ligature not in-situ at schedule 1	Pass
D7 M1	Ligature	190.7	2.057	1.753	NA	No: Ligature not in-situ at schedule 1	Pass
D7 M1	Control	224.2	2.065	2.044	NA	No: Ligature not in-situ at schedule 1	Pass
D7 M2	Ligature	307.3	2.081	2.136	NA	No: Ligature not in-situ at schedule 1	Pass
D7 M2	Control	170.3	2.049	1.969	NA	No: Ligature not in-situ at schedule 1	Pass
D7 M3	Ligature	119.0	2.041	0.582	8.90	Yes	Pass

Sample	Control or Ligature	Conc. ng/µl	A260:280	A260:230	RIN	Suitable for Profiler Array	RT2 Quality Control
D7 M3	Control	277.8	2.062	2.022	NA	No: Ligature not in-situ at schedule 1	Pass
D7 M4	Ligature	208.6	2.045	2.052	NA	Yes	Pass
D7 M4	Control	266.9	2.086	1.854	NA	Yes	Pass
D7 M5	Ligature	455.1	2.078	1.893	NA	Yes	Pass
D7 M5	Control	284.6	2.062	1.893	NA	Yes	Pass
D7 M6	Ligature	387.5	2.080	1.912	NA	Yes	Pass
D7 M6	Control	103.7	2.000	1.773	NA	Yes	Pass
D7 M7	Ligature	342.4	2.077	2.080	NA	Yes	Pass
D7 M7	Control	53.857	1.995	0.624	NA	Yes	Pass
D7 M8	Ligature	275.1	2.066	1.757	NA	Yes	Pass
D7 M8	Control	154.4	2.065	1.963	NA	Yes	Pass
D7 M9	Ligature	170.0	2.070	0.679	NA	No: Ligature not in-situ at schedule 1	Pass
D7 M9	Control	170.1	2.071	1.008	NA	No: Ligature not in-situ at schedule 1	Pass
D7 M10	Ligature	11.585	1.528	0.574	NA	No: Low RNA concentration	Pass
D7 M10	Control				NA	No: Sample missing	NA
D10 M1	Ligature	150.0	2.007	1.141	NA	No: Ligature not in-situ at schedule 1	Pass
D10 M1	Control	232.633	2.04	1.98	NA	No: Ligature not in-situ at schedule 1	Pass
D10 M2	Ligature	200.320	1.201	2.069	NA	Yes	Pass
D10 M2	Control	285.423	2.055	2.124	NA	Yes	Pass
D10 M3	Ligature	86.675	2.035	0.598	NA	Yes	Pass
D10 M3	Control	102.934	1.996	1.549	NA	Yes	Pass
D10 M4	Ligature	265.776	2.088	1.304	NA	Yes	Pass
D10 M4	Control	247.033	2.047	1.326	NA	Yes	Pass
D10 M5	Ligature	258.577	2.046	2.337	NA	Yes	Pass

Sample	Control or Ligature	Conc. ng/µl	A260:280	A260:230	RIN	Suitable for Profiler Array	RT2 Quality Control
D10 M5	Control	167.546	2.049	0.750	NA	Yes	Pass
D10 M6	Ligature	148.128	2.071	0.382	NA	Yes	Pass
D10 M6	Control	117.847	2.035	1.296	NA	Yes	Pass
D10 M7	Ligature	91.833	1.966	1.272	NA	Yes	Pass
D10 M7	Control	162.151	2.036	1.997	NA	Yes	Pass
D10 M8	Ligature	109.476	2.018	1.438	NA	No: Ligature not in-situ at schedule 1	Pass
D10 M8	Control	72.783	1.991	1.906	NA	No: Ligature not in-situ at schedule 1	Fail
D10 M9	Ligature	226.962	2.059	2.142	NA	Yes	Pass
D10 M9	Control	66.246	1.999	1.497	NA	Yes	Pass
D10 M10	Ligature	56.354	1.984	0.561	NA	Yes	Pass
D10 M10	Control	30.777	1.818	0.723	NA	Yes	Pass
H1	No Ligature Control	164.3	2.05	1.94	NA	Yes	Pass
H2	No Ligature Control	170.5	2.05	1.19	10	Yes	Pass
H3	No Ligature Control	162	2.05	1.34	9.50	Yes	Pass
H4	No Ligature Control	224.8	2.05	1.96	NA	Yes	Pass
H5	No Ligature Control	175.7	2.080	2.024	NA	No: Traumatised	Pass

Table 4. 2 Table of gingiva samples for RT2 Profiler Array

In resting gingiva (RG), from mice with no ligature applied, chemokines were readily detectable. In terms of inflammatory chemokines, there was high-level expression (expression levels above the third quartile) of *Cxcl5, Ccl6* and *Cxcl16* and lower-level expression (those with chemokine expression between the first and third quartiles) of *Ccl2, Ccl5, Ccl11* and *Cxcl2*. Of the homeostatic and dual

chemokines and those with unknown function, *Ccl19*, *Ccl20, Cxcl12*, *Cxcl13*, and *Cxcl17* were prominent, and *Ccl19* was the most highly expressed chemokine detected in RG. Expression of *Ccl22, Cxcl4* and *Cxcl14* was also detectable between the first and third quartiles. Chemokine receptor expression was generally lower than that of the chemokines. *Ackr3* displayed the highest expression level, and *Cxcr4, Ccr2* and *Ccr3* were also detectable between the median and third quartile **(Fig. 4.3).**

We evaluated chemokine expression, at the three time points, in both ligated gingiva (LG) and contralateral-control gingiva (CLCG) and compared the expression patterns between groups. Most chemokines exhibited similar levels of expression in these two groups which were also indistinguishable from those in the RG group. In both LG and CLCG *Ccl6, Ccl19, Cxcl12, Cxcl14, Cxcl16 Cxcl17* were highly expressed. Reflecting the findings in resting gingivae, *Cxcr4, Ackr3* and *Ackr4* were highly expressed in murine LG and CLCG **(Fig. 4.4)**.

A small number of chemokine and chemokine receptors were differentially expressed between CLCG, LG and RG. *Cxcl13* expression in D3 LG was significantly downregulated compared to RG and D3 CLCG. However, *Cxcl13* expression at D10 LG was significantly higher than at D3 LG. *Ccl20* was significantly downregulated in D3 LG compared to RG. Generally, *Ccl11, Cxcl4* and *Cxcl14* were expressed at slightly higher levels in the CLCG than RG, which may reflect a general induction of inflammation in the oral cavity in response to the contralateral ligature; these changes did not reach statistical significance **(Fig. 4.5)**.

Chemokine receptors had similar expression in LG, CLCG and RG compared to CLCG and RG. However, a significant decrease in *Ccr6* expression was observed between RG and D3 LG. *Ccr6* expression exhibited significantly higher expression in D10 LG compared to D3 LG. *Cxcr5* at D3 LG was significantly downregulated compared to D3 CLCG and RG. At D10 LG, CXCR5 was upregulated compared to D3 LG **(Fig. 4.5)**.

Cxcl12, Cxcr4 and *Ackr3* had consistent expression levels in all LG and CLCG samples. Although inflammatory and homeostatic chemokines were expressed in the gingiva, only modest differences were observed in ligature-induced periodontitis compared to contra-lateral control and resting gingiva. *Ackr4* was upregulated at D7 CLCG compared to RG, D3 CLCG and D10 CLCG.

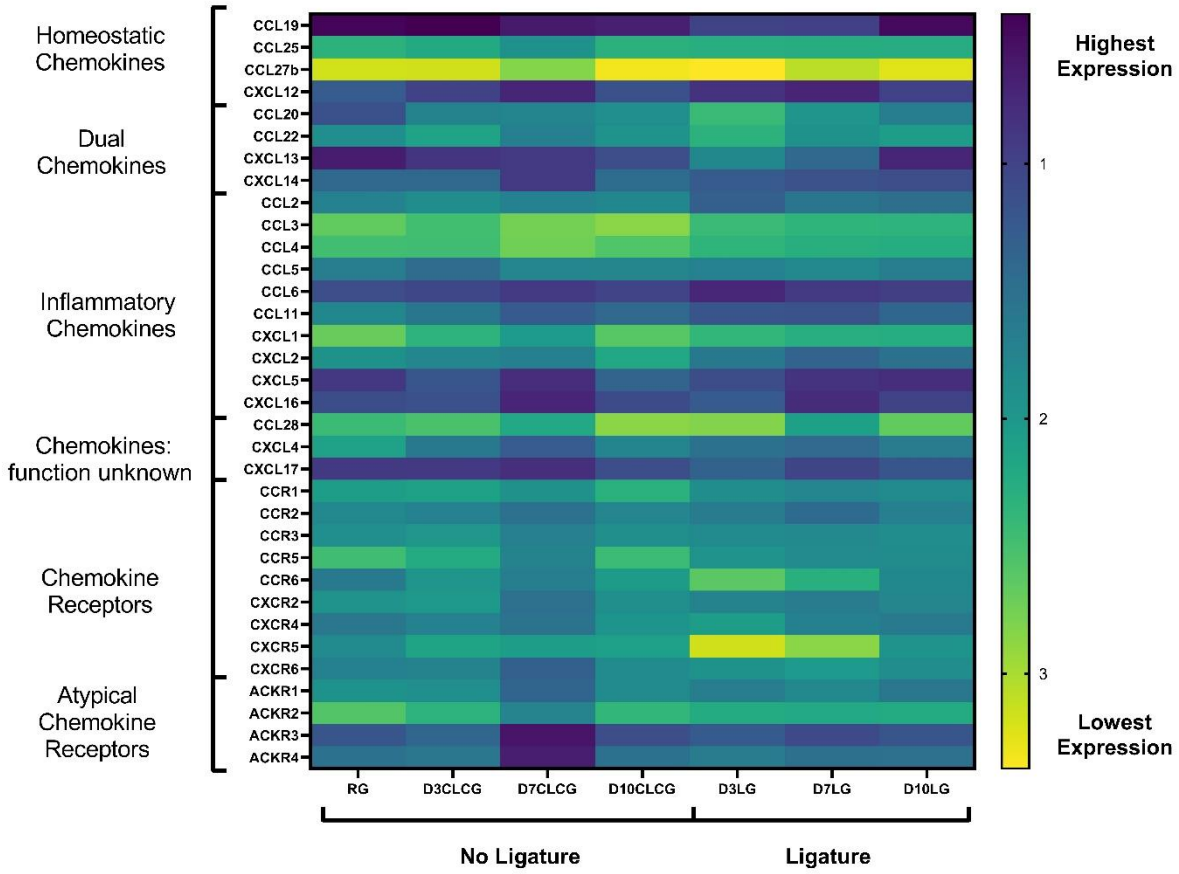

Figure 4.3 Heatmap of chemokine and chemokine receptor expression in ligature-induced periodontitis and controls

Ligatures were placed around the left maxillary first molar teeth (LG). The contralateral tooth served as control (CLCG). A further control group had no ligature (RG) (n=5). On day three (D3), day seven (D7) and day ten (D10), mice were culled, gingival tissue collected (n=10 mice/group/time point), and mice that failed to develop alveolar bone loss were excluded. RNA was isolated, and the expression of 34 chemokines and chemokine receptors was determined. Any outliers and samples that failed quality control were excluded from the analysis and were not graphed. The omitted samples are described in **Table 4.2**. Heatmap overview of analysed transcripts in control (*n* = 4), D3 (n = 8), D7 (n = 3), and D10 (n = 7) timepoints in ligature and control groups. Expression is displayed as the mean of each group.

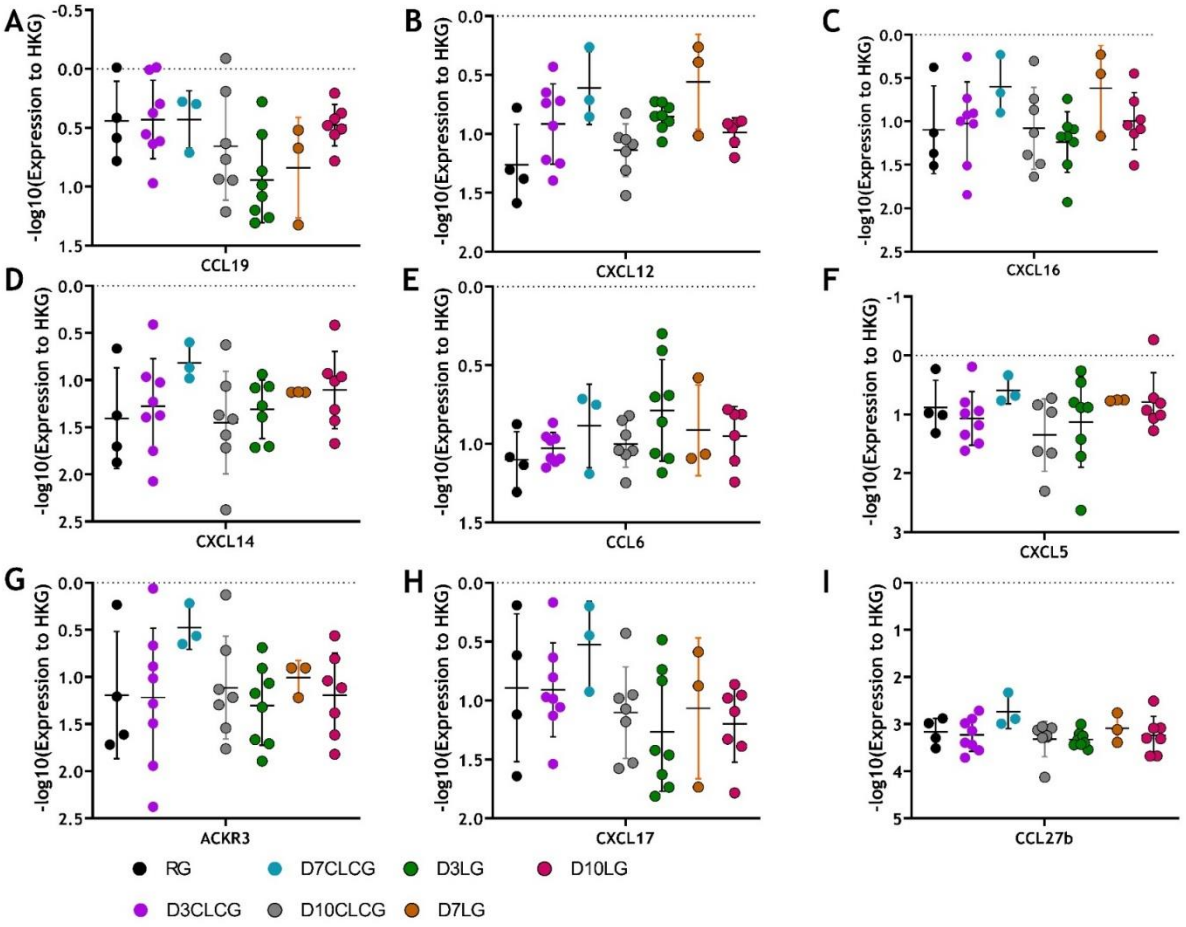

Figure 4.4 legend overleaf

Figure 4.4 Scatter plot of highly expressed transcripts in ligature induced periodontitis

Ligatures were placed around the left maxillary first molar teeth (LG). The contralateral tooth served as control (CLCG). A further control group had no ligature (RG). On day three (D3), day seven (D7) and day ten (D10), mice were culled, gingival tissue collected (n=10 mice/group/time point), and mice that failed to develop alveolar bone loss were excluded. RNA was isolated, and the expression of 34 chemokines and chemokine receptors was determined. Any outliers and samples that failed quality control were excluded from the analysis and were not graphed. The omitted samples are described in **Table 4.4**. Data are presented as the scaled expression of transcripts relative to housekeeping genes RG (n = 4), D3(n = 8), D7(n = 3), and D10(n = 7) timepoints in ligature and control groups. The horizontal bar represents the mean expression in each group, and the whiskers show the standard deviation of the mean. A 2-way-ANOVA, corrected for multiple comparisons, was used to detect significance.

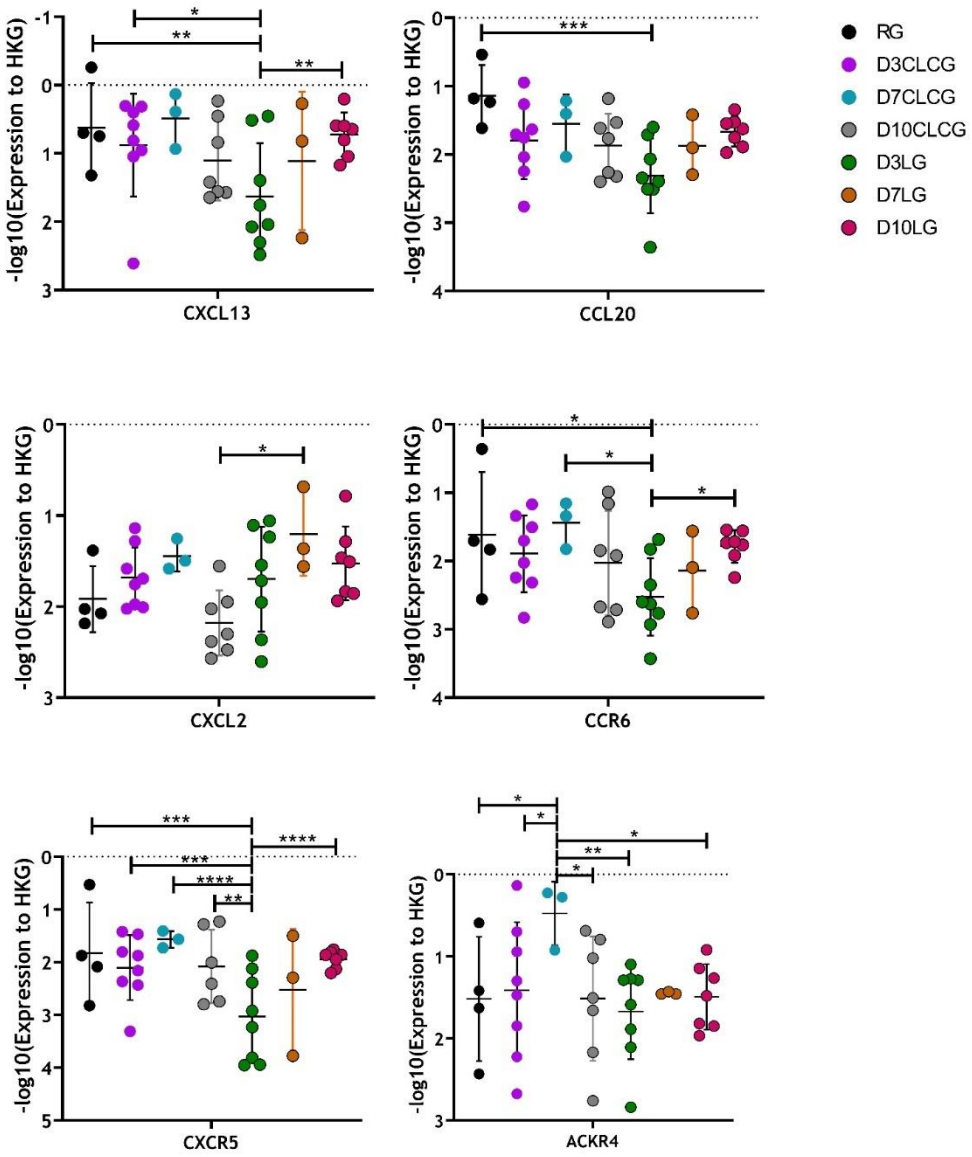

Figure 4.5 Scatter plot of significantly differentially expressed transcripts in ligature induced periodontitis

Ligatures were placed around the left maxillary first molar teeth (LG). The contralateral tooth served as control (CLCG). A further control group had no ligature (RG). On day three (D3), day seven (D7) and day ten (D10), mice were culled, gingival tissue collected (n=10 mice/group/time point), and mice that failed to develop alveolar bone loss were excluded. RNA was isolated, and the expression of 34 chemokines and chemokine receptors was determined. Any outliers and samples that failed quality control were excluded from the analysis and were not graphed. The omitted samples are described in **Table 4.2**. Data are presented as the scaled expression of transcripts relative to housekeeping genes RG (n = 4), D3 (n = 8), D7 (n = 3), and D10 (n = 7) timepoints in ligature and control groups. The horizontal bar represents the mean expression in each group, and the whiskers show the standard deviation of the mean. A 2-way-ANOVA, corrected for multiple comparisons, was used to detect significance. Stars denote the level of significance * $p \leq 0.05$, ** $p \leq 0.01$, *** $p \leq 0.001$ and **** $p \leq 0.0001$.

To identify if the chemokine and chemokine receptor expression changes were significantly different between time points, the fold change between LG and CLCG was evaluated. *Cxcl5* at D10 had the greatest fold change between CLCG and LG with a fold change of 7.15 (SD 8.69). Furthermore, the fold change observed at D10 was significantly higher compared to D3 and D7. *Cxcl2* also exhibited significantly greater fold change at D10 compared to D3. *Cxcr4* at D10 had the greatest differential expression between LG and CLCG with a log fold change of 4.33 (SD 4.88), which was also significantly higher than the differential expression between LG and CLCG at D3 **(Fig. 4.6)**.

A linear regression analysis was used to determine if the fold change from CLCG to LG was associated with alveolar bone loss. Only *Cxcr5* had a statistically significant association with alveolar bone loss and fold change between CLCG and LG. **(Fig. 4.7)**.

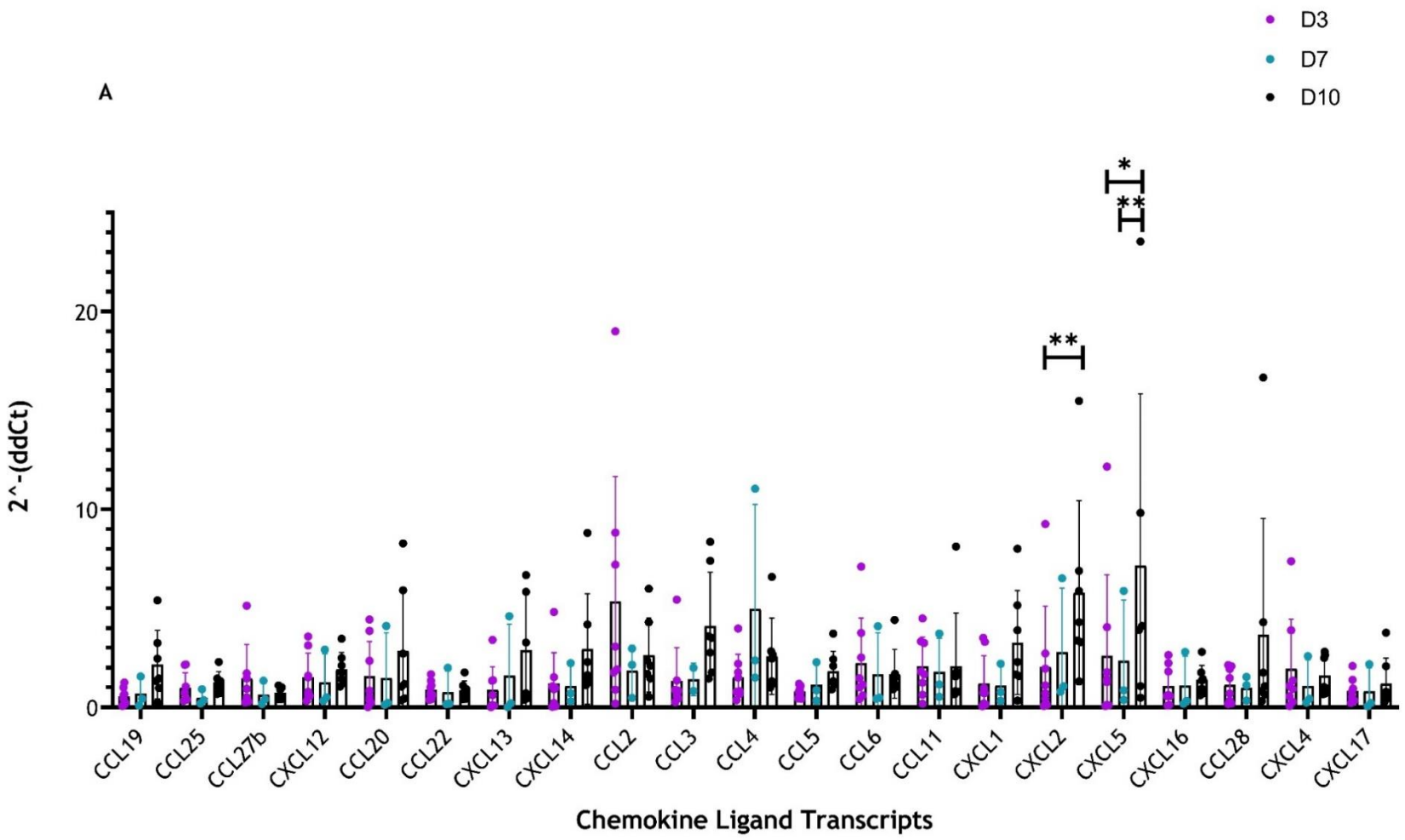

Figure 4.6 legend on page 118

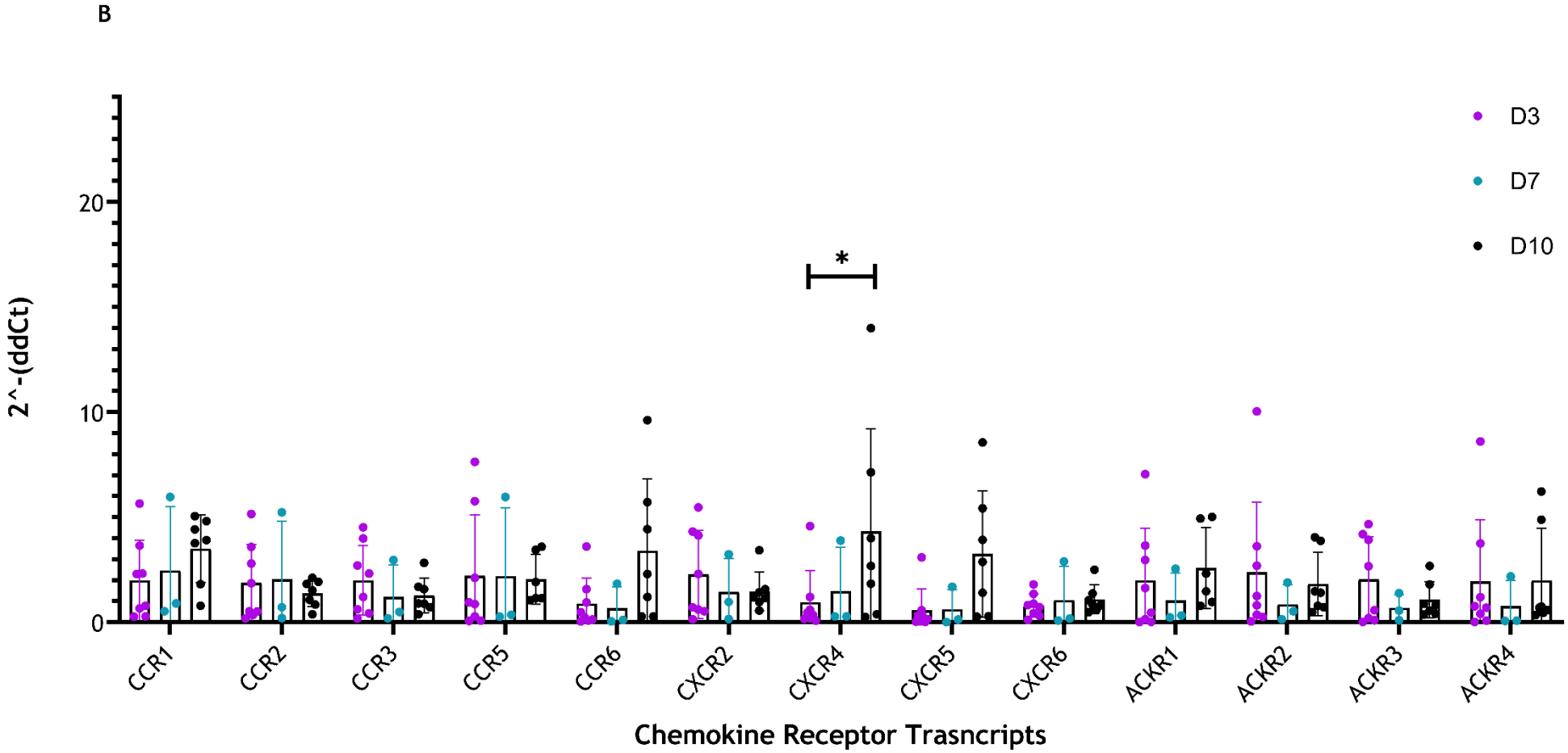

Figure 4.6 legend on page 118

Figure 4. 6 Chemokine and chemokine receptor fold change between control and ligature-induced periodontitis gingivae

Ligatures were placed around the left maxillary first molar teeth (LG). The contralateral tooth served as control (CLCG). On day three (D3), day seven (D7) and day ten (D10), mice were culled, gingival tissue collected (n=10 mice/group/time point), and mice that failed to develop alveolar bone loss were excluded. RNA was isolated, and the expression of 34 chemokines and chemokine receptors was determined. Any outliers and samples that failed quality control were excluded from the analysis. The data presented is the change in expression of chemokine and chemokine receptor transcripts from contra-lateral control to ligated gingiva, calculated by the formula 2^-(ddCT). The delta CT was measured relative to each sample's average of the housekeeping genes. **(A)** Chemokine Ligand Transcripts. **(B)** Chemokine Receptor Transcripts. The horizontal bar represents the mean expression in each group. Each dot represents one comparison D3 (n = 8), D7 (n = 3) and D10 (n = 7). The whiskers show the standard deviation of the mean. A 2-way-ANOVA, corrected for multiple comparisons, was used to detect significance. Stars denote the level of significance * $p \leq 0.05$, ** $p \leq 0.01$, *** $p \leq 0.001$ and **** $p \leq 0.0001$.

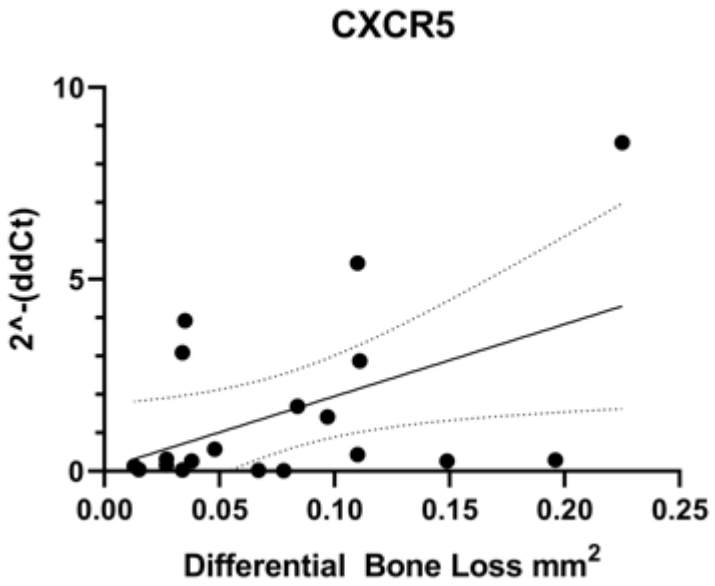

Figure 4. 7 Linear regression analysis of CXCR5 fold change and differential bone loss

Ligatures were placed around the left maxillary first molar teeth (LG). The contralateral tooth served as control (CLCG). On day three (D3), day seven (D7) and day ten (D10), mice were culled, gingival tissue collected (n=10 mice/group/time point), and bone loss measured, mice that failed to develop alveolar bone loss were excluded. Bone loss was measured as the area of exposed bone below the CEJ, and the CLCG area of bone was subtracted from the LG to ascertain the differential bone loss. The bone loss was plotted against the chemokine receptor fold change from CLCG to LG gingiva. A linear regression analysis was conducted to identify associations between bone loss and change in CXCR5 expression. Each dot represents one sample (n = 19). The dotted line represents the 95% confidence interval. The line equation is Y = 18.79*X + 0.06903, p=0.0322.

4.2.2 Transcriptional expression of chemokines in Non-Human Primates in Health and Periodontitis

To elaborate on our understanding of the chemokine landscape in mammals, we explored the chemokine and chemokine receptor landscape in NHPs. These data were obtained from a recently published microarray data set, which explored the transcriptional profile of NHP gingivae at different ages in health and experimental ligature-induced periodontitis. These data facilitated exploring the chemokine landscape between health and disease and identify if the chemokine landscape changes with age **(Table 4.3).**

	Young Healthy	Adolescent Healthy	Adult Healthy	Adult Periodontitis	Aged Healthy	Aged Periodontitis
Age Range (years)	3	7 – 12	13 – 17	13 - 17	> 17	> 17
Number	5	5	7	5	6	6

Table 4. 3 Non-human primate study samples

Table outlining the study groups, age NHPs, number of subjects per group and the abbreviation used to describe each group.

Gingival samples from NHPs in both health and disease showed high expression of *CCL19, CXCL6, CXCL12* and *CXCL14*, reflecting the murine gingivae findings. Most chemokines had similar levels of expression across sample groups **(Fig. 4.8)**. Ten chemokines were differentially expressed between groups. *CCL7* expression was increased in aged compared to healthy adolescent NHPs, whilst *CCL13* demonstrated increased expression in adults compared to young NHPs **(Figure 4.9 A and B**). *CCL15* expression significantly decreased between young and adult NHP and increased between adults and aged NHP.

Interestingly *CCL15* expression was higher in healthy young NHPs compared to healthy adult NHPs (**Figure 4.9 C**). *CCL17* expression was also higher in periodontal disease compared to health in adult NHP **(Figure 4.9 D)**. *CCL19* expression increased with age, showing higher expression in aged NHP compared to young and adolescent NHP. There was also higher expression in adults compared to adolescent NHP **(Figure 4.9 E)**. *CCL20* had higher expression in periodontitis than health in both adult and aged NHP **(Figure 4.9 F)**. *CXCL4(PF4V1)* expression was elevated in aged NHP compared to adults, adolescent and young NHP. Surprisingly, it also demonstrated lower expression in periodontitis compared to healthy NHP **(Figure 4.9 G)**. *CXCL6, CXCL11* and *CXCL13* exhibited significantly higher expression with age in NHP **(Figure 4.9 H-J).**

Finally, the log fold change was examined between Adult Healthy NHP chemokine expression and Adult Periodontitis, Aged Healthy, and Aged Periodontitis NHP. Few chemokines or chemokine receptors had large fold changes between the experimental groups. The greatest fold change was

observed in *CCL20* between Adult Healthy and Aged Healthy NHP (4.61). *CXCL9* exhibited the greatest downregulation, this was observed between Adult Healthy and Adult Periodontitis NHPs (0.60) (**Figure 4.10).**

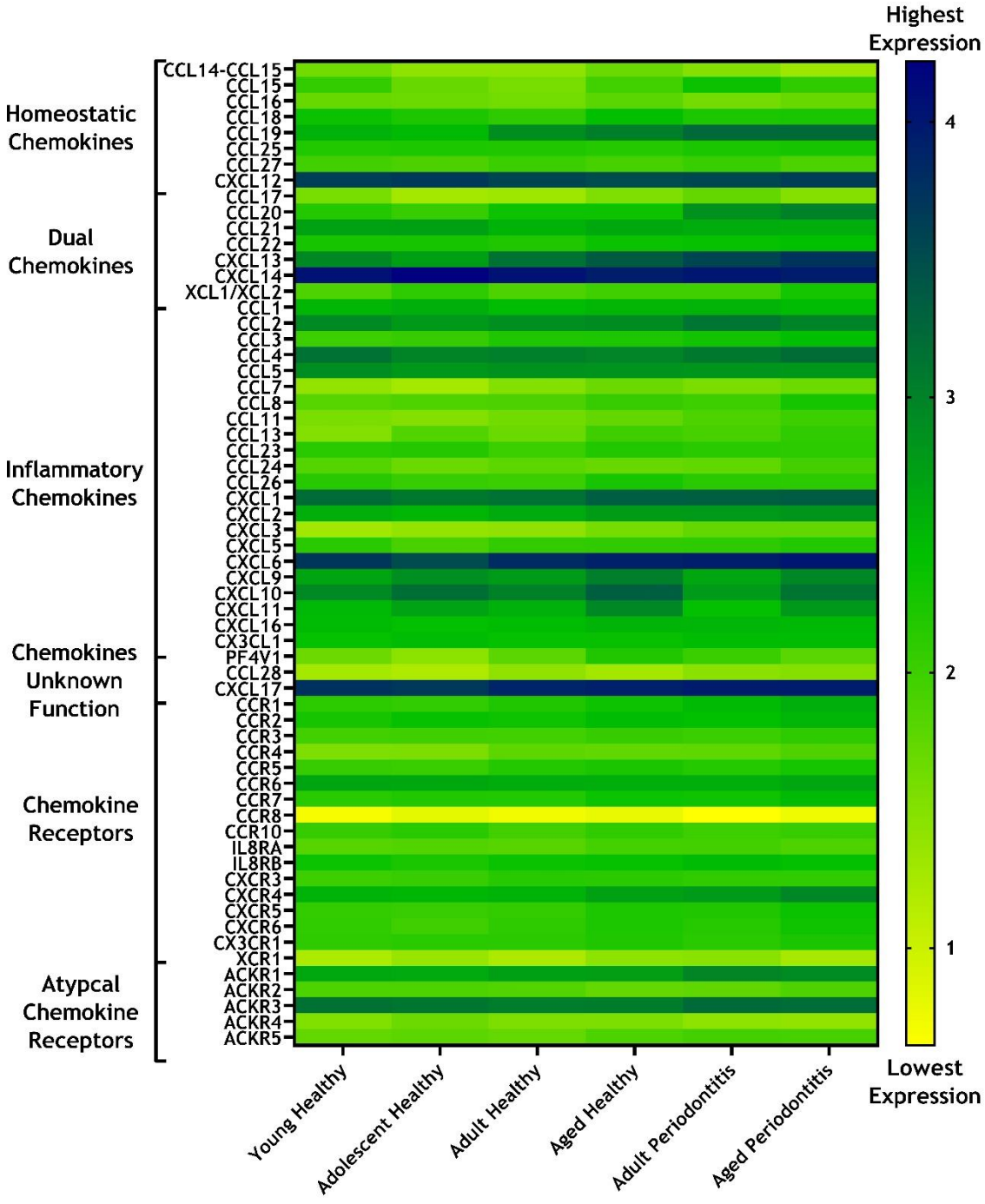

Figure 4. 8 Heatmap of non-human primate chemokine and chemokine receptor expression

Gingiva from NHPs in health and experimental periodontitis was harvested from NHPs of different ages. RNA was isolated and analysed on a microarray. The data shown is the log-transformed mean expression for chemokines and chemokine receptors.

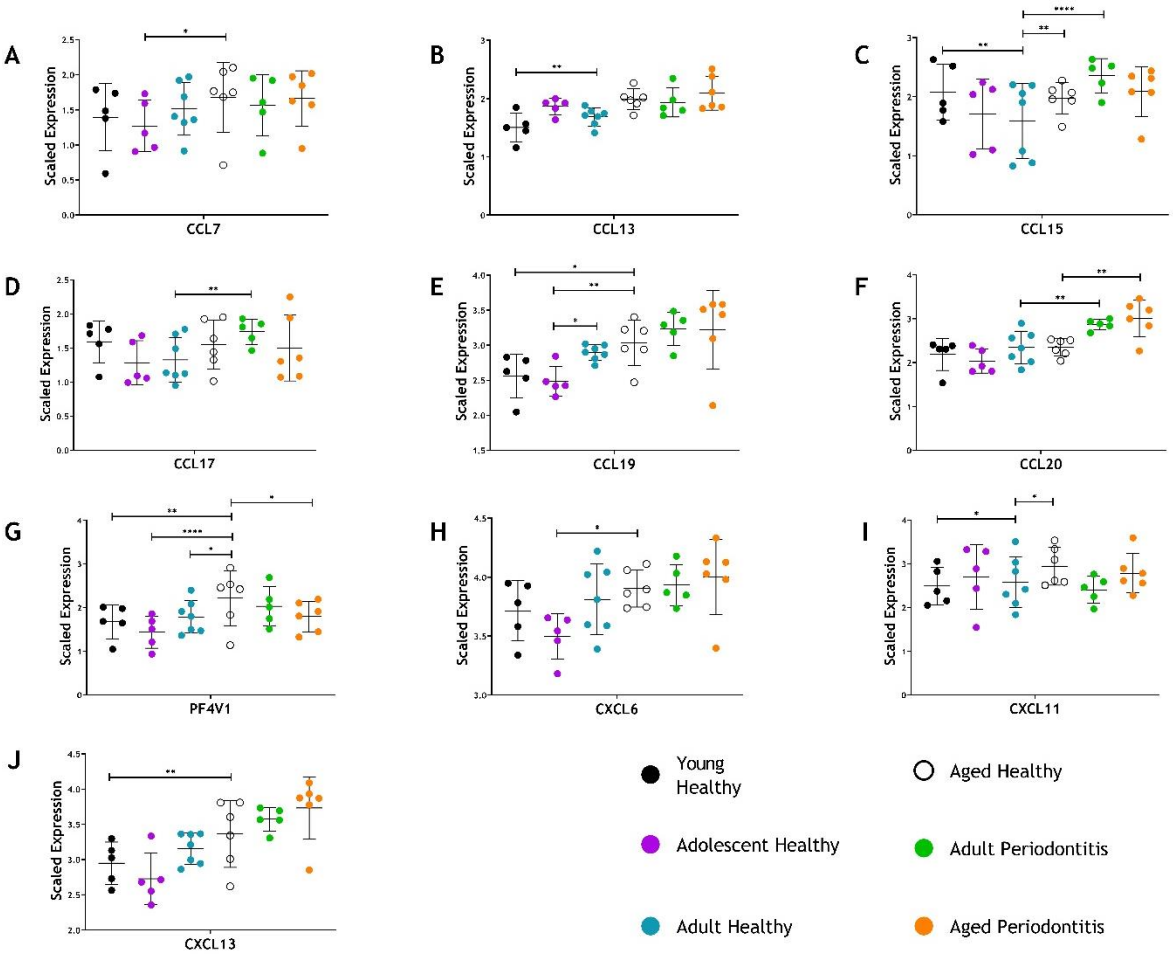

Figure 4.9 legend overleaf

Figure 4.9 Non-human primate chemokines and chemokine receptors with significant differential expression between age groups and disease status

Gingiva from NHPs in health and experimental periodontitis were harvested from NHPs of different ages Young Healthy (n = 5), Adolescent Healthy (n = 5), Adult Healthy (n = 7), Aged Healthy (n = 6), Adult Periodontitis (n = 5) and Aged Periodontitis (n = 6). RNA was isolated and analysed on a microarray. The data shown are the log-transformed mean expression for chemokines and chemokine receptors. Statistical analysis was conducted as a 2-way-ANOVA. Changes in expression were detected between experimental groups. Stars denote the level of significance * $p \leq 0.05$, ** $p \leq 0.01$, *** $p \leq 0.001$ and **** $p \leq 0.0001$. The horizontal bar is the mean expression from each group, and the whiskers represent the standard deviation.

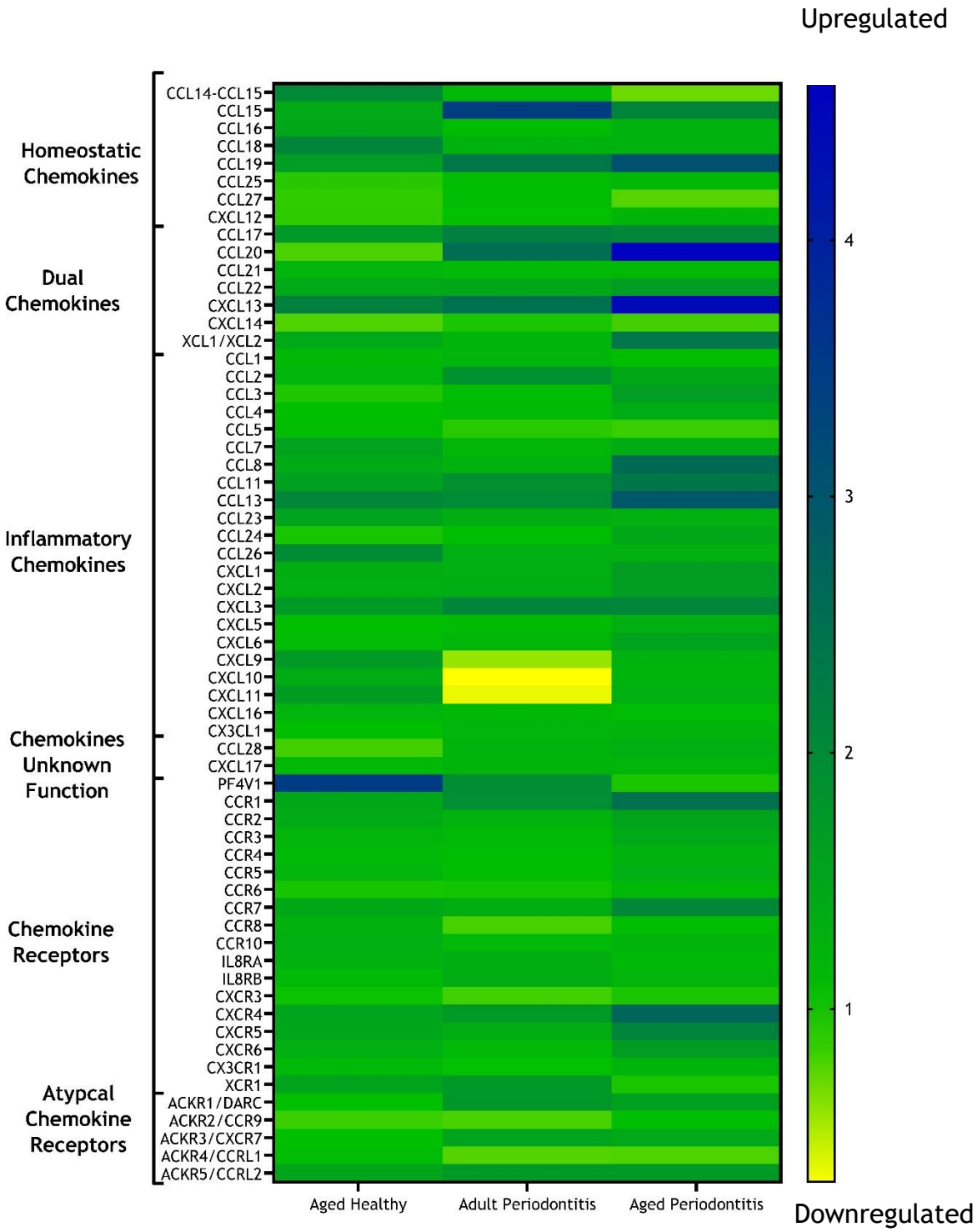

Figure 4. 10 Chemokine and chemokine receptor fold change compared to healthy adult non-human primates

Gingiva from NHPs in health and experimental periodontitis was harvested from NHPs of different ages. RNA was isolated and analysed on a microarray. The fold change was determined by dividing the expression in the experimental condition compared to healthy adult NHP expression. The colour represents the mean fold change. Any value less than one is downregulated.

4.2.3 Transcriptional expression of chemokines in human health and periodontitis

The chemokine landscape in human gingival tissue in health and periodontitis was analysed using a qPCR array. Healthy gingivae were obtained from patients undergoing periodontal plastic surgery – either surgical crown lengthening or from excess tissue following free gingival tissue grafting. Diseased gingivae were collected from patients with periodontitis undergoing open flap debridement. Prior to debridement, all periodontitis patients had periodontal probing depths greater than 5 mm, persisting following non-surgical periodontal therapy and in the presence of good oral hygiene (**Table 4.4)**. RNA was isolated from tissue samples, analysed by wavelength absorbance and bioanalysis, reverse transcribed and analysed using an RT^2 Profiler Array for chemokines and chemokine receptors **(Table 4.5).**

	Healthy gingival samples N = 5	**Diseased gingival samples N = 6**
Mean Age (years)	33	53
Age Range (years)	22-52	39-63
Male participants	0	4
Female participants	5	2

Table 4. 4 Demographic data of gingival tissue samples

In healthy human gingiva, homeostatic and inflammatory chemokines were readily detectable. Specifically, the homeostatic chemokines *CCL19* and *CXCL12* were prominently expressed. The dual chemokines *CCL20, CCL21* and *CXCL13* were also readily detectable, with *CXCL14* being the chemokine with the highest expression in health. *CXCL1* and *CXCL2* were the inflammatory chemokines with the highest expression, although relatively high levels of *CXCL6, CXCL8* and *CXCL10* were detected in healthy gingiva. ACKR1 was strongly expressed, and, in keeping with the data from the murine oral cavity, there was prominent expression of *CXCR4* and *ACKR3* **(Fig. 4.11)**.

Many of the same chemokines expressed in healthy gingiva were also detectable in periodontal disease. However, the expression of chemokines *CCL4* and *CXCL2* was higher. *CXCL1, CXCL6, CXCL8, CXCL10* and *CXCL13* as well as the dual chemokine *CCL20*, also exhibited increased expression but did not reach significance. There was downregulation of *CXCL14* in disease compared to health. The chemokine receptor *XCR2* and atypical chemokine receptor *ACKR1*

were significantly upregulated in the diseased tissue. The *CXCL12/CXCR4/ACKR3* axis was prominently represented in diseased gingivae, with *CXCR4* being the most highly expressed typical chemokine receptor. The log fold change of significantly differentially expressed chemokines was analysed. *CXCL6* had the greatest fold change in disease compared to health (**Fig. 4.12**).

Thus, some common patterns of chemokine and chemokine receptor expression levels were seen in both murine and human gingiva with prominent representation of CXCL12/CXCR4/ACKR3 in both healthy and diseased states.

Sample	A260:A230	A260:280	RIN	RNA concentration	Sample Used for Profiler Array
HG1	2.04	2.11	9.00	165 ng/µl	No
HG2	2.07	1.36	9.90	440 ng/µl	No
HG3	2.08	1.82	10.00	505 ng/µl	Yes
HG4	2.22	2.11	9.60	735 ng/µl	Yes
HG5	1.31	2.06	8.50	101 ng/µl	No
HG6	2.23	2.09	9.80	760 ng/µl	Yes
HG7	2.16	2.08	9.90	760 ng/µl	Yes
HG8	2.09	2.07	9.60	435 ng/µl	Yes
HG9	2.23	2.09	9.10	710 ng/µl	No
HG10	2.23	2.08	9.10	725 ng/µl	Yes
DG2	2.01	1.25	4.90	40 ng/µl	No
DG3	2.10	1.78	6.40	68 ng/µl	No
DG4	2.07	1.23	5.30	57.5 ng/µl	No
DG5	0.64	2.06	8.60	70 ng/µl	Yes
DG6	2.33	2.04	5.70	36 ng/µl	No
DG7	0.02	1.97	5.80	3.9 ng/µl	No
DG8	1.94	2.04	8.20	345 ng/µl	Yes
DG9	2.22	2.02	7.20	290 ng/µl	No
DG10	1.90	1.99	4.40	36 ng/µl	No
DG11	2.23	2.09	8	865 ng/µl	No
DG12	0.509	2.056	7.7	228 ng/µl	No
DG13	2.077	2.096	7.6	133 ng/µl	Yes
DG14	2.175	2.059	6.9	235 ng/µl	Yes
DG15	2.149	2.022	7.5	225 ng/µl	Yes
DG16	1.722	2.024	7.4	70 ng/µl	Yes

Table 4. 5 Human gingiva sample RNA Analysis of gingiva samples from health (HG) and gingiva samples from patients with periodontitis (DG)

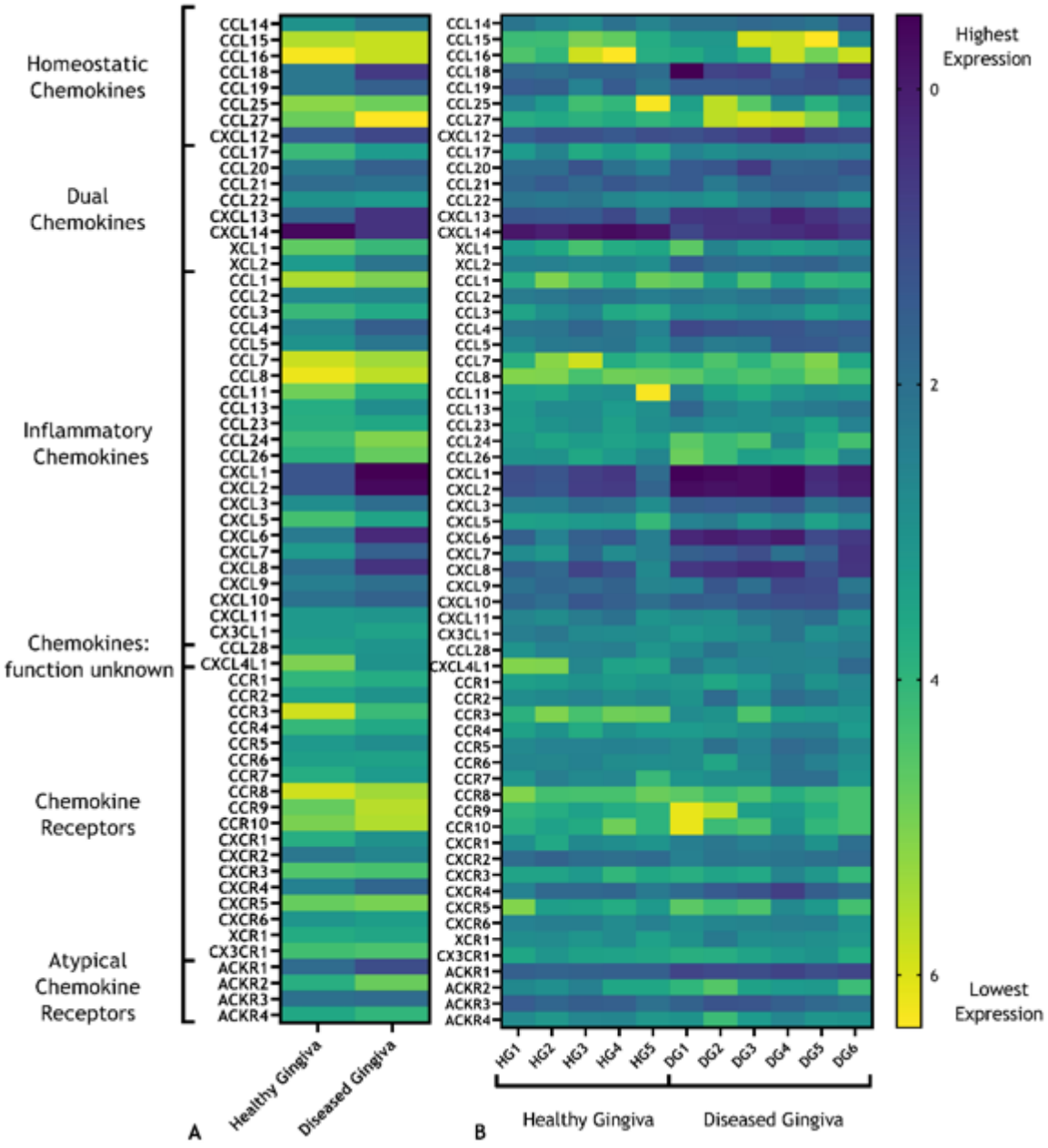

Figure 4. 11 Heatmap of chemokines and chemokine receptors in human gingiva in health and periodontal disease.

(A, B) Healthy (HG) (*n*= 5) and diseased (DG) (*n*= 6) human gingival tissues were obtained during routine periodontal surgery. RNA was isolated, and gene expression was determined by qPCR. **(A)** Heatmap of mean chemokine and chemokine receptor expression in healthy and diseased gingivae. **(B)** Heatmap of chemokine and chemokine receptor expression of individual samples from healthy and diseased gingiva groups.

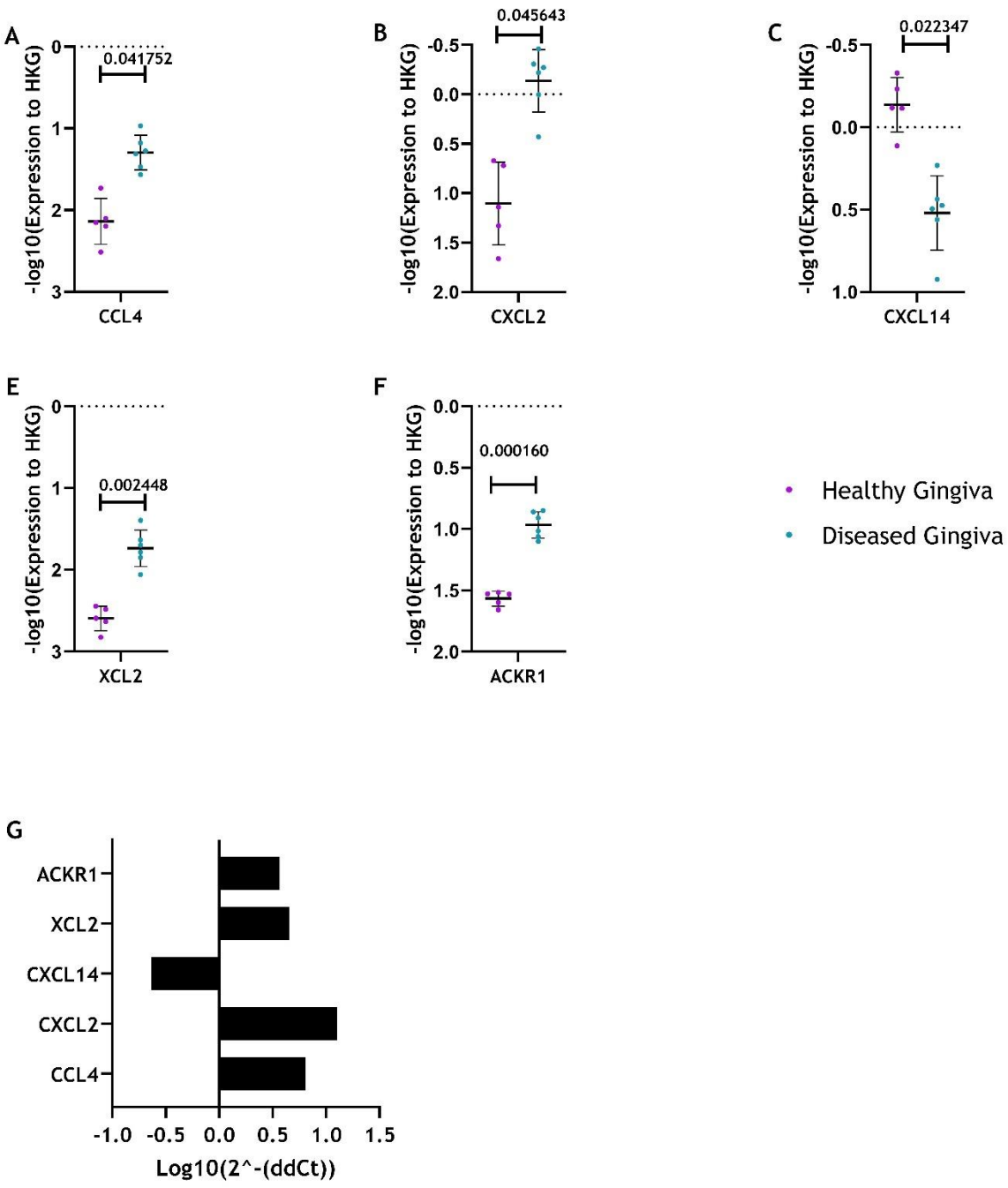

Figure 4. 12 Differentially expressed chemokine and chemokine receptor transcripts between healthy and diseased gingiva

Healthy (HG) (*n*=5) and diseased (DG) (*n*=6) human gingival tissues were obtained during routine periodontal surgery. RNA was isolated, and gene expression was determined by qPCR. **(A-F)** Expression of differentially expressed chemokine transcripts between healthy and diseased human gingiva, differential expression was determined using unpaired t-tests and corrected for multiple comparisons. **(G)** log fold change of significantly differentially expressed transcripts between healthy and diseased human gingiva.

4.2.4 Chemokine concentration in human saliva and gingival crevicular fluid in periodontitis and health

To evaluate the protein expression of chemokines in the oral cavity, chemokine concentrations in the saliva and gingival GCF were determined in patients with periodontitis (n = 10) compared to healthy controls (n = 10). Before periodontal treatment, saliva and GCF were collected from healthy volunteers and patients with periodontitis **(Table 4.6)**. Chemokine concentrations were determined by a custom LUMINEX panel and supplemental ELISAs for chemokines which were previously identified as highly expressed or of interest in gingiva in health or disease, IL-1β was also included as a positive marker of periodontitis. Overall, fewer chemokines were detected at the protein level. However, several chemokines had levels of detection that were below the limit of detection, in these instances their concentrations were extrapolated from the standard curve. Chemokine concentrations were similar in health and disease for both GCF and saliva. In saliva, CXCL5 was the chemokine with the highest concentration **(Table 4.7) (Fig. 4.13)**. Whilst IL-1β was upregulated in saliva this did not reach statistical significance (**Fig. 4.13**). CXCL16 was the only chemokine differentially expressed in GCF, which was downregulated in disease, no change was seen in saliva (**Fig. 4.14)**. In saliva CCL2 and CCL28 were both significantly downregulated in disease compared to health, no significant change was seen in GCF **(Fig. 4.14)**. CXCL8 expression increased in saliva but not GCF, this did not reach significance between periodontitis and healthy controls (**Fig. 4.13**).

	Healthy Controls	**Periodontal Disease Patients**
Number of participants	10	10
Male Participants	8	5
Female Participants	2	5
Age Range	25 – 53	32 - 54
Mean Age	33	39

Table 4. 6 Demographics of healthy volunteers and periodontal disease patients

In contrast to the gingival tissue chemokine mRNA expression profile, CXCL12 and CCL19 were not detected at protein level in GCF and saliva, and only low levels of CXCL14 were detected in saliva from patients with periodontal disease. However, the mucosal chemokine CCL28 was detected in all GCF and saliva

samples. Reflecting the transcriptional profile, there was low protein expression of CCL27 and CCL25 in all samples (**Fig. 4.12**).

	Health	Periodontitis
Average Age	33	39
Gender	Male = 8 Female = 2	Male = 5 Female = 5
Gingival Crevicular Fluid	**Concentration pg/mL**	
CXCL10	9.62 +/- 3.41	7.52 +/- 0.33
	ns	
CXCL13	0 +/- 0	0 +/- 0
	ns	
CXCL1	347.5 +/- 42.24	292.16 +/- 26.44
	ns	
CXCL5	0 +/- 0	0 +/- 0
	ns	
CCL11	584.47 +/- 8.65	583.97 +/- 10.78
	ns	
TNF-α	0 +/- 0	0 +/- 0
	ns	
IL-6	0.16 +/- 0.39	0.12 +/- 0.38
	ns	
CCL2	110.11 +/- 4.39	111.26 +/- 4.4
	ns	
IL-1B	479.48 +/- 408.36	437.08 +/- 284.87
	ns	
CCL20	21.1 +/- 66.72	0 +/- 0
	ns	
CCL3	400.73 +/- 35.26	402.36 +/- 29.26
	ns	
CCL22	648.85 +/- 1.29	647.46 +/- 3.03
	ns	
CCL4	1020.27 +/- 51.63	1003.48 +/- 35.3
	ns	
CXCL16	5.49 +/- 4.1	0.39 +/- 0.99
	Adjusted P= 0.0032	
CCL19	0 +/- 0	0 +/- 0
	ns	
CCL28	258.91 +/- 5.97	260.09 +/- 11.47
	ns	
CCL25	20.61 +/- 16.75	24.28 +/- 14.17
	ns	
CXCL7	7517.44 +/- 89.52	7495.95 +/- 59.71
	ns	

	Health	Periodontitis
CXCL9	2700.41 +/- 102.81	2683.34 +/- 80.88
	ns	
CXCL4	0 +/- 0	0 +/- 0
	ns	
CCL21	0 +/- 0	0 +/- 0
	ns	
CXCL14	0 +/- 0	0 +/- 0
	ns	
CCL27	0 +/- 0	0 +/- 0
	ns	
CCL5	0 +/- 0	0 +/- 0
	ns	
CXCL2	0 +/- 0	0 +/- 0
	ns	
Saliva	**Concentration pg/mL**	
CXCL10	92.35 +/- 115.85	30.67 +/- 23.74
	ns	
CXCL13	29.9 +/- 43.37	16.48 +/- 14.7
	ns	
CXCL1	670.91 +/- 587.72	1015.13 +/- 817.07
	ns	
CXCL5	9219.1 +/- 8878.55	2133.14 +/- 2278.21
	ns	
CCL11	149.5 +/- 37.2	123.62 +/- 5.54
	ns	
TNF-α	5.97 +/- 7.44	13.04 +/- 28.78
	ns	
IL-6	5.94 +/- 4.12	21.97 +/- 17.31
	ns	
CCL2	828.12 +/- 518.53	330.41 +/- 402.6
	Adjusted P = 0.0489	
IL-1β	639.81 +/- 331.12	2385.07 +/- 2554.13
	ns	
CCL20	17.97 +/- 23.01	24.34 +/- 52.19
	ns	
CCL3	106.56 +/- 14.45	119.39 +/- 21.03
	ns	
CCL22	131.98 +/- 1.21	130.47 +/- 1.14
	ns	
CCL4	241.45 +/- 18.85	271.81 +/- 45.68
	ns	
CXCL16	61.74 +/- 21.07	70.84 +/- 48.11
	ns	
CCL19	0.02 +/- 0.07	0.21 +/- 0.65
	ns	
CCL28	806 +/- 983.88	158.24 +/- 187.34

	Health	Periodontitis
	Adjusted P = 0.039	
CCL25	11.92 +/- 6.8	8.01 +/- 4.21
	ns	
CXCL7	1574.36 +/- 73.29	1547.79 +/- 35.2
	ns	
CXCL9	597.46 +/- 30.52	615.7 +/- 70.91
	ns	
CXCL4	0 +/- 0	0 +/- 0
	ns	
CCL21	8.41 +/- 13.64	10.3 +/- 21.98
	ns	
CXCL14	0 +/- 0	59.13 +/- 287
	ns	
CCL27	0 +/- 0	0 +/- 0
	ns	
CCL5	0 +/- 0	0 +/- 0
	ns	
CXCL2	175.95 +/- 187.86	178.72 +/- 148.68
	ns	

Table 4. 7 Summary of samples and analyte concentration in GCF and saliva

Table of sample demographics and analyte concentrations in saliva and GCF from patients with periodontitis and healthy controls. Chemokine concentration is presented as the mean and the standard deviation. If a significant difference in chemokine concentration was detected between periodontitis and healthy control, this was stated. Ns = non-significant. Significance was determined using a Mann-Whitney U test. The results were corrected for multiple comparisons using the Holm-Sidak method.

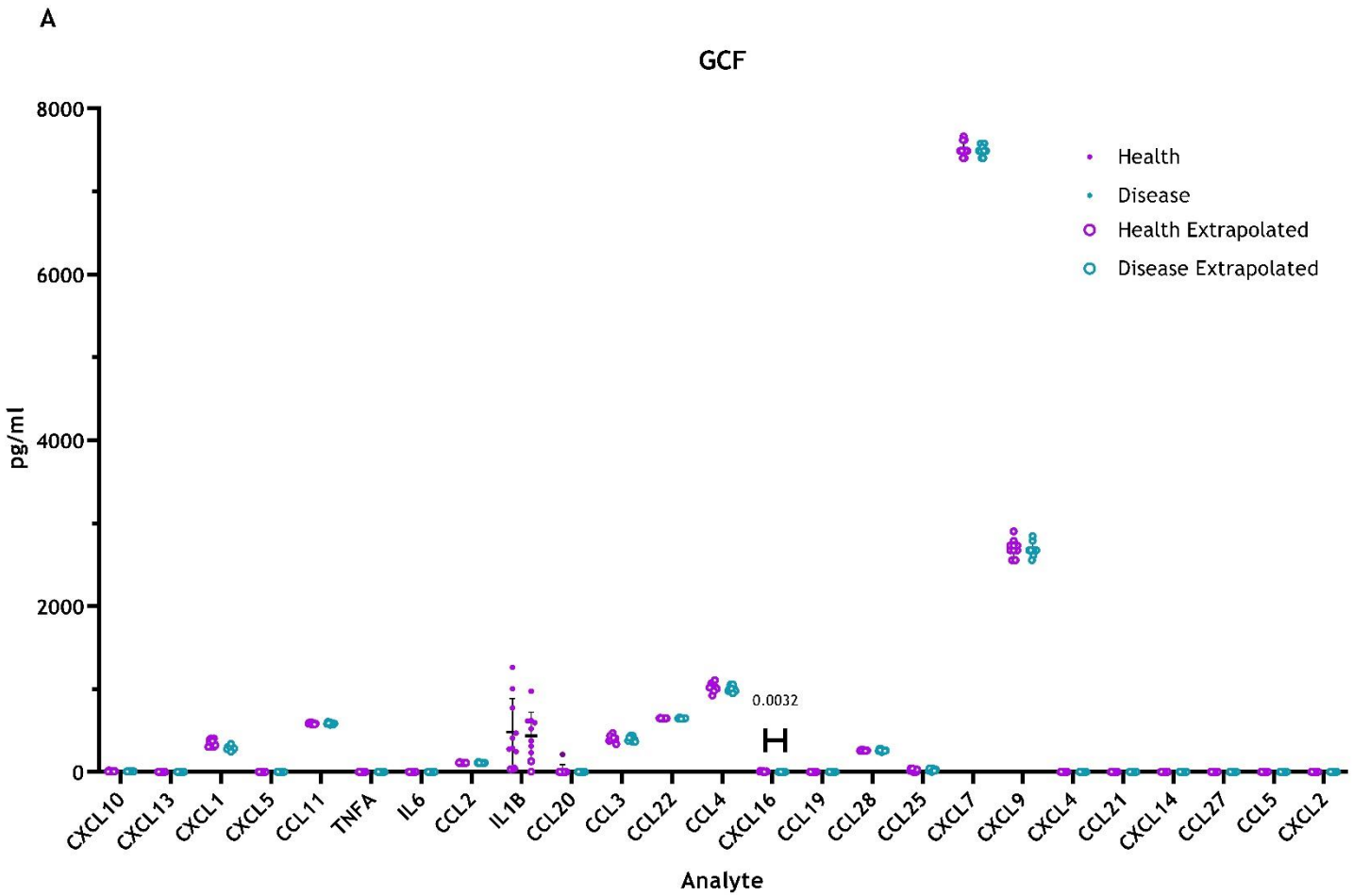

Figure 4.13 legend on page 136

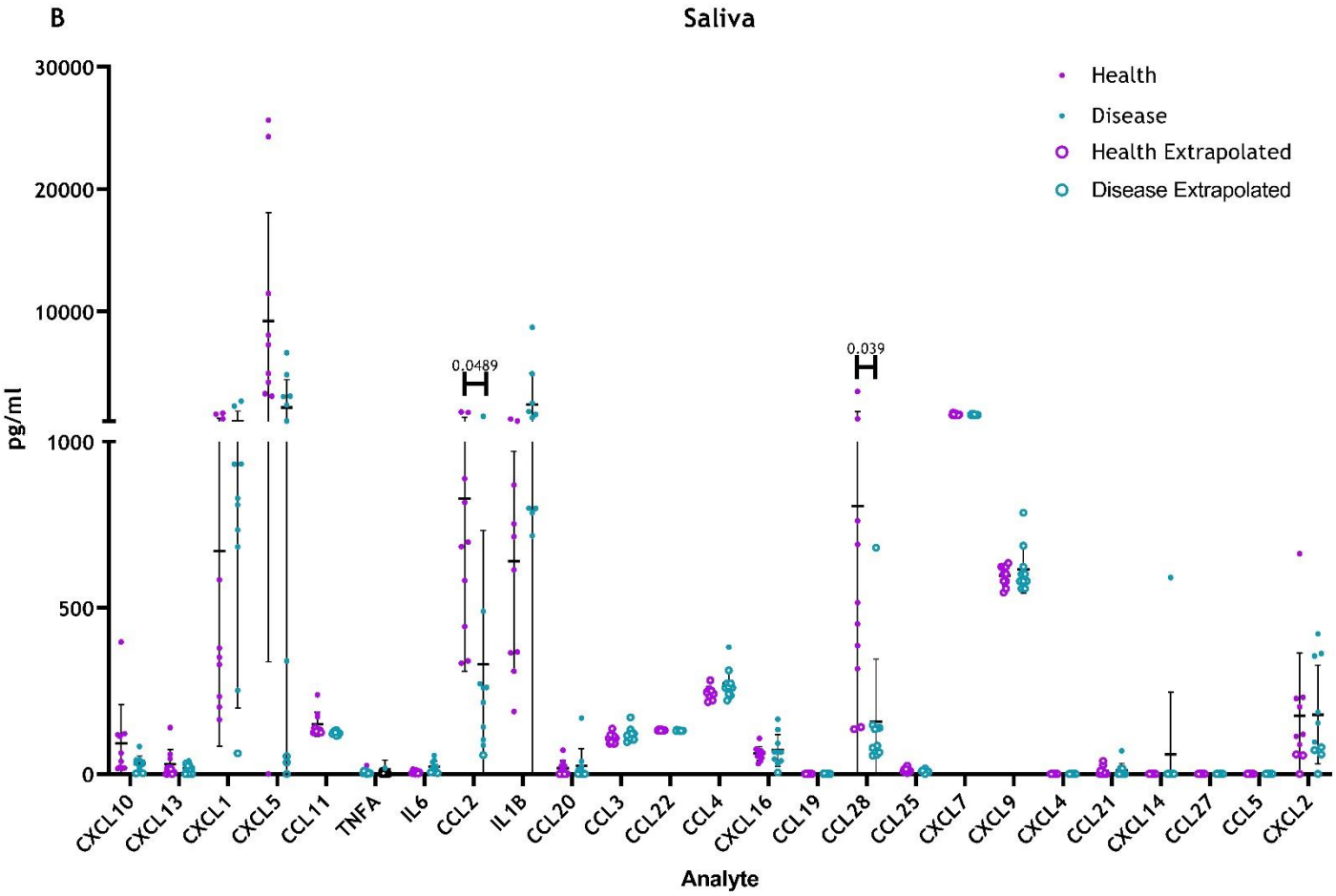

Figure 4.13 legend on page 136

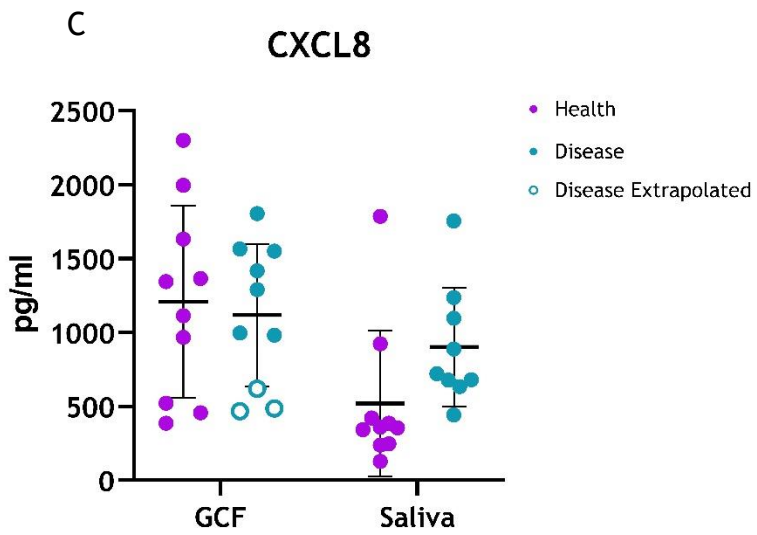

Figure 4. 13 Chemokine concentration in saliva and GCF in health and periodontitis

Saliva and GCF were obtained from healthy donors or patients with periodontal disease. Chemokine concentration in GCF **(A)** and saliva **(B)** in health and periodontitis. (n = 10) for each group. A custom LUMINEX assay determined chemokine concentration from GCF and saliva samples. The concentrations of chemokines in GCF was measured from the eluate from four Periostrips®. From each participant 2 mL of saliva was collected, and the concentrations of chemokines in saliva were measured from a sample of these. The concentrations were determined by interpolating the mean fluorescence intensity (MFI) of the samples to a standard. Values above or below the standard were extrapolated from the standard curve. Significance was determined using a 2-way ANOVA and corrected for multiple comparisons. The top of the coloured box represents the mean, and the whisker represents the standard deviation of the mean. **(C)** ELISA of CXCL8 concentration in GCF and saliva in health and periodontitis. The sample concentration was determined by interpolating a standard curve, a Mann-Whitney U test was used to assess the significance of differential concentrations between health and disease. The results were corrected for multiple comparisons using the Holm-Sidak method. Solid dots represent samples where the concentration was interpolated from the standard curve, rings represent samples that had fluorescence below the limit of detection and were extrapolated from the standard curve. The horizontal line represents the mean, and the whiskers the standard deviation of the mean.

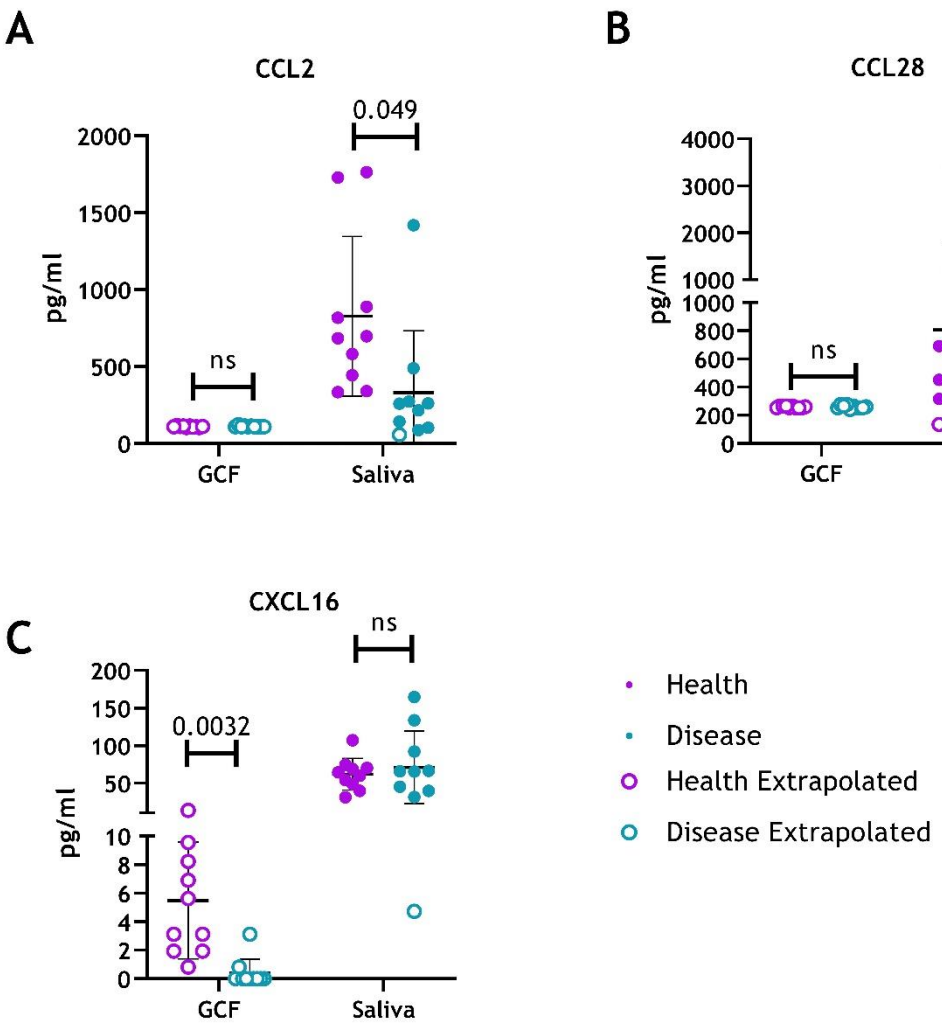

Figure 4. 14 Differentially expressed chemokines between health and periodontitis

Saliva and GCF were obtained from healthy donors or patients with periodontal disease. The concentrations of chemokines in GCF was measured from the eluate from four Periostrips®. From each participant 2 mL of saliva was collected, and the concentrations of chemokines in saliva were measured from a sample of these. The concentrations were determined by interpolating the mean fluorescence intensity (MFI) of the samples to a standard. **A** Scatter plot of CCL2 concentration in GCF and saliva. **B** Scatter plot of CCL28 concentration in GCF and saliva. **C** Scatter plot of CXCL16 concentration in GCF and saliva. A Mann-Whitney U test was used to assess the significance of differential concentrations between health and disease. The results were corrected for multiple comparisons using the Holm-Sidak method. Solid dots represent samples where the concentration was interpolated from the standard curve, rings represent samples that had fluorescence below the limit of detection and were extrapolated from the standard curve. The horizontal line represents the mean, and the whiskers the standard deviation of the mean. ns = not significant.

4.3 Discussion

These findings comprehensively detail the chemokine and chemokine receptor expression in human, mouse and NHP gingiva during health and periodontitis. The data show that the CXCL12/CXCR4/ACKR3 axis is prominently expressed in both resting gingiva and gingiva affected by periodontitis in mice, NHP and humans suggesting that it may be a significant contributor to cellular recruitment to the oral mucosa. Whilst other studies have investigated CXCL12 in the gingiva, these studies are the first analysis of CXCL12 and its receptors CXCR4 and ACKR3, expression relative to a broad array of chemokines and receptors in gingival health, disease and between mammalian species.

Surprisingly few chemokines exhibited significant differential expression between health and disease in humans or between health and ligature-induced periodontitis in mice and NHP. Interestingly multiple inflammatory chemokines were highly expressed in health and had similar expression in diseases such as CXCL6, 8, and 9 in humans, CXCL1,2 and 6 in NHP and CCL6, CXCL5 and CXCL16 in mice, the majority of which are responsible for neutrophil chemotaxis. Given the large neutrophil population in healthy gingiva, this is unsurprising but highlights that neutrophil migration to oral gingiva may be more nuanced than previously described, which has canonically relied on CXCL1,2 and 8, as other neutrophil chemoattractants, such as CXCL5, are also highly expressed. Furthermore, the presence of inflammatory chemokines during health is not overly surprising as the mouth is constantly exposed to masticatory forces and microbial insult and thus requires the presence of leukocytes and stem cells to protect and repair the oral mucosa, even in clinical health (Moutsopoulos and Konkel 2018; Zhang et al. 2012). As such, it is possible that inflammatory chemokines are constantly being induced; thus, only subtle changes in chemokine expression occur during overt inflammatory responses.

Multiple chemokines and chemokine receptors demonstrated significant changes in gingival tissues in periodontitis compared to health. Reinforcing previous human studies, an elevated CXCL1 and CXCL2 was observed in disease. CXCL6 was also elevated in periodontitis compared to health, which has also been described previously (Kebschull *et al.*, 2009). In mice, CXCL5 was upregulated in disease. Previous studies have shown CXCL8 to be highly expressed in

periodontitis. CXCL8 appeared to be upregulated in these studies but did not reach statistical significance, however, prior to correcting for multiple comparisons, CXCL8 was significantly upregulated in diseased compared to healthy gingiva ($p = 0.0087$). This may be due to a lack of statistical power due to the large number of analytes assessed. Previous murine immunohistochemistry and in-situ hybridisation studies have shown CXCL2 and 8 are expressed at the JE, and have increasing concentration towards the gingival sulcus. Further human immunohistochemistry studies have shown CXCL1 expression in diseased gingiva to increase, however, no comment was made on the location of expression within the gingiva (Rath-Deschner *et al.*, 2020). The spatial position for CXCL6 and CXCL5 has not been explored to date (Greer *et al.*, 2016; Tonetti, Imboden and Lang, 1998). These findings suggest that neutrophil trafficking to gingiva relies on various chemokines. It could be speculated that there is redundancy of function, and/or a nuanced and specific chemokine pattern to direct different neutrophil subsets or directing cells to specific sites within the gingiva. Further work is needed to understand this fully.

Of the homeostatic, dual, and chemokines with unknown functions, CXCL13 was highly expressed in healthy gingiva in humans, NHPs and mice and was upregulated in gingiva from patients and NHPs with periodontal disease, but this did not reach statistical significance. Moreover in mice *Cxcr5*, the receptor for CXCL13, expression was positively associated with alveolar bone loss. Given the abundant B cell populations observed in healthy gingiva and their abundance in periodontally diseased gingiva, this is likely to be the primary role of CXCL13 in the gingiva of mammalian species (Nakajima *et al.*, 2008; Figueredo, Lira-Junior and Love, 2019).

No other homeostatic chemokine was upregulated in disease across species. However, CXCL14 was significantly downregulated in periodontitis compared to healthy gingiva in humans. As described in chapter three, CXCL14 is thought to be a non-signalling ligand for CXCR4, which affects the ability of CXCL12 to signal through CXCR4. The relevance of CXCL14 in potentially regulating CXCL12 expression in gingiva is unclear.

In vitro studies have shown *P. gingivalis* stimulates CXCL14 expression on oral epithelial cells indirectly by gingipain proteases. Gingipains are proteinases released by *P. gingivalis* that modulate the local immune response to creating

favourable ecological niche (Li and Collyer, 2011). The *in vitro* data contradict these *in vivo* findings, however, it highlights the complexity of the chemokine system in the gingiva.

Chemokines have functions beyond leukocyte chemotaxis, including recruitment and regulation of non-leukocyte cells and antimicrobial functions (Hughes and Nibbs, 2018). Thus, chemokines may have functions that are essential to oral homeostasis, other than cellular recruitment, and these processes are required in both healthy and diseased gingiva. These functions may explain why most homeostatic chemokines had similar expression levels in health and disease.

Multiple chemokines were not detected at the protein level in GCF or saliva. In GCF, this may be due to the small volume available for analysis limiting detection of lowly expressed chemokines, or the platform used was not sensitive enough to accurately detect the concentrations of chemokines in the sample. Chemokines were more readily detected in saliva. Alternative methods of protein quantification such as proximity extension assays were considered, which are sensitive and have multiplexing capacity. However, multiple chemokines of interest were not available on these assays. Consideration of these techniques may be given to validate the findings from these studies or explore analytes that had low-abundance (Lundberg *et al.*, 2011). Moreover, to ascertain the concentration of multiple chemokines extrapolation below the limit of detection was necessary, thus reducing the accuracy of analysis.

Due to the low volume of GCF protein concentration was not determined in these studies. Whilst a standardised approach was taken to GCF and saliva collection, measuring the total protein concentration would allow for a more accurate comparison of chemokine expression between samples. An alternative method would be to standardise the concentrations of the chemokines to the volume of substrate, a periotron® was not available and as such the volume of GCF was not determined (Bevilacqua *et al.*, 2016).

Reflecting the transcriptional data salivary and GCF CXCL8 concentration was higher in disease then in health, but did not reach statistical significance, this may be due to lack of statistical power. It was anticipated that CXCL8 concentration in GCF would increase in periodontitis; these findings suggest it didn't change. This may reflect the low starting volumes of GCF for analysis, and

lack of sensitivity of the assay used. The literature is divided as to whether CXCL8 increases in GCF in periodontitis (Finoti *et al.*, 2017). Alternative handling methods of GCF strips could have improved yields such as snap freezing in liquid nitrogen (Barros *et al.*, 2016). To confirm the total protein yields BCA assay or alternative protein quantification could have been undertaken, this was not possible due to the low volume of eluate. However, multiple highly expressed chemokine transcripts were not detected or had low concentrations in saliva and GCF, such as CXCL13 and CXCL14. There are multiple explanations for this. Firstly, chemokines are susceptible to post-translation modification; thus, modified variants of chemokines may not be detected at the protein level (Hughes, 2018). Alternatively, chemokines, such as CXCL8, are degraded by *P. gingivalis (Jayaprakash, Khalaf and Bengtsson, 2014)*. Also, ACKRs may restrict chemokine concentrations through their scavenging functionality. It is also possible that some chemokines remain in tissue or are degraded in tissue, reducing their abundancy in saliva and GCF (Mortier *et al.*, 2011). A limitation of these experiments is that the protein expression was determined in GCF and saliva, not directly from the tissue, as such, not all chemokines of interest may leave the gingiva and be present in GCF or saliva.

Through NHP models, the chemokine landscape in gingiva has been analysed at different ages, providing novel insight into potential developmental-related chemokine changes. Multiple chemokines had differing levels of expression with age, including CXCL13, CXCL4 and CCL19. These results highlight a potential role for chemokines in the development and repair of gingival tissue and potentially periodontal disease susceptibility, as periodontal disease prevalence increases with age (Clark, Kotronia and Ramsay, 2021). It is important to elucidate the role of these chemokines and understand why they may change with age how that may modulate gingival homeostasis.

These data provide a comprehensive overview of the chemokine landscape in healthy and diseased gingiva in humans, mice and NHP. Specifically, we have shown that CXCL12, CXCR4, ACKR3 and CXCL14 are consistently highly expressed in mouse, NHP and human oral mucosa in health and disease. Given the interplay between these molecules and their indispensable biological roles, this axis may be crucial in gingivae homeostasis. Most chemokines have similar expression in health and disease. However, multiple neutrophil chemo-attractants are

upregulated across all species in disease compared to healthy gingiva. More work is required to identify the specific role of each of these in the context of health and periodontitis. In addition, the expression of multiple chemokines changed with age in NHP.

Further work is needed to elucidate if these changes are associated with changes in the cellular populations they are known for regulating to provide a greater appreciation of the relevance of these changes. The protein expression of chemokines in GCF and saliva did not accurately represent the transcriptional findings in these studies. In addition, there were subtle differences in chemokine and chemokine receptor expression between species. However, most chemokines demonstrated similar levels of expression, suggesting chemokine expression is conserved between mammalian species; thus, mice and NHP models are helpful in exploring chemokines' role in regulating cellular recruitment to the gingiva.

The key findings from the posed research questions for this chapter are:

- Does the expression of chemokine or chemokine receptor transcripts change between health and periodontitis in mice, non-human primates, and humans?
    - Most chemokines and chemokine receptors had similar expression levels in health and disease across mammalian species.
    - CXCL13, as well as multiple neutrophil chemo-attractants, were more highly expressed in periodontitis compared to healthy gingiva in mice, non-human primates, and humans.
- Does the transcriptional expression of chemokines and chemokine receptors differ between mice, non-human primates, and humans?
    - The chemokine and chemokine receptor landscape in periodontitis in humans and experimental periodontitis in mice and non-human primates were broadly similar

These findings support the hypotheses that the gingival chemokine and chemokine receptor landscape differ between health and periodontitis and the chemokine landscape is conserved amongst mammalian species.

Chapter 5 - The Murine Gingival CD4+ T cell Transcriptome in Health and Periodontitis

5.1 Introduction

The oral mucosa forms a barrier that is constantly exposed to the external environment and potentially harmful microbiota, as such homeostatic mechanisms must be active to maintain health. The cellular response, including the CD4+ T cell response is crucial to this. Patients with a defective CD4+ response experience viral, fungal and bacterial infections and mucosal stomatitis (Peacock, Arce and Cutler, 2017).

Although CD4+ subsets help maintain gingival homeostasis, they also have a role in periodontal disease, with all phenotypes implicated to some degree. Mice deficient in Th1 derived IFN-γ and IL-6 have reduced bone loss, even in the presence of *P. gingivalis* (Baker *et al.*, 1999). Increased alveolar bone loss is observed where IL-5 was increased (Myneni *et al.*, 2011). Th17 associated IL-17 and IL-23 are both increased at sites of attachment loss compared to in health (Vernal *et al.*, 2005).

Whilst T cells are important in oral homeostasis, there is limited insight into their specific function in oral mucosa and how they may traffic there in health or during inflammation.

Whole genome transcriptional analysis has provided insights into gene expression in gingival tissue biopsies. In human gingival samples from patients with periodontitis, upregulation of genes related to the antimicrobial response, chemotaxis and antigen presentation have been observed compared to healthy gingiva (Demmer *et al.*, 2008). In murine ligature induced periodontitis RNA-Sequencing analysis has shown that gene ontology sets for neutrophil chemotaxis, inflammatory responses and the positive regulation of inflammatory responses were upregulated in ligated gingiva compared to contra-lateral control tissue (Maekawa *et al.*, 2019). However, bulk RNA-Sequencing provides limited

insight into the transcriptional profiles of specific cell subtypes when whole tissue is analysed. Single cell RNA-Sequencing has also been conducted on human buccal and gingival mucosae. However, it too has limitations including greater variability and decreased sensitivity compared to bulk RNA sequencing (Haque *et al.*, 2017) (Williams *et al.*, 2021). There have also been no reports of differential expression between lymph node and gingivae CD4+ T cells. To overcome these limitations, bulk RNA sequencing can be conducted on purified cell types, offering optimal gene coverage and limiting cellular heterogeneity in the sample.

CD4+ T cells are essential to maintaining oral homeostasis and are implicated in the development of periodontal disease, yet no in-depth and unbiased analysis of the CD4+ T cell transcriptome in gingiva has been conducted. Herein, bulk RNA Sequencing of purified CD4+ T cells from gingivae and draining lymph nodes from mice with *P. gingivalis* infection or control infection control are analysed, providing some insights into T cell functions in the oral cavity and how this may differ between health and disease, as well as between lymphoid tissue and the gingivae.

Hypotheses:

- The transcriptional profile of murine gingival CD4+ T cells will differ between health and periodontitis.
- The transcriptional profile of murine CD4+ T cells will differ between cervical draining lymph node and gingiva.

The research questions posed to investigate this hypothesis included:

- Identify the transcriptional differences of isolated murine CD4+ T cells between:
    - Gingiva in health and periodontitis
    - Cervical draining lymph node in health and periodontitis
    - Gingiva and cervical draining lymph node in health
    - Gingiva and cervical draining lymph node in periodontitis

- Which chemokine receptors, integrins and selectin ligands are highly expressed on gingival CD4+ T cells, relative to cervical draining lymph node CD4+ T cells?

5.2 Results

5.2.1 Unbiased analysis

To understand the gingivae and cervical draining lymph node CD4+ T cell transcriptome in health and during alveolar bone loss, T cells were isolated from both tissues during *P. gingivalis* infection or CMC control infection via gavage. The transcriptome of isolated T cells were then analysed by RNA-Sequencing to provide an in-depth and unbiased evaluation of the transcriptome. Previous work has confirmed a robust adaptive immune response(through the presence of circulating *P. gingivalis* IgG anti-bodies) to *P. gingivalis* infection occurs 2-4 weeks following initial exposure. Bone loss begins at about 28 days after initial exposure to *P. gingivalis*, but does not reach statistical significance until around 6 weeks following *P. gingivalis* exposure (Campbell, 2017). T cells were thus isolated from gingivae and draining cervical lymph nodes at 28 days following initial infection with *P. gingivalis* or control CMC, as at this point a robust immune response has taken place and the process of alveolar bone loss is ongoing (**Table 5.1 and Table 5.2)**.

RNA, with a RIN score of at least 8.6 was obtained from between 1.2 x 10^4 and 3.5 x 10^4 gingival CD4+ T cells, obtained by FACS with 100% purity. From the draining lymph node, between 3.0 x 10^5 and 1.0 x 10^6 CD4+ T cells were isolated yielding RNA with a RIN score of least 9. RNA was amplified, reverse transcribed and all samples were diluted to 1 ng total cDNA prior to sequencing (Campbell, 2017).

Following next generation sequencing of purified CD4+ T cell RNA, and normalisation of mapped read counts, transcripts with expression less than <1 Fragments per Kilobase of transcript per Million mapped reads (FPKM) were excluded from subsequent analysis, which was conducted using R (**Fig. 5.1)**.

	Lymph Node	Gingiva
P. gingivalis infection	LN_PG (n = 3)	G_PG (n = 3)
Control Infection	LN_CMC (n = 3)	G_CMC (n = 3)

Table 5. 1 Sample nomenclature

The transcriptional profile of CD4+ T cells are being analysed in two conditions and from two tissues. Thus there are four experimental groups which have been analysed in biological triplicate. The groups are CD4+ T cells from Lymph Node in control infection (LN_CMC), Gingiva in control infection(G_CMC), Lymph node in *P. gingivalis* Infection (LN_PG) and Gingiva in *P. gingivalis* infection (G_PG).

	LN_PG	G_CMC
LN_CMC	LN_CMC_V_LN_PG	LN_CMC_V_G_CMC
G_PG	LN_PG_V_G_PG	G_CMC_V_G_PG

Table 5. 2 Differential expression comparisons

Comparisons of CD4+ T cell gene expression were made between gingiva in control infection *and P. gingivalis* infection (G_CMC_V_G_PG) as well as lymph node in control infection and *P. gingivalis* infection (LN_CMC_V_LN_PG). Comparisons were also made between gingiva and lymph node in control infection (LN_CMC_V_G_CMC) and *P. gingivalis* infection (LN_PG_V_G_PG) separately.

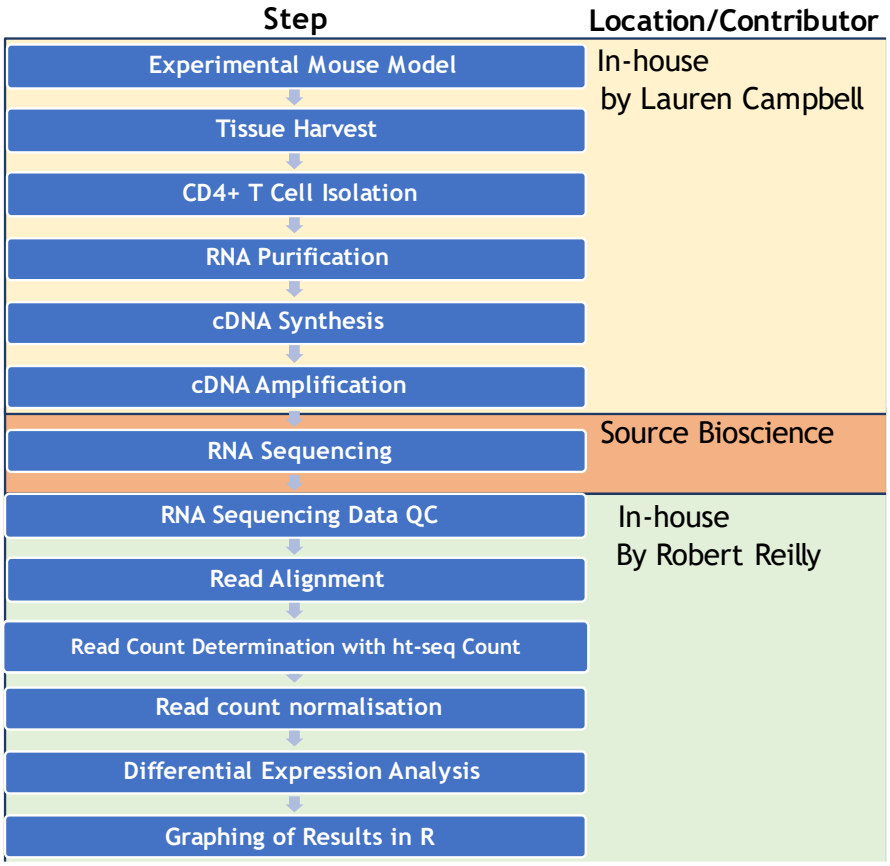

Figure 5. 1 RNA Sequencing work flow

Outline of the steps taken to generate RNA Sequencing data, where the step took place and primary contributor for each step.

The first aim was to identify if the CD4+ T cell transcriptome in gingivae and draining cervical lymph nodes differed between control infection and *P. gingivalis* infection. Principal component analysis revealed no differences in clustering patterns of CD4+ T cells between control and *P. gingivalis* infection in gingivae or draining lymph node. However, CD4+ T cells from gingivae and draining cervical lymph node clustered separately, irrespective of their infection state **(Fig. 5.2A)**. On further analysis, no genes were differentially expressed in gingivae or lymph node CD4+ T cells between control and *P. gingivalis* infection. In the control infection, 1405 genes were differentially expressed between gingivae and cervical lymph node CD4+ T cells; 1148 genes were upregulated and 257 were down regulated. In *P. gingivalis* infected animals, 1451 genes were differentially expressed between gingivae and cervical lymph node CD4+ T cells.1112 and 339 were up and down regulated respectively in the gingivae compared to cervical lymph node **(Fig. 5.2 B, C, D)**. Eight of the ten highest

expressed CD4+ T cell genes were common to all experimental groups. The genes with highest expression in lymph node were the same in both *P. gingivalis* and control infection **(Table 5.3)**. The CD4+ T cell transcripts with highest expression in gingivae were subtly different between *P. gingivalis* and control infection (**Table 5.4** and **5.5**). The ten genes with the greatest fold change between gingivae and lymph node were different in *P. gingivalis* and control infection **(Table 5.6** and **5.7**).

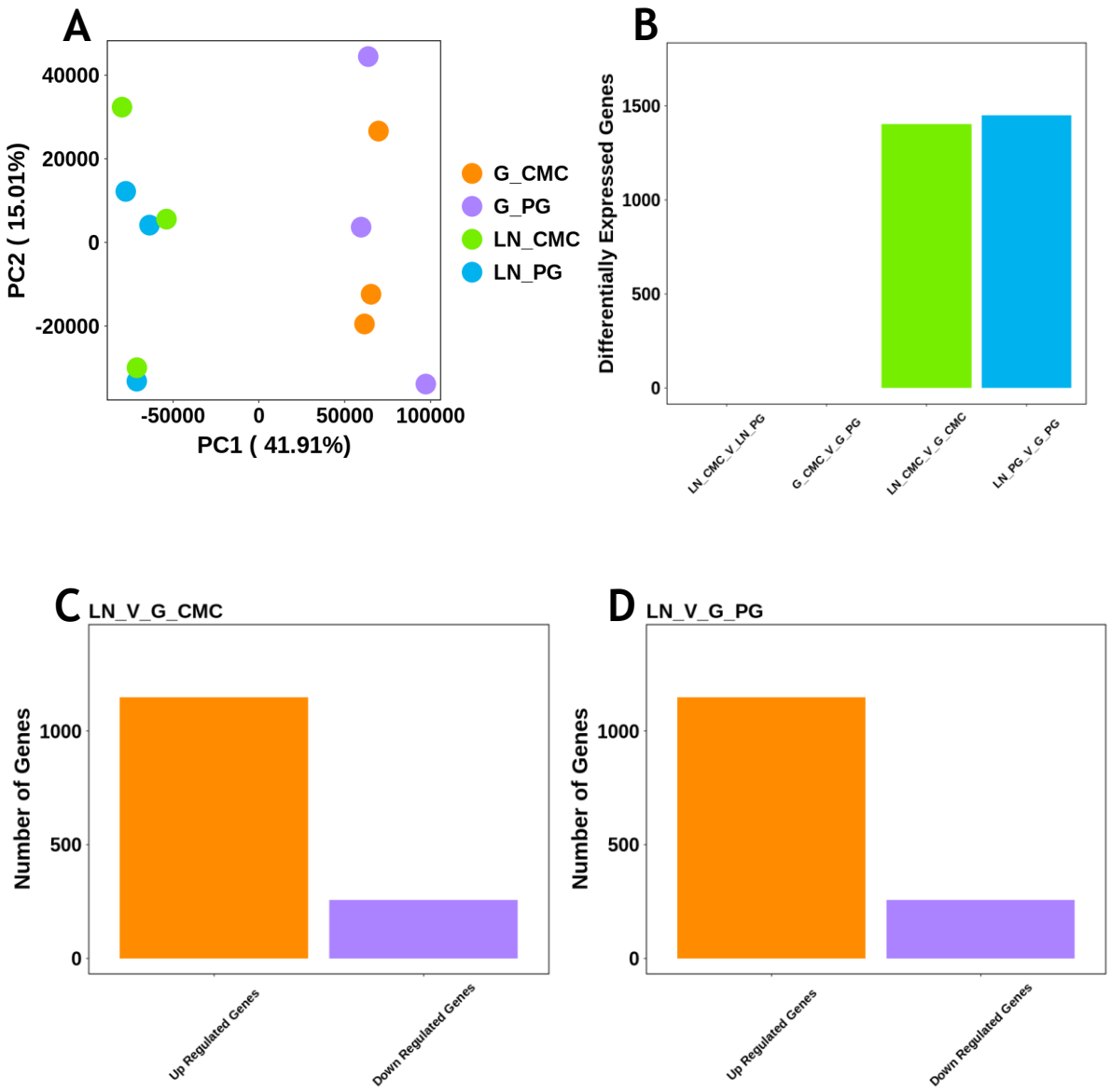

Figure 5. 2 Differential expression of genes in CD4+ T cells

CMC, only (n=3). At 28 days post infection, cells were isolated from gingivae and draining lymph nodes and CD4+ T cells were sorted. RNA was extracted, pre-amplified, then reverse transcribed for next-generation sequencing using NextSeq platform. DESeq2 was used to determine normalised gene expression and differential gene expression. A differentially expressed gene had

Figure 5.2 continued

a log2fold change of >1 and adjusted P value of <0.05 **(A)** Principal component analysis of normalised gene expression for each sample. Each data point represents the CD4+ T cell transcriptome from one sample. **(B)** Bar chart of differentially expressed genes between lymph nodes and gingivae CD4+ T cells in CMC(LN_CMC_V_G_CMC) or *P. gingivalis* (LN_PG_V_G_PG) infection and between CD4+ T cells from control and *P. gingivalis* infected lymph node (LN_CMC_V_LN_PG) and gingivae (G_CMC_V_GP_PG). **(C)** The number of significantly up and down regulated genes between lymph nodes and gingivae CD4+ T cells in CMC infection. **(D)** The number of significantly up and down regulated genes between lymph nodes and gingivae CD4+ T cells in *P. gingivalis* infection. The groups are CD4+ T cells from lymph node in control infection(LN_CMC), Gingiva in control infection(G_CMC), Lymph node in *P. gingivalis* Infection(LN_PG) and Gingiva in *P.gingivalis* infection (G_PG).

Gene	LN_CMC Mean Expression (FPKM)	LN_PG Mean Expression (FPKM)	Description	Reference
Actb	122019	126185	The protein Beta Actin supports the cytoskeleton framework.	https://medlineplus.gov/genetics/gene/actb/
CT010467.1	96368	106610	No data	
Tmsb4x	85576	79896	Actin polymerisation. Also involved in cell proliferation, migration, and differentiation	https://www.genecards.org/cgi-bin/carddisp.pl?gene=TMSB4X
mt-Rnr2	76143	65077	Enables G protein-coupled receptor binding activity	https://www.genecards.org/cgi-bin/carddisp.pl?gene=MT-RNR2
Lars2	50413	57508	encodes for mitochondrial leucyl-tRNA synthetase: responsible for protein synthesis in mitochondria	https://medlineplus.gov/genetics/gene/lars2/
mt-Co1	48130	45052	Contributes to cytochrome-c oxidase activity.	https://www.genecards.org/cgi-bin/carddisp.pl?gene=MT-CO1
Malat1	46215	43085	Produces a precursor transcript which plays a role in forming molecular scaffolds for ribonucleoprotein complexes.	https://www.genecards.org/cgi-bin/carddisp.pl?gene=MALAT1
B2m	44084	41194	Encodes a serum protein associated with the major histocompatibility complex (MHC) class I heavy chain on the surface of nucleated cells.	https://www.genecards.org/cgi-bin/carddisp.pl?gene=B2M
H2-D1	42139	41852	Encodes for H-2 class I histocompatibility antigen	https://www.uniprot.org/uniprot/P01899
Eef1a1	36772	36667	Encodes an isoform of the alpha subunit of the elongation factor-1 complex; responsible for the enzymatic delivery of aminoacyl tRNAs to the ribosome.	https://www.genecards.org/cgi-bin/carddisp.pl?gene=EEF1A1

Table 5. 3 Murine draining cervical lymph node CD4+ T cell genes with the highest mean expression

Gene	Mean Expression (FPKM)	Description	Reference
Actb	100326	The protein Beta Actin supports the cytoskeleton framework.	(https://medlineplus.gov/genetics/gene/actb/)
Junb	65826	Enables sequence-specific double-stranded DNA binding activity. Involved in positive regulation of transcription by RNA polymerase II.	https://www.genecards.org/cgi-bin/carddisp.pl?gene=JUNB
Tmsb4x	64629	Actin polymerisation. Also involved in cell proliferation, migration, and differentiation.	https://www.genecards.org/cgi-bin/carddisp.pl?gene=TMSB4X
H2-D1	50722	Encodes for H-2 class I histocompatibility antigen.	https://www.uniprot.org/uniprot/P01899
Lars2	50091	Encodes for mitochondrial leucyl-tRNA synthetase: responsible for protein synthesis in mitochondria.	https://medlineplus.gov/genetics/gene/lars2/
Malat1	46229	Produces a precursor transcript which plays a role in forming molecular scaffolds for ribonucleoprotein complexes.	https://www.genecards.org/cgi-bin/carddisp.pl?gene=MALAT1
mt-Rnr2	44651	Enables G protein-coupled receptor binding activity.	https://www.genecards.org/cgi-bin/carddisp.pl?gene=MT-RNR2
CT010467.1	40395	No data	
Hspa5	39696	Heat shock 70 protein family, involved in the folding and assembly of proteins in the endoplasmic reticulum (ER) and is a master regulator of ER homeostasis.	https://www.genecards.org/cgi-bin/carddisp.pl?gene=HSPA5
B2m	37084	Encodes a serum protein associated with the major histocompatibility complex (MHC) class I heavy chain on the surface of nucleated cells.	https://www.genecards.org/cgi-bin/carddisp.pl?gene=B2M

Table 5. 4 Gingivae CD4+ T cell genes with the highest mean expression from mice with control infection

Gene	Mean Expression (FPKM)	Description	Reference
Actb	91485	The protein Beta Actin supports the cytoskeleton framework.	(https://medlineplus.gov/genetics/gene/actb/)
Junb	68779	Enables sequence-specific double-stranded DNA binding activity. Involved in positive regulation of transcription by RNA polymerase II.	https://www.genecards.org/cgi-bin/carddisp.pl?gene=JUNB
Tmsb4x	64799	Actin polymerisation. Also involved in cell proliferation, migration, and differentiation.	https://www.genecards.org/cgi-bin/carddisp.pl?gene=TMSB4X
CT010467.1	56463	No data	
mt-Rnr2	53409	Enables G protein-coupled receptor binding activity.	https://www.genecards.org/cgi-bin/carddisp.pl?gene=MT-RNR2
H2-D1	52951	Encodes for H-2 class I histocompatibility antigen.	https://www.uniprot.org/uniprot/P01899
Lars2	50491	Encodes for mitochondrial leucyl-tRNA synthetase: responsible for protein synthesis in mitochondria.	https://medlineplus.gov/genetics/gene/lars2/
Hspa5	43743	Heat shock 70 protein family, involved in the folding and assembly of proteins in the endoplasmic reticulum (ER) and is a master regulator of ER homeostasis.	https://www.genecards.org/cgi-bin/carddisp.pl?gene=HSPA5
Malat1	42677	Produces a precursor transcript which plays a role in forming molecular scaffolds for ribonucleoprotein complexes.	https://www.genecards.org/cgi-bin/carddisp.pl?gene=MALAT1
Eef1a1	40536	Encodes an isoform of the alpha subunit of the elongation factor-1 complex; responsible for the enzymatic delivery of aminoacyl tRNAs to the ribosome.	https://www.genecards.org/cgi-bin/carddisp.pl?gene=EEF1A1

Table 5. 5 Gingivae CD4+ T cell genes with the highest mean expression from mice with *P. gingivalis* infection

Gene ID	Adjusted P Value	log2fold Change	Description	Reference
Il22	9.59E-10	9.01	Member of the IL10 family of cytokines that mediate cellular inflammatory responses. The encoded protein functions in antimicrobial defence at mucosal surfaces and in tissue repair.	https://www.genecards.org/cgi-bin/carddisp.pl?gene=IL22
Dusp8	1.84E-11	7.31	Phosphatase that inactivates target kinases by dephosphorylating both the phosphoserine/threonine and phosphotyrosine residues.	https://www.genecards.org/cgi-bin/carddisp.pl?gene=DUSP8
Olfr1342	3.97E-06	6.99	olfactory receptor 1342.	https://www.ncbi.nlm.nih.gov/gene/258708
Snai1	1.10E-06	6.68	Downregulates the expression of ectodermal genes within the mesoderm.	https://www.genecards.org/cgi-bin/carddisp.pl?gene=SNAI1
Cx3cl1	3.14E-09	5.64	Chemokine that is a ligand for CX3CR1	https://www.genecards.org/cgi-bin/carddisp.pl?gene=CX3CL1&keywords=Cx3cl1
Bpifa2	8.02E-08	-5.40	Proposed to play a role in the local antibacterial response in nose, mouth and upper respiratory pathways.	https://www.genecards.org/cgi-bin/carddisp.pl?gene=BPIFA2&keywords=Bpifa2
Clnk	1.80E-07	3.95	Plays a role in the regulation of immunoreceptor signalling.	https://www.genecards.org/cgi-bin/carddisp.pl?gene=CLNK&keywords=Clnk
Arhgef28	8.59E-07	3.33	The encoded protein interacts with low molecular weight neurofilament mRNA and may be involved in the formation of amyotrophic lateral sclerosis neurofilament aggregates.	https://www.genecards.org/cgi-bin/carddisp.pl?gene=ARHGEF28&keywords=Arhgef28
Gprc5a	9.97E-08	3.27	Encoded protein may be involved in interaction between retinoic acid and G protein signalling pathways.	https://www.genecards.org/cgi-bin/carddisp.pl?gene=GPRC5A&keywords=Gprc5a
Reg3g	0.00026	2.63	The protein encoded by this gene is an antimicrobial lectin with activity against Gram-positive bacteria.	https://www.genecards.org/cgi-bin/carddisp.pl?gene=REG3G&keywords=Reg3g

Table 5. 6 Ten genes with the greatest difference in expression between draining lymph node and Gingivae CD4+ T cell in control infection

Gene ID	Adjusted P Value	log2fold Change	Description	Reference
IL-22	1.25E-08	9.01	Member of the IL10 family of cytokines that mediate cellular inflammatory responses. The encoded protein functions in antimicrobial defence at mucosal surfaces and in tissue repair.	https://www.genecards.org/cgi-bin/carddisp.pl?gene=IL22
Serinc2	1.36E-08	7.95	Its related pathways are responsible for metabolism and peptide chain elongation.	https://www.genecards.org/cgi-bin/carddisp.pl?gene=SERINC2&keywords=Serinc2
Hes1	1.27E-08	7.94	Transcriptional repressor of genes that require a basic helix-loop-helix protein for their transcription.	https://www.genecards.org/cgi-bin/carddisp.pl?gene=HES1&keywords=Hes1
4930438A08Rik	3.05E-10	7.49	Predicted to enable L-amino-acid oxidase activity and polyamine oxidase activity.	https://www.ncbi.nlm.nih.gov/gene/73988
Dusp8	2.33E-10	7.31	Phosphatase that inactivates target kinases by dephosphorylating both the phosphoserine/threonine and phosphotyrosine residues.	https://www.genecards.org/cgi-bin/carddisp.pl?gene=DUSP8
Olfr1342	6.72E-06	6.99	Olfactory receptor 1342	https://www.ncbi.nlm.nih.gov/gene/258708
Dkk3	1.39E-06	6.97	The secreted protein contains two cysteine rich regions and is involved in embryonic development.	https://www.genecards.org/cgi-bin/carddisp.pl?gene=DKK3&keywords=Dkk3
Lilrb4a	2.87E-05	6.95	Receptor expressed on immune cells where it binds to MHC class I molecules on antigen-presenting cells and transduces a negative signal that inhibits stimulation of an immune response.	https://www.genecards.org/cgi-bin/carddisp.pl?gene=LILRB4&keywords=Lilrb4a
Mapk10	2.70E-06	6.92	The protein encoded by this gene is a member of the MAP kinase family. MAP kinases act as integration points for multiple biochemical signals, and are involved in a wide variety of cellular processes.	https://www.genecards.org/cgi-bin/carddisp.pl?gene=MAPK10&keywords=Mapk10
Kcnk1	5.36E-07	6.92	Encodes one of the members of the superfamily of potassium channel proteins containing two pore-forming P domains.	https://www.genecards.org/cgi-bin/carddisp.pl?gene=KCNK1&keywords=Kcnk1

Table 5. 7 Ten genes with the greatest difference in expression between draining lymph node and Gingivae CD4+ T cell in *P. gingivalis* infection

To further explore differential gene expression patterns, the log2fold change and mean expression of transcripts between gingivae and lymph node CD4+ T cells in control infection **(Fig. 5.3 A)** and *P. gingivalis* infection **(Fig. 5.3 B)** were analysed. The majority of significant transcriptional changes occurred at low levels of expression. Differential CD4+ T cell expression patterns between lymph node and gingivae were similar in control and *P. gingivalis* infection. Furthermore, CD4+ T cell differential gene expression between control and *P. gingivalis* infection were similar in gingivae and lymph node, whilst some genes did show differential expression these did not reach statistical significance **(Fig. 5.3 C, D)**. To identify the relationship between significance and fold change volcano plots were used. This demonstrated that between lymph node and gingivae CD4+ T cells more genes were significantly upregulated then downregulated in both control and *P. gingivalis* infection in the gingivae (**Fig. 5.4 A**, **B**). In comparison, both gingivae and draining lymph node CD4+ T cell transcripts had similar differential expression between control an *P. gingivali*s infection (**Fig. 5.4 C, D**). When comparing the log2fold change of transcripts between gingivae and draining lymph node in both control infection and *P. gingivalis* infection, a linear relationship exists. Spearman co-efficient analysis showed a Rho = 0.73, a strong linear relationship, suggesting the log 2-fold change of genes between dLN and gingiva CD4+ T cells is similar in control and *P. gingivalis* infection **(Fig. 5.5)**

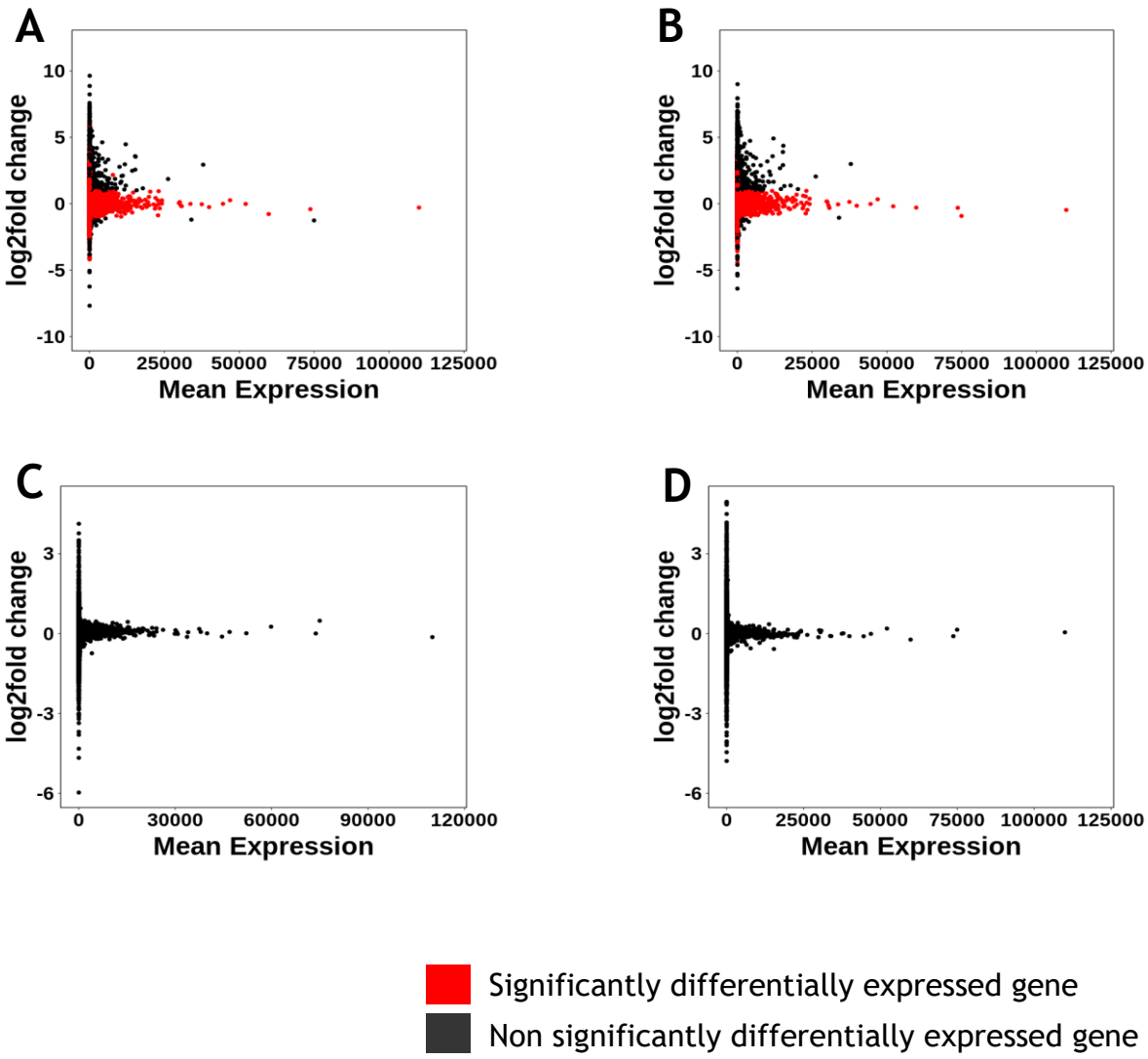

Figure 5. 3 MA plots of differential gene expression

Samples were prepared as described in figure 5.1. The total mean gene expression across all samples was used. **(A)** MA plot of gene expression change between lymph nodes and gingivae CD4+ T cells in CMC infection. **(B)** MA plot of gene expression change between lymph nodes and gingivae CD4+ T cells in *P. gingivalis* infection. **(C)** MA plot of gene expression change in gingivae CD4+ T cells in between CMC and *P. gingivalis* infection. **(D)** MA plot of gene expression change in lymph nodes CD4+ T cells in between CMC and *P. gingivalis* infection. Red points denote genes with significant differential gene expression, black points denotes genes that are not significantly differentially expressed.

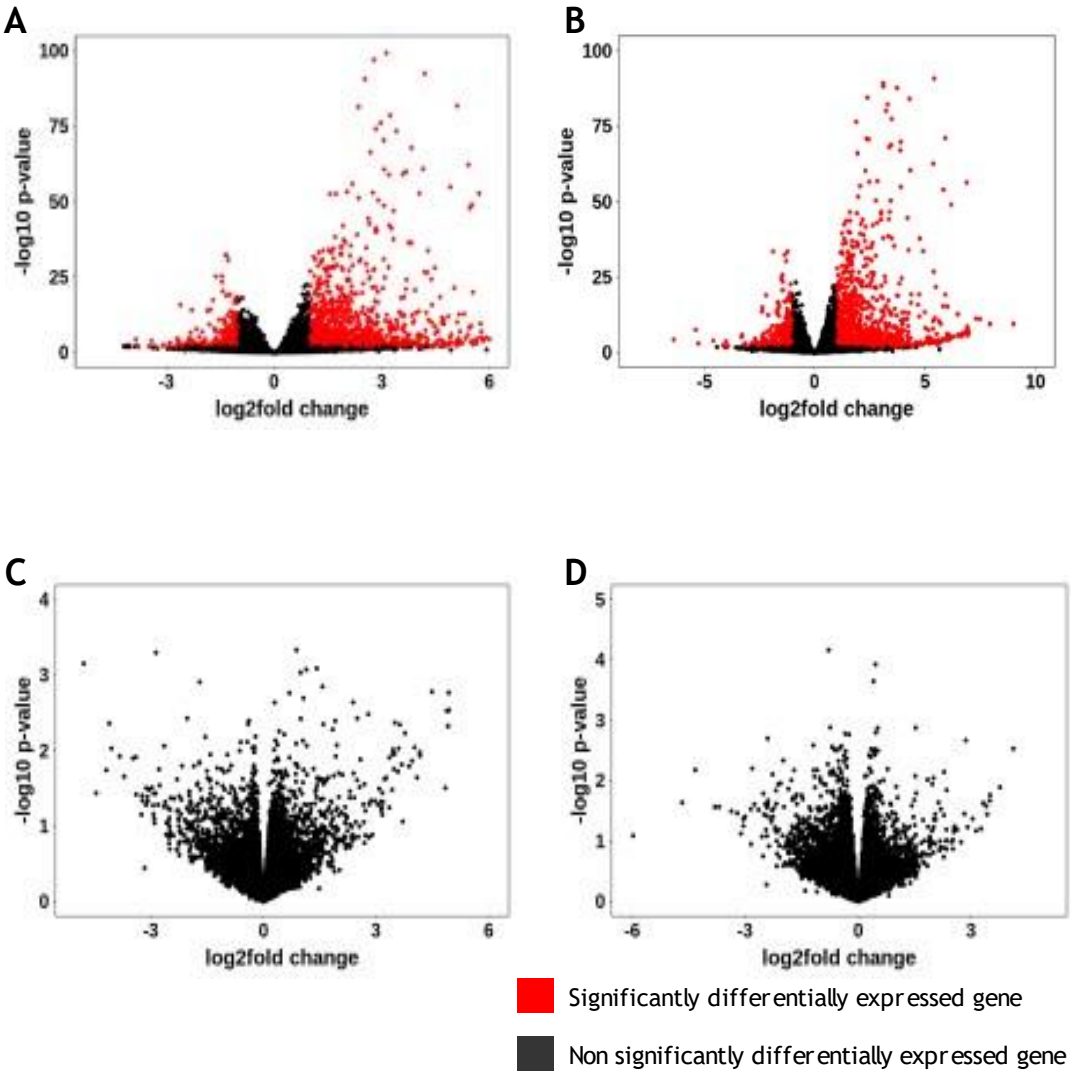

Figure 5. 4 Volcano plots of gene differential expression

Samples were prepared as described in figure 5.1. Significantly differentially expressed genes are coloured red. **(A)** Volcano plot of differential gene expression between lymph nodes and gingivae CD4+ T cells in CMC infection. **(B)** Volcano plot of differential gene expression between lymph nodes and gingivae CD4+ T cells in *P. gingivalis* infection. **(C)** Volcano plot of gene expression change in gingivae CD4+ T cells in between CMC and *P. gingivalis* infection. **(D)** Volcano plot of gene expression change in lymph nodes CD4+ T cells in between CMC and *P. gingivalis* infection. Red points denote genes with significant differential gene expression, black points denotes genes that are not significantly differentially expressed.

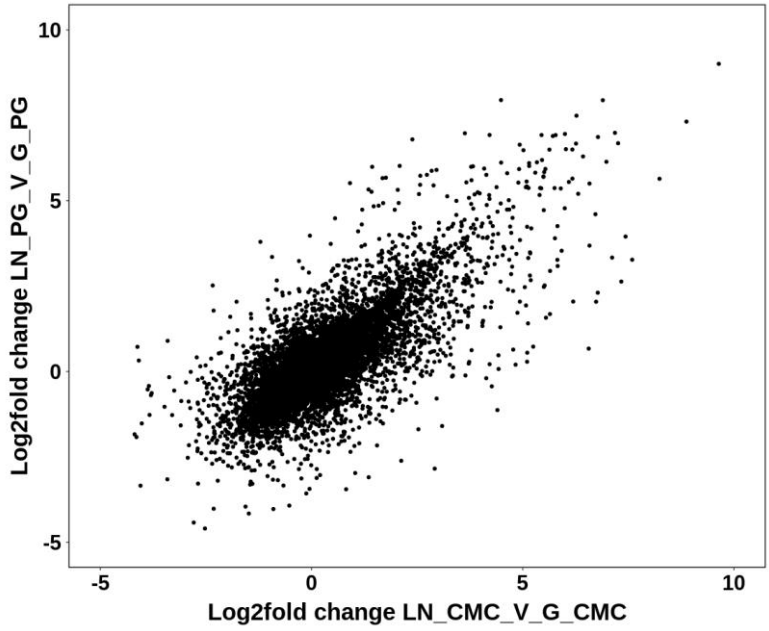

Figure 5. 5 Log2fold change in gene expression scatter-plot

Samples were prepared as described in figure 5.1 The log 2-fold change between lymph nodes and gingivae CD4+ T cells in control infection (x-axis) and *P. gingivalis* infection (y-axis) were plotted. A Spearman coefficient analysis was conducted to assess the relationship in gene expression change in control infection compared to *P. gingivalis* infection, this showed a Rho = 0.73.

In total 1898 genes exhibited differential expression between gingiva and lymph node. Between gingiva and lymph node CD4+ T cells, in mice with control infection, 1405 genes were differentially expressed. In *P. gingivalis* infection 1451 genes were differentially expressed between lymph node and gingiva CD4+ T cells. In total 958 genes were differentially expressed between gingivae and lymph nodes in both control and *P. gingivalis* infection, 447 and 493 were differentially expressed only in control and *P. gingivalis* infection respectively **(Fig. 5.6 A)**. To visualise expression patterns for individual samples a heatmap was used, with gene expression clustering, to identify differentially expressed genes between samples and groups. This revealed that individual genes had similar expression levels across samples in each respective tissue. This also highlighted the clear differential expression of genes between tissues in control and *P. gingivalis* infection (**Fig. 5.6 B**).

To identify if genes with related functions were differentially expressed, gene set enrichment analysis was conducted. Multiple gene sets were significantly differentially expressed between lymph node and gingivae CD4+ T cells in control or *P. gingivalis* infection (**Fig. 5.7**). The gene set with the highest level of significance of differential expression was that for the regulation of protein serine/threonine kinase activity. Reflecting our previous observations, most of these genes were upregulated in gingival CD4+ T cells compared to draining lymph nodes. Furthermore, similar differential expression patterns were seen in control and *P. gingivalis* infection (**Fig. 5.8 and Fig. 5.9**).

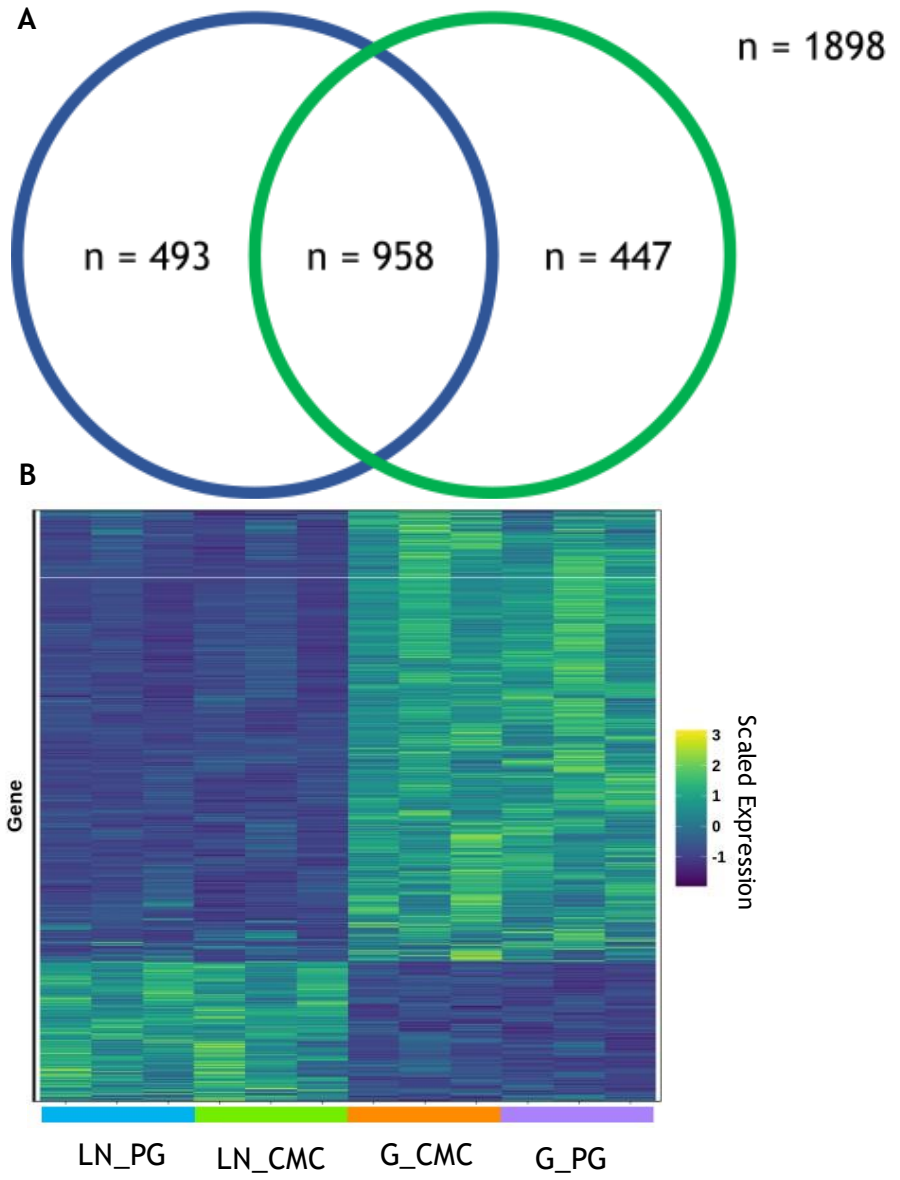

Figure 5. 6 Differentially expressed genes in draining lymph nodes and gingivae CD4+ T cells

Samples were prepared as described in figure 5.1. **(A)** Venn diagram of the number of differentially expressed genes between draining lymph nodes and gingivae CD4+ T cells in CMC (green circle) and P. *ginigvalis* infection (blue circle). **(B)** Heatmap of all significantly differentially expressed CD4+ T cell genes between draining lymph nodes and gingivae. The heatmap was clustered based on gene expression.

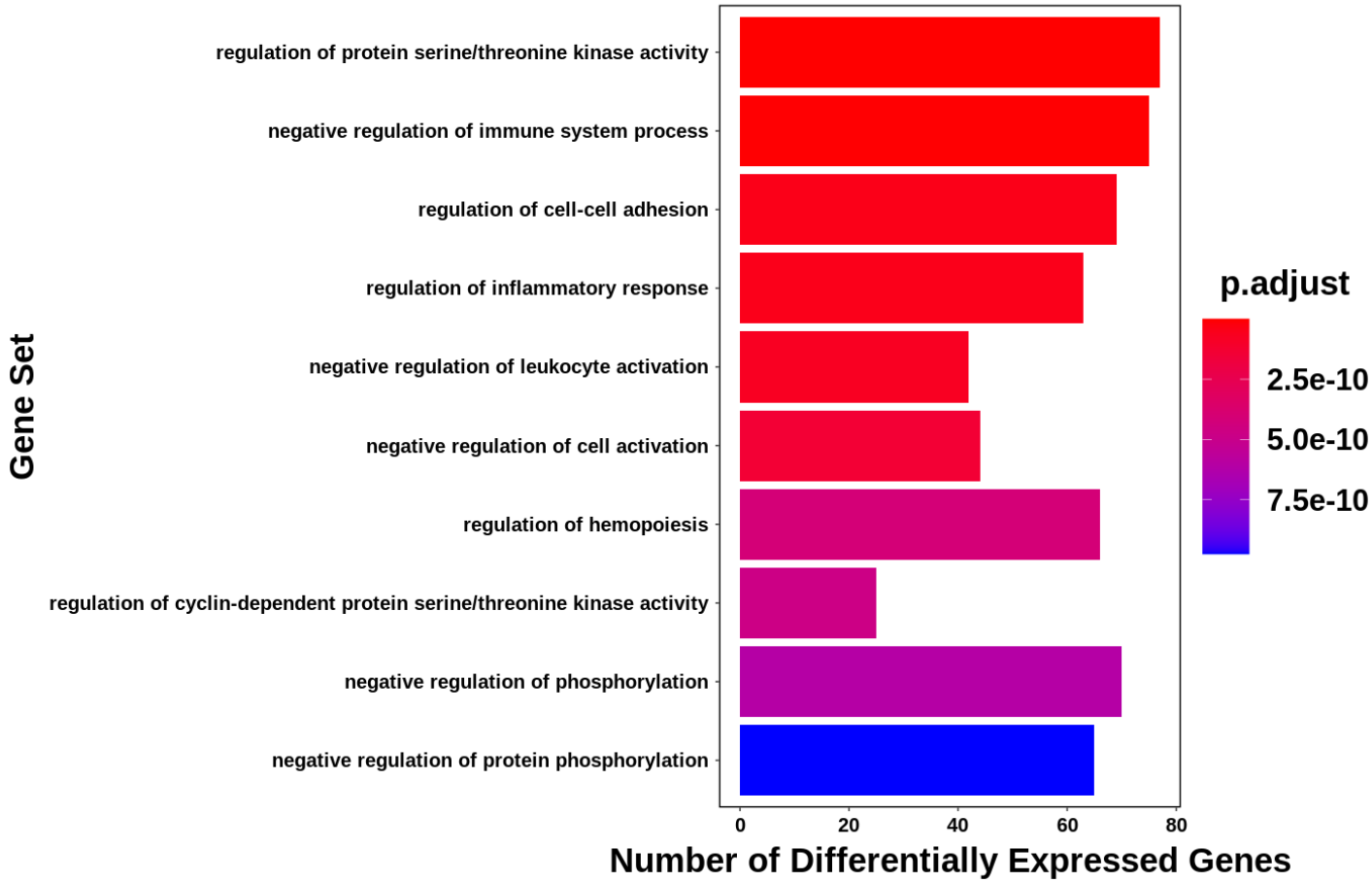

Figure 5. 7 Over representation analysis of differentially expressed genes between lymph nodes and gingivae CD4+ T cells in CMC or *P. gingivalis* infection

Samples were prepared as described in figure 5.1 and differential expression between lymph nodes and gingivae CD4+ T cells in CMC and *P. gingivalis* infection was determined using DESeq2. **(A)** Boxplot of significantly differentially expressed Gene Sets in genes that were differentially expressed lymph nodes or gingivae CD4+ T cells in CMC or *P. gingivalis* infection, using ClusterProfiler in R, the number and significance of differentially expressed genes in different gene sets were analysed.

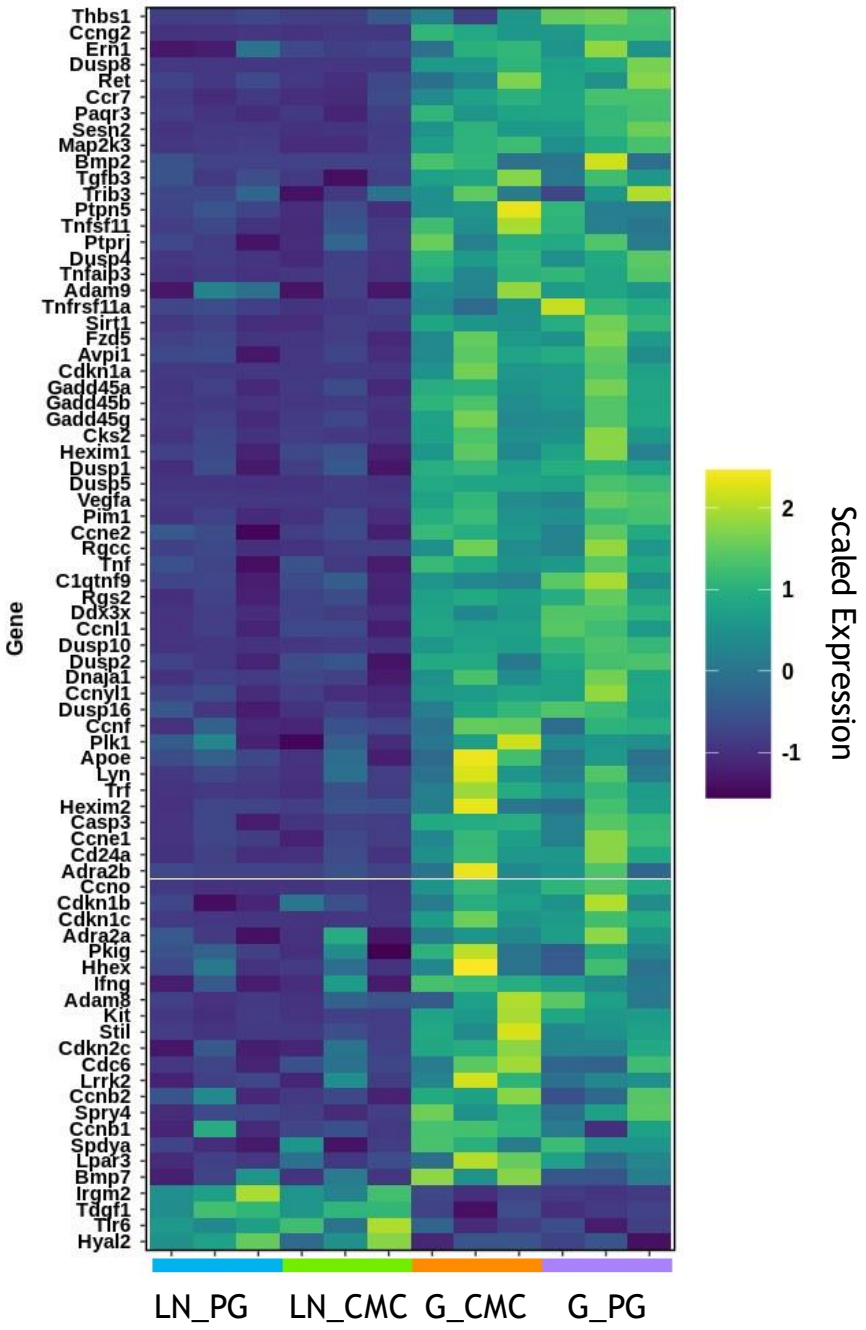

Figure 5. 8 Heatmap of significantly differentially expressed genes in the regulation of protein serine/threonine kinase activity gene set

Samples were prepared as described in figure 5.1, and differential expression between lymph nodes and gingivae CD4+ T cells in CMC and *P. gingivalis* infection was determined using DESeq2, gene expression was subsequently scaled for heatmap analysis and clustered based on gene expression.

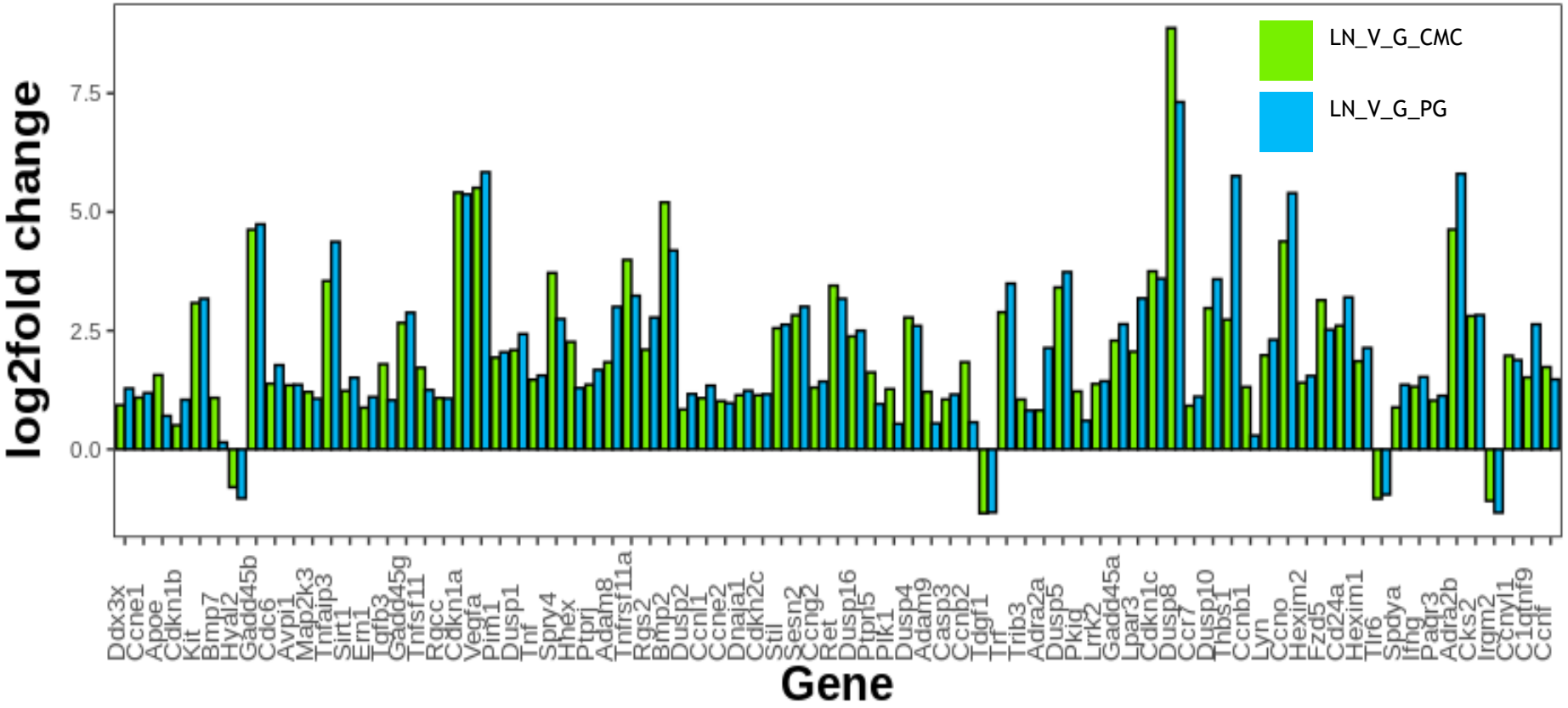

Figure 5. 9 Bar chart of log 2-fold change of significantly differentially expressed genes from the regulation of protein serine/threonine kinase activity gene set.

Samples were prepared as described in figure 5.1 and differential expression between lymph nodes and gingivae CD4+ T cells in CMC and *P. gingivalis* infection was determined using DESeq2.

Next, gene set enrichment analysis was conducted for genes that were significantly differentially expressed between draining lymph node and gingivae CD4+ T cells in both control and *P. gingivalis* infection. The gene sets that were significantly enriched in control and *P. gingivalis* infection were, unsurprisingly, similar to those enriched in *P. gingivalis* infection or control infection. However, there were differences, most notably the gene set with the greatest significance was for regulation of cell-cell adhesion (**Fig. 5.10**). A heatmap analysis of these genes revealed most genes in this set were upregulated in gingiva CD4+ T cells compared to lymph node CD4+ T cells. Whilst CD4+ T cell gene expression was different between tissues, it was similar between control and *P. gingivalis* infection in each tissue **(Fig. 5.11)**. Once again, the individual differentially expressed genes between draining cervical lymph node and gingivae CD4+ T cells in this set exhibited similar expression changes in both *P. gingivalis* and control infection **(Fig. 5.12)**.

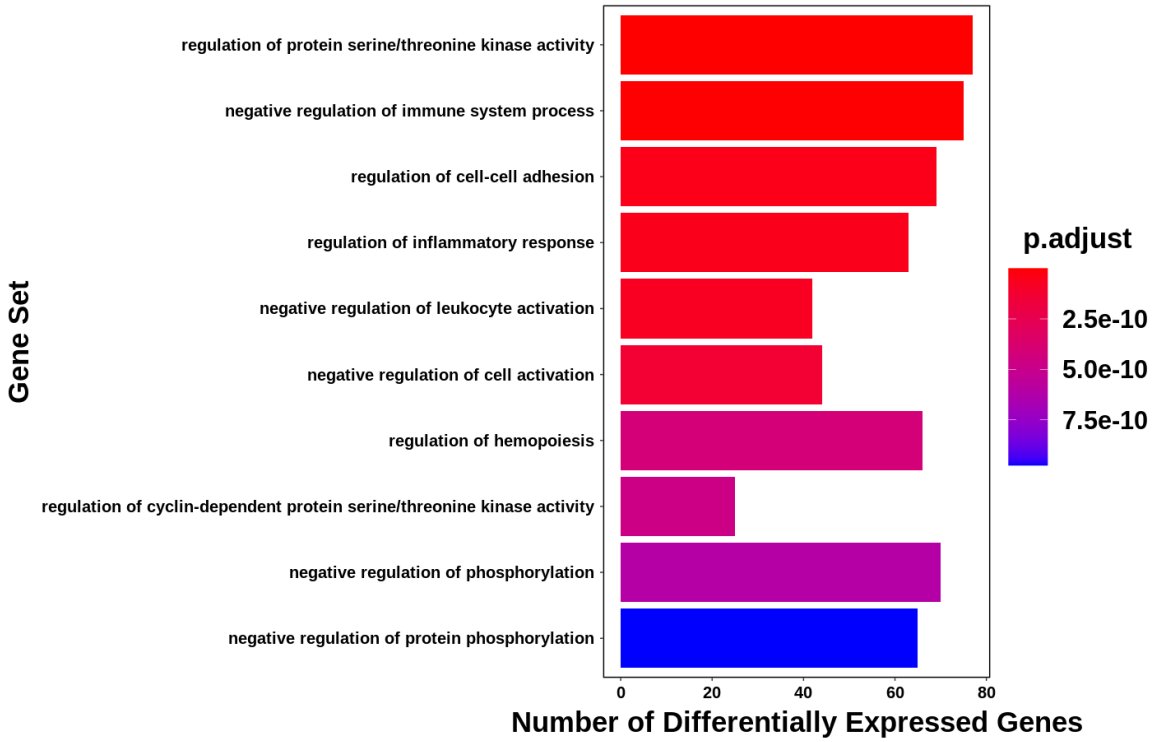

Figure 5. 10 Over Representation Analysis (ORA) of differentially expressed genes from lymph nodes and gingivae CD4+ T cells in CMC or *P. gingivalis* infection

Samples were prepared as described in figure 5.1 and differential expression between lymph nodes and gingivae CD4+ T cells in CMC and *P. gingivalis* infection was determined using DESeq2. A boxplot shows the ten most significantly differentially expressed gene sets in genes that were differentially expressed lymph nodes and gingivae CD4+ T cells in CMC and *P. gingivalis* infection.

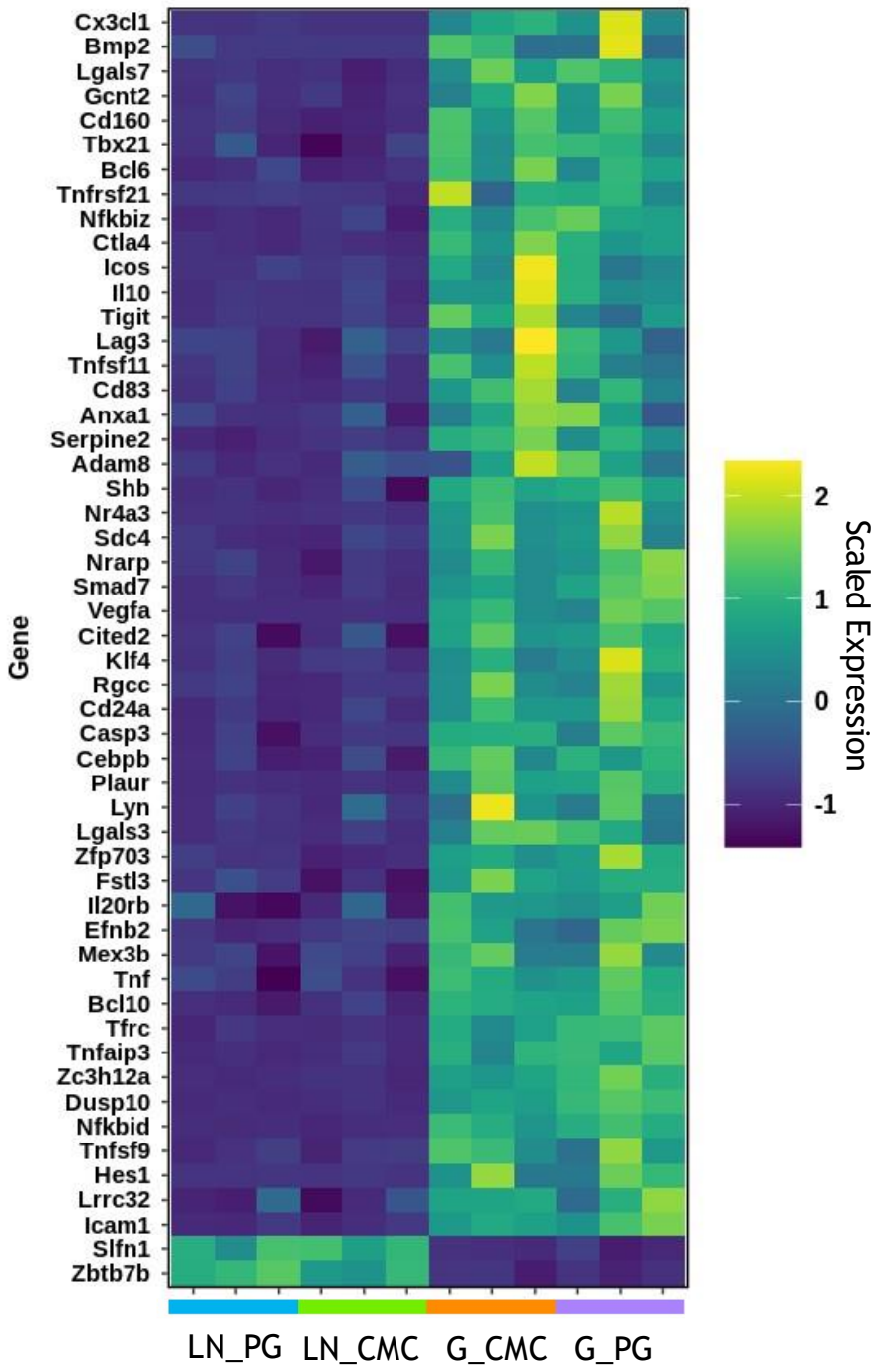

Figure 5. 11 Heatmap of significantly differentially expressed genes in the regulation of cell-cell adhesion gene set

Samples were prepared as described in figure 5.1 and differential expression between lymph nodes and gingivae CD4+ T cells in CMC and *P. gingivalis* infection was determined using DESeq2, gene expression was subsequently scaled for heatmap analysis of genes in the regulation of cell-cell adhesion gene set and clustered based on gene expression.

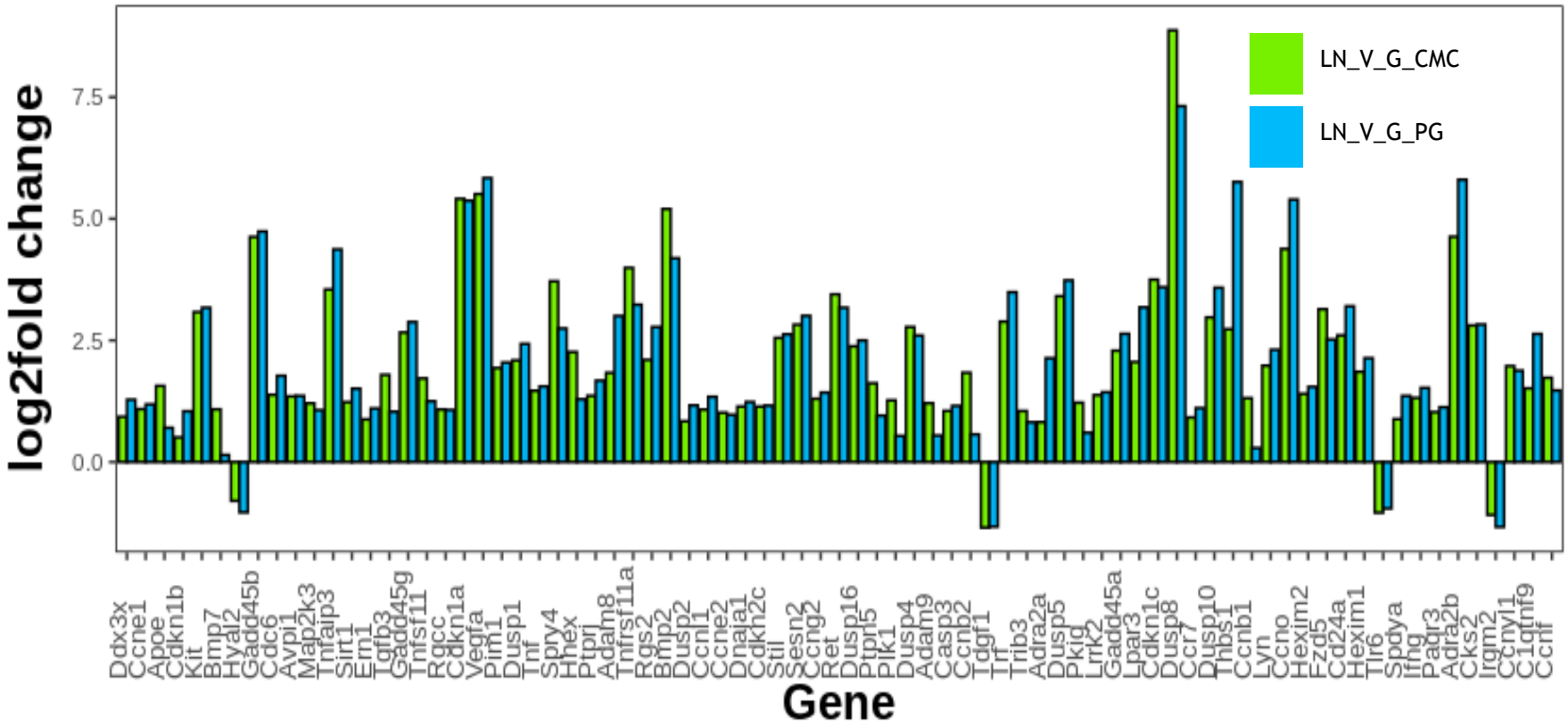

Figure 5. 12 Bar chart of log-2-fold change of significantly differentially expressed genes from the regulation of cell-cell adhesion gene set

Bar chart of log 2-fold change of significantly differentially expressed genes from the regulation of cell-cell adhesion gene set. Samples were prepared as described in figure 5.1 and differential expression between lymph nodes and gingivae CD4+ T cells in CMC and *P. gingivalis* infection was determined using DESeq2. Bar charts of log2fold change were plotted using R.

5.2.2 Targeted analysis

G protein-coupled receptors (GPCR) are the largest family of cell membrane receptors (Sriram and Insel, 2018). They are also one of the most common therapeutic targets in medicine with 30% of drugs designed to target GPCRs (Santos *et al.*, 2017). To identify potential therapeutic targets for the treatment of T cell mediated oral disease differentially expressed GPCR were identified. In total, 176 GPCRs had detectable levels of expression in CD4+ T cells. Thirty-five GPCR exhibited differential expression between lymph node and gingivae, the majority of which were up regulated in gingival CD4+ T cells (**Fig. 5.13**).

Of the thirty-five differentially expressed GPCR, 11 of these were chemokine receptors, the majority of which were upregulated. In total, 21 typical or atypical chemokine receptors had detectable expression in gingivae or lymph node CD4+ T cells. (**Fig. 5.14)**.

Alongside chemokine receptors, integrins and selectin ligands also play a significant role in cellular navigation. In total, 17 integrins and three selectin ligands had detectable levels of expression in gingivae or lymph node CD4+ T cells, although none of these exhibited significant differential expression between tissue sites (**Fig. 5.15)**.

Chemokine expression was then analysed to investigate the impact that T cells may have on cellular recruitment to the gingivae, 19 chemokines had detectable levels of expression in CD4+ T cells. Of the genes these five chemokines were significantly upregulated in gingivae CD4+ T cells compared to draining lymph node (**Fig. 5.16)**.

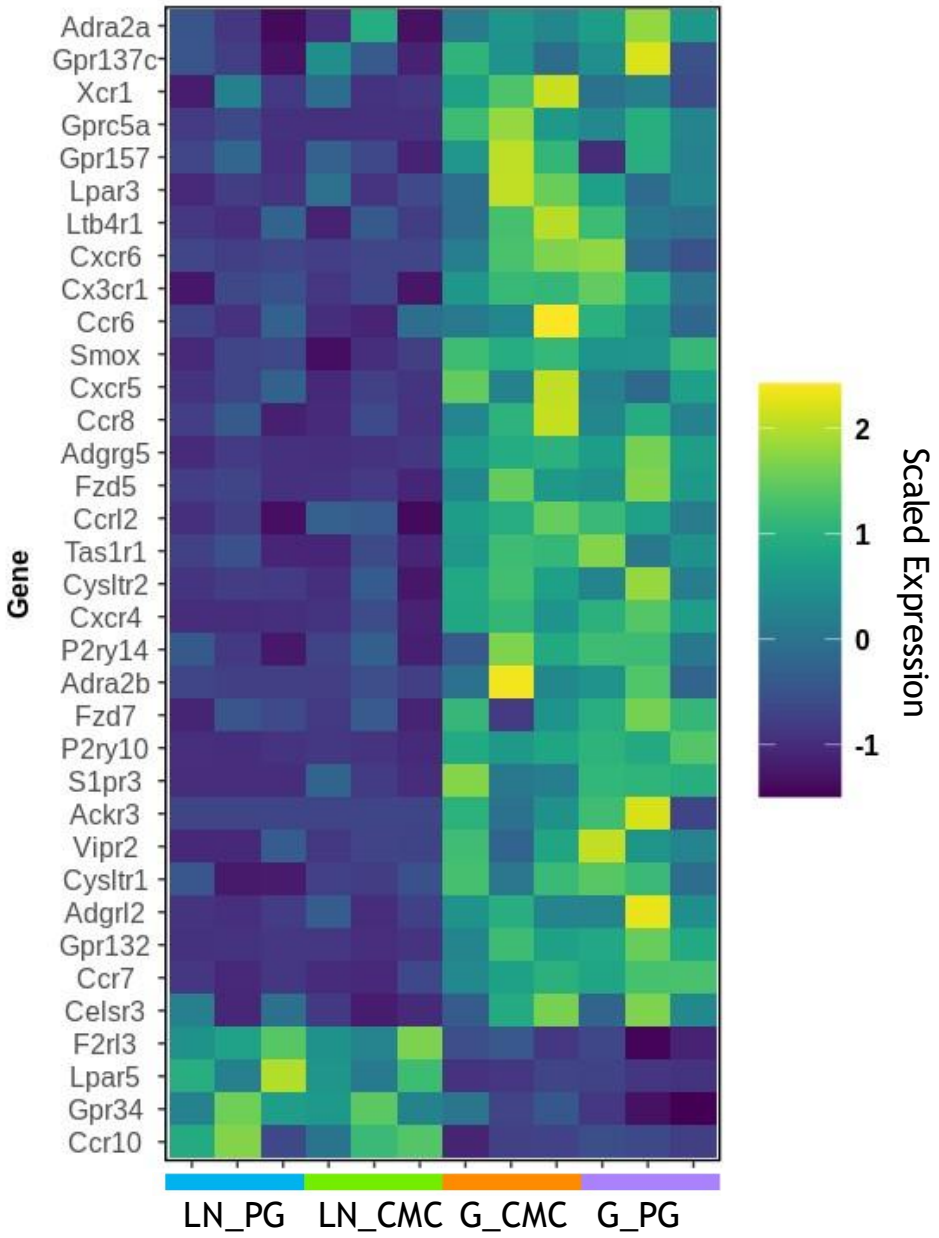

Figure 5. 13 Heatmap of significantly differentially expressed genes G-Protein Coupled Receptors

Samples were prepared as described in figure 5.1 and differential expression between lymph nodes and gingivae CD4+ T cells in CMC and *P. gingivalis* infection was determined using DESeq2, gene expression values of GPCRs were scaled and clustered based on gene expression.

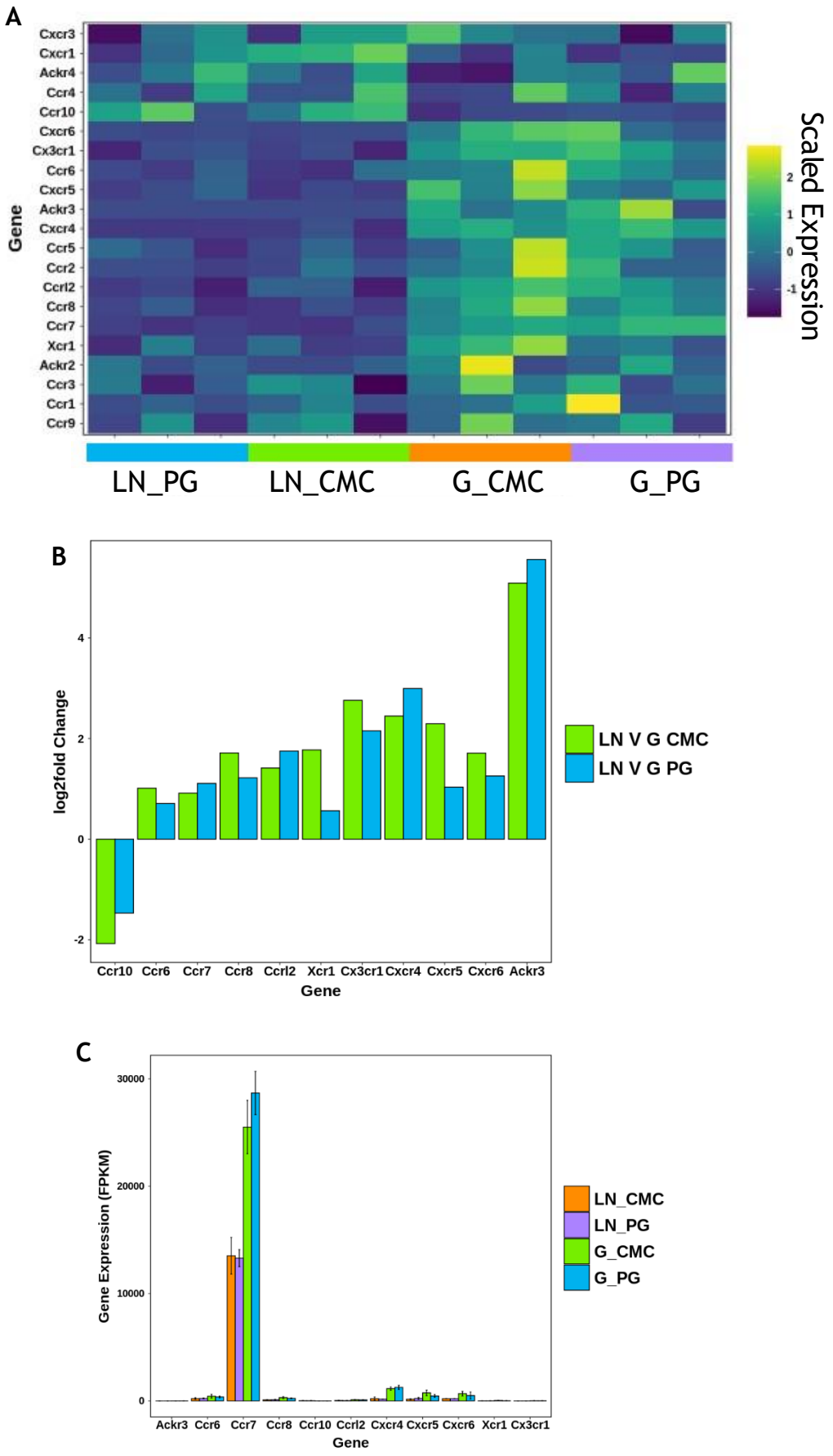

Figure 5.14 legend overleaf

Figure 5.4 CD4+ T cell chemokine receptor expression

Samples were prepared as described in figure 5.1 and differential expression between lymph nodes and gingivae CD4+ T cells in CMC and *P. gingivalis* infection was determined using DESeq2. **(A)** Heatmap of chemokine receptors with detectable levels of expression, all values were scaled. **(B)** Boxplot of chemokine receptor expression with significant differential expression between gingiva and lymph node CD4+ T cells. The top of each bar represents the mean, the whiskers are the standard deviation of the mean. **(C)** Log 2-fold change of chemokine receptor expression between lymph nodes and gingivae in control and *P. gingivalis* infection.

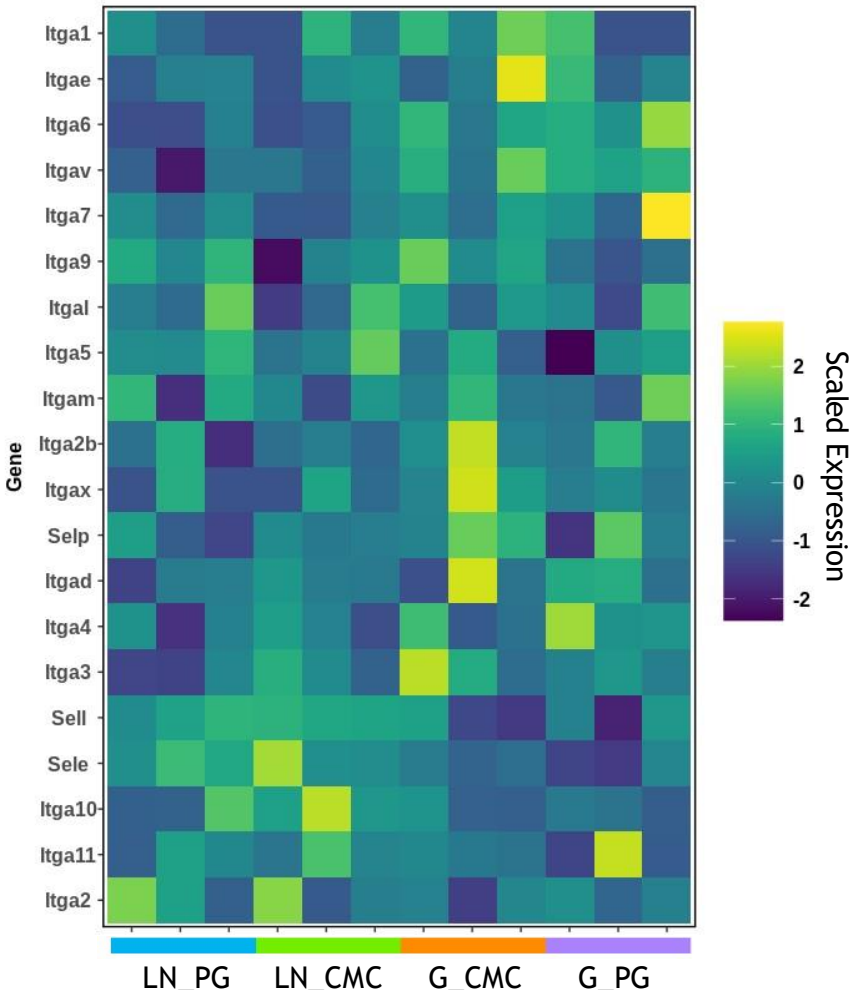

Figure 5.15 Heatmap of integrin and selectin ligand expression

Samples were prepared as described in figure 5.1 and differential expression between lymph nodes and gingivae CD4+ T cells in CMC and *P. gingivalis* infection was determined using DESeq2, gene expression values of integrins and selectin ligands were scaled for and clustered based on gene expression.

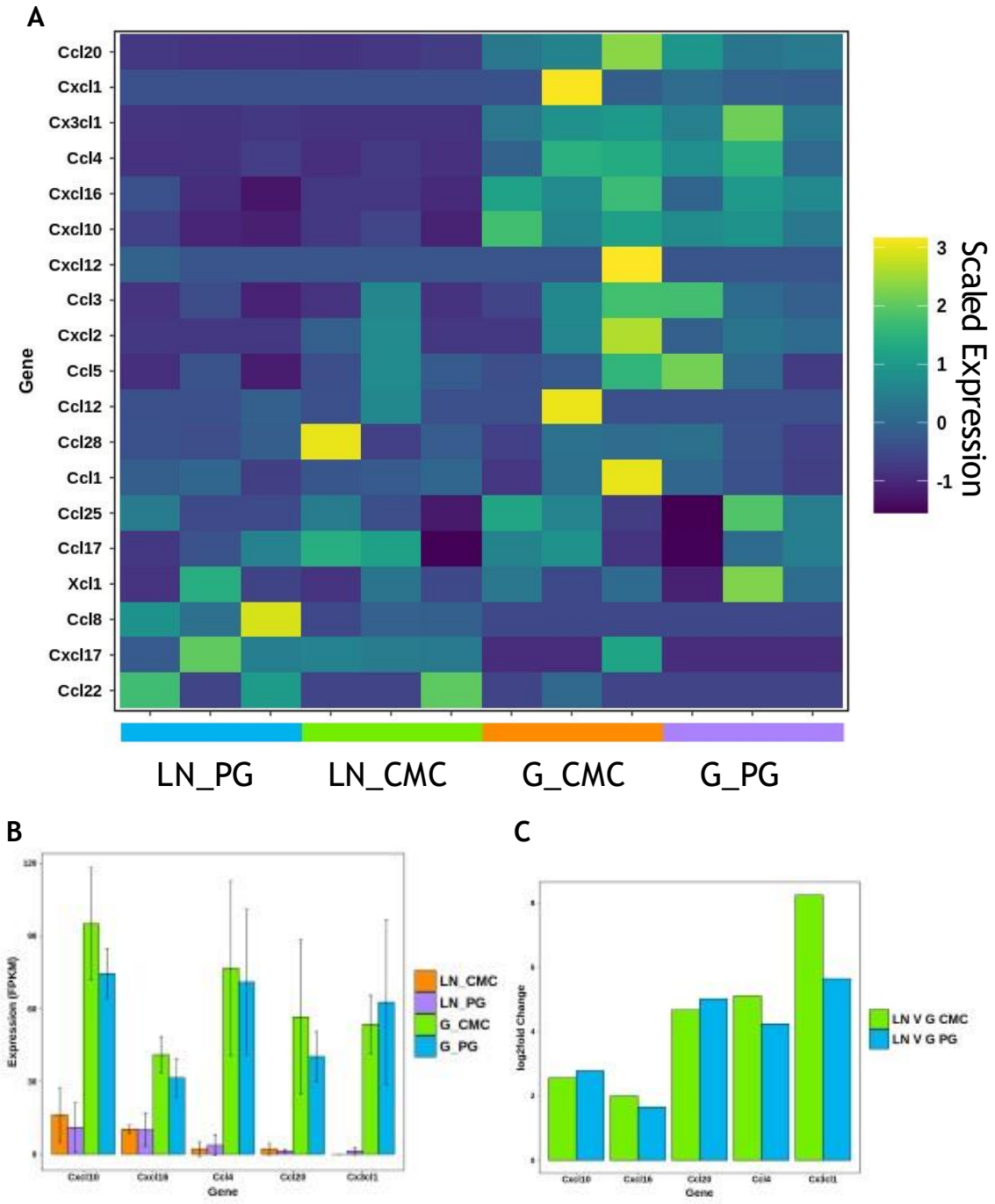

Figure 5. 14 CD4+ T cell chemokine expression

Samples were prepared as described in figure 5.1 and differential expression between lymph nodes and gingivae CD4+ T cells in CMC and *P. gingivalis* infection was determined using DESeq2. **(A)** Heatmap of scaled chemokine ligand with detectable levels of expressions, all values were scaled. **(B)** Boxplot of chemokine ligand expression with differential expression between gingiva and lymph nodes. The top of each bar represents the mean, the whiskers are the standard deviation of the mean. **(C)** Log 2-fold change of chemokine ligand expression between lymph nodes and gingivae in control and *P. gingivalis* infection.

5.3 Discussion

The findings from this chapter provide an in depth and unbiased overview of the CD4+ T cell transcriptome in murine gingivae and lymph node in health and during *P. gingivalis* infection, and a targeted analysis of transcripts important in cell migration.

These data show the CD4+ T cell transcriptome in both gingivae and lymph node were similar between *P. gingivalis* and control infection. This was surprising as T cells are essential to maintaining health and crucial to the development of periodontitis, thus a difference in transcriptome was hypothesised (Baker *et al.*, 1999; Baker *et al.*, 2002). This suggests that another mechanism is responsible for the development of alveolar bone loss in periodontitis, but T cells play a role in initiating these pathways; as T cell deficient mice have diminished alveolar bone loss when exposed to *P. gingivalis*. Several genes did exhibit differential expression without significance, as such, the experiment may have lacked statistical power to detect more subtle changes in the transcriptome that may contribute to the development of periodontitis. The experimental design may have contributed to this too. Murine palate was used to facilitate the collection of enough CD4+ T cells for transcriptional analysis, this may have diluted the number of T cells that are present specifically at the junctional epithelium and potentially responsible for the development of alveolar bone loss. Furthermore, palatal tissue was harvested at one time point, and whilst efforts were made to identify the most relevant time point for analysis, changes in the T cell transcriptome in gingiva may occur earlier or later in this process. Furthermore, the similarity of the transcriptome reinforces the concept of murine palate being perpetual exposed to pathogens, thus an active immune response is present even in apparent health. The limited sample size is also an important limitation of these data.

Despite no transcriptional differences being detected in tissue between *P. gingivalis* infection and control, 1898 genes were differentially expressed between CD4+ T cells in gingivae compared to draining lymph node. This suggests that their transcriptome changes to reflect the needs of their local tissue environment. Whilst, most differentially expressed genes between draining lymph node and gingivae CD4+ T cells were common to both control and

P. gingivalis infection, some were unique to each experimental condition, however, a strong linear relationship was observed between the levels of differential expression, showing that gene expression change was similar between dLN and gingivae in *P. gingivalis* infection and controls. Most differentially expressed genes are upregulated in gingivae compared to lymph node CD4+ T cells, which may reflect T cells in tissue being activated, compared to a potentially large pool of naïve T cells in the lymph node.

Serine/threonine kinase activity gene sets were upregulated in gingival CD4+ T cells compared to lymph node, in both control and *P. gingivalis* infections, this gene set consists of 356 genes that are responsible for phosphorylation of serine or threonine hydroxyl groups (JAX, 2022). This is crucial to regulating process that rely on molecule phosphorylation, and has important implications for post translational modification of proteins (Fulcher and Sapkota, 2020). This impacts pathways related to regulation of cell proliferation, programmed cell death (apoptosis), cell differentiation, and embryonic development (McCubrey *et al.*, 2000). The functionality of this group of molecules is broad, and future work would be important to elucidate the importance of this group set in gingiva.

When exploring the 958 significantly differentially expressed genes between gingivae and draining lymph nodes, common to both *P. gingivalis* and control, the gene set for regulation of cell-cell adhesion had the greatest significance. This gene set can be broken into multiple subsets, including positive and negative regulation of cell-cell adhesion. Negative regulation of cell-cell adhesion featured highly in terms of significantly differentially expressed gene set enrichment terms, suggesting that CD4+ T cells in gingivae have a reduced the rate of cell adhesion compared to those in lymph node. This may be reflective of having an active T cell population that can egress from lymph node due to decreased adhesion ability (Hunter, Teijeira and Halin, 2016). However, this remained surprising as typically there would be activation of adhesion markers, allowing T cells to migrate and remain in tertiary tissue (Denucci, Mitchell and Shimizu, 2009).

To identify potential therapeutic targets on gingival CD4+ T cells GPCR expression was analysed. Drugs that target GPCR represent over 30% of approved medicines, as such GPCRs on gingival CD4+ T cells represent potential therapeutic targets in managing a plethora of immune mediated oral diseases

(Santos *et al.*, 2017). Multiple GPCRs had detectable levels of expression and 35 GPCR transcripts were differentially expressed in gingivae compared to lymph node CD4+ T cells. The majority of which were upregulated in gingivae compared to lymph node. Interestingly C*cr7* was upregulated in gingivae compared to lymph nodes, given the well described roles of CCR7 and its ligand, CCL19, in lymphocyte homing to lymphoid organs this was surprising (Asperti-Boursin *et al.*, 2007; Yan *et al.*, 2019). However, we have also shown CCL19 to be expressed in human and murine gingivae, suggesting a role for this axis regulating T cell recruitment to the gingiva. There is also high expression of CXCR4 which again is upregulated in gingival CD4+ T cells, and thus may regulate T cell recruitment to the gingivae, however, this is mechanism of T cell recruitment is not unique to the oral environment (Scimone *et al.*, 2004).

There is also a significant downregulation of *Ccr10* on CD4+ T cells in gingivae compared to lymph node. CCR10 is the primary signalling receptor for CCL27, and in the context of T cells is pivotal to skin homing. The cervical draining lymph node would likely have leukocytes destined for skin as well as oral mucosa, however, given the downregulation of CCR10 in gingivae, this suggests the CCL27-CCR10 axis is not an important medicator of T cell recruitment to the gingiva (Homey *et al.*, 2002; Xia *et al.*, 2014).

CX3CR1 is also upregulated on CD4+ T cells in this analysis, this has well a well-documented role, with its ligand CX3CL1 in T cell chemoattraction (Siddiqui *et al.*, 2016; Nukiwa *et al.*, 2006). In all, multiple T cell chemo-attractant receptors are expressed on gingival CD4+ T cells, this suggests multiple ligands and receptors are responsible for T cell homing in the gingiva. This may be a result of redundancy and robustness, or alternatively a precise network of chemokine-chemokine receptor relationship designed to direct T cells to specific locations in gingivae in particular conditions, future work is necessary to understand the roles of each chemokine receptor and potential ligands in the gingiva.

The diverse chemokine receptor profile also raises the possibility of different CD4+ T cell subsets having varying chemokine receptor expression profiles. Alternatively, varying chemokine ligand-receptor interactions may direct T cells to specific anatomical sites within gingiva.

No selectin or integrins demonstrated differential expression between gingivae and lymph node, although multiple had detectable levels of expression. To identify integrins or selectin ligands responsible for oral mucosa homing, it would be beneficial to compare the integrin and selectin ligand expression at the protein and transcriptional level to skin and small intestine, this may identify cell adhesion molecules important for CD4+ T cell recruitment to the gingiva.

Chemokine ligands play a crucial role in cellular recruitment, CD4+ T cells in gingivae were transcriptionally active for a wide array of chemokines, and five ligands were upregulated in gingivae compared to cervical draining lymph node CD4+ T cells, including *Cx3cl1*.

Whilst our data shows there to be no transcriptional differences in the CD4+ T cell transcriptome in experimental periodontitis compared to controls, and thus no clearly targetable pathway for its treatment, it provides an in-depth and unbiased analysis of CD4+ T cells in gingivae compared to lymph node. This is vitally important as tissue specific immunity is highly compartmentalised and has begun to elicit the gingival CD4+ T cell transcriptional signature. To explore this further, the transcriptomes of CD4+ T cells of other barrier tissue should be compared to oral mucosa, such as skin and small intestine, which have been defined in greater detail. This would aid our understanding of tissue specific immune cell signatures and provide greater insight to potential therapeutic targets for managing T cell mediated oral disease. Furthermore, the T cell transcriptome may differ at alternative timepoints. Exploring the CD4+ T cell transcriptome at timepoints where there is established bone loss would provide further useful insight, as would using alternative models of murine periodontitis such as the ligature model.

The key findings from the posed research questions for this chapter are:

- Are there transcriptional differences of isolated murine CD4+ T cells between:
    - Gingiva in health and periodontitis
        - No differences were detected
    - Cervical draining lymph node in health and periodontitis
        - No differences were detected

    - Gingiva and cervical draining lymph node in health
        - There were 1405 genes that were differentially expressed
    - Gingiva and cervical draining lymph node in periodontitis
        - There were 1451 genes that were differentially expressed

- Which chemokine receptors, integrins and selectin ligands are highly expressed on gingival CD4+ T cells, relative to cervical draining lymph node CD4+ T cells?

    - Multiple chemokine receptors, including CXCR4, were upregulated on gingival CD4+ T cells compared to those from lymph node.

These findings reject the hypothesis that the murine gingival CD4+ T cell transcriptome differs between controls and periodontitis.

These findings support the hypothesis that the murine gingival CD4+ T cell transcriptome differs from the cervical draining lymph node CD4+ T cell transcriptome.

Chapter 6 – General Discussion

This thesis aimed to understand better the chemokines and chemokine receptors that contribute to gingival homeostasis and identify how these change during periodontitis. The importance of this is founded on the ability of chemokines to mediate cellular recruitment to the gingiva. Excessive and ineffective cellular responses are both associated with oral pathology. Thus, identifying the chemokines and chemokine receptors that contribute to maintaining health or perpetuating periodontitis pathogenesis are central to understanding homeostasis at the gingival barrier. An improved understanding of gingival chemokines and their receptors may identify novel therapeutic targets for numerous immune-mediated oral conditions. There is a detailed discussion at the end of each chapter; herein, a summary of these findings is provided, along with limitations of the work and potential avenues for future research.

6.1 The Chemokine Landscape in Healthy Gingiva

These data show the chemokine landscape in healthy gingiva in mice is unique compared to skin and small intestine in mice. In particular, CCL25 and CCL27, chemokines that direct small intestine and skin T cells in health, were expressed at low levels in the gingivae. If a gingiva-specific T cell population exist, it is therefore doubtful their presence in the gingival tissues is the result of signalling through these pathways. The importance of neutrophil recruitment has been well described in maintaining health and in periodontitis pathogenesis, and this was reflected across mammalian species with high expression levels of neutrophil chemo-attractants such as CXCL1, CXCL2, CXCL6 and CXCL8. High expression of the homeostatic chemokines CXCL17, CXCL14 and CXCL12, were observed and highly conserved in the gingival tissues across all three mammalian species (human, NHP, mouse). In-situ hybridisation revealed that these homeostatic chemokines have specific spatial expression patterns and may be responsible for regulating cellular recruitment in particular tissue niches. CXCL17 was uniquely highly expressed in the gingiva, compared to skin and small intestine, however, its receptor and precise function are unknown. It was also highly expressed in non-human primates. Unfortunately, CXCL17 was not

included on the human RT^2 profiler assay, supplemental qPCR would be useful to ascertain it's levels of expression in human gingiva.

6.2 The Chemokine Landscape in Periodontitis

The murine, NHP and human periodontitis data show a broadly similar chemokine landscape in gingival health and strikingly few chemokines were differentially expressed between health and disease in all models. Neutrophil chemo-attractants and CXCL13 were the exception; they are highly expressed in health and expression significantly increased during periodontitis, in line with previous studies (Tonetti, Imboden and Lang, 1998). The similarities in chemokine expression between health and disease may be reflective of the continual necessity for immuno-surveillance at the JE. Alternatively, this may support the recently established hypothesis of a resident extra-medullary HSC population, in the gingiva, with differentiation capacity, which would limit the necessity for leukocyte recruitment from the vasculature (Krishnan *et al.*, 2021). In support of this hypothesis the CXCL12, CXCR4 and ACRK3 axis, vital in regulating HSC populations, are highly expressed in gingival tissues, and are conserved between mammalian species. *CXCL14* is highly expressed across mammalian species, suggesting this may be a key contributor to gingival homeostasis, but was markedly downregulated in periodontitis. A further study has suggested a potential function for CXCL14 regulating osteogenesis in the periodontium (Ko *et al.*, 2020). Delineating the function of CXCL14 may reveal this as a therapeutic target in periodontitis **(Fig. 6.1)**.

6.3 The Gingival CD4+ T cell Transcriptome

No gingival CD4+ T cell genes were differentially expressed between health and *P. gingivalis* infection. The lack of transcriptional change suggests CD4+ T cells do not directly contribute to periodontitis pathogenesis in this model, at this time point. This contrasts with previous findings where CD4+ T cells are indispensable for periodontitis pathogenesis (Baker *et al.*, 1999). These findings suggest periodontitis may not develop without CD4+ T cells but may not be the main contributor to disease progression, in this model of periodontitis.

CD4+ T cells in the gingiva were – as expected - distinct from their counterparts in the lymph node. The majority of differentially expressed genes were upregulated in gingiva CD4+ T cells compared to lymph node, and the changes in gene expression between lymph node and gingiva CD4+ T cells were similar in control and *P. gingivalis* infection. Gene ontology analysis revealed regulation of protein serine/threonine kinase activity and regulation of cell-cell adhesion were amongst the most highly expressed gene sets. These findings may reflect an increased frequency of activated T cells in the gingiva compared to lymph node, yet some features may be fundamental to maintaining homeostasis at the gingival barrier. To explore this further, the transcriptomes of CD4+ T cells from other barrier sites, such as the skin and small intestine, could be compared to those from the gingiva, to identify unique transcripts or enriched gene sets and provide insight into the potential functional differences of CD4+ T cells between barrier tissues.

6.4 The chemokine receptor expression of CD4+ T cells

Multiple chemokines were differentially expressed between the gingiva and lymph node, suggesting T cell recruitment may be reliant on multiple chemokine receptors, including *Ccr7* and *Cxcr4*. Interestingly, *Ccr10* was downregulated on gingiva CD4+ T cells, suggesting that this is not required for gingival tropism, as it is for the skin.

6.5 Limitations of the study

The exploratory nature of these studies has provided a broad overview of the chemokine landscape. The group sizes were based on expected differences in clinical features, namely alveolar bone loss. Taking this approach potentially limited experimental power; thus, subtle changes in chemokine and chemokine receptors, and indeed transcriptional changes of CD4+ T cells may not have been detected. Non-significance must be interpreted with caution – the studies were not powered to detect equivalence. The data generated here can be used to design studies with sufficient statistical power, to validate or refute these findings.

An array-based approach was taken to analyse the transcriptional expression of chemokines and their receptors in health and periodontitis in humans, and in murine palate, skin, small intestine. In doing so, a small number of chemokines were not analysed in humans, due to them being unavailable on the array. Chemokines that were lowly expressed in exploratory analysis were also omitted from murine studies. This introduces an element of selection bias as well as potential chemokines of interest being omitted. For example, CXCL17 was not present on the human assay, it would be beneficial to undertake supplemental qPCR on individual chemokines of interest that have not been analysed. To reduce the element of selection bias, now I would more likely use a transcriptomic approach to these studies, due to the development of skills in this area and the reducing cost associated with RNA Sequencing.

Human studies were based on a population from the West of Scotland, due to geographical differences in diet, lifestyle and microbiomes the findings here may not translate to a global population (Gupta, Paul and Dutta, 2017). Moreover, the small sample size used limited the ability to detect differences in expression of some chemokines and receptors between health and periodontal disease.

Results from protein analysis must be viewed with some caution. Tissue lysates were generated from small intestine, palate, skin, and lymph nodes from mice following an established protocol, yet many chemokines were detected with low abundance. These findings should be validated using other protein detection and quantification platforms, such as flow cytometry, western blot, or proximity extension assays. Given the time constraints, this has not been possible in this thesis. Whilst the protein concentration of chemokines was analysed in human saliva and GCF, it was not evaluated in tissue. Use of a periotron® to determine total GCF volume from samples and standardising the saliva results per mL of collected saliva would allow for more detailed comparisons between samples. All stored tissues available were preserved in RNA preservation media, unsuitable for subsequent protein analysis. Collection of fresh tissue from patients undergoing surgery paused from February 2020 and has not yet restarted, and so tissue was not available during the time experiments were carried out. GCF and saliva were evaluated due to the ease of collecting control samples and availability of stored samples from patients with periodontitis. Using GCF and saliva provided some insight, but to achieve an accurate

reflection of chemokine concentration in tissue, the lysate of gingiva should be analysed in the future. Due to the limited volume of GCF a BCA assay to quantify protein concentration, was not possible.

There are advantages and limitations of each animal model of periodontitis. To explore the chemokine landscape, the ligature model was selected, due to the rapid and localised development of alveolar bone loss. Limitations of this were the failure of ligatures, and trauma to the alveolus upon ligature placement and tissue harvesting, resulting in the inability to assess alveolar bone loss in some animals. If this was repeated, it would likely yield more robust findings due to fewer mice being lost because of experimental error. A gavage model would have afforded a more direct comparison to the CD4+ T cell RNA Sequencing results, but requires greater group sizes for controls, and disease progression is slower. The split mouth approach and rapid disease development offered by the ligature model offers was of more value in this instance. It also does not fully replicate the disease we see in humans, due to the rapid development of alveolar bone loss.

The gavage model of periodontitis was employed for CD4+ T cell transcriptome analysis. T cells were isolated from the gingiva, following *P. gingivalis* infection, but prior to bone loss. This was identified as the time point where transcriptional changes would be most likely to occur yet changes in the T cell may occur early or later in this process. T cells were isolated from the whole murine palate. This increased the numbers of T cells available downstream analysis but diluted the population of T cells present at the gingival barrier, which are most likely to change transcriptionally. Moreover, all CD4+ T cell populations in the palate were analysed. If transcriptional changes occurred in specific T cell subsets, the experimental design might not have been sufficiently sensitive to detect this. In the future single-cell RNA Sequencing could be used to provide more granular detail on transcriptional changes in each of these subsets. Furthermore, the gavage model also does not fully replicate the disease we see in humans, as it requires artificially high abundances of *P. gingivalis* to initiate bone loss and may not replicate the complex host immune response that is seen in periodontitis associated with a complex polymicrobial biofilm.

6.6 Future work

The results presented in this thesis suggest multiple avenues of enquiry that would be prime future research opportunities. It would be worthwhile exploring the chemokine landscape in periodontitis by employing the gavage model, which uses an infective as opposed to mechanical model to initiate alveolar bone loss, may validate these findings from the ligature model presented herein, or indeed, suggest that the induction of chemokines differs depending on the insult experienced. Moreover, the contribution of normal occlusal trauma to the chemokine profile could be examined by placing mice on a soft diet – which has previously been demonstrated to result in changes in the gingival tissue immune network (Dutzan *et al.*, 2017). In relation to the human data generated; it would be beneficial to conduct a larger study, including investigation of tissue protein expression. Parallel investigation of the adjacent microbiome and an 'infecotgenomics' approach to analysis would permit evaluation of whether microbiome features associate with chemokine expression. A multi-national study could further identify if regional idiosyncrasies influence the chemokine repertoire in humans. A biobank of tissue, available internationally would help address this (Sivolella *et al.*, 2022). Methods with greater sensitivity such as proximity extension assays or high sensitivity ELISAs or with less inherent bias such as mass spectrometry can be used to further explore the chemokine network in oral mucosa, saliva and GCF. To standardise results between GCF and saliva samples total volume quantification or total protein concentraion methods, as previously discussed, could be employed.It is unclear if the minimal transcriptional changes observed is unique to periodontitis or shared in other gingival inflammatory pathologies. The similarities in chemokine landscapes in health and disease is itself interesting, yet identifying the contributing factors in gingival health is challenging due to environmental and microbial challenges. To explore microbial mechanisms that regulate gingival chemokine expression in health, chemokine in SPF and GF mice could be compared (Dutzan *et al.*, 2017).

Identifying the chemokine landscape in other inflammatory gingival conditions such as lichen planus and pemphigoid would provide some insight into this. It would identify if the minimal transcriptional changes seen in periodontitis was disease specific, or a reflection of gingival inflammation irrespective of the pathological mechanism. Both conditions are rarer than periodontitis but are

associated with significant morbidity and in the case of lichen planus are potentially malignant (Reilly, Johnston and Culshaw, 2019).

The CXCL12, CXCL14, CXCR4, and ACKR3 axis represents a potentially fascinating therapeutic target and CXCL17 being uniquely highly expressed in gingiva warrants further exploration too. In the gingiva, the logical next steps are to identify cells producing these chemokines, and the cells expressing receptors for CXCL12 and CXCL14. Some efforts were made during these studies; however, due to notoriously poor chemokine antibodies, this was challenging, no interpretable data were generated. Experimental techniques such as PrimeFlow, the use of reporter mice, single cell RNA-Sequencing or the use of labelled chemokines may help address this. A simple next step could be to use immunohistochemistry, coupled with in-situ hybridisation to identify the cell types, histologically, that expressed the aforementioned transcripts.

Exploring the functionality of CXCL12 has been challenging due the perinatally lethal phenotype of CXCL12 homozygote knockout mice (Tzeng *et al.*, 2011; Nagasawa *et al.*, 1996). Similarly, CXCL14 knock out mice, are susceptible to premature death and potential perinatally mortality, making husbandry and experimentation challenging (Benarafa and Wolf, 2015; Tanegashima *et al.*, 2010). However, conditional deletion models of CXCL12 and CXCL14 deficient mice have been successful (Hara and Tanegashima, 2012; Tanegashima *et al.*, 2010; Meuter *et al.*, 2007). Developing collaborations with laboratories with success with these mice may afford the opportunity to explore the functionality of CXCL12 and CXCL14 in gingival homeostasis and experimental periodontitis. Moreover, oral epithelial cell conditional knock out and knock down models have been developed, by generating similar mouse models for CXCL12 and CXCL14 the local function of these molecules can be explored, without systemic disruption (Delitto *et al.*, 2018).

The CD4+ T cell transcriptome in gingiva was distinct from the lymph node; however, the analysis conducted does not differentiate between T cells recruited to the gingiva and those that were resident. Due to the experimental design, it is impossible to determine if the T cells present responded to *P. gingivalis* or were resident in the tissue prior to infection. An initial aim of this PhD was to explore how T cells specifically trafficked to the oral mucosa. The intention was to adoptively transfer ovalbumin-specific CD4+ T cells from an OTII

donor mouse, to a wild type recipient, and challenge the recipient mouse with ovalbumin and CpG via a micro-needle. OTII T cells would be isolated from the palate, thus having T cells that had trafficked in response to ovalbumin. However, due to the COVID-19 pandemic, and the disruption to the laboratory and intended collaborators this was not feasible. These experiments would represent an exciting opportunity to improve the understanding of T cell recruitment in the gingiva. Such a study would require extensive optimisation due to the highly technical nature of the proposed work.

The use of Kaede transgenic mice offer an alternative model for understanding the trafficking mechanisms of T cells to palate. Kaede mice have a photoconvertible protein that upon exposure to violet light photo switches from a green to a red signal. This can then be used to track T cells that have migrated from lymph node to gingiva. Cervical draining lymph nodes could be could be exposed to ultra-violet light, photo-switching the fluorescent protein on T cells. Upon fluorescence-activated cell sorting red signal expressing T cells, resident in the lymph node at the time of ultra-violet light exposure, can then be positively selected; providing a T cell population that had migrated from the lymph node to the palate. This model could be used in conjunction with a gavage or ligature model of periodontitis and explore the transcriptomes of those CD4+ T cells that have migrated following initiation of the disease model (Kitamoto *et al.*, 2020).

6.7 Overall Conclusions

In conclusion, the data generated in this thesis has provided novel insights into the chemokine landscape in healthy and diseased gingiva in mice, NHPs and humans. Furthermore, these studies have begun to define the gingival CD4+ T cell transcriptome and identify chemokine receptors that may regulate CD4+ T cell gingival tropism.

The key findings are:

- The chemokine landscape in the palate of mice is distinct from the skin and small intestine.
- The CXCL12/CXCL14/CXCR4/ACKR3 axis is highly expressed at the oral barrier and is conserved between mammalian species.
- Homeostatic chemokines in the palate of mice have distinct patterns of spatial expression.
- The gingival chemokine landscape was similar in health and periodontitis in mice NHPs and humans.
- No gingival CD4+ T cell genes were differentially expressed between health and *P. gingivalis* infection.
- CD4+ T cells in the gingiva have a distinct transcriptional signature compared to lymph node CD4+ T cells.
- The chemokine receptors *Ccr6, Ccr7, Ccr8, Cxcr4, Cxcr5, Cxcr6, Xcr1,* and *Cx3cr1* were upregulated in gingivae compared to lymph node CD4+ T cells.

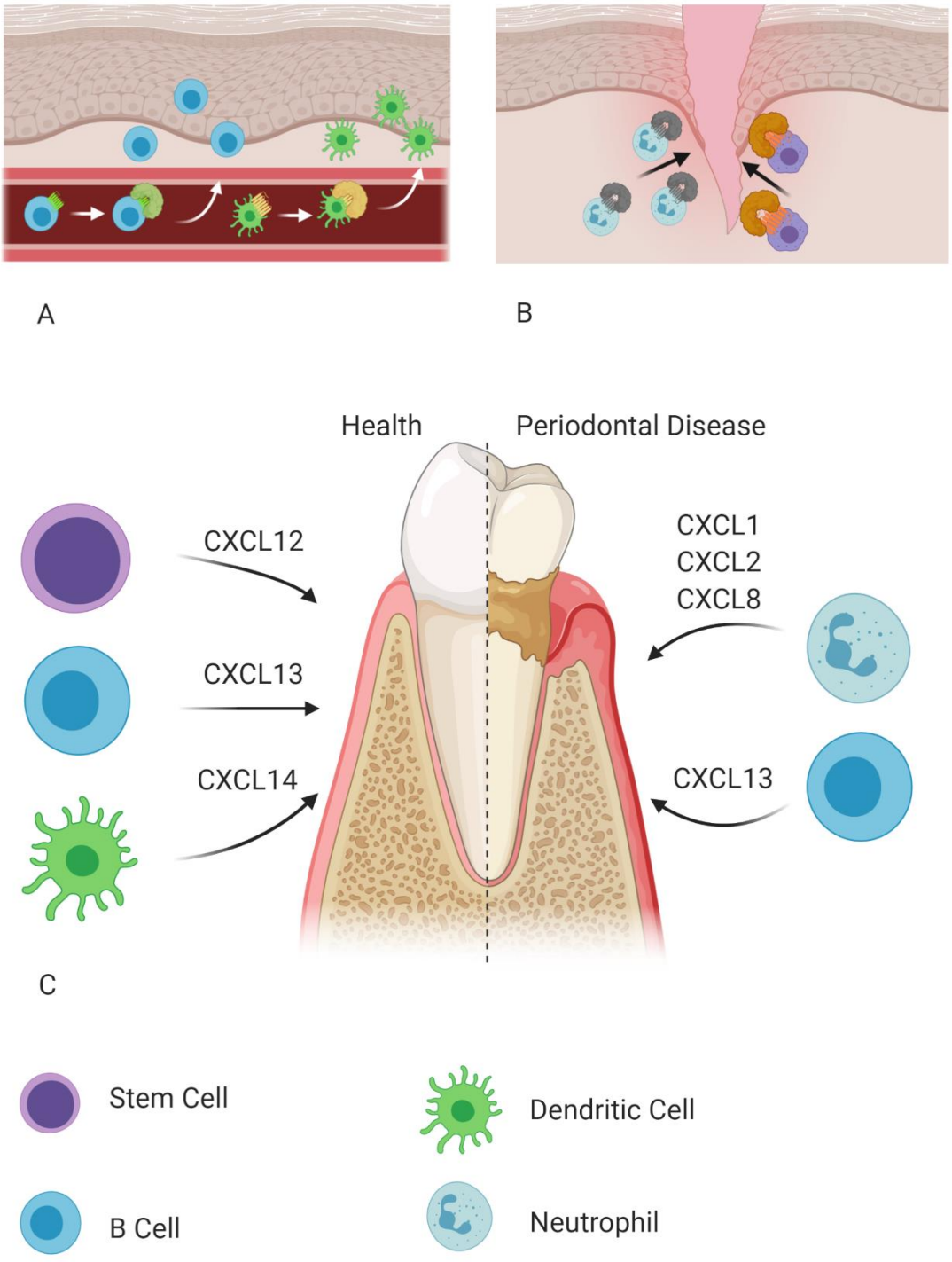

Figure 6. 1 The role of chemokines in gingiva

(A) Homeostatic chemokines maintain health by recruiting leukocytes for immune surveillance and tolerance. Chemokines also play a key role in tissue repair and development through hematopoietic stem cell and progenitor cell trafficking. The homeostatic chemokine landscape therefore differs between tissues depending on the function and environment of the ecological niche. **(B)** Inflammatory chemokines direct cells during inflammatory responses. In contrast to

Figure 6.1 continued

homeostatic chemokines, similar inflammatory chemokines profiles are seen at different body sites. (**C)** Potential roles for chemokines in the gingiva: CXCL12, and it's receptor CXCR4, were highly expressed in healthy and diseased human gingiva, studies have shown these play a role in lymphocyte, stem cell and mesenchymal cell migration at other body sites. CXCL13 was highly expressed in both health and disease, this has been shown to be chemotactic for B Cells in other tissues, and studies suggested the same role in gingiva. CXCL14 was highly expressed in health and downregulated in disease, the receptor for CXCL14 is unknown, it has been suggested that it plays a role in dendritic cell precursor recruitment and expression is modulated by *P. gingivalis* exposure. It may also be and allosteric modulator of CXCR4, thus influencing CXCL12 to direct cellular recruitment. The inflammatory chemokines CXCL1, CXCL2 and CXCL8 were upregulated in disease - their primary function is neutrophil chemotaxis, this would be their most likely role in periodontitis. Figure created with BioRender.com.

References

Abe, T. and Hajishengallis, G. (2013) 'Optimization of the ligature-induced periodontitis model in mice', *J Immunol Methods,* 394(1-2), pp. 49-54.

Asperti-Boursin, F., Real, E., Bismuth, G., Trautmann, A. and Donnadieu, E. (2007) 'CCR7 ligands control basal T cell motility within lymph node slices in a phosphoinositide 3-kinase-independent manner', *J Exp Med,* 204(5), pp. 1167-79.

Baker, P. J., Dixon, M., Evans, R. T., Dufour, L., Johnson, E. and Roopenian, D. C. (1999) 'CD4(+) T cells and the proinflammatory cytokines gamma interferon and interleukin-6 contribute to alveolar bone loss in mice', *Infect Immun,* 67(6), pp. 2804-9.

Baker, P. J., Evans, R. T. and Roopenian, D. C. (1994) 'Oral infection with Porphyromonas gingivalis and induced alveolar bone loss in immunocompetent and severe combined immunodeficient mice', *Arch Oral Biol,* 39(12), pp. 1035-40.

Baker, P. J., Howe, L., Garneau, J. and Roopenian, D. C. (2002) 'T cell knockout mice have diminished alveolar bone loss after oral infection with Porphyromonas gingivalis', *FEMS Immunol Med Microbiol,* 34(1), pp. 45-50.

Barros, S. P., Williams, R., Offenbacher, S. and Morelli, T. (2016) 'Gingival crevicular fluid as a source of biomarkers for periodontitis', *Periodontol 2000,* 70(1), pp. 53-64.

Bell, D., Chomarat, P., Broyles, D., Netto, G., Harb, G. M., Lebecque, S., Valladeau, J., Davoust, J., Palucka, K. A. and Banchereau, J. (1999) 'In breast carcinoma tissue, immature dendritic cells reside within the tumor, whereas mature dendritic cells are located in peritumoral areas', *J Exp Med,* 190(10), pp. 1417-26.

Benarafa, C. and Wolf, M. (2015) 'CXCL14: the Swiss army knife chemokine', *Oncotarget,* 6(33), pp. 34065-6.

Bendre, M. S., Montague, D. C., Peery, T., Akel, N. S., Gaddy, D. and Suva, L. J. (2003) 'Interleukin-8 stimulation of osteoclastogenesis and bone resorption is a mechanism for the increased osteolysis of metastatic bone disease', *Bone,* 33(1), pp. 28-37.

Bernabe, E., Marcenes, W., Hernandez, C. R., Bailey, J., Abreu, L. G., Alipour, V., Amini, S., Arabloo, J., Arefi, Z., Arora, A., Ayanore, M. A., Barnighausen, T. W., Bijani, A., Cho, D. Y., Chu, D. T., Crowe, C. S., Demoz, G. T., Demsie, D. G., Dibaji Forooshani, Z. S., Du, M., El Tantawi, M., Fischer, F., Folayan, M. O., Futran, N. D., Geramo, Y. C. D., Haj-Mirzaian, A., Hariyani, N., Hasanzadeh, A., Hassanipour, S., Hay, S. I., Hole, M. K., Hostiuc, S., Ilic, M. D., James, S. L., Kalhor, R., Kemmer, L., Keramati, M., Khader, Y. S., Kisa, S., Kisa, A., Koyanagi,

A., Lalloo, R., Le Nguyen, Q., London, S. D., Manohar, N. D., Massenburg, B. B., Mathur, M. R., Meles, H. G., Mestrovic, T., Mohammadian-Hafshejani, A., Mohammadpourhodki, R., Mokdad, A. H., Morrison, S. D., Nazari, J., Nguyen, T. H., Nguyen, C. T., Nixon, M. R., Olagunju, T. O., Pakshir, K., Pathak, M., Rabiee, N., Rafiei, A., Ramezanzadeh, K., Rios-Blancas, M. J., Roro, E. M., Sabour, S., Samy, A. M., Sawhney, M., Schwendicke, F., Shaahmadi, F., Shaikh, M. A., Stein, C., Tovani-Palone, M. R., Tran, B. X., Unnikrishnan, B., Vu, G. T., Vukovic, A., Warouw, T. S. S., Zaidi, Z., Zhang, Z. J. and Kassebaum, N. J. (2020) 'Global, Regional, and National Levels and Trends in Burden of Oral Conditions from 1990 to 2017: A Systematic Analysis for the Global Burden of Disease 2017 Study', *J Dent Res,* 99(4), pp. 362-373.

Bevilacqua, L., Biasi, M. D., Lorenzon, M. G., Frattini, C. and Angerame, D. (2016) 'Volumetric Analysis of Gingival Crevicular Fluid and Peri-Implant Sulcus Fluid in Healthy and Diseased Sites: A Cross-Sectional Split-Mouth Pilot Study', *Open Dent J,* 10, pp. 131-8.

Bhusal, R. P., Foster, S. R. and Stone, M. J. (2020) 'Structural basis of chemokine and receptor interactions: Key regulators of leukocyte recruitment in inflammatory responses', *Protein Sci,* 29(2), pp. 420-432.

Bonecchi, R. and Graham, G. J. (2016) 'Atypical Chemokine Receptors and Their Roles in the Resolution of the Inflammatory Response', *Front Immunol,* 7, pp. 224.

Bosshardt, D. D. and Lang, N. P. (2005) 'The junctional epithelium: from health to disease', *J Dent Res,* 84(1), pp. 9-20.

Botelho, J., Machado, V., Leira, Y., Proenca, L., Chambrone, L. and Mendes, J. J. (2022) 'Economic burden of periodontitis in the United States and Europe: An updated estimation', *J Periodontol,* 93(3), pp. 373-379.

Brizuela, M. and Winters, R. (2022) 'Histology, Oral Mucosa', *StatPearls*. Treasure Island (FL).

Campbell, L., Millhouse, E., Malcolm, J. and Culshaw, S. (2016) 'T cells, teeth and tissue destruction - what do T cells do in periodontal disease?', *Mol Oral Microbiol,* 31(6), pp. 445-456.

Campbell, L. D. (2017) *'The Role of CD4+ T cells in Periodontal Disease'*. University of Glasgow, Glasgow.

Capucetti, A., Albano, F. and Bonecchi, R. (2020) 'Multiple Roles for Chemokines in Neutrophil Biology', *Front Immunol,* 11, pp. 1259.

Cardona, A. E., Sasse, M. E., Liu, L., Cardona, S. M., Mizutani, M., Savarin, C., Hu, T. and Ransohoff, R. M. (2008) 'Scavenging roles of chemokine receptors: chemokine receptor deficiency is associated with increased levels of ligand in circulation and tissues', *Blood,* 112(2), pp. 256-63.

Cardoso, E. M. and Arosa, F. A. (2017) 'CD8(+) T Cells in Chronic Periodontitis: Roles and Rules', *Front Immunol,* 8, pp. 145.

Casanova, L., Hughes, F. J. and Preshaw, P. M. (2015) 'Diabetes and periodontal disease', *BDJ Team,* 1(1).

Cekici, A., Kantarci, A., Hasturk, H. and Van Dyke, T. E. (2014) 'Inflammatory and immune pathways in the pathogenesis of periodontal disease', *Periodontol 2000,* 64(1), pp. 57-80.

Chapple, I. L. and Genco, R. (2013) 'Diabetes and periodontal diseases: consensus report of the Joint EFP/AAP Workshop on Periodontitis and Systemic Diseases', *J Periodontol,* 84(4 Suppl), pp. S106-12.

Chapple, I. L. C., Mealey, B. L., Van Dyke, T. E., Bartold, P. M., Dommisch, H., Eickholz, P., Geisinger, M. L., Genco, R. J., Glogauer, M., Goldstein, M., Griffin, T. J., Holmstrup, P., Johnson, G. K., Kapila, Y., Lang, N. P., Meyle, J., Murakami, S., Plemons, J., Romito, G. A., Shapira, L., Tatakis, D. N., Teughels, W., Trombelli, L., Walter, C., Wimmer, G., Xenoudi, P. and Yoshie, H. (2018) 'Periodontal health and gingival diseases and conditions on an intact and a reduced periodontium: Consensus report of workgroup 1 of the 2017 World Workshop on the Classification of Periodontal and Peri-Implant Diseases and Conditions', *J Periodontol,* 89 Suppl 1, pp. S74-S84.

Chen, B., Wu, W., Sun, W., Zhang, Q., Yan, F. and Xiao, Y. (2014) 'RANKL expression in periodontal disease: where does RANKL come from?', *Biomed Res Int,* 2014, pp. 731039.

Chen, K., Bao, Z., Tang, P., Gong, W., Yoshimura, T. and Wang, J. M. (2018) 'Chemokines in homeostasis and diseases', *Cell Mol Immunol,* 15(4), pp. 324-334.

Clark, D., Kotronia, E. and Ramsay, S. E. (2021) 'Frailty, aging, and periodontal disease: Basic biologic considerations', *Periodontol 2000,* 87(1), pp. 143-156.

Clore, G. M. and Gronenborn, A. M. (1995) 'Three-dimensional structures of alpha and beta chemokines', *FASEB J,* 9(1), pp. 57-62.

Collins, P. J., McCully, M. L., Martinez-Munoz, L., Santiago, C., Wheeldon, J., Caucheteux, S., Thelen, S., Cecchinato, V., Laufer, J. M., Purvanov, V., Monneau, Y. R., Lortat-Jacob, H., Legler, D. F., Uguccioni, M., Thelen, M., Piguet, V., Mellado, M. and Moser, B. (2017) 'Epithelial chemokine CXCL14 synergizes with CXCL12 via allosteric modulation of CXCR4', *FASEB J,* 31(7), pp. 3084-3097.

Conti, H. R., Peterson, A. C., Brane, L., Huppler, A. R., Hernandez-Santos, N., Whibley, N., Garg, A. V., Simpson-Abelson, M. R., Gibson, G. A., Mamo, A. J., Osborne, L. C., Bishu, S., Ghilardi, N., Siebenlist, U., Watkins, S. C., Artis, D., McGeachy, M. J. and Gaffen, S. L. (2014) 'Oral-resident natural Th17 cells and gammadelta T cells control opportunistic Candida albicans infections', *J Exp Med,* 211(10), pp. 2075-84.

Curiel, T. J., Coukos, G., Zou, L., Alvarez, X., Cheng, P., Mottram, P., Evdemon-Hogan, M., Conejo-Garcia, J. R., Zhang, L., Burow, M., Zhu, Y., Wei, S., Kryczek, I., Daniel, B., Gordon, A., Myers, L., Lackner, A., Disis, M. L., Knutson, K. L., Chen, L. and Zou, W. (2004) 'Specific recruitment of regulatory T cells in ovarian carcinoma fosters immune privilege and predicts reduced survival', *Nat Med,* 10(9), pp. 942-9.

Darre, L., Vergnes, J. N., Gourdy, P. and Sixou, M. (2008) 'Efficacy of periodontal treatment on glycaemic control in diabetic patients: A meta-analysis of interventional studies', *Diabetes Metab,* 34(5), pp. 497-506.

Davila, M. L., Xu, M., Huang, C., Gaddes, E. R., Winter, L., Cantorna, M. T., Wang, Y. and Xiong, N. (2022) 'CCL27 is a crucial regulator of immune homeostasis of the skin and mucosal tissues', *iScience,* 25(6), pp. 104426.

Davison, E., Johnston, W., Piela, K., Rosier, B. T., Paterson, M., Mira, A. and Culshaw, S. (2021) 'The Subgingival Plaque Microbiome, Systemic Antibodies Against Bacteria and Citrullinated Proteins Following Periodontal Therapy', *Pathogens,* 10(2).

de Mattos, B. R., Garcia, M. P., Nogueira, J. B., Paiatto, L. N., Albuquerque, C. G., Souza, C. L., Fernandes, L. G., Tamashiro, W. M. and Simioni, P. U. (2015) 'Inflammatory Bowel Disease: An Overview of Immune Mechanisms and Biological Treatments', *Mediators Inflamm,* 2015, pp. 493012.

Delitto, A. E., Rocha, F., Decker, A. M., Amador, B., Sorenson, H. L. and Wallet, S. M. (2018) 'MyD88-mediated innate sensing by oral epithelial cells controls periodontal inflammation', *Arch Oral Biol,* 87, pp. 125-130.

Demmer, R. T., Behle, J. H., Wolf, D. L., Handfield, M., Kebschull, M., Celenti, R., Pavlidis, P. and Papapanou, P. N. (2008) 'Transcriptomes in healthy and diseased gingival tissues', *J Periodontol,* 79(11), pp. 2112-24.

Denucci, C. C., Mitchell, J. S. and Shimizu, Y. (2009) 'Integrin function in T-cell homing to lymphoid and nonlymphoid sites: getting there and staying there', *Crit Rev Immunol,* 29(2), pp. 87-109.

DeVries, M. E., Kelvin, A. A., Xu, L., Ran, L., Robinson, J. and Kelvin, D. J. (2006) 'Defining the origins and evolution of the chemokine/chemokine receptor system', *J Immunol,* 176(1), pp. 401-15.

Dewhirst, F. E., Chen, T., Izard, J., Paster, B. J., Tanner, A. C., Yu, W. H., Lakshmanan, A. and Wade, W. G. (2010) 'The human oral microbiome', *J Bacteriol,* 192(19), pp. 5002-17.

Dimberg, A. (2010) 'Chemokines in angiogenesis', *Curr Top Microbiol Immunol,* 341, pp. 59-80.

Dufty, J., Gkranias, N. and Donos, N. (2017) 'Necrotising Ulcerative Gingivitis: A Literature Review', *Oral Health Prev Dent,* 15(4), pp. 321-327.

Dutzan, N., Abusleme, L., Bridgeman, H., Greenwell-Wild, T., Zangerle-Murray, T., Fife, M. E., Bouladoux, N., Linley, H., Brenchley, L., Wemyss, K., Calderon, G., Hong, B. Y., Break, T. J., Bowdish, D. M. E., Lionakis, M. S., Jones, S. A., Trinchieri, G., Diaz, P. I., Belkaid, Y., Konkel, J. E. and Moutsopoulos, N. M. (2017) 'On-going Mechanical Damage from Mastication Drives Homeostatic Th17 Cell Responses at the Oral Barrier', *Immunity,* 46(1), pp. 133-147.

Dutzan, N., Kajikawa, T., Abusleme, L., Greenwell-Wild, T., Zuazo, C. E., Ikeuchi, T., Brenchley, L., Abe, T., Hurabielle, C., Martin, D., Morell, R. J., Freeman, A. F., Lazarevic, V., Trinchieri, G., Diaz, P. I., Holland, S. M., Belkaid, Y., Hajishengallis, G. and Moutsopoulos, N. M. (2018) 'A dysbiotic microbiome triggers TH17 cells to mediate oral mucosal immunopathology in mice and humans', *Sci Transl Med,* 10(463).

Ebersole, J., Kirakodu, S., Chen, J., Nagarajan, R. and Gonzalez, O. A. (2020) 'Oral Microbiome and Gingival Transcriptome Profiles of Ligature-Induced Periodontitis', *J Dent Res,* 99(6), pp. 746-757.

Ebersole, J. L., Kirakodu, S., Novak, M. J., Stromberg, A. J., Shen, S., Orraca, L., Gonzalez-Martinez, J., Burgos, A. and Gonzalez, O. A. (2014) 'Cytokine gene expression profiles during initiation, progression and resolution of periodontitis', *J Clin Periodontol,* 41(9), pp. 853-61.

Ebersole, J. L., Steffen, M. J., Gonzalez-Martinez, J. and Novak, M. J. (2008) 'Effects of age and oral disease on systemic inflammatory and immune parameters in nonhuman primates', *Clin Vaccine Immunol,* 15(7), pp. 1067-75.

Ertugrul, A. S., Sahin, H., Dikilitas, A., Alpaslan, N. and Bozoglan, A. (2013) 'Comparison of CCL28, interleukin-8, interleukin-1beta and tumor necrosis factor-alpha in subjects with gingivitis, chronic periodontitis and generalized aggressive periodontitis', *J Periodontal Res,* 48(1), pp. 44-51.

Figueredo, C. M., Lira-Junior, R. and Love, R. M. (2019) 'T and B Cells in Periodontal Disease: New Functions in A Complex Scenario', *Int J Mol Sci,* 20(16).

Fine, N., Hassanpour, S., Borenstein, A., Sima, C., Oveisi, M., Scholey, J., Cherney, D. and Glogauer, M. (2016) 'Distinct Oral Neutrophil Subsets Define Health and Periodontal Disease States', *J Dent Res,* 95(8), pp. 931-8.

Finoti, L. S., Nepomuceno, R., Pigossi, S. C., Corbi, S. C., Secolin, R. and Scarel-Caminaga, R. M. (2017) 'Association between interleukin-8 levels and chronic periodontal disease: A PRISMA-compliant systematic review and meta-analysis', *Medicine (Baltimore),* 96(22), pp. e6932.

Forster, R., Davalos-Misslitz, A. C. and Rot, A. (2008) 'CCR7 and its ligands: balancing immunity and tolerance', *Nat Rev Immunol,* 8(5), pp. 362-71.

Forster, R., Mattis, A. E., Kremmer, E., Wolf, E., Brem, G. and Lipp, M. (1996) 'A putative chemokine receptor, BLR1, directs B cell migration to defined lymphoid organs and specific anatomic compartments of the spleen', *Cell,* 87(6), pp. 1037-47.

Forster, R., Schubel, A., Breitfeld, D., Kremmer, E., Renner-Muller, I., Wolf, E. and Lipp, M. (1999) 'CCR7 coordinates the primary immune response by establishing functional microenvironments in secondary lymphoid organs', *Cell,* 99(1), pp. 23-33.

Fricker, S. P. (2013) 'Physiology and pharmacology of plerixafor', *Transfus Med Hemother,* 40(4), pp. 237-45.

Fulcher, L. J. and Sapkota, G. P. (2020) 'Functions and regulation of the serine/threonine protein kinase CK1 family: moving beyond promiscuity', *Biochem J,* 477(23), pp. 4603-4621.

Garlet, G. P., Cardoso, C. R., Campanelli, A. P., Garlet, T. P., Avila-Campos, M. J., Cunha, F. Q. and Silva, J. S. (2008) 'The essential role of IFN-gamma in the control of lethal Aggregatibacter actinomycetemcomitans infection in mice', *Microbes Infect,* 10(5), pp. 489-96.

Gemmell, E., Carter, C. L. and Seymour, G. J. (2001) 'Chemokines in human periodontal disease tissues', *Clin Exp Immunol,* 125(1), pp. 134-41.

Gonzalez, O. A., Stromberg, A. J., Huggins, P. M., Gonzalez-Martinez, J., Novak, M. J. and Ebersole, J. L. (2011) 'Apoptotic genes are differentially expressed in aged gingival tissue', *J Dent Res,* 90(7), pp. 880-6.

Granger DN, S. E. (2010) 'Chapter 7, Leukocyte–Endothelial Cell Adhesion', *Inflammation and the Microcirculation*.

Graves, D. T., Fine, D., Teng, Y. T., Van Dyke, T. E. and Hajishengallis, G. (2008) 'The use of rodent models to investigate host-bacteria interactions related to periodontal diseases', *J Clin Periodontol,* 35(2), pp. 89-105.

Greer, A., Irie, K., Hashim, A., Leroux, B. G., Chang, A. M., Curtis, M. A. and Darveau, R. P. (2016) 'Site-Specific Neutrophil Migration and CXCL2 Expression in Periodontal Tissue', *J Dent Res,* 95(8), pp. 946-52.

Griffen, A. L., Beall, C. J., Campbell, J. H., Firestone, N. D., Kumar, P. S., Yang, Z. K., Podar, M. and Leys, E. J. (2012) 'Distinct and complex bacterial profiles in human periodontitis and health revealed by 16S pyrosequencing', *ISME J,* 6(6), pp. 1176-85.

Grossi, S. G., Genco, R. J., Machtei, E. E., Ho, A. W., Koch, G., Dunford, R., Zambon, J. J. and Hausmann, E. (1995) 'Assessment of risk for periodontal disease. II. Risk indicators for alveolar bone loss', *J Periodontol,* 66(1), pp. 23-9.

Grossi, S. G., Zambon, J. J., Ho, A. W., Koch, G., Dunford, R. G., Machtei, E. E., Norderyd, O. M. and Genco, R. J. (1994) 'Assessment of risk for periodontal disease. I. Risk indicators for attachment loss', *J Periodontol,* 65(3), pp. 260-7.

Guo, L., Feng, K., Wang, Y. C., Mei, J. J., Ning, R. T., Zheng, H. W., Wang, J. J., Worthen, G. S., Wang, X., Song, J., Li, Q. H. and Liu, L. D. (2017) 'Critical role of CXCL4 in the lung pathogenesis of influenza (H1N1) respiratory infection', *Mucosal Immunol,* 10(6), pp. 1529-1541.

Gupta, V. K., Paul, S. and Dutta, C. (2017) 'Geography, Ethnicity or Subsistence-Specific Variations in Human Microbiome Composition and Diversity', *Front Microbiol,* 8, pp. 1162.

Hajishengallis, E. and Hajishengallis, G. (2014) 'Neutrophil homeostasis and periodontal health in children and adults', *J Dent Res,* 93(3), pp. 231-7.

Hajishengallis, G. (2014) 'The inflammophilic character of the periodontitis-associated microbiota', *Mol Oral Microbiol,* 29(6), pp. 248-57.

Hajishengallis, G. and Chavakis, T. (2013) 'Endogenous modulators of inflammatory cell recruitment', *Trends Immunol,* 34(1), pp. 1-6.

Hajishengallis, G., Darveau, R. P. and Curtis, M. A. (2012) 'The keystone-pathogen hypothesis', *Nat Rev Microbiol,* 10(10), pp. 717-25.

Hajishengallis, G. and Korostoff, J. M. (2017) 'Revisiting the Page & Schroeder model: the good, the bad and the unknowns in the periodontal host response 40 years later', *Periodontol 2000,* 75(1), pp. 116-151.

Hajishengallis, G., Lamont, R. J. and Graves, D. T. (2015) 'The enduring importance of animal models in understanding periodontal disease', *Virulence,* 6(3), pp. 229-35.

Hajishengallis, G., Liang, S., Payne, M. A., Hashim, A., Jotwani, R., Eskan, M. A., McIntosh, M. L., Alsam, A., Kirkwood, K. L., Lambris, J. D., Darveau, R. P. and Curtis, M. A. (2011) 'Low-abundance biofilm species orchestrates inflammatory periodontal disease through the commensal microbiota and complement', *Cell Host Microbe,* 10(5), pp. 497-506.

Hajishengallis, G., Maekawa, T., Abe, T., Hajishengallis, E. and Lambris, J. D. (2015) 'Complement Involvement in Periodontitis: Molecular Mechanisms and Rational Therapeutic Approaches', *Adv Exp Med Biol,* 865, pp. 57-74.

Han, J. H., Choi, S. J., Kurihara, N., Koide, M., Oba, Y. and Roodman, G. D. (2001) 'Macrophage inflammatory protein-1alpha is an osteoclastogenic factor in myeloma that is independent of receptor activator of nuclear factor kappaB ligand', *Blood,* 97(11), pp. 3349-53.

Hanazawa, S., Kawata, Y., Takeshita, A., Kumada, H., Okithu, M., Tanaka, S., Yamamoto, Y., Masuda, T., Umemoto, T. and Kitano, S. (1993) 'Expression of monocyte chemoattractant protein 1 (MCP-1) in adult periodontal disease: increased monocyte chemotactic activity in crevicular fluids and induction of MCP-1 expression in gingival tissues', *Infect Immun,* 61(12), pp. 5219-24.

Handel, T. M., Johnson, Z., Crown, S. E., Lau, E. K. and Proudfoot, A. E. (2005) 'Regulation of protein function by glycosaminoglycans--as exemplified by chemokines', *Annu Rev Biochem,* 74, pp. 385-410.

Haque, A., Engel, J., Teichmann, S. A. and Lonnberg, T. (2017) 'A practical guide to single-cell RNA-sequencing for biomedical research and clinical applications', *Genome Med,* 9(1), pp. 75.

Hara, T. and Tanegashima, K. (2012) 'Pleiotropic functions of the CXC-type chemokine CXCL14 in mammals', *J Biochem,* 151(5), pp. 469-76.

Heidari, Z., Moudi, B. and Mahmoudzadeh-Sagheb, H. (2019) 'Immunomodulatory factors gene polymorphisms in chronic periodontitis: an overview', *BMC Oral Health,* 19(1), pp. 29.

Heusinkveld, L. E., Majumdar, S., Gao, J. L., McDermott, D. H. and Murphy, P. M. (2019) 'WHIM Syndrome: from Pathogenesis Towards Personalized Medicine and Cure', *J Clin Immunol,* 39(6), pp. 532-556.

Hillyer, P., Mordelet, E., Flynn, G. and Male, D. (2003) 'Chemokines, chemokine receptors and adhesion molecules on different human endothelia: discriminating the tissue-specific functions that affect leucocyte migration', *Clin Exp Immunol,* 134(3), pp. 431-41.

Hocking, A. M. (2015) 'The Role of Chemokines in Mesenchymal Stem Cell Homing to Wounds', *Adv Wound Care (New Rochelle),* 4(11), pp. 623-630.

Homey, B., Alenius, H., Muller, A., Soto, H., Bowman, E. P., Yuan, W., McEvoy, L., Lauerma, A. I., Assmann, T., Bunemann, E., Lehto, M., Wolff, H., Yen, D., Marxhausen, H., To, W., Sedgwick, J., Ruzicka, T., Lehmann, P. and Zlotnik, A. (2002) 'CCL27-CCR10 interactions regulate T cell-mediated skin inflammation', *Nat Med,* 8(2), pp. 157-65.

Hovav, A. H. (2014) 'Dendritic cells of the oral mucosa', *Mucosal Immunol,* 7(1), pp. 27-37.

Hu, C., Yong, X., Li, C., Lu, M., Liu, D., Chen, L., Hu, J., Teng, M., Zhang, D., Fan, Y. and Liang, G. (2013) 'CXCL12/CXCR4 axis promotes mesenchymal stem cell mobilization to burn wounds and contributes to wound repair', *J Surg Res,* 183(1), pp. 427-34.

Hughes, C. E. and Nibbs, R. J. B. (2018) 'A guide to chemokines and their receptors', *FEBS J,* 285(16), pp. 2944-2971.

Hunter, M. C., Teijeira, A. and Halin, C. (2016) 'T Cell Trafficking through Lymphatic Vessels', *Front Immunol,* 7, pp. 613.

Hussain, S., Peng, B., Cherian, M., Song, J. W., Ahirwar, D. K. and Ganju, R. K. (2020) 'The Roles of Stroma-Derived Chemokine in Different Stages of Cancer Metastases', *Front Immunol,* 11, pp. 598532.

Iwata, M., Hirakiyama, A., Eshima, Y., Kagechika, H., Kato, C. and Song, S. Y. (2004) 'Retinoic acid imprints gut-homing specificity on T cells', *Immunity,* 21(4), pp. 527-38.

Janssens, R., Struyf, S. and Proost, P. (2018) 'The unique structural and functional features of CXCL12', *Cell Mol Immunol,* 15(4), pp. 299-311.

JAX (2022) *Gene Ontology Browser regulation of protein serine/threonine kinase activity* Available at: http://www.informatics.jax.org/vocab/gene_ontology/GO:0071900 (Accessed: 06/09/2022 2022).

Jayaprakash, K., Khalaf, H. and Bengtsson, T. (2014) 'Gingipains from Porphyromonas gingivalis play a significant role in induction and regulation of CXCL8 in THP-1 cells', *BMC Microbiol,* 14, pp. 193.

Jiang, Q., Zhao, Y., Shui, Y., Zhou, X., Cheng, L., Ren, B., Chen, Z. and Li, M. (2021) 'Interactions Between Neutrophils and Periodontal Pathogens in Late-Onset Periodontitis', *Front Cell Infect Microbiol,* 11, pp. 627328.

Jiang, Y., Zhou, X., Cheng, L. and Li, M. (2020) 'The Impact of Smoking on Subgingival Microflora: From Periodontal Health to Disease', *Front Microbiol,* 11, pp. 66.

Jiang, Z., Li, Y., Ji, X., Tang, Y., Yu, H., Ding, L., Yu, M., Cui, Q., Zhang, M., Ma, Y. and Li, M. (2017) 'Protein profiling identified key chemokines that regulate the maintenance of human pluripotent stem cells', *Sci Rep,* 7(1), pp. 14510.

Jin, Q., Altenburg, J. D., Hossain, M. M. and Alkhatib, G. (2011) 'Role for the conserved N-terminal cysteines in the anti-chemokine activities by the chemokine-like protein MC148R1 encoded by Molluscum contagiosum virus', *Virology,* 417(2), pp. 449-56.

Johnson, G. K. and Guthmiller, J. M. (2007) 'The impact of cigarette smoking on periodontal disease and treatment', *Periodontol 2000,* 44, pp. 178-94.

Johnston, W. (2021) *The host and microbial response to non-surgical periodontal therapy*. PhD, University of Glasgow, Glasgow.

Johnston, W., Paterson, M., Piela, K., Davison, E., Simpson, A., Goulding, M., Ramage, G., Sherriff, A. and Culshaw, S. (2020) 'The systemic inflammatory

response following hand instrumentation versus ultrasonic instrumentation-A randomized controlled trial', *J Clin Periodontol,* 47(9), pp. 1087-1097.

Kabashima, H., Yoneda, M., Nagata, K., Hirofuji, T. and Maeda, K. (2002) 'The presence of chemokine (MCP-1, MIP-1alpha, MIP-1beta, IP-10, RANTES)-positive cells and chemokine receptor (CCR5, CXCR3)-positive cells in inflamed human gingival tissues', *Cytokine,* 20(2), pp. 70-7.

Kakinuma, T., Nakamura, K., Wakugawa, M., Mitsui, H., Tada, Y., Saeki, H., Torii, H., Asahina, A., Onai, N., Matsushima, K. and Tamaki, K. (2001) 'Thymus and activation-regulated chemokine in atopic dermatitis: Serum thymus and activation-regulated chemokine level is closely related with disease activity', *J Allergy Clin Immunol,* 107(3), pp. 535-41.

Kakinuma, T., Sugaya, M., Nakamura, K., Kaneko, F., Wakugawa, M., Matsushima, K. and Tamaki, K. (2003) 'Thymus and activation-regulated chemokine (TARC/CCL17) in mycosis fungoides: serum TARC levels reflect the disease activity of mycosis fungoides', *J Am Acad Dermatol,* 48(1), pp. 23-30.

Kapoor, A., Malhotra, R., Grover, V. and Grover, D. (2012) 'Systemic antibiotic therapy in periodontics', *Dent Res J (Isfahan),* 9(5), pp. 505-15.

Kashem, S. W. and Kaplan, D. H. (2018) 'Isolation of Murine Skin Resident and Migratory Dendritic Cells via Enzymatic Digestion', *Curr Protoc Immunol,* 121(1), pp. e45.

Kebschull, M., Demmer, R., Behle, J. H., Pollreisz, A., Heidemann, J., Belusko, P. B., Celenti, R., Pavlidis, P. and Papapanou, P. N. (2009) 'Granulocyte chemotactic protein 2 (gcp-2/cxcl6) complements interleukin-8 in periodontal disease', *J Periodontal Res,* 44(4), pp. 465-71.

Khan, W. I., Motomura, Y., Wang, H., El-Sharkawy, R. T., Verdu, E. F., Verma-Gandhu, M., Rollins, B. J. and Collins, S. M. (2006) 'Critical role of MCP-1 in the pathogenesis of experimental colitis in the context of immune and enterochromaffin cells', *Am J Physiol Gastrointest Liver Physiol,* 291(5), pp. G803-11.

Kitamoto, S., Nagao-Kitamoto, H., Jiao, Y., Gillilland, M. G., 3rd, Hayashi, A., Imai, J., Sugihara, K., Miyoshi, M., Brazil, J. C., Kuffa, P., Hill, B. D., Rizvi, S. M., Wen, F., Bishu, S., Inohara, N., Eaton, K. A., Nusrat, A., Lei, Y. L., Giannobile, W. V. and Kamada, N. (2020) 'The Intermucosal Connection between the Mouth and Gut in Commensal Pathobiont-Driven Colitis', *Cell,* 182(2), pp. 447-462 e14.

Ko, H. M., Moon, J. S., Shim, H. K., Lee, S. Y., Kang, J. H., Kim, M. S., Chung, H. J. and Kim, S. H. (2020) 'Inhibitory effect of C-X-C motif chemokine ligand 14 on the osteogenic differentiation of human periodontal ligament cells through transforming growth factor-beta1', *Arch Oral Biol,* 115, pp. 104733.

Krijgsveld, J., Zaat, S. A., Meeldijk, J., van Veelen, P. A., Fang, G., Poolman, B., Brandt, E., Ehlert, J. E., Kuijpers, A. J., Engbers, G. H., Feijen, J. and Dankert, J. (2000) 'Thrombocidins, microbicidal proteins from human blood platelets, are C-terminal deletion products of CXC chemokines', *J Biol Chem,* 275(27), pp. 20374-81.

Krishnan, S., Wemyss, K., Prise, I. E., McClure, F. A., O'Boyle, C., Bridgeman, H. M., Shaw, T. N., Grainger, J. R. and Konkel, J. E. (2021) 'Hematopoietic stem and progenitor cells are present in healthy gingiva tissue', *J Exp Med,* 218(4).

Kryczek, I., Lange, A., Mottram, P., Alvarez, X., Cheng, P., Hogan, M., Moons, L., Wei, S., Zou, L., Machelon, V., Emilie, D., Terrassa, M., Lackner, A., Curiel, T. J., Carmeliet, P. and Zou, W. (2005) 'CXCL12 and vascular endothelial growth factor synergistically induce neoangiogenesis in human ovarian cancers', *Cancer Res,* 65(2), pp. 465-72.

Kufareva, I., Salanga, C. L. and Handel, T. M. (2015) 'Chemokine and chemokine receptor structure and interactions: implications for therapeutic strategies', *Immunol Cell Biol,* 93(4), pp. 372-83.

Kunkel, E. J. and Butcher, E. C. (2002) 'Chemokines and the tissue-specific migration of lymphocytes', *Immunity,* 16(1), pp. 1-4.

Kunkel, E. J. and Ley, K. (1996) 'Distinct phenotype of E-selectin-deficient mice. E-selectin is required for slow leukocyte rolling in vivo', *Circ Res,* 79(6), pp. 1196-204.

Kuritani, M., Sakai, N., Karakawa, A., Isawa, M., Chatani, M., Negishi-Koga, T., Funatsu, T. and Takami, M. (2018) 'Anti-mouse RANKL Antibodies Inhibit Alveolar Bone Destruction in Periodontitis Model Mice', *Biol Pharm Bull,* 41(4), pp. 637-643.

Kwon, T., Lamster, I. B. and Levin, L. (2020) 'Current concepts in the management of periodontitis', *Int Dent J.*

Lai, W. Y. and Mueller, A. (2021) 'Latest update on chemokine receptors as therapeutic targets', *Biochem Soc Trans,* 49(3), pp. 1385-1395.

Lazennec, G. and Richmond, A. (2010) 'Chemokines and chemokine receptors: new insights into cancer-related inflammation', *Trends Mol Med,* 16(3), pp. 133-44.

Lee, J., Taneja, V. and Vassallo, R. (2012) 'Cigarette smoking and inflammation: cellular and molecular mechanisms', *J Dent Res,* 91(2), pp. 142-9.

Legler, D. F. and Thelen, M. (2018) 'New insights in chemokine signaling', *F1000Res,* 7, pp. 95.

Ley, K., Laudanna, C., Cybulsky, M. I. and Nourshargh, S. (2007) 'Getting to the site of inflammation: the leukocyte adhesion cascade updated', *Nat Rev Immunol,* 7(9), pp. 678-89.

Li, F., Adase, C. A. and Zhang, L. J. (2017) 'Isolation and Culture of Primary Mouse Keratinocytes from Neonatal and Adult Mouse Skin', *J Vis Exp,* (125).

Li, N. and Collyer, C. A. (2011) 'Gingipains from Porphyromonas gingivalis - Complex domain structures confer diverse functions', *Eur J Microbiol Immunol (Bp),* 1(1), pp. 41-58.

Li, W., Zhang, Z. and Wang, Z. M. (2020) 'Differential immune cell infiltrations between healthy periodontal and chronic periodontitis tissues', *BMC Oral Health,* 20(1), pp. 293.

Listgarten, M. A., Schifter, C. C. and Laster, L. (1985) '3-year longitudinal study of the periodontal status of an adult population with gingivitis', *J Clin Periodontol,* 12(3), pp. 225-38.

Löe, H., Anerud, A., Boysen, H. and Morrison, E. (1986) 'Natural history of periodontal disease in man. Rapid, moderate and no loss of attachment in Sri Lankan laborers 14 to 46 years of age', *J Clin Periodontol,* 13(5), pp. 431-45.

Loos, B. G. and Van Dyke, T. E. (2020) 'The role of inflammation and genetics in periodontal disease', *Periodontol 2000,* 83(1), pp. 26-39.

Lorant, D. E., Topham, M. K., Whatley, R. E., McEver, R. P., McIntyre, T. M., Prescott, S. M. and Zimmerman, G. A. (1993) 'Inflammatory roles of P-selectin', *J Clin Invest,* 92(2), pp. 559-70.

Lundberg, M., Eriksson, A., Tran, B., Assarsson, E. and Fredriksson, S. (2011) 'Homogeneous antibody-based proximity extension assays provide sensitive and specific detection of low-abundant proteins in human blood', *Nucleic Acids Res,* 39(15), pp. e102.

Maekawa, S., Onizuka, S., Katagiri, S., Hatasa, M., Ohsugi, Y., Sasaki, N., Watanabe, K., Ohtsu, A., Komazaki, R., Ogura, K., Miyoshi-Akiyama, T., Iwata, T., Nitta, H. and Izumi, Y. (2019) 'RNA sequencing for ligature induced periodontitis in mice revealed important role of S100A8 and S100A9 for periodontal destruction', *Sci Rep,* 9(1), pp. 14663.

Mahanonda, R., Champaiboon, C., Subbalekha, K., Sa-Ard-Iam, N., Rattanathammatada, W., Thawanaphong, S., Rerkyen, P., Yoshimura, F., Nagano, K., Lang, N. P. and Pichyangkul, S. (2016) 'Human Memory B Cells in Healthy Gingiva, Gingivitis, and Periodontitis', *J Immunol,* 197(3), pp. 715-25.

Malcolm, J., Awang, R. A., Oliver-Bell, J., Butcher, J. P., Campbell, L., Adrados Planell, A., Lappin, D. F., Fukada, S. Y., Nile, C. J., Liew, F. Y. and Culshaw, S.

(2015) 'IL-33 Exacerbates Periodontal Disease through Induction of RANKL', *J Dent Res,* 94(7), pp. 968-75.

Mantovani, A. (1999) 'The chemokine system: redundancy for robust outputs', *Immunol Today,* 20(6), pp. 254-7.

Mantovani, A., Cassatella, M. A., Costantini, C. and Jaillon, S. (2011) 'Neutrophils in the activation and regulation of innate and adaptive immunity', *Nat Rev Immunol,* 11(8), pp. 519-31.

Marchesan, J., Girnary, M. S., Jing, L., Miao, M. Z., Zhang, S., Sun, L., Morelli, T., Schoenfisch, M. H., Inohara, N., Offenbacher, S. and Jiao, Y. (2018) 'An experimental murine model to study periodontitis', *Nat Protoc,* 13(10), pp. 2247-2267.

Masopust, D., Sivula, C. P. and Jameson, S. C. (2017) 'Of Mice, Dirty Mice, and Men: Using Mice To Understand Human Immunology', *J Immunol,* 199(2), pp. 383-388.

Matthews, J. B., Wright, H. J., Roberts, A., Ling-Mountford, N., Cooper, P. R. and Chapple, I. L. (2007) 'Neutrophil hyper-responsiveness in periodontitis', *J Dent Res,* 86(8), pp. 718-22.

McCubrey, J. A., May, W. S., Duronio, V. and Mufson, A. (2000) 'Serine/threonine phosphorylation in cytokine signal transduction', *Leukemia,* 14(1), pp. 9-21.

Medina-Ruiz, L., Bartolini, R., Wilson, G. J., Dyer, D. P., Vidler, F., Hughes, C. E., Schuette, F., Love, S., Pingen, M., Hayes, A. J., Fu, J., Stewart, A. F. and Graham, G. J. (2022) 'Analysis of combinatorial chemokine receptor expression dynamics using multi-receptor reporter mice', *Elife,* 11.

Menon, G. K., Cleary, G. W. and Lane, M. E. (2012) 'The structure and function of the stratum corneum', *Int J Pharm,* 435(1), pp. 3-9.

Meuter, S., Schaerli, P., Roos, R. S., Brandau, O., Bosl, M. R., von Andrian, U. H. and Moser, B. (2007) 'Murine CXCL14 is dispensable for dendritic cell function and localization within peripheral tissues', *Mol Cell Biol,* 27(3), pp. 983-92.

Michalowicz, B. S., Diehl, S. R., Gunsolley, J. C., Sparks, B. S., Brooks, C. N., Koertge, T. E., Califano, J. V., Burmeister, J. A. and Schenkein, H. A. (2000) 'Evidence of a substantial genetic basis for risk of adult periodontitis', *J Periodontol,* 71(11), pp. 1699-707.

Middleton, J., Patterson, A. M., Gardner, L., Schmutz, C. and Ashton, B. A. (2002) 'Leukocyte extravasation: chemokine transport and presentation by the endothelium', *Blood,* 100(12), pp. 3853-60.

Millhouse, E., Jose, A., Sherry, L., Lappin, D. F., Patel, N., Middleton, A. M., Pratten, J., Culshaw, S. and Ramage, G. (2014) 'Development of an in vitro

periodontal biofilm model for assessing antimicrobial and host modulatory effects of bioactive molecules', *BMC Oral Health,* 14, pp. 80.

Miyauchi, M., Kitagawa, S., Hiraoka, M., Saito, A., Sato, S., Kudo, Y., Ogawa, I. and Takata, T. (2004) 'Immunolocalization of CXC chemokine and recruitment of polymorphonuclear leukocytes in the rat molar periodontal tissue after topical application of lipopolysaccharide', *Histochem Cell Biol,* 121(4), pp. 291-7.

Mollica Poeta, V., Massara, M., Capucetti, A. and Bonecchi, R. (2019) 'Chemokines and Chemokine Receptors: New Targets for Cancer Immunotherapy', *Front Immunol,* 10, pp. 379.

Monteclaro, F. S. and Charo, I. F. (1996) 'The amino-terminal extracellular domain of the MCP-1 receptor, but not the RANTES/MIP-1alpha receptor, confers chemokine selectivity. Evidence for a two-step mechanism for MCP-1 receptor activation', *J Biol Chem,* 271(32), pp. 19084-92.

Moore, D. C., Elmes, J. B., Shibu, P. A., Larck, C. and Park, S. I. (2020) 'Mogamulizumab: An Anti-CC Chemokine Receptor 4 Antibody for T-Cell Lymphomas', *Ann Pharmacother,* 54(4), pp. 371-379.

Moore, J. E., Jr., Brook, B. S. and Nibbs, R. J. B. (2018) 'Chemokine Transport Dynamics and Emerging Recognition of Their Role in Immune Function', *Curr Opin Biomed Eng,* 5, pp. 90-95.

Mora, J. R. and von Andrian, U. H. (2006) 'T-cell homing specificity and plasticity: new concepts and future challenges', *Trends Immunol,* 27(5), pp. 235-43.

Mortier, A., Gouwy, M., Van Damme, J. and Proost, P. (2011) 'Effect of posttranslational processing on the in vitro and in vivo activity of chemokines', *Exp Cell Res,* 317(5), pp. 642-54.

Moutsopoulos, N. M., Konkel, J., Sarmadi, M., Eskan, M. A., Wild, T., Dutzan, N., Abusleme, L., Zenobia, C., Hosur, K. B., Abe, T., Uzel, G., Chen, W., Chavakis, T., Holland, S. M. and Hajishengallis, G. (2014) 'Defective neutrophil recruitment in leukocyte adhesion deficiency type I disease causes local IL-17-driven inflammatory bone loss', *Sci Transl Med,* 6(229), pp. 229ra40.

Moutsopoulos, N. M. and Konkel, J. E. (2018) 'Tissue-Specific Immunity at the Oral Mucosal Barrier', *Trends Immunol,* 39(4), pp. 276-287.

Muller, W. A. (2013) 'Getting leukocytes to the site of inflammation', *Vet Pathol,* 50(1), pp. 7-22.

Murayama, Y., Kurihara, H., Nagai, A., Dompkowski, D. and Van Dyke, T. E. (1994) 'Acute necrotizing ulcerative gingivitis: risk factors involving host defense mechanisms', *Periodontol 2000,* 6, pp. 116-24.

Murphy, P. M. and Heusinkveld, L. (2018) 'Multisystem multitasking by CXCL12 and its receptors CXCR4 and ACKR3', *Cytokine,* 109, pp. 2-10.

Myneni, S. R., Settem, R. P., Connell, T. D., Keegan, A. D., Gaffen, S. L. and Sharma, A. (2011) 'TLR2 signaling and Th2 responses drive Tannerella forsythia-induced periodontal bone loss', *J Immunol,* 187(1), pp. 501-9.

Nagarsheth, N., Wicha, M. S. and Zou, W. (2017) 'Chemokines in the cancer microenvironment and their relevance in cancer immunotherapy', *Nat Rev Immunol,* 17(9), pp. 559-572.

Nagasawa, T., Hirota, S., Tachibana, K., Takakura, N., Nishikawa, S., Kitamura, Y., Yoshida, N., Kikutani, H. and Kishimoto, T. (1996) 'Defects of B-cell lymphopoiesis and bone-marrow myelopoiesis in mice lacking the CXC chemokine PBSF/SDF-1', *Nature,* 382(6592), pp. 635-8.

Nahian, A. and Chauhan, P. R. (2022) 'Histology, Periosteum And Endosteum', *StatPearls*. Treasure Island (FL).

Nakajima, T., Amanuma, R., Ueki-Maruyama, K., Oda, T., Honda, T., Ito, H. and Yamazaki, K. (2008) 'CXCL13 expression and follicular dendritic cells in relation to B-cell infiltration in periodontal disease tissues', *J Periodontal Res,* 43(6), pp. 635-41.

Nazir, M. A. (2017) 'Prevalence of periodontal disease, its association with systemic diseases and prevention', *Int J Health Sci (Qassim),* 11(2), pp. 72-80.

NC3R (2022) *National Centre for the Replacement, Refinement and Reduction of Animals in Research*. Available at: https://nc3rs.org.uk/who-we-are/3rs 2022).

Nesse, W., Abbas, F., van der Ploeg, I., Spijkervet, F. K., Dijkstra, P. U. and Vissink, A. (2008) 'Periodontal inflamed surface area: quantifying inflammatory burden', *J Clin Periodontol,* 35(8), pp. 668-73.

Nibbs, R., Graham, G. and Rot, A. (2003) 'Chemokines on the move: control by the chemokine "interceptors" Duffy blood group antigen and D6', *Semin Immunol,* 15(5), pp. 287-94.

Nibbs, R. J. and Graham, G. J. (2013) 'Immune regulation by atypical chemokine receptors', *Nat Rev Immunol,* 13(11), pp. 815-29.

Nukiwa, M., Andarini, S., Zaini, J., Xin, H., Kanehira, M., Suzuki, T., Fukuhara, T., Mizuguchi, H., Hayakawa, T., Saijo, Y., Nukiwa, T. and Kikuchi, T. (2006) 'Dendritic cells modified to express fractalkine/CX3CL1 in the treatment of preexisting tumors', *Eur J Immunol,* 36(4), pp. 1019-27.

Oo, Y. H., Shetty, S. and Adams, D. H. (2010) 'The role of chemokines in the recruitment of lymphocytes to the liver', *Dig Dis,* 28(1), pp. 31-44.

Otte, M., Kliewer, A., Schutz, D., Reimann, C., Schulz, S. and Stumm, R. (2014) 'CXCL14 is no direct modulator of CXCR4', *FEBS Lett,* 588(24), pp. 4769-75.

Oz, H. S. and Puleo, D. A. (2011) 'Animal models for periodontal disease', *J Biomed Biotechnol,* 2011, pp. 754857.

Page, R. C. and Schroeder, H. E. (1976) 'Pathogenesis of inflammatory periodontal disease. A summary of current work', *Lab Invest,* 34(3), pp. 235-49.

Peacock, M. E., Arce, R. M. and Cutler, C. W. (2017) 'Periodontal and other oral manifestations of immunodeficiency diseases', *Oral Dis,* 23(7), pp. 866-888.

Peddis, N., Musu, D., Ideo, F., Rossi-Fedele, G. and Cotti, E. (2019) 'Interaction of biologic therapy with apical periodontitis and periodontitis: a systematic review', *Aust Dent J,* 64(2), pp. 122-134.

Pejcic, A., Djordjevic, V., Kojovic, D., Zivkovic, V., Minic, I., Mirkovic, D. and Stojanovic, M. (2014) 'Effect of periodontal treatment in renal transplant recipients', *Med Princ Pract,* 23(2), pp. 149-53.

Perez-Chaparro, P. J., Goncalves, C., Figueiredo, L. C., Faveri, M., Lobao, E., Tamashiro, N., Duarte, P. and Feres, M. (2014) 'Newly identified pathogens associated with periodontitis: a systematic review', *J Dent Res,* 93(9), pp. 846-58.

Portella, L., Bello, A. M. and Scala, S. (2021) 'CXCL12 Signaling in the Tumor Microenvironment', *Adv Exp Med Biol,* 1302, pp. 51-70.

Prates, T. P., Taira, T. M., Holanda, M. C., Bignardi, L. A., Salvador, S. L., Zamboni, D. S., Cunha, F. Q. and Fukada, S. Y. (2014) 'NOD2 contributes to Porphyromonas gingivalis-induced bone resorption', *J Dent Res,* 93(11), pp. 1155-62.

Puel, A., Cypowyj, S., Bustamante, J., Wright, J. F., Liu, L., Lim, H. K., Migaud, M., Israel, L., Chrabieh, M., Audry, M., Gumbleton, M., Toulon, A., Bodemer, C., El-Baghdadi, J., Whitters, M., Paradis, T., Brooks, J., Collins, M., Wolfman, N. M., Al-Muhsen, S., Galicchio, M., Abel, L., Picard, C. and Casanova, J. L. (2011) 'Chronic mucocutaneous candidiasis in humans with inborn errors of interleukin-17 immunity', *Science,* 332(6025), pp. 65-8.

Raman, D., Sobolik-Delmaire, T. and Richmond, A. (2011) 'Chemokines in health and disease', *Exp Cell Res,* 317(5), pp. 575-89.

Raport, C. J., Gosling, J., Schweickart, V. L., Gray, P. W. and Charo, I. F. (1996) 'Molecular cloning and functional characterization of a novel human CC chemokine receptor (CCR5) for RANTES, MIP-1beta, and MIP-1alpha', *J Biol Chem,* 271(29), pp. 17161-6.

Rath-Deschner, B., Memmert, S., Damanaki, A., Nokhbehsaim, M., Eick, S., Cirelli, J. A., Gotz, W., Deschner, J., Jager, A. and Nogueira, A. V. B. (2020) 'CXCL1, CCL2, and CCL5 modulation by microbial and biomechanical signals in periodontal cells and tissues-in vitro and in vivo studies', *Clin Oral Investig,* 24(10), pp. 3661-3670.

Reilly, R. J. R., Johnston, W. and Culshaw, S. (2019) 'Autoimmunity and the Oral Cavity', *Current Oral Health Reports,* 6(1), pp. 1-8.

Reiss, Y., Proudfoot, A. E., Power, C. A., Campbell, J. J. and Butcher, E. C. (2001) 'CC chemokine receptor (CCR)4 and the CCR10 ligand cutaneous T cell-attracting chemokine (CTACK) in lymphocyte trafficking to inflamed skin', *J Exp Med,* 194(10), pp. 1541-7.

Roberts, H. M., Ling, M. R., Insall, R., Kalna, G., Spengler, J., Grant, M. M. and Chapple, I. L. (2015) 'Impaired neutrophil directional chemotactic accuracy in chronic periodontitis patients', *J Clin Periodontol,* 42(1), pp. 1-11.

Rot, A. and von Andrian, U. H. (2004) 'Chemokines in innate and adaptive host defense: basic chemokinese grammar for immune cells', *Annu Rev Immunol,* 22, pp. 891-928.

Sahingur, S. E. and Yeudall, W. A. (2015) 'Chemokine function in periodontal disease and oral cavity cancer', *Front Immunol,* 6, pp. 214.

Salvi, G. E., Carollo-Bittel, B. and Lang, N. P. (2008) 'Effects of diabetes mellitus on periodontal and peri-implant conditions: update on associations and risks', *J Clin Periodontol,* 35(8 Suppl), pp. 398-409.

Santos, R., Ursu, O., Gaulton, A., Bento, A. P., Donadi, R. S., Bologa, C. G., Karlsson, A., Al-Lazikani, B., Hersey, A., Oprea, T. I. and Overington, J. P. (2017) 'A comprehensive map of molecular drug targets', *Nat Rev Drug Discov,* 16(1), pp. 19-34.

Schaerli, P., Willimann, K., Ebert, L. M., Walz, A. and Moser, B. (2005) 'Cutaneous CXCL14 targets blood precursors to epidermal niches for Langerhans cell differentiation', *Immunity,* 23(3), pp. 331-42.

Schall, T. J. (1991) 'Biology of the RANTES/SIS cytokine family', *Cytokine,* 3(3), pp. 165-83.

Scimone, M. L., Felbinger, T. W., Mazo, I. B., Stein, J. V., Von Andrian, U. H. and Weninger, W. (2004) 'CXCL12 mediates CCR7-independent homing of central memory cells, but not naive T cells, in peripheral lymph nodes', *J Exp Med,* 199(8), pp. 1113-20.

Scott, D. A. and Krauss, J. (2012) 'Neutrophils in periodontal inflammation', *Front Oral Biol,* 15, pp. 56-83.

SDCEP (2014) 'Prevention and Treatment of Periodontal Diseases in Primary Care'.

Seymour, G. J., Powell, R. N. and Aitken, J. F. (1983) 'Experimental gingivitis in humans. A clinical and histologic investigation', *J Periodontol,* 54(9), pp. 522-8.

Shen, Z., Kuang, S., Zhang, M., Huang, X., Chen, J., Guan, M., Qin, W., Xu, H. H. K. and Lin, Z. (2021) 'Inhibition of CCL2 by bindarit alleviates diabetes-associated periodontitis by suppressing inflammatory monocyte infiltration and altering macrophage properties', *Cell Mol Immunol,* 18(9), pp. 2224-2235.

Siddiqui, I., Erreni, M., van Brakel, M., Debets, R. and Allavena, P. (2016) 'Enhanced recruitment of genetically modified CX3CR1-positive human T cells into Fractalkine/CX3CL1 expressing tumors: importance of the chemokine gradient', *J Immunother Cancer,* 4, pp. 21.

Sigmundsdottir, H., Pan, J., Debes, G. F., Alt, C., Habtezion, A., Soler, D. and Butcher, E. C. (2007) 'DCs metabolize sunlight-induced vitamin D3 to 'program' T cell attraction to the epidermal chemokine CCL27', *Nat Immunol,* 8(3), pp. 285-93.

Silva, T. A., Garlet, G. P., Fukada, S. Y., Silva, J. S. and Cunha, F. Q. (2007) 'Chemokines in oral inflammatory diseases: apical periodontitis and periodontal disease', *J Dent Res,* 86(4), pp. 306-19.

Singh, U. P., Singh, N. P., Murphy, E. A., Price, R. L., Fayad, R., Nagarkatti, M. and Nagarkatti, P. S. (2016) 'Chemokine and cytokine levels in inflammatory bowel disease patients', *Cytokine,* 77, pp. 44-9.

Sivolella, S., Scanu, A., Xie, Z., Vianello, S. and Stellini, E. (2022) 'Biobanking in dentistry: A review', *Jpn Dent Sci Rev,* 58, pp. 31-40.

Smith, C. and Martinez, C. (2018) 'Wound Healing in the Oral Mucosa', *Oral Mucosa in Health and Disease*, pp. 77-90.

Socransky, S. S., Haffajee, A. D., Cugini, M. A., Smith, C. and Kent, R. L., Jr. (1998) 'Microbial complexes in subgingival plaque', *J Clin Periodontol,* 25(2), pp. 134-44.

Song, L., Dong, G., Guo, L. and Graves, D. T. (2018) 'The function of dendritic cells in modulating the host response', *Mol Oral Microbiol,* 33(1), pp. 13-21.

Soriano, S. F., Serrano, A., Hernanz-Falcon, P., Martin de Ana, A., Monterrubio, M., Martinez, C., Rodriguez-Frade, J. M. and Mellado, M. (2003) 'Chemokines integrate JAK/STAT and G-protein pathways during chemotaxis and calcium flux responses', *Eur J Immunol,* 33(5), pp. 1328-33.

Sriram, K. and Insel, P. A. (2018) 'G Protein-Coupled Receptors as Targets for Approved Drugs: How Many Targets and How Many Drugs?', (1521-0111 (Electronic)).

Sugaya, M. (2015) 'Chemokines and skin diseases', *Arch Immunol Ther Exp (Warsz),* 63(2), pp. 109-15.

Surmi, B. K. and Hasty, A. H. (2010) 'The role of chemokines in recruitment of immune cells to the artery wall and adipose tissue', *Vascul Pharmacol,* 52(1-2), pp. 27-36.

Tan, Q., Zhu, Y., Li, J., Chen, Z., Han, G. W., Kufareva, I., Li, T., Ma, L., Fenalti, G., Li, J., Zhang, W., Xie, X., Yang, H., Jiang, H., Cherezov, V., Liu, H., Stevens, R. C., Zhao, Q. and Wu, B. (2013) 'Structure of the CCR5 chemokine receptor-HIV entry inhibitor maraviroc complex', *Science,* 341(6152), pp. 1387-90.

Tanegashima, K., Okamoto, S., Nakayama, Y., Taya, C., Shitara, H., Ishii, R., Yonekawa, H., Minokoshi, Y. and Hara, T. (2010) 'CXCL14 deficiency in mice attenuates obesity and inhibits feeding behavior in a novel environment', *PLoS One,* 5(4), pp. e10321.

Tanegashima, K., Suzuki, K., Nakayama, Y., Tsuji, K., Shigenaga, A., Otaka, A. and Hara, T. (2013) 'CXCL14 is a natural inhibitor of the CXCL12-CXCR4 signaling axis', *FEBS Lett,* 587(12), pp. 1731-5.

Thelen, M. and Stein, J. V. (2008) 'How chemokines invite leukocytes to dance', *Nat Immunol,* 9(9), pp. 953-9.

Tomar, S. L. and Asma, S. (2000) 'Smoking-attributable periodontitis in the United States: findings from NHANES III. National Health and Nutrition Examination Survey', *J Periodontol,* 71(5), pp. 743-51.

Tonetti, M. S., Imboden, M. A. and Lang, N. P. (1998) 'Neutrophil migration into the gingival sulcus is associated with transepithelial gradients of interleukin-8 and ICAM-1', *J Periodontol,* 69(10), pp. 1139-47.

Tzeng, Y. S., Li, H., Kang, Y. L., Chen, W. C., Cheng, W. C. and Lai, D. M. (2011) 'Loss of Cxcl12/Sdf-1 in adult mice decreases the quiescent state of hematopoietic stem/progenitor cells and alters the pattern of hematopoietic regeneration after myelosuppression', *Blood,* 117(2), pp. 429-39.

Usui, M., Onizuka, S., Sato, T., Kokabu, S., Ariyoshi, W. and Nakashima, K. (2021) 'Mechanism of alveolar bone destruction in periodontitis - Periodontal bacteria and inflammation', *Jpn Dent Sci Rev,* 57, pp. 201-208.

Van der Weijden, G. A. F., Dekkers, G. J. and Slot, D. E. (2019) 'Success of non-surgical periodontal therapy in adult periodontitis patients: A retrospective analysis', *Int J Dent Hyg,* 17(4), pp. 309-317.

Van Dyke, T. E. and Sheilesh, D. (2005) 'Risk factors for periodontitis', *J Int Acad Periodontol,* 7(1), pp. 3-7.

Vandercappellen, J., Van Damme, J. and Struyf, S. (2011) 'The role of the CXC chemokines platelet factor-4 (CXCL4/PF-4) and its variant (CXCL4L1/PF-4var) in inflammation, angiogenesis and cancer', *Cytokine Growth Factor Rev,* 22(1), pp. 1-18.

Vanheule, V., Metzemaekers, M., Janssens, R., Struyf, S. and Proost, P. (2018) 'How post-translational modifications influence the biological activity of chemokines', *Cytokine,* 109, pp. 29-51.

Vernal, R., Dutzan, N., Chaparro, A., Puente, J., Antonieta Valenzuela, M. and Gamonal, J. (2005) 'Levels of interleukin-17 in gingival crevicular fluid and in supernatants of cellular cultures of gingival tissue from patients with chronic periodontitis', *J Clin Periodontol,* 32(4), pp. 383-9.

Votta, B. J., White, J. R., Dodds, R. A., James, I. E., Connor, J. R., Lee-Rykaczewski, E., Eichman, C. F., Kumar, S., Lark, M. W. and Gowen, M. (2000) 'CKbeta-8 [CCL23], a novel CC chemokine, is chemotactic for human osteoclast precursors and is expressed in bone tissues', *J Cell Physiol,* 183(2), pp. 196-207.

Weber, M., Hauschild, R., Schwarz, J., Moussion, C., de Vries, I., Legler, D. F., Luther, S. A., Bollenbach, T. and Sixt, M. (2013) 'Interstitial dendritic cell guidance by haptotactic chemokine gradients', *Science,* 339(6117), pp. 328-32.

Wermers, J. D., McNamee, E. N., Wurbel, M. A., Jedlicka, P. and Rivera-Nieves, J. (2011) 'The chemokine receptor CCR9 is required for the T-cell-mediated regulation of chronic ileitis in mice', *Gastroenterology,* 140(5), pp. 1526-35 e3.

Williams, D. W., Greenwell-Wild, T., Brenchley, L., Dutzan, N., Overmiller, A., Sawaya, A. P., Webb, S., Martin, D., Genomics, N. N., Computational Biology, C., Hajishengallis, G., Divaris, K., Morasso, M., Haniffa, M. and Moutsopoulos, N. M. (2021) 'Human oral mucosa cell atlas reveals a stromal-neutrophil axis regulating tissue immunity', *Cell,* 184(15), pp. 4090-4104 e15.

Wolf, M. and Moser, B. (2012) 'Antimicrobial activities of chemokines: not just a side-effect?', *Front Immunol,* 3, pp. 213.

Wu, R. Q., Zhang, D. F., Tu, E., Chen, Q. M. and Chen, W. (2014) 'The mucosal immune system in the oral cavity-an orchestra of T cell diversity', *Int J Oral Sci,* 6(3), pp. 125-32.

Wurbel, M. A., Malissen, M., Guy-Grand, D., Malissen, B. and Campbell, J. J. (2007) 'Impaired accumulation of antigen-specific CD8 lymphocytes in chemokine CCL25-deficient intestinal epithelium and lamina propria', *J Immunol,* 178(12), pp. 7598-606.

Wurbel, M. A., Malissen, M., Guy-Grand, D., Meffre, E., Nussenzweig, M. C., Richelme, M., Carrier, A. and Malissen, B. (2001) 'Mice lacking the CCR9 CC-chemokine receptor show a mild impairment of early T- and B-cell development and a reduction in T-cell receptor gammadelta(+) gut intraepithelial lymphocytes', *Blood,* 98(9), pp. 2626-32.

Wurbel, M. A., McIntire, M. G., Dwyer, P. and Fiebiger, E. (2011) 'CCL25/CCR9 interactions regulate large intestinal inflammation in a murine model of acute colitis', *PLoS One,* 6(1), pp. e16442.

Xia, M., Hu, S., Fu, Y., Jin, W., Yi, Q., Matsui, Y., Yang, J., McDowell, M. A., Sarkar, S., Kalia, V. and Xiong, N. (2014) 'CCR10 regulates balanced maintenance and function of resident regulatory and effector T cells to promote immune homeostasis in the skin', *J Allergy Clin Immunol,* 134(3), pp. 634-644 e10.

Xiao, W., Dong, G., Pacios, S., Alnammary, M., Barger, L. A., Wang, Y., Wu, Y. and Graves, D. T. (2015) 'FOXO1 deletion reduces dendritic cell function and enhances susceptibility to periodontitis', *Am J Pathol,* 185(4), pp. 1085-93.

Yan, Y., Chen, R., Wang, X., Hu, K., Huang, L., Lu, M. and Hu, Q. (2019) 'CCL19 and CCR7 Expression, Signaling Pathways, and Adjuvant Functions in Viral Infection and Prevention', *Front Cell Dev Biol,* 7, pp. 212.

Yau, J. C. Y., Fong, T. C. T., Wan, A. H. Y. and Ho, R. T. H. (2022) 'Comparison of passive drool and cotton-based collection methods for salivary C-reactive protein measurement', *Am J Hum Biol,* 34(9), pp. e23782.

Yu, J. J., Ruddy, M. J., Wong, G. C., Sfintescu, C., Baker, P. J., Smith, J. B., Evans, R. T. and Gaffen, S. L. (2007) 'An essential role for IL-17 in preventing pathogen-initiated bone destruction: recruitment of neutrophils to inflamed bone requires IL-17 receptor-dependent signals', *Blood,* 109(9), pp. 3794-802.

Yucel-Lindberg, T. and Bage, T. (2013) 'Inflammatory mediators in the pathogenesis of periodontitis', *Expert Rev Mol Med,* 15, pp. e7.

Zenobia, C., Luo, X. L., Hashim, A., Abe, T., Jin, L., Chang, Y., Jin, Z. C., Sun, J. X., Hajishengallis, G., Curtis, M. A. and Darveau, R. P. (2013) 'Commensal bacteria-dependent select expression of CXCL2 contributes to periodontal tissue homeostasis', *Cell Microbiol,* 15(8), pp. 1419-26.

Zhang, Q. Z., Nguyen, A. L., Yu, W. H. and Le, A. D. (2012) 'Human oral mucosa and gingiva: a unique reservoir for mesenchymal stem cells', *J Dent Res,* 91(11), pp. 1011-8.

Zimmerman, N. P., Vongsa, R. A., Wendt, M. K. and Dwinell, M. B. (2008) 'Chemokines and chemokine receptors in mucosal homeostasis at the intestinal epithelial barrier in inflammatory bowel disease', *Inflamm Bowel Dis,* 14(7), pp. 1000-11.

Zlotnik, A., Burkhardt, A. M. and Homey, B. (2011) 'Homeostatic chemokine receptors and organ-specific metastasis', *Nat Rev Immunol,* 11(9), pp. 597-606.

Zlotnik, A., Yoshie, O. and Nomiyama, H. (2006) 'The chemokine and chemokine receptor superfamilies and their molecular evolution', *Genome Biol,* 7(12), pp. 243.

Zou, W. and Restifo, N. P. (2010) 'T(H)17 cells in tumour immunity and immunotherapy', *Nat Rev Immunol,* 10(4), pp. 248-56.

Appendix: RNA Sequencing R Code

```
#load the datasets for gingiva sham
G_CMC_3 = read.table("HT_SEQ_READCOUNTS/Galaxy216-[G_CMC_3].tabular",header=FALSE, sep="\t")
G_CMC_4 = read.table("HT_SEQ_READCOUNTS/Galaxy218-[G_CMC_4].tabular",header=FALSE, sep="\t")
G_CMC_5 = read.table("HT_SEQ_READCOUNTS/Galaxy220-[G_CMC_5].tabular",header=FALSE, sep="\t")

#column names
column_names = c("GENE_ID", "READCOUNTS")
names(G_CMC_3) = column_names
names(G_CMC_4) = column_names
names(G_CMC_5) = column_names

#merge the files and rename columns
G_CMC_merged = merge(G_CMC_3, G_CMC_4, by = "GENE_ID")

G_CMC_merged = merge(G_CMC_merged, G_CMC_5, by = "GENE_ID")

newcols= c("GENE_ID","G_CMC_3","G_CMC_4","G_CMC_5")
names(G_CMC_merged) = newcols

#load the datasets for gingiva Pg

G_PG_3 = read.table("HT_SEQ_READCOUNTS/Galaxy228-[G_Pg_3].tabular",header=FALSE, sep="\t")
G_PG_4 = read.table("HT_SEQ_READCOUNTS/Galaxy230-[G_Pg_4].tabular",header=FALSE, sep="\t")
G_PG_5 = read.table("HT_SEQ_READCOUNTS/Galaxy232-[G_Pg_5].tabular",header=FALSE, sep="\t")

#col names

column_names3 = c("GENE_ID", "G_PG_3")
column_names4 = c("GENE_ID", "G_PG_4")
column_names5 = c("GENE_ID", "G_PG_5")
names(G_PG_3) = column_names3
names(G_PG_4) = column_names4
names(G_PG_5) = column_names5

#merge the files

G_PG_merged = merge(G_PG_3, G_PG_4, by = "GENE_ID")
G_PG_merged = merge(G_PG_merged, G_PG_5, by = "GENE_ID")

#load the files for all LN
LN_CMC_3 = read.table("HT_SEQ_READCOUNTS/Galaxy222-[LN_CMC_3].tabular",header=FALSE, sep="\t")
LN_CMC_4 = read.table("HT_SEQ_READCOUNTS/Galaxy224-[LN_CMC_4].tabular",header=FALSE, sep="\t")
LN_CMC_5 = read.table("HT_SEQ_READCOUNTS/Galaxy226-[LN_CMC_5].tabular",header=FALSE, sep="\t")
LN_PG_3 = read.table("HT_SEQ_READCOUNTS/Galaxy234-[LN_PG_3].tabular",header=FALSE, sep="\t")
LN_PG_4 = read.table("HT_SEQ_READCOUNTS/Galaxy236-[LN_Pg_4].tabular",header=FALSE, sep="\t")
LN_PG_5 = read.table("HT_SEQ_READCOUNTS/Galaxy238-[LN_Pg_5].tabular",header=FALSE, sep="\t")

#col names 1
column_names3 = c("GENE_ID", "LN_PG_3")
column_names4 = c("GENE_ID", "LN_PG_4")
column_names5 = c("GENE_ID", "LN_PG_5")
names(LN_PG_3) = column_names3
names(LN_PG_4) = column_names4
names(LN_PG_5) = column_names5

#col names 2
column_names3 = c("GENE_ID", "LN_CMC_3")
column_names4 = c("GENE_ID", "LN_CMC_4")
column_names5 = c("GENE_ID", "LN_CMC_5")
names(LN_CMC_3) = column_names3
names(LN_CMC_4) = column_names4
names(LN_CMC_5) = column_names5

#merge the files

LN_Merged = merge(LN_PG_3,LN_PG_4, by = "GENE_ID")
LN_Merged = merge(LN_Merged,LN_PG_5, by = "GENE_ID")
LN_Merged = merge(LN_Merged,LN_CMC_3, by = "GENE_ID")
LN_Merged = merge(LN_Merged,LN_CMC_4, by = "GENE_ID")
LN_Merged = merge(LN_Merged,LN_CMC_5, by = "GENE_ID")

#READCOUNT MASTER TABLE
G_Merged = merge(G_CMC_merged, G_PG_merged, by = "GENE_ID")
```

```
READCOUNT_MASTER = merge(LN_Merged, G_Merged, by = "GENE_ID")

#load the sample sheet
Sample_Sheet = read.table("sample_sheet.csv", header = TRUE, row.names = 1, sep = '\t')

#change the READCOUNT table row names to GENE ID

row.names(READCOUNT_MASTER) = READCOUNT_MASTER$GENE_ID

keep = c(2:13)

READCOUNT_MASTER = READCOUNT_MASTER[,keep]

#keep only counts >=1

counts = subset(READCOUNT_MASTER,apply(READCOUNT_MASTER, 1, mean) >=1)
nrow(counts)
nrow(READCOUNT_MASTER)

#matrix of counts

counts = as.matrix(counts)

#make sample groups

sample_group = factor(Sample_Sheet$Sample_Group)

#make a new data frame with the groups names

sample_data = data.frame(row.names=colnames(counts), sample_group)

#DeSeq2

#run DESEq2

library(DESeq2)

dds = DESeqDataSetFromMatrix(countData = counts, colData = sample_data, design =~sample_group)
dds = DESeq(dds)

#normalised readcounts
norm_counts = as.data.frame(counts(dds, normalized=TRUE))
norm_counts = round(norm_counts,2)

#Differential expression
de = results(dds, c("sample_group","G_PG", "LN_PG"))
de_table = as.data.frame(de)

de_table = de_table[order(de_table$pvalue),]

#LN PG v CMC
de = results(dds, c("sample_group","LN_PG","LN_CMC")) # note the first group will become the one where a positive fold is
a greater expression value
de_out = as.data.frame(de)
de_out = de_out[order(de_out$padj), ]
de_out$id = row.names(de_out)
de_out = de_out[,c(7,2,5,6)]
colnames(de_out) = c("id","log2fold","p","p.adj")

DE_LN_CMC_V_PG = de_out

#G PG v CMC
de = results(dds, c("sample_group","G_PG","G_CMC")) # note the first group will become the one where a positive fold is a
greter expression value
de_out = as.data.frame(de)
de_out = de_out[order(de_out$padj), ]
de_out$id = row.names(de_out)
de_out = de_out[,c(7,2,5,6)]
colnames(de_out) = c("id","log2fold","p","p.adj")

DE_G_CMC_V_PG = de_out

#LN_CMC v G_CMC
de = results(dds, c("sample_group","G_CMC","LN_CMC")) # note the first group will become the one where a positive fold
is a greter expression value
de_out = as.data.frame(de)
de_out = de_out[order(de_out$padj), ]
de_out$id = row.names(de_out)
de_out = de_out[,c(7,2,5,6)]
```

```
colnames(de_out) = c("id","log2fold","p","p.adj")

DE_LN_CMC_V_G_CMC = de_out

#LN_PG v G_PG
de = results(dds, c("sample_group","G_PG","LN_PG")) # note the first group will become the one where a positive fold is a greter expression value
de_out = as.data.frame(de)
de_out = de_out[order(de_out$padj), ]
de_out$id = row.names(de_out)
de_out = de_out[,c(7,2,5,6)]
colnames(de_out) = c("id","log2fold","p","p.adj")

DE_LN_PG_V_G_PG = de_out

#Load annotations
annotations = read.table("MOUSE_BACKGROUND.txt", header=TRUE,row.names = 1, sep='\t', quote='',check.names = TRUE)

Keep = c(1,2)
annotations = annotations[,Keep]
annotations$GENE_ID = row.names(annotations)



#Organizing annotations
annotations = read.table("MOUSE_BACKGROUND1.txt", header=TRUE, row.names=1, sep="\t")

keepers= c(1,2)
annotations = annotations[,keepers]

annotations$GENE_ID = row.names(annotations)

annotations = annotations[order(annotations$GENE_ID),]

norm_counts$GENE_ID = row.names(norm_counts)
norm_counts = norm_counts[order(norm_counts$GENE_ID),]

norm_counts_annotated = merge(norm_counts, annotations, by = "GENE_ID")

row.names(norm_counts_annotated) = norm_counts_annotated$SYMBOL

#Merge DE tables
DE_G_CMC_V_PG$GENE_ID = row.names(DE_G_CMC_V_PG)
DE_G_CMC_V_PG = DE_G_CMC_V_PG[order(DE_G_CMC_V_PG$GENE_ID),]

DE_LN_CMC_V_PG$GENE_ID = row.names(DE_LN_CMC_V_PG)
DE_LN_CMC_V_PG = DE_LN_CMC_V_PG[order(DE_LN_CMC_V_PG$GENE_ID),]

DE_LN_CMC_V_G_CMC$GENE_ID = row.names(DE_LN_CMC_V_G_CMC)
DE_LN_CMC_V_G_CMC = DE_LN_CMC_V_G_CMC[order(DE_LN_CMC_V_G_CMC$GENE_ID),]

DE_LN_PG_V_G_PG$GENE_ID = row.names(DE_LN_PG_V_G_PG)
DE_LN_PG_V_G_PG = DE_LN_PG_V_G_PG[order(DE_LN_PG_V_G_PG$GENE_ID),]

DE_merged1 = merge(DE_G_CMC_V_PG, DE_LN_CMC_V_PG, by="GENE_ID", suffixes = c("_DE_G_CMC_V_PG", "_DE_LN_CMC_V_PG" ))
DE_merged2 = merge(DE_LN_CMC_V_G_CMC, DE_LN_PG_V_G_PG, by = "GENE_ID", suffixes = c("_DE_LN_CMC_V_G_CMC", "_DE_LN_PG_V_G_PG") )

DE_MERGED = merge(DE_merged1, DE_merged2, by = "GENE_ID")

MASTERTABLE = merge(DE_MERGED, norm_counts_annotated, by = "GENE_ID")

row.names(MASTERTABLE) = MASTERTABLE$SYMBOL

MASTERTABLE = na.omit(MASTERTABLE)


#add-log10p column

MASTERTABLE$mlog10p_DE_G_CMC_V_PG = -log(MASTERTABLE$p_DE_G_CMC_V_PG,10)
MASTERTABLE$mlog10p_DE_LN_CMC_V_PG = -log(MASTERTABLE$p_DE_LN_CMC_V_PG,10)
MASTERTABLE$mlog10p_DE_LN_CMC_V_G_CMC = -log(MASTERTABLE$p_DE_LN_CMC_V_G_CMC,10)
MASTERTABLE$mlog10p_DE_LN_PG_V_G_PG = -log(MASTERTABLE$p_DE_LN_PG_V_G_PG,10)

#Add a column for significance
MASTERTABLE$Sig_DE_G_CMC_V_PG = as.factor(MASTERTABLE$p.adj_DE_G_CMC_V_PG <0.05 & abs(MASTERTABLE$log2fold_DE_G_CMC_V_PG) > 1)
```

```
MASTERTABLE$Sig_DE_LN_CMC_V_PG = as.factor(MASTERTABLE$p.adj_DE_LN_CMC_V_PG <0.05 &
abs(MASTERTABLE$log2fold_DE_LN_CMC_V_PG) > 1)
MASTERTABLE$Sig_DE_LN_CMC_V_G_CMC = as.factor(MASTERTABLE$p.adj_DE_LN_CMC_V_G_CMC <0.05 &
abs(MASTERTABLE$log2fold_DE_LN_CMC_V_G_CMC) > 1)
MASTERTABLE$Sig_DE_LN_PG_V_G_PG = as.factor(MASTERTABLE$p.adj_DE_LN_PG_V_G_PG <0.05 &
abs(MASTERTABLE$log2fold_DE_LN_PG_V_G_PG) > 1)



#List the sig genes for each DE analysis

DE_sig_G_CMC_V_PG = subset(MASTERTABLE, p.adj_DE_G_CMC_V_PG  <0.05 & abs(log2fold_DE_G_CMC_V_PG) > 1)
DE_sig_LN_CMC_V_PG = subset(MASTERTABLE,p.adj_DE_LN_CMC_V_PG <0.05 & abs(log2fold_DE_LN_CMC_V_PG) > 1)
DE_sig_LN_CMC_V_G_CMC = subset(MASTERTABLE,p.adj_DE_LN_CMC_V_G_CMC <0.05 &
abs(log2fold_DE_LN_CMC_V_G_CMC) > 1)
DE_sig_LN_PG_V_G_PG = subset(MASTERTABLE,p.adj_DE_LN_PG_V_G_PG <0.05 & abs(log2fold_DE_LN_PG_V_G_PG) > 1)

Sig_Gene_Names_DE_sig_LN_CMC_V_G_CMC = row.names(DE_sig_LN_CMC_V_G_CMC )
Sig_Gene_Names_DE_sig_LN_PG_V_G_PG = row.names(DE_sig_LN_PG_V_G_PG)

#change the levels
MASTERTABLE$Sig_DE_G_CMC_V_PG = factor(MASTERTABLE$Sig_DE_G_CMC_V_PG, levels = c(TRUE, FALSE))
MASTERTABLE$Sig_DE_LN_CMC_V_PG = factor(MASTERTABLE$Sig_DE_LN_CMC_V_PG, levels = c(TRUE, FALSE))
MASTERTABLE$Sig_DE_LN_CMC_V_G_CMC = factor(MASTERTABLE$Sig_DE_LN_CMC_V_G_CMC, levels = c(TRUE, FALSE))
MASTERTABLE$Sig_DE_LN_PG_V_G_PG = factor(MASTERTABLE$Sig_DE_DE_LN_PG_V_G_PG, levels = c(TRUE, FALSE))

#Rename norm_counts_annotated to EM
EM = norm_counts_annotated


#Figure 1


##---- Theme ----##
theme_SL2 <- function () {
  theme_bw() %+replace%
    theme(
      panel.grid = element_blank(),
      panel.background = element_blank(),
      panel.border = element_rect(colour = "black", fill=NA, size=1),
      plot.background = element_blank(),
      legend.background = element_rect(fill="transparent", colour=NA),
      legend.key = element_rect(fill="transparent", colour=NA),
      plot.title = element_text(size=12, margin = margin(b = 5),hjust=0,vjust=0.5, family="Arial", face="bold"),
      title = element_text(size = 12, margin = margin(b = 5),hjust=0,vjust=0.5, family="Arial", face="bold"),
      axis.text.y = element_text(size = 23, margin = margin(r = 5),hjust=1,vjust=0.5, family="Arial",
face="bold",colour="black"),
      axis.text.x = element_text(size = 23, margin = margin(t = 5),hjust=0.5,vjust=1, family="Arial",
face="bold",colour="black"),
      axis.title.y = element_text(size = 26, margin = margin(r = 10),angle = 90,hjust=0.5,vjust=0.5, family="Arial",
face="bold"),
      axis.title.x = element_text(size = 26, margin = margin(t = 10),hjust=0.5,vjust=1, family="Arial", face="bold"),
      legend.text=element_text(size=23, family="Arial", face="bold"),
      legend.title=element_blank(),
      legend.key.size=unit(2.5,"line"),
      plot.margin=unit(c(0.4,0.4,0.4,0.4), "cm")
    )
}

theme_SL2_Volc <- function () {
  theme_bw() %+replace%
    theme(
      panel.grid = element_blank(),
      panel.background = element_blank(),
      panel.border = element_rect(colour = "black", fill=NA, size=1),
      plot.background = element_blank(),
      legend.position = "none",
      plot.title = element_text(size=12, margin = margin(b = 5),hjust=0,vjust=0.5, family="Arial", face="bold"),
      title = element_text(size = 12, margin = margin(b = 5),hjust=0,vjust=0.5, family="Arial", face="bold"),
      axis.text.y = element_text(size = 23, margin = margin(r = 5),hjust=1,vjust=0.5, family="Arial",
face="bold",colour="black"),
      axis.text.x = element_text(size = 23, margin = margin(t = 5),hjust=0.5,vjust=1, family="Arial",
face="bold",colour="black"),
      axis.title.y = element_text(size = 26, margin = margin(r = 10),angle = 90,hjust=0.5,vjust=0.5, family="Arial",
face="bold"),
      axis.title.x = element_text(size = 26, margin = margin(t = 10),hjust=0.5,vjust=1, family="Arial", face="bold"),
      plot.margin=unit(c(0.4,0.4,0.4,0.4), "cm")
    )
}
```

```
theme_SL2_MA <- function () {
  theme_bw() %+replace%
    theme(
      panel.grid = element_blank(),
      panel.background = element_blank(),
      panel.border = element_rect(colour = "black", fill=NA, size=1),
      plot.background = element_blank(),
      legend.position = "none",
      plot.title = element_text(size=12, margin = margin(b = 5),hjust=0,vjust=0.5, family="Arial", face="bold"),
      title = element_text(size = 12, margin = margin(b = 5),hjust=0,vjust=0.5, family="Arial", face="bold"),
      axis.text.y = element_text(size = 25, margin = margin(r = 5),hjust=1,vjust=0.5, family="Arial",
face="bold",colour="black"),
      axis.text.x = element_text(size = 25, margin = margin(t = 5),hjust=0.5,vjust=1, family="Arial",
face="bold",colour="black"),
      axis.title.y = element_text(size = 34, margin = margin(r = 10),angle = 90,hjust=0.5,vjust=0.5, family="Arial",
face="bold"),
      axis.title.x = element_text(size = 34, margin = margin(t = 10),hjust=0.5,vjust=1, family="Arial", face="bold"),
      plot.margin=unit(c(2,2,2,2), "cm")
    )
}



#pca

#Part 1

#KEEP ONLY EXPESSION VALUE COLUMNS

keep = c(2:13)

EM= EM[,keep]
#scale the EM

EM_scaled = scale(EM)

EM_scaled = data.frame(EM)
#make a numeric matrix
EMPCA = as.matrix(sapply(EM, as.numeric))


#Zscore PCA
as.matrix(sapply(EM_scaled, as.numeric))
pcaZscore= prcomp(t(EM_scaled))
pcaZscore_coordinates = data.frame(pcaZscore$x)


#add percentage to axis
percentage <- round(pcaZscore$sdev / sum(pcaZscore$sdev) * 100, 2)
percentage <- paste( colnames(pcaZscore_coordinates), "(", paste( as.character(percentage), "%", ")", sep="") )

#make plot
PCA_PC1_v_PC2_Z_Score = ggplot (pcaZscore_coordinates, aes (x = PC1, y = PC2, color=sample_group))+
  geom_point(size=10) +
  theme_SL2()+
  xlab(percentage[1]) + ylab(percentage[2])+
  scale_color_manual(values= c("darkorange","mediumpurple1","chartreuse2","deepskyblue2"))


#Volcano Plots

###LN_CMC_V_G_CMC###

master_up_LN_CMC_V_G_CMC = subset(MASTERTABLE,p.adj_DE_LN_CMC_V_G_CMC  < 0.05 &
log2fold_DE_LN_CMC_V_G_CMC > 1)

master_up_LN_CMC_V_G_CMC_sorted = master_up_LN_CMC_V_G_CMC
[order(master_up_LN_CMC_V_G_CMC$log2fold_DE_LN_CMC_V_G_CMC,decreasing = TRUE),]

master_up_LN_CMC_V_G_CMC_top5 = master_up_LN_CMC_V_G_CMC_sorted [1:5,]

master_down_LN_CMC_V_G_CMC = subset(MASTERTABLE,p.adj_DE_LN_CMC_V_G_CMC  < 0.05 &
log2fold_DE_LN_CMC_V_G_CMC < -1)

master_down_LN_CMC_V_G_CMC_sorted = master_down_LN_CMC_V_G_CMC
[order(master_down_LN_CMC_V_G_CMC$log2fold_DE_LN_CMC_V_G_CMC, decreasing = FALSE),]
```

```
master_down_LN_CMC_V_G_CMC_top5 = master_down_LN_CMC_V_G_CMC_sorted[1:5,]



#DE_LN_CMC_V_G_CMC
ggp_DE_LN_CMC_V_G_CMC_VOLC = ggplot (MASTERTABLE, aes (x = log2fold_DE_LN_CMC_V_G_CMC, y =
mlog10p_DE_LN_CMC_V_G_CMC, fill = Sig_DE_LN_CMC_V_G_CMC, colour= Sig_DE_LN_CMC_V_G_CMC))+
  geom_point(size = 2)+
  theme_SL2_Volc() + xlim(c(-5,6)) + ylim(c(0,100)) +
  labs(x = "log2fold change", y= "-log10 p-value")+
  scale_color_manual(values = c("red", "black"))

 #DE_LN_PG_V_G_PG
ggp_DE_LN_PG_V_G_PG_VOLC = ggplot (MASTERTABLE, aes (x = log2fold_DE_LN_PG_V_G_PG, y =
mlog10p_DE_LN_PG_V_G_PG, fill = Sig_DE_LN_PG_V_G_PG, colour= Sig_DE_LN_PG_V_G_PG))+
  geom_point(size = 2)+
  theme_SL2_Volc()+
  xlim(c(-8,10)) + ylim(c(0,100)) +
  labs(x = "log2fold change", y= "-log10 p-value")+
  scale_color_manual(values = c("black", "red"))

#DE_LN_CMC_V_LN_PG
ggp_DE_LN_CMC_V_LN_PG_VOLC = ggplot (MASTERTABLE, aes (x = log2fold_DE_LN_CMC_V_PG, y =
mlog10p_DE_LN_CMC_V_PG, fill = Sig_DE_LN_CMC_V_PG, colour= Sig_DE_LN_CMC_V_PG))+
  geom_point(size = 2)+
  theme_SL2_Volc() + xlim(c(-5,6)) + ylim(c(0,4)) +
  labs(x = "log2fold change", y= "-log10 p-value")+
  scale_color_manual(values = c("black", "red"))

#DE_G_CMC_V_G_PG
ggp_DE_G_CMC_V_G_PG_VOLC = ggplot (MASTERTABLE, aes (x = log2fold_DE_G_CMC_V_PG, y =
mlog10p_DE_G_CMC_V_PG, fill = Sig_DE_G_CMC_V_PG, colour= Sig_DE_G_CMC_V_PG))+
  geom_point(size = 2)+
  theme_SL2_Volc() + xlim(c(-6,5)) + ylim(c(0,5)) +
  labs(x = "log2fold change", y= "-log10 p-value")+
  scale_color_manual(values = c("black", "red"))

###MA_PLOT####

#Add mean expression

MASTERTABLE$Mean_Expression  = rowMeans(MASTERTABLE[,(18:29)])

 #MA Plots

#DE_LN_CMC_V_G_CMC
ggp_DE_LN_CMC_V_G_CMC_MA = ggplot (MASTERTABLE, aes ( x = Mean_Expression, y = log2fold_DE_LN_CMC_V_G_CMC,
fill = Sig_DE_LN_CMC_V_G_CMC, colour= Sig_DE_LN_CMC_V_G_CMC))+
  geom_point(size = 2)+
  theme_SL2_MA() + xlim(c(0,120000)) + ylim(c(-10,12)) +
  labs(x = "Mean Expression", y="log2fold change" )+
  scale_color_manual(values = c("black", "red"))

#DE_LN_PG_V_G_PG
ggp_DE_LN_PG_V_G_PG_MA = ggplot (MASTERTABLE, aes ( x = Mean_Expression, y = log2fold_DE_LN_PG_V_G_PG, fill =
Sig_DE_LN_PG_V_G_PG, colour= Sig_DE_LN_PG_V_G_PG))+
  geom_point(size = 2)+
  theme_SL2_MA() + xlim(c(0,120000)) + ylim(c(-10,12)) +
  labs(x = "Mean Expression", y="log2fold change" )+
  scale_color_manual(values = c("red", "black"))

#DE_LN_CMC_V_PG
ggp_DE_LN_CMC_V_PG_MA = ggplot (MASTERTABLE, aes ( x = Mean_Expression, y = log2fold_DE_LN_CMC_V_PG, fill =
Sig_DE_LN_CMC_V_PG, colour= Sig_DE_LN_CMC_V_PG))+
  geom_point(size = 2)+
  theme_SL2_MA() + xlim(c(0,120000)) + ylim(c(-6,5)) +
  labs(x = "Mean Expression", y="log2fold change" )+
  scale_color_manual(values = c("black", "red"))

#DE_G_CMC_V_PG
ggp_DE_G_CMC_V_PG_MA = ggplot (MASTERTABLE, aes ( x = Mean_Expression, y = log2fold_DE_G_CMC_V_PG, fill =
Sig_DE_G_CMC_V_PG, colour= Sig_DE_G_CMC_V_PG))+
  geom_point(size = 2)+
  theme_SL2_MA() + xlim(c(0,115000)) + ylim(c(-6,5)) +
  labs(x = "Mean Expression", y="log2fold change" )+
  scale_color_manual(values = c("black", "red"))
```

```
#Bar chart of Differentially Expressed genes

####THEME####
theme_SL2_bar <- function () {
  theme_bw() %+replace%
    theme(
      panel.grid = element_blank(),
      panel.background = element_blank(),
      panel.border = element_rect(colour = "black", fill=NA, size=1),
      plot.background = element_blank(),
      legend.position = "none",
      plot.title = element_text(size=12, margin = margin(b = 5),hjust=0,vjust=0.5, family="Arial", face="bold"),
      title = element_text(size = 12, margin = margin(b = 5),hjust=0,vjust=0.5, family="Arial", face="bold"),
      axis.text.y = element_text(size = 23, margin = margin(r = 5),hjust=1,vjust=0.5, family="Arial",
face="bold",colour="black"),
      axis.text.x = element_text(size = 23, margin = margin(r = 5),hjust=1, angle = 45, vjust=1, family="Arial",
face="bold",colour="black"),
      axis.title.y = element_text(size = 26, margin = margin(r = 10),angle = 90,hjust=0.5,vjust=0.5, family="Arial",
face="bold"),
      axis.title.x = element_blank(),
      plot.margin=unit(c(0.4,0.4,0.4,0.4), "cm")
    )
}


Diff_exp_genes = data.frame(nrow(DE_sig_LN_CMC_V_PG),nrow(DE_sig_G_CMC_V_PG), nrow(DE_sig_LN_CMC_V_G_CMC),
nrow(DE_sig_LN_PG_V_G_PG))


row.names(Diff_exp_genes)[1] = "Number_of_Differentially_Expressed_Gene"
New_names = c("LN_CMC_V_LN_PG", "G_CMC_V_G_PG", "LN_CMC_V_G_CMC", "LN_PG_V_G_PG")

colnames(Diff_exp_genes) = New_names


Diff_exp_genes = data.frame(Diff_exp_genes)

gene_data.m = melt(Diff_exp_genes)

names(gene_data.m) = c("Comparison", "Number_of_Differentially_Expressed_Genes")


ggp_Diff_exp_genes = ggplot(gene_data.m, aes(x= Comparison, y=Number_of_Differentially_Expressed_Genes, fill =
Comparison)) +
  theme_SL2_bar()+
  geom_col()+
  scale_fill_manual(values= c("darkorange","mediumpurple1","chartreuse2","deepskyblue2"))+
  scale_color_manual(values = "black")+
  ylab("Number of Differentially Expressed Genes")+
  ylim(c(0,1750))


#Column of significantly up and down regulated genes LN_CMC_V_G_CMC


####THEME#####
theme_SL2_bar_2 <- function () {
  theme_bw() %+replace%
    theme(
      panel.grid = element_blank(),
      panel.background = element_blank(),
      panel.border = element_rect(colour = "black", fill=NA, size=1),
      plot.background = element_blank(),
      legend.background = element_rect(fill="transparent", colour=NA),
      legend.key = element_rect(fill="transparent", colour=NA),
      plot.title = element_text(size=12, margin = margin(b = 5),hjust=0,vjust=0.5, family="Arial", face="bold"),
      title = element_text(size = 12, margin = margin(b = 5),hjust=0,vjust=0.5, family="Arial", face="bold"),
      axis.text.y = element_text(size = 23, margin = margin(r = 5),hjust=1,vjust=0.5, family="Arial",
face="bold",colour="black"),
      axis.text.x = element_blank(),
      axis.title.y = element_text(size = 26, margin = margin(r = 10),angle = 90,hjust=0.5,vjust=0.5, family="Arial",
face="bold"),
      axis.title.x = element_text(size = 26, margin = margin(t = 10),hjust=0.5,vjust=1, family="Arial", face="bold"),
      legend.text=element_text(size=23, family="Arial", face="bold"),
      legend.title=element_blank(),
      legend.key.size=unit(2.5,"line"),
      plot.margin=unit(c(0.4,0.4,0.4,0.4), "cm")
    )
}
```

```
DE_sig_UP_LN_CMC_V_G_CMC = subset(MASTERTABLE,p.adj_DE_LN_CMC_V_G_CMC <0.05 &
log2fold_DE_LN_CMC_V_G_CMC > 1)
DE_sig_DOWN_LN_CMC_V_G_CMC = subset(MASTERTABLE,p.adj_DE_LN_CMC_V_G_CMC <0.05 &
log2fold_DE_LN_CMC_V_G_CMC < -1)

Diff_CMC_up = nrow(DE_sig_UP_LN_CMC_V_G_CMC)
Diff_CMC_down = nrow(DE_sig_DOWN_LN_CMC_V_G_CMC)

CMC_Diff = merge(Diff_CMC_up, Diff_CMC_down)
names = c( "Up Regulated Genes", "Down Regulated Genes")
colnames(CMC_Diff) = names
row.names(CMC_Diff) = "Number of Genes"


gene_data.m = melt(CMC_Diff)

ggp_CMC_Diff= ggplot(gene_data.m, aes(x= variable, y=value, fill = variable)) +
  theme_SL2_bar()+
  geom_col()+
  scale_fill_manual(values= c("darkorange","mediumpurple1"))+
  scale_color_manual(values = "black")+
  ylab("Number of Genes")+
  ylim(c(0,1400))+
  xlab("G_V_LN_CMC")


#Column of significantly up and down regulated genes LN_PG_V_G_PG
DE_sig_UP_LN_PG_V_G_PG = subset(MASTERTABLE,p.adj_DE_LN_PG_V_G_PG <0.05 & log2fold_DE_LN_PG_V_G_PG > 1)
DE_sig_DOWN_LN_PG_V_G_PG = subset(MASTERTABLE,p.adj_DE_LN_PG_V_G_PG <0.05 & log2fold_DE_LN_PG_V_G_PG < -
1)

Diff_PG_up = nrow(DE_sig_UP_LN_PG_V_G_PG)
Diff_PG_down = nrow(DE_sig_DOWN_LN_PG_V_G_PG)

PG_Diff = merge(Diff_PG_up, Diff_PG_down)
names = c( "Up Regulated Genes", "Down Regulated Genes")
colnames(PG_Diff) = names
row.names(PG_Diff) = "Number of Genes"

gene_data.m = melt(PG_Diff)

 ggp_PG_Diff= ggplot(gene_data.m, aes(x= variable, y=value, fill = variable)) +
  theme_SL2_bar()+
  geom_col()+
  scale_fill_manual(values= c("darkorange","mediumpurple1"))+
  scale_color_manual(values = "black")+
  ylim(c(0,1400))+
  ylab("Number of Genes")+
  xlab("G_V_LN_PG")


#Venn Diagram Data

DE_sig_LN_CMC_V_G_CMC_ONLY = subset(MASTERTABLE, Sig_DE_LN_CMC_V_G_CMC == TRUE & Sig_DE_LN_PG_V_G_PG ==
FALSE)
DE_sig_LN_PG_V_G_PG_ONLY = subset(MASTERTABLE, Sig_DE_LN_PG_V_G_PG == TRUE & Sig_DE_LN_CMC_V_G_CMC ==
FALSE)
DE_sig_overlap = subset(MASTERTABLE, Sig_DE_LN_CMC_V_G_CMC == TRUE & Sig_DE_LN_PG_V_G_PG == TRUE)
DE_genes_LN_V_G = subset(MASTERTABLE, Sig_DE_LN_CMC_V_G_CMC == TRUE | Sig_DE_LN_PG_V_G_PG == TRUE)

#Heatmaps

#theme

theme_SL2_HM <- function () {
  theme_bw() %+replace%
    theme(
      panel.grid = element_blank(),
      panel.background = element_blank(),
      panel.border = element_rect(colour = "black", fill=NA, size=1),
      plot.background = element_blank(),
      legend.background = element_rect(fill="transparent", colour=NA),
      legend.key = element_rect(fill="transparent", colour=NA),
      plot.title = element_text(size=12, margin = margin(b = 5),hjust=0,vjust=0.5, family="Arial", face="bold"),
      title = element_text(size = 12, margin = margin(b = 5),hjust=0,vjust=0.5, family="Arial", face="bold"),
      axis.text.y = element_blank(),
      axis.text.x = element_blank(),
```

```
    axis.title.y = element_text(size = 24, margin = margin(r = 10),angle = 90,hjust=0.5,vjust=0.5, family="Arial",
face="bold"),
    axis.title.x = element_blank(),
    legend.text=element_text(size=18, family="Arial", face="bold"),
    legend.title=element_blank(),
    legend.key.size=unit(2.5,"line"),
    plot.margin=unit(c(0.4,0.4,0.4,0.4), "cm")
   )
}

 # get an expression table of all sig genes
sig_all = subset(MASTERTABLE, Sig_DE_LN_CMC_V_G_CMC == TRUE | Sig_DE_LN_PG_V_G_PG == TRUE)
keep = c(18:29)
sig_all_expression = sig_all[,keep]


data.s = data.frame(t(scale(t(sig_all_expression))))
hm.matrix = as.matrix(data.s)

hm.matrix = na.omit(hm.matrix)

y.dist = Dist(hm.matrix, method="spearman")
y.cluster = hclust(y.dist, method="average")
y.dd = as.dendrogram(y.cluster)
y.dd.reorder = reorder(y.dd,0,FUN="average")
y.order = order.dendrogram(y.dd.reorder)
hm.matrix_clustered = hm.matrix[y.order,]

hm.matrix_clustered = melt(hm.matrix_clustered)

ggp_HM_sig_Genes = ggplot(hm.matrix_clustered, aes(x=Var2, y=Var1, fill=value)) +
  geom_tile(linetype="blank") +
  scale_fill_viridis() +
  theme_SL2_HM()+
  labs(x="Sample",y="Gene")

#group rug
group_rug = as.matrix(as.numeric(sample_data$sample_group))
group_rug = melt(group_rug)
colours = c("darkorange","mediumpurple1","chartreuse2","deepskyblue2")
hm.palette= colorRampPalette(colours)
ggp_HM_group_rug = ggplot(group_rug, aes(x=X1, y=X2, fill=value))+
  geom_tile(linetype="blank")+
  ylab('') +
  xlab('') +
  theme(axis.text.x = element_blank(),axis.text.y = element_blank(), axis.ticks=element_blank(), legend.position =
"none") +
  scale_x_discrete(expand=c(0,0)) +
  scale_y_discrete(expand=c(0,0)) +
  scale_fill_gradientn(colours = hm.palette(100))

 #Correlation Scatter plot

ggp_fold_v_fold_change = ggplot(MASTERTABLE, aes(x=log2fold_DE_LN_CMC_V_G_CMC, y=log2fold_DE_LN_PG_V_G_PG))
+
  geom_point()+
  theme_SL2_Volc()+
  xlim(c(-5,10))+
  ylim(c(-5,10))+
  labs( x = "Log2fold change LN_CMC_V_G_CMC", y = "Log2fold change LN_PG_V_G_PG")


cor.test(MASTERTABLE$log2fold_DE_LN_CMC_V_G_CMC, MASTERTABLE$log2fold_DE_LN_PG_V_G_PG, method =
"spearman")


#pathway analysis

#Make a vector of all sig genes that overlap

sig_genes_overlap = row.names(DE_sig_overlap)
sig_genes_LN_CMC_v_G_CMC = row.names(DE_sig_LN_CMC_V_G_CMC)
sig_genes_LN_PG_v_G_PG = row.names(DE_sig_LN_PG_V_G_PG)
sig_genes_LN_CMC_v_G_CMC_ONLY = row.names(DE_sig_LN_CMC_V_G_CMC_ONLY)
sig_genes_LN_PG_v_G_PG_ONLY = row.names(DE_sig_LN_PG_V_G_PG_ONLY)
sig_genes_ALL_DIFF = row.names(DE_genes_LN_V_G)

#change ID to entrez
```

```
sig_genes_overlap_entrez = bitr(sig_genes_overlap, fromType = "SYMBOL", toType = c("ENTREZID"), OrgDb =
org.Mm.eg.db)


sig_genes_ALL_DIFF_entrez = bitr(sig_genes_ALL_DIFF, fromType = "SYMBOL", toType = c("ENTREZID"), OrgDb =
org.Mm.eg.db)

#ORA Analysis

go_enrich_overlap = enrichGO(gene = sig_genes_overlap_entrez$ENTREZID, OrgDb = org.Mm.eg.db,readable = T, ont =
"BP", pvalueCutoff = 0.05, qvalueCutoff = 0.10)

go_enrich_ALL_DIFF = enrichGO(gene = sig_genes_ALL_DIFF_entrez$ENTREZID, OrgDb = org.Mm.eg.db,readable = T, ont =
"BP", pvalueCutoff = 0.05, qvalueCutoff = 0.10)
###THEME###

theme_SL2_GENE_SET <- function () {
  theme_bw() %+replace%
    theme(
      panel.grid = element_blank(),
      panel.background = element_blank(),
      panel.border = element_rect(colour = "black", fill=NA, size=1),
      plot.background = element_blank(),
      legend.background = element_rect(fill="transparent", colour=NA),
      legend.key = element_rect(fill="transparent", colour=NA),
      plot.title = element_text(size=12, margin = margin(b = 5),hjust=0,vjust=0.5, family="Arial", face="bold"),
      title = element_text(size = 12, margin = margin(b = 5),hjust=0,vjust=0.5, family="Arial", face="bold"),
      axis.text.y = element_text(size = 15, margin = margin(r = 5),hjust=1,vjust=0.5, family="Arial",
face="bold",colour="black"),
      axis.text.x = element_text(size = 15, margin = margin(t = 5),hjust=0.5,vjust=1, family="Arial",
face="bold",colour="black"),
      axis.title.y = element_text(size = 26, margin = margin(r = 10),angle = 90,hjust=0.5,vjust=0.5, family="Arial",
face="bold"),
      axis.title.x = element_text(size = 26, margin = margin(t = 10),hjust=0.5,vjust=1, family="Arial", face="bold"),
      legend.text=element_text(size=23, family="Arial", face="bold"),
      legend.title=element_text(size = 26, margin = margin(t = 10),hjust=0.5,vjust=1, family="Arial", face="bold"),
      legend.key.size=unit(2.5,"line"),
      plot.margin=unit(c(0.4,0.4,0.4,0.4), "cm")
    )
}
ggp_bar_overlap_ORA = barplot(go_enrich_overlap, showCategory = 10)+
  theme_SL2_GENE_SET()+
  labs( x = "Number of Differentially Expressed Genes", y = "Gene Set")

ggp_bar_ALL_DIFF_ORA = barplot(go_enrich_ALL_DIFF, showCategory = 10)+
  theme_SL2_GENE_SET()+
  labs( x = "Number of Differentially Expressed Genes", y = "Gene Set")



#heatmap of regulation of protein/serine/threonine kinase activity

#get the gene set list for overlap

gene_sets = go_enrich_overlap$geneID
description = go_enrich_overlap$Description
p.adj = go_enrich_overlap$p.adjust
ora_overlap_results =data.frame( cbind(gene_sets,description,p.adj) )

results_top_overlap = as.character(ora_overlap_results[1,1])
regulation_of_cell_cell_adhesion_genes = unlist(strsplit(results_top_overlap,"/"))

#get gene list for ALL DIFF ORA
gene_sets_2 = go_enrich_ALL_DIFF$geneID
description_2 = go_enrich_ALL_DIFF$Description
p.adj_2 = go_enrich_ALL_DIFF$p.adjust
ora_ALL_DIFF_results =data.frame( cbind(gene_sets_2,description_2,p.adj_2) )

results_top_ALL_DIFF = as.character(ora_ALL_DIFF_results[1,1])
reg_of_protein_serine_threonine_kinas_activity_genes = unlist(strsplit(results_top_ALL_DIFF,"/"))



###THEME####

theme_SL2_HM_2 <- function () {
  theme_bw() %+replace%
    theme(
      panel.grid = element_blank(),
```

```
      panel.background = element_blank(),
      panel.border = element_rect(colour = "black", fill=NA, size=1),
      plot.background = element_blank(),
      legend.background = element_rect(fill="transparent", colour=NA),
      legend.key = element_rect(fill="transparent", colour=NA),
      plot.title = element_text(size=12, margin = margin(b = 5),hjust=0,vjust=0.5, family="Arial", face="bold"),
      title = element_text(size = 12, margin = margin(b = 5),hjust=0,vjust=0.5, family="Arial", face="bold"),
      axis.text.y = element_text(size = 14, margin = margin(r = 5),hjust=1,vjust=0.5, family="Arial",
face="bold",colour="black"),
      axis.text.x = element_blank(),
      axis.title.y = element_text(size = 20, margin = margin(r = 10),angle = 90,hjust=0.5,vjust=0.5, family="Arial",
face="bold"),
      axis.title.x = element_blank(),
      legend.text=element_text(size=12, family="Arial", face="bold"),
      legend.title=element_blank(),
      legend.key.size=unit(2.5,"line"),
      plot.margin=unit(c(0.4,0.4,0.4,0.4), "cm")
    )
}

 #HM_OVERLAP
HM_OVERLAP = MASTERTABLE[regulation_of_cell_cell_adhesion_genes,]

keep=c(18:29)

HM_OVERLAP = HM_OVERLAP[,keep]

data.s = data.frame(t(scale(t(HM_OVERLAP))))
hm.matrix = as.matrix(data.s)


y.dist = Dist(hm.matrix, method="spearman")
y.cluster = hclust(y.dist, method="average")
y.dd = as.dendrogram(y.cluster)
y.dd.reorder = reorder(y.dd,0,FUN="average")
y.order = order.dendrogram(y.dd.reorder)
hm.matrix_clustered = hm.matrix[y.order,]


hm.matrix_clustered = melt(hm.matrix_clustered)


ggp_HM_OVERLAP = ggplot(hm.matrix_clustered, aes(x=Var2, y=Var1, fill=value)) +
  geom_tile(linetype="blank") +
  scale_fill_viridis() +
  theme_SL2_HM_2()+
  labs(x="Sample",y="Gene")


#heatmap of ALL_DIFF

HM_ALL_DIFF= MASTERTABLE[reg_of_protein_serine_threonine_kinas_activity_genes,]

keep=c(18:29)
HM_ALL_DIFF = HM_ALL_DIFF[,keep]

data.s = data.frame(t(scale(t(HM_ALL_DIFF))))
hm.matrix = as.matrix(data.s)


y.dist = Dist(hm.matrix, method="spearman")
y.cluster = hclust(y.dist, method="average")
y.dd = as.dendrogram(y.cluster)
y.dd.reorder = reorder(y.dd,0,FUN="average")
y.order = order.dendrogram(y.dd.reorder)
hm.matrix_clustered = hm.matrix[y.order,]


hm.matrix_clustered = melt(hm.matrix_clustered)


ggp_HM_ALL_DIFF = ggplot(hm.matrix_clustered, aes(x=Var2, y=Var1, fill=value)) +
  geom_tile(linetype="blank") +
  scale_fill_viridis() +
  theme_SL2_HM_2()+
  labs(x="Sample",y="Gene")


#Make a Gene Set Boxplot of overlap
```

```
#overlap
 gene_sets = go_enrich_overlap$geneID
description = go_enrich_overlap$Description
p.adj = go_enrich_overlap$p.adjust
ora_overlap_results =data.frame( cbind(gene_sets,description,p.adj) )

 keep = c(11,15)
Diff_Expression_Values = DE_genes_LN_V_G[,keep]

samples_1 = c("DE_LN_CMC_V_G_CMC","DE_LN_PG_V_CMC")

samples_1 = data.frame(samples_1)

Diff_Expression_Values_regulation_of_cell_cell_adhesion_genes =
Diff_Expression_Values[regulation_of_cell_cell_adhesion_genes,]
gene_data = Diff_Expression_Values_regulation_of_cell_cell_adhesion_genes
gene_data = data.frame(t(gene_data))
gene_data$sample_group = samples_1$samples_1

gene_data.m = melt(gene_data)

  names(gene_data.m) = c("Comparison", "Gene", "log2fold")

 ggp_overlap_box_plot = ggplot(gene_data.m,aes(x=Gene,y=log2fold, fill=Comparison)) +
  geom_col(position = "dodge", colour="black")+
  theme(panel.background = element_blank(),axis.text.x = element_text(size=10,angle=90, hjust=0, vjust=0),
panel.border=element_rect(fill=NA),  axis.title.x = element_text(size = 18, margin = margin(r = 10),hjust=0.5,vjust=0.5,
angle=0, family="Arial", face="bold"), axis.title.y = element_text(size = 18, margin = margin(r = 10),hjust=0.5,vjust=0.5,
family="Arial", face="bold"), legend.position = "none")+
  labs(x = "Gene", y="log2fold change")+
  scale_fill_manual(values= c("chartreuse2","deepskyblue2"))



#all diff
Diff_Expression_Values_regulation_of_protein_genes =
Diff_Expression_Values[reg_of_protein_serine_threonine_kinas_activity_genes,]
gene_data = Diff_Expression_Values_regulation_of_protein_genes
gene_data = data.frame(t(gene_data))
gene_data$sample_group = samples_1$samples_1

gene_data.m = melt(gene_data)


names(gene_data.m) = c("Comparison", "Gene", "log2fold")


ggp_ALL_DIFF_box_plot = ggplot(gene_data.m,aes(x=Gene,y=log2fold, fill=Comparison)) +
  geom_col(position = "dodge", colour="black")+
  theme(panel.background = element_blank(),axis.text.x = element_text(size=10,angle=90, hjust=0, vjust=0),
panel.border=element_rect(fill=NA),  axis.title.x = element_text(size = 18, margin = margin(r = 10),hjust=0.5,vjust=0.5,
angle=0, family="Arial", face="bold"), axis.title.y = element_text(size = 18, margin = margin(r = 10),hjust=0.5,vjust=0.5,
family="Arial", face="bold"), legend.position = "none")+
  labs(x = "Gene", y="log2fold change")+
  scale_fill_manual(values= c("chartreuse2","deepskyblue2"))

#Highest Expressed Transcripts LN_PG
keep= c(1:3)
LN_PG_ALL_TRANSCRIPTS = EM[,keep]
LN_PG_ALL_TRANSCRIPTS$Mean = rowMeans(LN_PG_ALL_TRANSCRIPTS)

LN_PG_ALL_TRANSCRIPTS = LN_PG_ALL_TRANSCRIPTS[order(LN_PG_ALL_TRANSCRIPTS$Mean, decreasing = TRUE),]

LN_PG_TOP_10 = head(LN_PG_ALL_TRANSCRIPTS, 10)
write.table(LN_PG_TOP_10, file="TOP EXPRESSED GENES/LN_PG_TOP_10.csv", sep="\t")

#Highest Expressed Transcripts LN_CMC
keep= c(4:6)
LN_CMC_ALL_TRANSCRIPTS = EM[,keep]
LN_CMC_ALL_TRANSCRIPTS$Mean = rowMeans(LN_CMC_ALL_TRANSCRIPTS)

LN_CMC_ALL_TRANSCRIPTS = LN_CMC_ALL_TRANSCRIPTS[order(LN_CMC_ALL_TRANSCRIPTS$Mean, decreasing = TRUE),]

LN_CMC_TOP_10 = head(LN_CMC_ALL_TRANSCRIPTS, 10)
write.table(LN_CMC_TOP_10, file="TOP EXPRESSED GENES/LN_CMC_TOP_10.csv", sep="\t")

#Highest Expressed Transcripts G_PG
keep= c(10:12)
```

```
G_PG_ALL_TRANSCRIPTS = EM[,keep]
G_PG_ALL_TRANSCRIPTS$Mean = rowMeans(G_PG_ALL_TRANSCRIPTS)

G_PG_ALL_TRANSCRIPTS = G_PG_ALL_TRANSCRIPTS[order(G_PG_ALL_TRANSCRIPTS$Mean, decreasing = TRUE),]

G_PG_TOP_10 = head(G_PG_ALL_TRANSCRIPTS, 10)
write.table(G_PG_TOP_10, file="TOP EXPRESSED GENES/G_PG_TOP_10.csv", sep="\t")

#Highest Expressed Transcripts G_CMC
keep= c(7:9)
G_CMC_ALL_TRANSCRIPTS = EM[,keep]
G_CMC_ALL_TRANSCRIPTS$Mean = rowMeans(G_CMC_ALL_TRANSCRIPTS)

G_CMC_ALL_TRANSCRIPTS = G_CMC_ALL_TRANSCRIPTS[order(G_CMC_ALL_TRANSCRIPTS$Mean, decreasing = TRUE),]

G_CMC_TOP_10 = head(G_CMC_ALL_TRANSCRIPTS, 10)
write.table(G_CMC_TOP_10, file="TOP EXPRESSED GENES/G_CMC_TOP_10.csv", sep="\t")

#Most deferentially expressed genes G v LN CMC(which are significant)

DE_sig_LN_CMC_V_G_CMC = DE_sig_LN_CMC_V_G_CMC[order(
abs(DE_sig_LN_CMC_V_G_CMC$log2fold_DE_LN_CMC_V_G_CMC), decreasing = TRUE),]

DE_sig_LN_CMC_V_G_CMC_top_10_diff_exp_Genes = head(DE_sig_LN_CMC_V_G_CMC,10)
keep=c(13:16)
DE_sig_LN_CMC_V_G_CMC_top_10_diff_exp_Genes= DE_sig_LN_CMC_V_G_CMC_top_10_diff_exp_Genes[,keep]
DE_sig_LN_CMC_V_G_CMC_top_10_diff_exp_Genes =
DE_sig_LN_CMC_V_G_CMC_top_10_diff_exp_Genes[order(abs(DE_sig_LN_CMC_V_G_CMC_top_10_diff_exp_Genes$log2fold
_DE_LN_PG_V_G_PG), decreasing = TRUE),]
write.table(DE_sig_LN_CMC_V_G_CMC_top_10_diff_exp_Genes, file="Thesis_Figures/Top_10_diff_expressed_genes.csv",
sep="\t")

#Most differentially expressed genes G v LN pg(which are significant)
DE_sig_LN_PG_V_G_PG = DE_sig_LN_PG_V_G_PG[order( abs(DE_sig_LN_PG_V_G_PG$log2fold_DE_LN_PG_V_G_PG),
decreasing = TRUE),]

DE_sig_LN_PG_V_G_PG_top_10_diff_exp_Genes = head(DE_sig_LN_PG_V_G_PG,10)
keep=c(15:17)
DE_sig_LN_PG_V_G_PG_top_10_diff_exp_Genes= DE_sig_LN_PG_V_G_PG_top_10_diff_exp_Genes[,keep]
DE_sig_LN_PG_V_G_PG_top_10_diff_exp_Genes =
DE_sig_LN_PG_V_G_PG_top_10_diff_exp_Genes[order(abs(DE_sig_LN_PG_V_G_PG_top_10_diff_exp_Genes$log2fold_DE_L
N_PG_V_G_PG), decreasing = TRUE),]

write.table(DE_sig_LN_PG_V_G_PG_top_10_diff_exp_Genes,
file="Thesis_Figures//DE_sig_LN_PG_V_G_PG_top_10_diff_exp_Genes.csv", sep="\t")

 #expression density plots

ggp_Exp_Dens_LN_PG_3 = ggplot (MASTERTABLE, aes (x = log10(LN_PG_3)))+
  theme_SL2_Volc()+
  geom_density(fill="red")+
  labs(title ="Expression Density Plot LN PG 3", x = "Expression(log10)", y= "Density")

ggp_Exp_Dens_LN_PG_4 = ggplot (MASTERTABLE, aes (x = log10(LN_PG_4)))+
  geom_density(fill="red")+
  labs(title ="Expression Density Plot LN PG 4", x = "Expression(log10)")

ggp_Exp_Dens_LN_PG_5 = ggplot (MASTERTABLE, aes (x = log10(LN_PG_5)))+
  geom_density(fill="red")+
  labs(title ="Expression Density Plot LN PG 5", x = "Expression(log10)")

ggp_Exp_Dens_LN_CMC_3 = ggplot (MASTERTABLE, aes (x = log10(LN_CMC_3)))+
  geom_density(fill="red")+
  labs(title ="Expression Density Plot LN CMC 3", x = "Expression(log10)")

ggp_Exp_Dens_LN_CMC_4 = ggplot (MASTERTABLE, aes (x = log10(LN_CMC_4)))+
  geom_density(fill="red")+
  labs(title ="Expression Density Plot LN CMC 4", x = "Expression(log10)")

ggp_Exp_Dens_LN_CMC_5 = ggplot (MASTERTABLE, aes (x = log10(LN_CMC_5)))+
  geom_density(fill="red")+
  labs(title ="Expression Density Plot LN CMC 5", x = "Expression(log10)")

ggp_Exp_Dens_G_PG_3 = ggplot (MASTERTABLE, aes (x = log10(G_PG_3)))+
  geom_density(fill="red")+
  labs(title ="Expression Density Plot G PG 3", x = "Expression(log10)")

ggp_Exp_Dens_G_PG_4 = ggplot (MASTERTABLE, aes (x = log10(G_PG_4)))+
  geom_density(fill="red")+
```

```
  labs(title ="Expression Density Plot G PG 4", x = "Expression(log10)")

ggp_Exp_Dens_G_PG_5 = ggplot (MASTERTABLE, aes (x = log10(G_PG_5)))+
  geom_density(fill="red")+
  labs(title ="Expression Density Plot G PG 5", x = "Expression(log10)")

ggp_Exp_Dens_G_CMC_3 = ggplot (MASTERTABLE, aes (x = log10(G_CMC_3)))+
  geom_density(fill="red")+
  labs(title ="Expression Density Plot G CMC 3", x = "Expression(log10)")

ggp_Exp_Dens_G_CMC_4 = ggplot (MASTERTABLE, aes (x = log10(G_CMC_4)))+
  geom_density(fill="red")+
  labs(title ="Expression Density Plot G CMC 4", x = "Expression(log10)")

ggp_Exp_Dens_G_CMC_5 = ggplot (MASTERTABLE, aes (x = log10(G_CMC_5)))+
  geom_density(fill="red")+
  labs(title ="Expression Density Plot G CMC 5", x = "Expression(log10)")

#Chemokine Receptor Analysis

#All Chemokine receptor analysis
Chemokine_Receptors = c("Ccr1", "Ccr2","Ccr3","Ccr4","Ccr5","Ccr6", "Ccr7", "Ccr8", "Ccr9", "Ccr10", "Ackr4", "Ccrl2",
"Ackr2", "Xcr1", "Cx3cr1", "Cxcr1", "Cxcr2", "Cxcr3", "Cxcr4", "Cxcr5", "Cxcr6", "Ackr3", "Ackr")


#All_chemokine_receptor_Heatmap
Chemokine_Receptors_EM_Scaled= EM_scaled[Chemokine_Receptors,]

Chemokine_Receptors_EM_Scaled= na.omit(Chemokine_Receptors_EM_Scaled)

gene_data = Chemokine_Receptors_EM_Scaled

data.s = data.frame(t(scale(t(gene_data))))
hm.matrix = as.matrix(data.s)

y.dist = Dist(hm.matrix, method="spearman")
y.cluster = hclust(y.dist, method="average")
y.dd = as.dendrogram(y.cluster)
y.dd.reorder = reorder(y.dd,0,FUN="average")
y.order = order.dendrogram(y.dd.reorder)
hm.matrix_clustered = hm.matrix[y.order,]

hm.matrix_clustered = melt(hm.matrix_clustered)

ggp_HM_All_Chemokine_Receptors = ggplot(hm.matrix_clustered, aes(x=Var2, y=Var1, fill=value)) +
  geom_tile(linetype="blank") +
  scale_fill_viridis() +
  theme_SL2_HM_2()+
  labs(x="Sample",y="Gene")

#Significant chemokine receptor bar chart, overlap

DE_G_V_LN_Chemokine_Receptors = EM_scaled[sig_genes_ALL_DIFF,]

DE_G_V_LN_Chemokine_Receptors = DE_G_V_LN_Chemokine_Receptors[Chemokine_Receptors,]

DE_G_V_LN_Chemokine_Receptors = na.omit(DE_G_V_LN_Chemokine_Receptors)

keep = c(1,2,3,4,6,7,8,9,10,11,12)

DE_G_V_LN_Chemokine_Receptors = DE_G_V_LN_Chemokine_Receptors[keep,]


gene_data = DE_G_V_LN_Chemokine_Receptors
gene_data = data.frame(t(gene_data))
gene_data$sample_group = Sample_Sheet$Sample_Group

gene_data.m = melt(gene_data)
names(gene_data.m) = c("Sample_Group", "Gene", "Expression")


data_summary <- function(data, varname, groupnames){
  require(plyr)
  summary_func <- function(x, col){
    c(mean = mean(x[[col]], na.rm=TRUE),
      sd = sd(x[[col]], na.rm=TRUE))
  }
  data_sum<-ddply(data, groupnames, .fun=summary_func,
                  varname)
```

```
  data_sum <- rename(data_sum, c("mean" = varname))
  return(data_sum)
}

df2 = data_summary(gene_data.m, varname = "Expression", groupnames = c("Sample_Group", "Gene"))
df2$Gene = as.factor(df2$Gene)

df2$Gene = factor(df2$Gene, levels = c("Ackr2", "Ackr3", "Ackr4", "Ccr1", "Ccr2", "Ccr3", "Ccr4", "Ccr5", "Ccr6", "Ccr7",
"Ccr8", "Ccr9", "Ccr10", "Ccrl2", "Cxcr1", "Cxcr3", "Cxcr4", "Cxcr5", "Cxcr6", "Xcr1", "Cx3cr1"),labels = c("Ackr2", "Ackr3",
"Ackr4", "Ccr1", "Ccr2", "Ccr3", "Ccr4", "Ccr5", "Ccr6", "Ccr7", "Ccr8", "Ccr9", "Ccr10", "Ccrl2", "Cxcr1", "Cxcr3", "Cxcr4",
"Cxcr5", "Cxcr6", "Xcr1", "Cx3cr1"))
df2$Sample_Group = factor(df2$Sample_Group, levels = c("LN_CMC", "LN_PG", "G_CMC", "G_PG"),labels =
c("LN_CMC","LN_PG", "G_CMC","G_PG"))



####THEME####
theme_SL2_bar_4 <- function () {
  theme_bw() %+replace%
    theme(
      panel.grid = element_blank(),
      panel.background = element_blank(),
      panel.border = element_rect(colour = "black", fill=NA, size=1),
      plot.background = element_blank(),
      legend.background = element_rect(fill="transparent", colour=NA),
      legend.key = element_rect(fill="transparent", colour=NA),
      plot.title = element_text(size=12, margin = margin(b = 5),hjust=0,vjust=0.5, family="Arial", face="bold"),
      title = element_text(size = 12, margin = margin(b = 5),hjust=0,vjust=0.5, family="Arial", face="bold"),
      axis.text.y = element_text(size = 14, margin = margin(r = 5),hjust=1,vjust=0.5, family="Arial",
face="bold",colour="black"),
      axis.text.x = element_text(size = 16, family="Arial", face="bold",colour="black"),
      axis.title.y = element_text(size = 20, margin = margin(r = 10),angle = 90,hjust=0.5,vjust=0.5, family="Arial",
face="bold"),
      axis.title.x = element_text(size = 20, margin = margin(t = 10),hjust=0.5,vjust=1, family="Arial", face="bold"),
      legend.text=element_text(size=23, family="Arial", face="bold"),
      legend.title=element_blank(),
      legend.key.size=unit(2.5,"line"),
      plot.margin=unit(c(0.4,0.4,0.4,0.4), "cm")
    )
}


ggp_sig_chemokine_receptors = ggplot(df2, aes(x=Gene, y=Expression, fill=Sample_Group)) +
  geom_bar(stat="identity", color="black",
           position=position_dodge()) +
  geom_errorbar(aes(ymin=Expression-sd, ymax=Expression+sd), width=.2,
                position=position_dodge(.9))+
  theme_SL2_bar_4()+
  scale_fill_manual(values= c("darkorange","mediumpurple1","chartreuse2","deepskyblue2"))+
  ylab("Gene Expression (FPKM)")

#Bar chart of chemokine fold change all diff genes

Fold_change_sig_chemokine_receptors = DE_genes_LN_V_G[Chemokine_Receptors,]

keep = c(11,15)
Fold_change_sig_chemokine_receptors = Fold_change_sig_chemokine_receptors[,keep]

Fold_change_sig_chemokine_receptors = na.omit(Fold_change_sig_chemokine_receptors)

keep = c(1,2,3,4,6,7,8,9,10,11,12)

Fold_change_sig_chemokine_receptors = Fold_change_sig_chemokine_receptors[keep,]

Fold_change_sig_chemokine_receptors.m = as.matrix(Fold_change_sig_chemokine_receptors)

Fold_change_sig_chemokine_receptors = melt(Fold_change_sig_chemokine_receptors.m)

ggp_sig_chemokine_receptors_fold_change_ALL = ggplot(Fold_change_sig_chemokine_receptors, aes(x= Var1, y=value,
fill = Var2)) +
  geom_bar(stat="identity", color="black", position=position_dodge()) +
  theme_SL2_bar_4()+
  scale_fill_manual(values= c("chartreuse2","deepskyblue2"), labels = c("LN V G CMC","LN V G PG"))+
  ylab("log2fold Change")+
  xlab("Gene")


#Chemokine Ligands
```

```
Chemokine_ligands = c("Cxcl1", "Cxcl2", "Cxcl4", "Cxcl5", "Cxcl7", "Cxcl9", "Cxcl10", "Cxcl11", "Cxcl12", "Cxcl13", "Cxcl14",
"Cxcl15", "Cxcl16", "Cxcl17", "Ccl1", "Ccl2", "Ccl3", "Ccl4", "Ccl5", "Ccl6", "Ccl7", "Ccl8", "Ccl9", "Ccl11", "Ccl12", "Ccl17",
"Ccl19", "Ccl20", "Ccl21a", "Ccl21b", "Ccl21c", "Ccl21d", "Ccl21", "Ccl22", "Ccl24", "Ccl25" ,"Ccl26l", "Ccl27", "Ccl27a",
"Ccl27b", "Ccl28", "Xcl1", "Cx3cl1")

EM_chemokines = EM[Chemokine_ligands,]

EM_chemokines = na.omit(EM_chemokines)

EM_chemokines_scaled = data.frame(scale(EM_chemokines))

data.s = data.frame(t(scale(t(EM_chemokines))))
hm.matrix = as.matrix(data.s)

# cluster Y
y.dist = Dist(hm.matrix, method="spearman")
y.cluster = hclust(y.dist, method="average")
y.dd = as.dendrogram(y.cluster)
y.dd.reorder = reorder(y.dd,0,FUN="average")
y.order = order.dendrogram(y.dd.reorder)
hm.matrix_clustered = hm.matrix[y.order,]

#untangled geneorder
y.order = order.dendrogram(y.dd.reorder)
hm.matrix_clustered = hm.matrix[y.order,]


# melt and plot
hm.matrix_clustered = melt(hm.matrix_clustered)
ggp_HM_Chemokines = ggplot(hm.matrix_clustered, aes(x=Var2, y=Var1, fill=value)) +
  geom_tile(linetype="blank") +
  scale_fill_viridis() +
  theme_SL2_HM_2()+
  labs(x="Sample",y="Gene")

#Significant chemokine ligand bar chart, overlap

DE_G_V_LN_Chemokine_ligands = EM_scaled[sig_genes_ALL_DIFF,]

DE_G_V_LN_Chemokine_ligands = DE_G_V_LN_Chemokine_ligands[Chemokine_ligands,]

DE_G_V_LN_Chemokine_ligands = na.omit(DE_G_V_LN_Chemokine_ligands)

keep = c(1,2,3,4,6)

DE_G_V_LN_Chemokine_ligands = DE_G_V_LN_Chemokine_ligands[keep,]

gene_data = DE_G_V_LN_Chemokine_ligands
gene_data = data.frame(t(gene_data))
gene_data$sample_group = Sample_Sheet$Sample_Group

gene_data.m = melt(gene_data)
names(gene_data.m) = c("Sample_Group", "Gene", "Expression")


data_summary <- function(data, varname, groupnames){
  require(plyr)
  summary_func <- function(x, col){
    c(mean = mean(x[[col]], na.rm=TRUE),
      sd = sd(x[[col]], na.rm=TRUE))
  }
  data_sum<-ddply(data, groupnames, .fun=summary_func,
                  varname)
  data_sum <- rename(data_sum, c("mean" = varname))
  return(data_sum)
}

df2 = data_summary(gene_data.m, varname = "Expression", groupnames = c("Sample_Group", "Gene"))
df2$Gene = as.factor(df2$Gene)

df2$Gene = factor(df2$Gene, levels = c("Cxcl1", "Cxcl2", "Cxcl4", "Cxcl5", "Cxcl7", "Cxcl9", "Cxcl10", "Cxcl11", "Cxcl12",
"Cxcl13", "Cxcl14", "Cxcl15", "Cxcl16", "Cxcl17", "Ccl1", "Ccl2", "Ccl3", "Ccl4", "Ccl5", "Ccl6", "Ccl7", "Ccl8", "Ccl9", "Ccl11",
"Ccl12", "Ccl17", "Ccl19", "Ccl20", "Ccl21a", "Ccl21b", "Ccl21c", "Ccl21d", "Ccl21", "Ccl22", "Ccl24", "Ccl25" ,"Ccl26l", "Ccl27",
"Ccl27a", "Ccl27b", "Ccl28", "Xcl1", "Cx3cl1"),labels = c("Cxcl1", "Cxcl2", "Cxcl4", "Cxcl5", "Cxcl7", "Cxcl9", "Cxcl10",
"Cxcl11", "Cxcl12", "Cxcl13", "Cxcl14", "Cxcl15", "Cxcl16", "Cxcl17", "Ccl1", "Ccl2", "Ccl3", "Ccl4", "Ccl5", "Ccl6", "Ccl7",
"Ccl8", "Ccl9", "Ccl11", "Ccl12", "Ccl17", "Ccl19", "Ccl20", "Ccl21a", "Ccl21b", "Ccl21c", "Ccl21d", "Ccl21", "Ccl22", "Ccl24",
"Ccl25" ,"Ccl26l", "Ccl27", "Ccl27a", "Ccl27b", "Ccl28", "Xcl1", "Cx3cl1"))
df2$Sample_Group = factor(df2$Sample_Group, levels = c("LN_CMC", "LN_PG", "G_CMC", "G_PG"),labels =
c("LN_CMC","LN_PG", "G_CMC","G_PG"))
```

```
ggp_sig_chemokine_ligands = ggplot(df2, aes(x=Gene, y=Expression, fill=Sample_Group)) +
  geom_bar(stat="identity", color="black",
           position=position_dodge()) +
  geom_errorbar(aes(ymin=Expression-sd, ymax=Expression+sd), width=.2,
                position=position_dodge(.9))+
  theme_SL2_bar_4()+
  scale_fill_manual(values= c("darkorange","mediumpurple1","chartreuse2","deepskyblue2"))+
  ylab("Expression (FPKM)")


###Log Change plots####
Fold_change_sig_chemokine_ligands = DE_genes_LN_V_G[Chemokine_ligands,]

keep = c(11,15)
Fold_change_sig_chemokine_ligands = Fold_change_sig_chemokine_ligands[,keep]

Fold_change_sig_chemokine_ligands = na.omit(Fold_change_sig_chemokine_ligands)

keep = c(1,2,3,4,6)

Fold_change_sig_chemokine_ligands = Fold_change_sig_chemokine_ligands[keep,]

Fold_change_sig_chemokine_ligands.m = as.matrix(Fold_change_sig_chemokine_ligands)

Fold_change_sig_chemokine_ligands = melt(Fold_change_sig_chemokine_ligands.m)

ggp_sig_chemokine_ligands_fold_change_ALL = ggplot(Fold_change_sig_chemokine_ligands, aes(x= Var1, y=value, fill =
Var2)) +
  geom_bar(stat="identity", color="black", position=position_dodge()) +
  theme_SL2_bar_4()+
  scale_fill_manual(values= c("chartreuse2","deepskyblue2"), labels = c("LN V G CMC","LN V G PG"))+
  ylab("log2fold Change")+
  xlab("Gene")

#GPCR analysis

GPCR_LIST= read.table("GPCRLIST.csv", header=TRUE,row.names=1, sep="\t")

GPCR = GPCR_LIST$MGI.symbol

 EM_GPCR = EM[GPCR,]

EM_GPCR = na.omit(EM_GPCR)

EM_GPCR_scaled = data.frame(scale(EM_GPCR))

data.s = data.frame(t(scale(t(EM_GPCR))))
hm.matrix = as.matrix(data.s)

# cluster Y
y.dist = Dist(hm.matrix, method="spearman")
y.cluster = hclust(y.dist, method="average")
y.dd = as.dendrogram(y.cluster)
y.dd.reorder = reorder(y.dd,0,FUN="average")
y.order = order.dendrogram(y.dd.reorder)
hm.matrix_clustered = hm.matrix[y.order,]

#untangled geneorder
y.order = order.dendrogram(y.dd.reorder)
hm.matrix_clustered = hm.matrix[y.order,]

 ###theme####

theme_SL2_HM_GPCR <- function () {
  theme_bw() %+replace%
    theme(
      panel.grid = element_blank(),
      panel.background = element_blank(),
      panel.border = element_rect(colour = "black", fill=NA, size=1),
      plot.background = element_blank(),
      legend.background = element_rect(fill="transparent", colour=NA),
      legend.key = element_rect(fill="transparent", colour=NA),
      plot.title = element_text(size=12, margin = margin(b = 5),hjust=0,vjust=0.5, family="Arial", face="bold"),
      title = element_text(size = 12, margin = margin(b = 5),hjust=0,vjust=0.5, family="Arial", face="bold"),
      axis.text.y = element_text(size = 12, face="bold"),
      axis.text.x = element_blank(),
      axis.title.y = element_text(size = 12, margin = margin(r = 10),angle = 90,hjust=0.5,vjust=0.5, family="Arial",
face="bold"),
```

```
    axis.title.x = element_blank(),
    legend.text=element_text(size=12, family="Arial", face="bold"),
    legend.title=element_blank(),
    legend.key.size=unit(2.5,"line"),
    plot.margin=unit(c(0.4,0.4,0.4,0.4), "cm")
   )
}


 # melt and plot
hm.matrix_clustered = melt(hm.matrix_clustered)
ggp_HM_GPCR = ggplot(hm.matrix_clustered, aes(x=Var2, y=Var1, fill=value)) +
  geom_tile(linetype="blank") +
  scale_fill_viridis() +
  theme_SL2_HM_GPCR()+
  labs(x="Sample",y="Gene")


#sig diff GPCRs

DE_genes_LN_V_G
keep = c(18:29)
sig_diff_GPCR= DE_genes_LN_V_G[,keep]

sig_diff_GPCR = na.omit(sig_diff_GPCR[GPCR,])

sig_diff_GPCR = sig_diff_GPCR[-c(3,9,19,38),]


data.s = data.frame(t(scale(t(sig_diff_GPCR))))
hm.matrix = as.matrix(data.s)

# cluster Y
y.dist = Dist(hm.matrix, method="spearman")
y.cluster = hclust(y.dist, method="average")
y.dd = as.dendrogram(y.cluster)
y.dd.reorder = reorder(y.dd,0,FUN="average")
y.order = order.dendrogram(y.dd.reorder)
hm.matrix_clustered = hm.matrix[y.order,]

#untangled geneorder
y.order = order.dendrogram(y.dd.reorder)
hm.matrix_clustered = hm.matrix[y.order,]


# melt and plot
hm.matrix_clustered = melt(hm.matrix_clustered)
ggp_HM_GPCR_Sig_Diff = ggplot(hm.matrix_clustered, aes(x = Var2, y=Var1, fill=value)) +
  geom_tile(linetype="blank") +
  scale_fill_viridis() +
  theme_SL2_HM_GPCR()+
  labs(x="Sample",y="Gene")


###integrin analysis###
#Integrin vector

Integrins_and_selectins = c("Sele", "Sell", "Selp","Itgad", "Itgae", "Itgal", "Itgam", "Itgav", "Itgax", "Itga1", "Itga2", "Itga2b",
"Itga2", "Itga3", "Itga4", "Itga5", "Itga6", "Itga7", "Itga8", "Itga9", "Itga10", "Itga11")

#EM of Integrins_and_selectins

EM_Integrins_and_selectins = EM[Integrins_and_selectins,]

EM_Integrins_and_selectins = na.omit(EM_Integrins_and_selectins)

EM_Integrins_and_selectins = EM_Integrins_and_selectins[-c(13),]

data.s = data.frame(t(scale(t(EM_Integrins_and_selectins))))
hm.matrix = as.matrix(data.s)

# cluster Y
y.dist = Dist(hm.matrix, method="spearman")
y.cluster = hclust(y.dist, method="average")
y.dd = as.dendrogram(y.cluster)
y.dd.reorder = reorder(y.dd,0,FUN="average")
y.order = order.dendrogram(y.dd.reorder)
hm.matrix_clustered = hm.matrix[y.order,]
```

```
#untangled geneorder
y.order = order.dendrogram(y.dd.reorder)
hm.matrix_clustered = hm.matrix[y.order,]


# melt and plot
hm.matrix_clustered = melt(hm.matrix_clustered)
ggp_HM_EM_Integrins_and_selectins = ggplot(hm.matrix_clustered, aes(x = Var2, y=Var1, fill=value)) +
  geom_tile(linetype="blank") +
  scale_fill_viridis() +
  theme_SL2_HM_GPCR()+
  labs(x="Sample",y="Gene")

EM_integrins_Diff = DE_genes_LN_V_G[Integrins,]


#Selectin Analysis#

selectins = c("Sele", "Sell", "Selp")

EM_selectins = EM[selectins,]

data.s = data.frame(t(scale(t(EM_selectins))))
hm.matrix = as.matrix(data.s)

# cluster Y
y.dist = Dist(hm.matrix, method="spearman")
y.cluster = hclust(y.dist, method="average")
y.dd = as.dendrogram(y.cluster)
y.dd.reorder = reorder(y.dd,0,FUN="average")
y.order = order.dendrogram(y.dd.reorder)
hm.matrix_clustered = hm.matrix[y.order,]

#untangled geneorder
y.order = order.dendrogram(y.dd.reorder)
hm.matrix_clustered = hm.matrix[y.order,]


# melt and plot
hm.matrix_clustered = melt(hm.matrix_clustered)
ggp_HM_Selectins = ggplot(hm.matrix_clustered, aes(x = Var2, y=Var1, fill=value)) +
  geom_tile(linetype="blank") +
  scale_fill_viridis() +
  theme_SL2_HM_GPCR()+
  labs(x="Sample",y="Gene")

#diff expressed selectins

EM_selectins_Diff = DE_genes_LN_V_G[selectins,]
```